UNIVERSITY OF CAPE TOWN
MINERAL PROCESSING RESEARCH UNIT

SEGREGATION AND MATERIAL FLOW ALONG LOW ASPECT SAG MILLS

by

Sonny Mwansa

B Min Sc (Metallurgy & Mineral processing), UNZA

A thesis submitted in fulfillment of the requirements for the award of the degree of Master of Science in Engineering, MSc (Eng)

Comminution Research Group
Department of Mechanical Engineering

August 2006

Declaration

I know the meaning of plagiarism, therefore, I hereby declare that the work in this dissertation, save for that which is properly acknowledged is my own. The material contained herein has also not been submitted either in whole or in part, for a degree at this or any other University.

Signed: Signed by candidate

Sonny Mwansa

Dedication

I dedicate this thesis to my mother Theresa Mulenga Mwansa for her inspiration in my education, for her love and for always having been there for me. I thank the almighty God for my existence.

Acknowledgements

I wish to thank the following individuals and institutions for their contribution towards the successful completion of this thesis:

- Dr. Malcolm Powell, my supervisor for his enthusiastic guidance, support and encouragement throughout the course of this research work. To Malcolm, I do not only convey my sincere gratitude for your overall support but I also thank you for facilitating my scholarship with the MPRU to undertake the MSc.
- Dr. Aubrey Mainza, for his involvement in my site work and sharing his knowledge of sampling Comminution circuits, his critical views as well as his general support.
- Dr. Toni Kojovic of the JKMRC, for his technical input to improve the quality of this thesis.
- Dr. Hakan Benzer of the Hacettepe University – Turkey, for the technical discussions and for his vision on the modeling benefits that could come out from this work.
- Dr. Frank Shi of the JKMRC for his suggestions at the initial stage of the project.
- Percy Condori, my Peruvian friend and colleague for his suggestions, being present on most of my site work, his criticism and most importantly for his good friendship.
- Special thanks to my girlfriend Bridgette Anastasia Sholtz for her encouragements and support.
- My colleagues Reuben Moalosi, Musa Mathye and Michael Bekapi, for their assistance and endurance during the emptying out of the charge from the Amandelbult SAG mill.
- Douglas Phillips and Vusumuzi Mahlangu (Anglo platinum) for their commitment and excellent support with the segregation samples and drop weight tests respectively.
- Dr. Richard Williams (University of Leeds), for his provision, in part, of papers on lab scale segregation techniques; such as Magnetic Resonance imaging (MRI).
- Professor Richard Hogg (The Pennsylvania State University), one of the pioneers of segregation research, for his suggestions and help with articles of segregation history.
- Dr. Abdelzaher Abouzeid (University of Cairo), for his valuable information on the history of Residence time distribution of particles in rotary mixers.
- Dr. Indresan Govender, Andrew McBride and Chisenga Kulya, for their input in DEM.
- Comminution group colleagues, for making my stay in the Mineral Processing Research Unit (MPRU) a worthwhile experience
- Finally but not the least, the AMIRA P9N sponsors; Anglo platinum Ltd and LonMin Platinum Ltd for the opportunity to conduct this study on their plants, for funding the P9 project and for their enthusiasm in promoting research in the mining industry.

Synopsis

A distinctive axial segregation study of particles (steel balls, rocks and slurry-fines) within the charge of long, South African style Semi-autogenous (SAG) mills is reported in this thesis.

The significance of this study is primarily intended to provide better understanding of axial segregation and flow of particles along SAG mills. Additionally, the current SAG mill models developed using "short" Australian and North American style mills exposes inaccuracies when applied to predict the performance of "long" mills. Thus the results of this study are expected to be useful for improving modelling of long SAG mills.

Several studies of radial and axial segregation in tumbling horizontal devices at laboratory-scale and a few on pilot-scale have been conducted in the past by various researchers. Recently, industrial-scale studies of axial segregation in kilns and dry milling, particularly in the cement industry have also been conducted. However, there seems to be no work reported and cited in the literature on axial segregation studies along SAG mills. Thus the lack of previous segregation research along SAG mills has exposed a knowledge gap in the subject.

Due to the unavailability of reported methodologies to survey particle axial segregation in large-scale tumbling mills, novel sampling techniques have been formulated and used in this present study to collect the charge particles at different positions along the mill, and to drain slurry from the mill at different points along its shell.

Results from the testwork of emptying out the entire mill contents into four separate slices along the mill length and sizing the emptied out charge independently, are reported. The sizing results showed that most of the big rocks resided within the inlet section of the mill whilst the fine particles had segregated towards the mill discharge position. The steel balls on the other hand, were found to be uniformly distributed across the mill length.

Further, drop weight tests have been performed to study hardness of rocks with respect to the position along the mill from where they were located. The drop weight test results have revealed that for identical sizes, the rocks located at the discharge position of the mill absorbed more specific comminution energy (Ecs) for breakage and were therefore harder than those from the inlet section.

Finally, discrete element modelling (DEM) has been used to simulate the particle collision interactions to produce the energy spectra for rocks located at the inlet position and those from the discharge section. The simulation outcomes reveal that the impact events of particles were different

for the two positions, being higher at the discharge than at the inlet. The predicted progeny rocks size distribution and rate of fines production were also significantly different, suggesting that long mills should not be modelled as perfectly mixed.

From all the testwork results, it can be tentatively concluded that segregation of particles along SAG mills is a product of the *transport* and *breakage* mechanisms. The transport mechanism is responsible for segregation by *size*. Fine particles with lower residence times migrate with the aid of the carrier fluid through the voids towards the mill discharge whilst the bigger rocks are preferentially retained and dominate the inlet section. The breakage mechanism is responsible for size reduction of particles, but some competent rocks survive and make it to the mill discharge, and could even flow backwards. Therefore, survivability (resistance of rocks to breakage) leads to segregation by particle *hardness*. The fact that the steel balls revealed no segregation, imply that rock hardness has a more significant influence than the particle size effect on the observed segregation.

Table of Contents

List of Figures

List of Tables

Nomenclature

The main terminology and the symbols adopted in this thesis are described in this section

Aspect ratio – A term used by Chemical Engineers and Minerals Engineers to describe or relate the diameter and length fraction of a cylindrical unit

Axial – Along the axis of rotation which is horizontal down the length of the mill

Collision class – A categorization of impact events.

Collision rate – The number of collisions per unit time of DEM simulation

Comminution – A processing technique of reducing large rocks to smaller sizes in order to liberate or free the minerals of interest

Competence / hardness – A term used to describe the structural stability of a particle and is measured by indenting or scratching a specific solid

Energy spectra – A plot of the number of collisions recorded in a fixed simulation time against the energy lost for each impact event of a given collision class.

Fines – Very small rock particles which have been ground to the size of powder

Mill – A rotary cylindrical device used in the Mineral processing industry to grind rocks in order to reduce them into fines and liberate the 'locked' mineral/s

Modal peak – The energy on the energy spectra for which the highest number of collisions is recorded within each impact class

Particle – A solid portion of matter e.g. rock or steel ball

Perfect mixing – A state of homogeneity where particles are evenly distributed in the mill

Progeny – The offspring (fines) particles broken out from big rocks

Radial – the cross –section outwards that is perpendicular to the axis of rotation

Sample – A part of material or specimen collected from the bulk quantity that is expected to represent the population from which that part is drawn

Screening/Sizing – A separation technique used to classify rocks according to their size

Segregation – A naturally occurring phenomenon where particles isolate or separate from the mass and collect together due to distinct physical properties such as size

Simulation – To mimic industrial-scale machine operations using a computer program

Slice – A segment or portion containing particles which was a fraction of the mill volume

DEM – Discrete Element Modelling

DWT – Drop Weight Test used for impact ore characterisation

MPRU – Mineral Processing Research Unit of the University of Cape Town

PSD – Particle Size distribution

SAG/AG – Semi-Autogenous milling/Autogenous milling

$\mathbf{E_{cs}}$ – Specific comminution input energy (kWh/t)

$\mathbf{E_{crit}}$ – Minimum energy to cause breakage from a single impact

$\mathbf{E_h}$ – Energy causing breakage after several hits or cyclic impacts

$\mathbf{E_o}$ – Minimum energy to cause breakage from several impacts

F80 – Size at which 80 % of the feed passes

P80 – Size at which 80 % of the product passes

S80 – Size at which 80 % of the particles in a mill slice pass

t_{10} – Fraction of broken product that is smaller than one tenth of the original particle size

Chapter 1

1 INTRODUCTION

This chapter describes the background, motivation, objectives of the present study, Hypotheses, and outlines the structure for this dissertation. From Powell *et al* (2000), the current Autogenous/Semi-Autogenous Grinding (AG/SAG) mill models based on Australian and North American style mills used in industry fall short in accurate prediction of mill performance of South African style mills. This is mainly due to the difference in design of these mill types, and the goal of this work is to provide better understanding of particles axial segregation along SAG mills and in part to suggest ways of incorporating the observed segregation in the current JK AG/SAG mill model. This thesis on *segregation and material flow along SAG mills* describes the methodology and the challenges of sampling the charge from production mills. It further highlights outcomes from emptying out and sizing the entire mill charge from a 4.8 m diameter by 3.5 m long industrial SAG mill.

1.1 BACKGROUND

The contribution of mining and mineral processing (metallurgical) products to technology and the subsequent social impact of these products on modern society is so huge that there has always been continuous research to improving and optimising current operating techniques in the mining and metallurgical processing industry.

Comminution is the process of breaking the ore into smaller fragments to liberate the mineral of interest and recover that particular mineral in the subsequent metallurgical processes. It is comprised of the crushing and milling processes. Crushing may have up to three stages; primary, secondary, and tertiary crushing involving screening in between the stages. The Fully Autogenous grinding (FAG) and Semi-Autogenous (SAG) mills or Run of Mine (RoM) ball mills as they are commonly referred to in the South African industry, combine both the crushing and milling processes within the mill. The comminution process requires an intense application of energy to break the particles. In milling particularly, lots of energy is expended especially during fine grinding as was demonstrated by early researchers Kick (1883), Rittinger (1867), Bond (1961) and reviewed further by Hukki (1961). The research efforts focused on energy reduction in tumbling mills are phenomenally high. Even with a better way of predicting mill power draw developed by Morrell (1993), the interactions of the charge particles inside a production mill is so dynamically complex that it is not easy to correlate the energy directly involved in breaking these particles to the power drawn by the mill

without having knowledge of the charge breakage characteristics, and mixedness or the *segregation* and flow of these particles along the SAG mill. Kavetsky and Whiten, (1984) conducted studies which showed that long mills were not perfectly mixed and had segregation. Thus the complexity of particle interactions inside industrial mills and non-peferct mixing in long mills motivated the topic for this dissertation. This research project was initiated by Dr. Malcolm Powell of the Mineral Processing research Unit (MPRU) at the University of Cape Town. This study is part of the two P9N projects aimed at accurately predicting performance of all types of SAG mills – the consolidated tumbling mill, and the measuring flow and segregation along SAG mills projects coordinated by the Australian Mineral Industry Research Association (AMIRA) International.

Segregation is a de-mixing phenomenon that has been long observed in heaping and storage of granular materials and occurs naturally during processing of these materials. The cause of segregation is believed to be the difference in physical properties; size, shape, hardness, and density of the flowing solids. While segregation has been found to be useful in some processes like screening, tabling, jigging, pelletization, etc, Abouzeid (2000), it is judged to be a source of inaccuracies when modelling long SAG mills. In tumbling horizontal cylinders and SAG mills, segregation is an act of particles to isolate from a mass and collect together. This negates mixing with other particles and may be detrimental to milling as the charge particles are exposed to different breakage zones. Axial segregation along mills has been found to exist in previous and current research studies but no quantitative studies have been conducted to determine the extent to which this phenomenon occurs. From the qualitative information available, it has been reported that segregation occurs both radially and axially (longitudinally), Donald and Roseman (1962), Rogers and Clements (1971), and Ding *et al* (2001). Radial segregation occurs faster than axial segregation and is expected to be more pronounced in shorter mills with large diameters while axial segregation is expected to occur more significantly in long mills, probably due to the higher residence time required for the motion of these particles to the discharge end as a result of the long length of the mill, Khakhar et al (2002). Segregation in industrial mills has not been thoroughly studied due to the difficulty in physical measurement of the charge.

The current autogenous grinding (AG) and SAG mill models used in JKSimMet do not take into account segregation of the charge and material flow along the mill. Particle segregation in the charge and material flow along the mill are thought to be important parameters in grinding operations but in the current models the charge is assumed to be perfectly mixed. The assumption of perfectly mixed charge in SAG mills has been used due to a lack of data on particle segregation and material

flow along mills and also because these models were developed on short mills in which the charge is thought to be reasonably perfectly mixed.

1.2 MOTIVATION

The difference in the design and window of operation for the Australian and North American SAG mills to that of the South African style SAG (RoM) ball mills given in Table 1-1, was highlighted by the extensive collaborative work conducted by the CMR of the University of Cape Town and the Julius Kruttschnitt Mineral Research Centre (JKMRC), Queensland University, Powell *et al* (2000).

Table 1-1: Comparison of RoM and SAG mill operating regimes (Powell et al 2000).

	AG/SAG	South African RoM
Speed, % critical	70 - 80 %	75 - 90%
Charge filling, % total mill volume	20 - 30 %	35 - 45%
Ball filling, % total mill volume	4 - 15%	15 - 35%
Internal Length	3 - 5 m	5 - 12 m
Aspect ratio, diameter / length	0.7 - 2	0.5 - 0.8
Recycle stream	Trommel oversize & pebble crusher	Cyclone underflow / fine screen
Application	Primary grind	Single stage to final product

It is evident from Table 1-1 that these two types of mills are different in dimension and their operating regimes are clearly different. Empirical models developed for Australian mills would not be expected to accurately predict the performance of South African mills, but more fundamental models should work on both types of mills. The huge operational difference shown in Table 1-1 suggests that it either would be useful to formulate a "Unified SAG model" that would incorporate all mill design types or to just improve the existing model by incorporating the aspects of charge behavior such as segregation and charge flow which have been previously omitted in the current model. The latter motivates the need to conduct this research work.

1.3 KNOWLEDGE GAP

Although reference can be given to many researchers conducting studies at laboratory scale on segregation in milling and other process industries, the literature has shown a clear lack of previous research on segregation and material flow in production SAG mills, Abouzeid (2000). The observations and statements made by the investigators clearly point out that flow of particles and segregation or mixedness of material in SAG mills is not well understood and they suggest that segregation is not required in milling, Donald and Roseman (1962), Shoji *et al* (1973), Hogg (1984),

and Tang and Puri (2004). There is however, no reported research on how to minimize segregation in milling or even how to incorporate it in the existing SAG model.

1.4 GENERAL RESEARCH OBJECTIVES

The underlying objective of this work is to improve liberation in milling circuits, through reduction of energy consumption in SAG mills.

The major task of this study is to quantify the effects of particle segregation and material transport along the charge of SAG mills and thus provide a sound understanding of this phenomenon. The long term goal which falls beyond the scope of this project is to use the segregation and flow data in updating and refinement of the current JK SAG model.

The general objectives of this research are summarized as:

1. Provide a better understanding of segregation and flow of material along SAG mills and fill the knowledge gap in this field.
2. Provide a reliable and tested methodology of sampling the charge and slurry to determine the extent of segregation and flow of material along SAG mills.
3. Provide quality data that could be used for continued research into SAG model refinement (updating) for accurate prediction of grind in all mill design types.

1.5 THESIS STRUCTURE

In light of the project objectives, this thesis is comprised of nine chapters tailored to achieve these project goals. The detailed outline of the thesis and the contents of each chapter are summarized as follows:

Chapter 1 describes the background to this work, introduces the objectives of this research study by giving the motivation to carry out this work, points out the knowledge gap due to insufficient literature on the subject, and then presents the thesis outline.

Chapter 2 reviews four aspects of particles' behavior in tumbling cylindrical devices based on the available literature. This chapter first presents the history of material flow and residence time of particulates in cylindrical rotary devices and highlights the techniques that have been previously used to measure and study segregation at a laboratory scale. A few published papers on the advances in segregation research are covered in section two. The studies in pilot and batch ball mills, and the

recent developments in discrete element modeling (DEM) are given in this section. A review of mill models in the mineral processing industry with emphasis on the perfect mixing model is given in detail in section three. Finally a critical overview of SAG mill operations and design is included to provide a correlation of motion of particles and charge behavior to tumbling mill design. The knowledge gap mentioned above imposed a restriction on reviewing a substantial amount of literature in this chapter.

Chapter 3 revisits the causes and trends of the observed segregation reported in literature. The hypotheses for the current segregation study are outlined and the specific objectives of this dissertation are described in this chapter.

Chapter 4 discusses the preliminary plant trials which suggested the course of direction for this research project. The analysis of improving the methodology and adjusting the sampling technique for better results is discussed.

Chapter 5 presents the results obtained from several snap surveys conducted at different Concentrators and on different SAG mill designs. The surveys were aimed at studying the influence of mill length on the observed segregation. Split Desktop Software is used to analyze mill charge surface pictures collected along SAG mills to examine the extent of segregation. This chapter also presents the results of residence time of different size particles conducted along an autogenous mill.

Chapter 6 demonstrates the adopted methodology used when emptying out the entire charge of a full production SAG mill. The pressures on mill production downtime as well as the challenges to plan and accurately cope with huge samples in the magnitude of tons to minimize errors are given in this chapter.

Chapter 7 is the heart of this research work and presents the detailed results and discussion of the segregation research work from the major plant campaign at Amandelbult.

Chapter 8 reports the energy spectra (collision frequency per energy range) simulations of particles obtained from the inlet and discharge mill positions (slices) of the Amandelbult SAG mill, using discrete element modelling (DEM). A discussion of the DEM simulations outcomes is given as well as the predicted fines production at the two slices.

Chapter 9 completes the thesis by presenting the overall summary of findings in the conclusions section and gives the recommendations for future research.

Chapter 2

2 LITERATURE REVIEW

This chapter presents a review of literature on segregation and flow of material in tumbling horizontal vessels. An overview of SAG mill operations and design is included to provide a correlation of motion of particles and charge behavior to tumbling mill design. The review covers four aspects of the subject in light of the thesis objectives given in Chapter 1. The first section reports earlier studies on material flow and residence time of particulates in cylindrical rotary devices at laboratory scale. The clear presence of particle segregation at this scale is highlighted. The second section covers latest advances in segregation research and gives a critical review of selected papers on topics such as the batch ball mill studies and discrete element modeling (DEM) methods. The third section briefly reviews the SAG mill model. Finally, an overview of SAG mill operations and design deemed relevant to this study is presented. The literature shows a clear lack of segregation research on production mills in the mineral processing industry and especially on wet milling.

2.1 SEGREGATION AND MATERIAL FLOW HISTORY

The early research on material transport and motion of particulates in mineral processing systems was mainly concentrated on residence time distribution (RTD) studies and most of this work was conducted in rotary kilns, Henein *et al.* (1985). Both radial and axial segregation have been studied at laboratory scale and some segregation models have been proposed although none of them have been satisfactory and hence have not been adapted to industrial applications.

2.1.1 Residence time distribution (RTD) studies

The work done by Sullivan *et al.* (1927) at the United States Bureau of Mines (USBM) is believed to be the first extensive experimental study done on material flow in mineral processing rotating cylindrical devices. Sullivan *et al.* related the time of passage of solids through rotary kilns to the measurable kiln variables. From the experimental measurements, they formulated a relationship in an empirical expression given by equation (2.1)

$$t = 1.77L(\theta)^{1/2} / 2Rn\varphi^{\circ} \qquad (2.1)$$

Where:

t = time of passage through the kiln, in minutes.

L = Length of the kiln, in ft.

θ = the angle of repose of material, in degrees.

R = the kiln radius, in ft.

n = rotation speed of the kiln, in rpm.

φ = the angle of inclination of the kiln axis, in degrees.

The relationship formulated by Sullivan *et al.* in equation (2.1) did not incorporate the segregation description of material through the kiln and similar studies conducted later by Oyama (1933) were based on relating the residence time of material to the kiln variables.

Pickering *et al* (1951), conducted work to represent the passage of particles from first principles and this was well presented by Saeman (1951). The expression for calculating the mean residence time derived by Saeman is given by equation (2.2)

$$t = LSin\theta^{\circ} / 2\pi rn\varphi^{\circ} \qquad (2.2)$$

Where:

r = passage of the particle in the material bed, in ft.

n = rotation speed of the kiln, in rpm.

The two equations (2.1), and (2.2) have been historically used to compute the mean residence time for passage of material in kilns, and under normal kiln operating conditions, an average angle of repose of material (θ) is set to 40°, and the difference in the mean residence time calculated from both equations above is less than 5%, Abouzeid (2000).

Like Sullivan *et al.*'s relationship, Saeman's equation (2.2) is a purely RTD expression and does not incorporate the segregation description of material through the kiln. Both expressions are less relevant to this study but at least trace the history of segregation research.

2.1.2 Radial and axial segregation in horizontal drum mixers

Rotating drums have been used historically to conduct experiments for the studies of segregation and mixing in the batch laboratory setup. This is because rotating drums play a key role in processing granular materials in the chemical, metallurgical, pharmaceutical and food industries, in which they perform chemical reactions, mixing, and drying, Ding (2001) However, due to the huge difference existing between the charge behavior in industrial mills and that of pre-mixed batch feed (usually sands and glass beads) in horizontal drum mixers, previous research has not contributed to the effect

of using these results in production mills, and prominent researchers of segregation in horizontal drum mixers attest to this fact.

"The fact that the axial movement of the grinding media and very large particles is constrained by the discharge grate causes major changes in the transport mechanisms, since finer material has to percolate through the interstices in the media charge rather than simply flow over the free surface of a rotating powder bed" – Richard Hogg (2005).

The first reported work on axial segregation of particles along a rotary cylinder was conducted by Oyama (1939) and was comprehensively reported by Weidenbaum (1958). Oyama performed experiments of studying the mixing behavior of a rotary charge and noticed that the binary mixture of large and small grained sand segregated into axial bands when tumbled in a horizontal drum mixer. A few more studies were performed in the next two decades but were not of as high note as the work conducted by Donald and Roseman (1962).

2.1.2.1 Mechanisms in a horizontal drum mixer by Donald and Roseman.

The work of Donald and Roseman (1962) is deemed to have thoroughly tackled segregation in drum mixers and most of the citations on the subject are referred to the study by these two investigators. They used an electrically driven drum mixer constructed from Perspex tube with a segment of the wall removable to allow vertical sampling. A binary component of sand and ballotini differing in particle size was used as the test material in the drum mixer.

Donald and Roseman based the mechanism of mixing on the independent description by Carley – Macauly (1954) and Lacey (1954) who each explained segregation as a statistical process expressed by the variance given in equations (2.3) and (2.4) respectively.

$$M = 1 - \frac{S^2 - S_R{}^2}{S_O{}^2 - S_R{}^2} \text{ (Lacey equation)} \qquad \textbf{(2.3)}$$

Where:

M = Degree of mixing corrected for sampling errors

S = Standard deviation of the sample composition, measured value

S_O = Standard deviation for unmixed material

S_R = Standard deviation for completely randomised mixture

At the start of mixing $S^2 = S_O{}^2$ and M = 0, while at completion $S^2 = S_R{}^2$ and M = 1

$$V_P = S^2 - S_R{}^2 \text{ (Carley – Macauly equation)} \quad \textbf{(2.4)}$$

Where:

V_P = Degree of mixing corrected for sampling errors

When the particles were distinguishable only by color, $S_R{}^2$ was given by the standard statistical term shown in equation (2.5).

$$S_R{}^2 = p(1-p)/n \quad \textbf{(2.5)}$$

Where:

$p(1-p)$ = initial proportions of the components

n = number of particles in a sample.

If the size of the particles differs, a bias is introduced into the sampling system and the correction to the variance is now given by equation

$$S_R{}^2 = \frac{p(1-p)}{n}\{pV_{01-p} + (1-p)V_{op}\} \quad \textbf{(2.6)}$$

Where: V_{op} and V_{01-p} = Volume of particles

The terms inside the brackets accounts for the size difference.

From equations (2.3) to (2.6), Lacey, Donald and Roseman all claim that every mixer utilizes three principal mixing mechanisms which they classified as follows.

i. The transfer of groups of adjacent particles from one location in the mass to another – "convective mixing."
ii. The distribution of particles over a freshly developed surface – "diffusive mixing."
iii. The setting up of slip planes within the mass – "shear mixing."

They further asserted that in horizontal drum mixers, the mixing or segregation of particles is of diffusional nature, (type ii). However, studies by several authors such as Rogers and Clements (1971), Hogg (1984), Henein *et al.* (1985), Hill *et al.* (1997), Wightman and Muzzio (1998), Abouzeid (2000), etc. have revealed that all of the above three mixing mechanism can occur at the same time in a

the rotating cylinder was operated and to the size ratio between the small and large particles. They reported that operating the cylinder at higher speeds could reverse the pattern of the observed radial segregation, where large particles would concentrate in the central core and the surrounding smaller particles occupying the peripheral next to the cylinder shell. They claimed that for mixtures with few large particles, large particles could concentrate at any radial position in the bed depending on the size ratio.

The work of Khakhar *et al.* (1996) showed that the length of a horizontal cylinder, drum or mill has a huge influence on the observed segregation, the fact that no axial segregation was observed in the short cylinder used for the study, indicated that increasing the length of the cylinder might promote scatter of particles and axial segregation along the cylinder as the particles would spend longer times to reach the other end of the cylinder. It appeared that larger diameters promote radial segregation while shorter lengths of the cylinders promote good axial mixing of the particles within the bed. The length and diameter length relationship effects in short cylinders are expected to have similar influence in SAG mills.

2.2 ADVANCES IN SEGREGATION RESEARCH

As much as the research of mixing and segregation in horizontal rotating drums has progressed, the reality is that the results obtained are still very far from being applicable to SAG mill operations. The studies in pilot and batch ball mills, and the recent developments in discrete element modeling (DEM) to simulate particle behavior in mills has raised the hope of understanding and applying segregation effects in the current SAG model.

2.2.1 Axial mixing of particles in batch ball mills by Shoji, Hogg and Austin

Shoji et al, (1973) used a batch mill constructed from Lucite tube, measuring 9.5 cm in diameter and 25 cm long, with 8 lifters, to study axial mixing of dry powders. The ball mill was rotated at 67 % of the critical speed and fed with silicon carbide crystals, garnet tracer, and 14 mm diameter vinyl balls.

These investigators claimed that axial mixing occurred through a diffusional mechanism while radial mixing was assumed to take place through convection of particles. The diffusional process could be described by a one-dimensional equation, (2.7).

$$\frac{\partial C}{\partial t} = D\frac{\partial^2 C}{\partial x^2} \qquad (2.7)$$

The mixing state achieved was attributed to the rocking perturbations applied to the system. After 1000 rotational revolutions, Wightman and Muzzio observed the core formation predicted by Hill and Kakalios at high speeds, where large blue beads formed a horizontal core in the bed surrounded by the smaller red beads.

The claim of rocking perturbations which are analogous to collisions and breakage in SAG mills, promoting mixing in drum mixers does not seem to be true as rocking perturbations promote chaos and generally after a collision, the particles involved scatter away from the rest of the particles in a bed. Donald and Roseman in their description of mixing stated that collisions or in this case rocking perturbations would result in a possibility of particles to be freed from the rest position and initiate segregation. Thus, it appears that the rocking perturbations would promote segregation rather than encourage mixing of particles in a bed.

2.1.2.5 Flow, mixing and radial segregation in short rotating cylinders - Khakhar et al.

Khakhar *et al.* (1996 and 2002) studies initially revealed no segregation of particles along a small 14 cm diameter by 6.5 cm short rotating cylinder when they operated it at low speeds of about 10 rpm. In their later studies on similar short (high aspect ratio) cylinders, they observed radial segregation in form of a radial core of smaller particles surrounded by larger particles. They claimed that coupling of the bed composition with flow led to instability that resulted in a pattern of segregation they termed "radial streaks" shown in Figure 2-7.

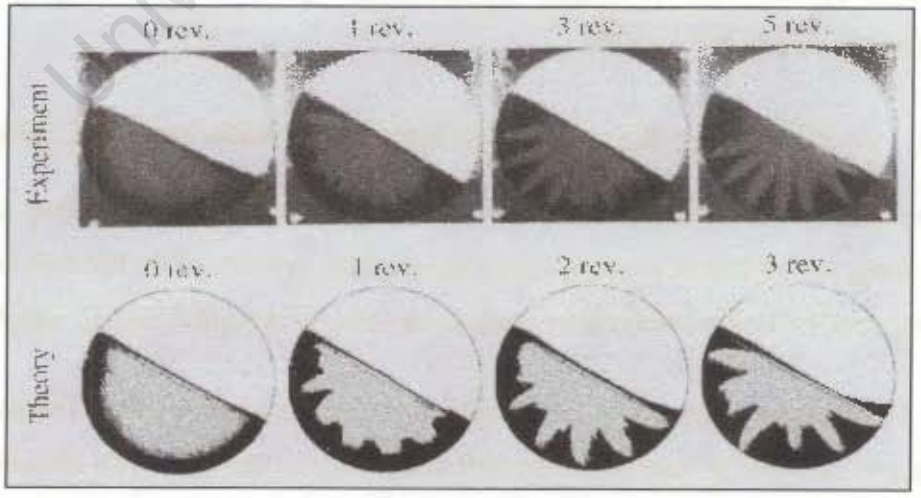

Figure 2-7: Experimental and computational results showing streak formation at 0.75 rpm. A 50 % vol/vol mixture of 3 mm (dark) and 1 mm (light) glass beads used, (after Khakhar *et al.* 2002)

Khakhar *et al.* (2002) ascribed the observed segregation where the small particles form a central core that is surrounded by large particles on the periphery, to the low rotation speed (0.75 rpm) at which

The banding segregation observed by Hill *et al.* bore some resemblance to the core formation segregation first observed by Donald and Roseman (1962).

The work of Hill and Kakalios highlighted the influence of the horizontal cylinder/drum speed on the observed segregation. They showed that for longer rotational times and at very high speeds, the observed bands merged into one central band of large beads with bands of small beads adjacent on either side

Choo *et al.* (1998) also observed axial banding segregation of particles along a 2.7 cm diameter by 1m long Pyrex drum mixer (Figure 2-6). As the length of the mixer was very long, the observed axial segregation was attributed to diffusion of small particles through the bed and was described by the dynamic angle of repose, mixer rotational speed and the local concentration within the bed, expressed through a first order diffusion equation. Choo *et al* claimed that their work was supported by the findings of Hill and Kakalios, (1994).

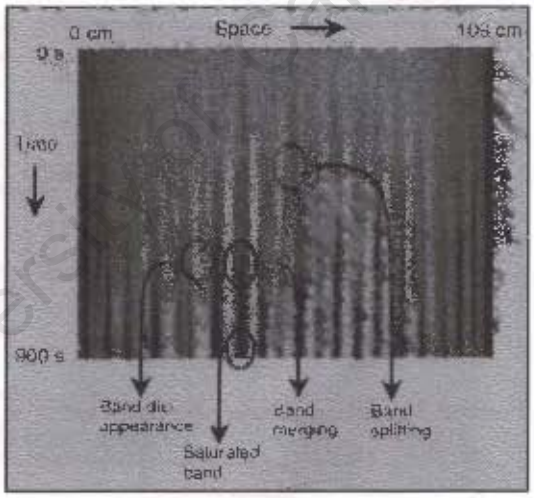

Figure 2-6: Example of transient dynamics exhibited by a mixture with a fixed composition, $\emptyset = 0.5$, showing band splitting, merging, and disappearance, (After Choo *et al*, 1998)

Wightman and Muzzio (1998) used a 10.6 cm diameter by 14 cm long drum mixer rotated at 5 rpm and fed with 66 µm mean diameter red particles and blue particles with mean diameter of 180 µm, to study mixing within the drum mixer. They chose a size ratio of 2.7 between the diameter of small and large particles because they claimed it was a typical value found to result in segregating systems.

Wightman and Roseman expected their segregation results to fall into any of the three patterns described by Donald and Roseman (1962). They claimed that by applying time–periodic rocking perturbations, the binary mixture would change from a segregation state to a homogenous mixture.

claimed that the phenomenon of regained segregation could only be achieved for binary mixture of large glass (2.85 mm) beads and small (0.5 – 0.75 mm) glass beads. Other combinations could reveal segregation but upon change of cylinder rotational speed from high to low and back to high, axial segregation could not be regained. They further claim that smooth round beads were not responsible for the regained segregation observed, as they noticed axial segregation of a mixture of split peas and uncooked rice. They observed a central band of peas formed with two side bands of rice after a cylinder rotation for about 2 hours at a speed of 14 rpm.

Further work by Hill *et al.* (1997), using magnetic resonance imaging (MRI) and using the same 12.7 cm diameter by 60 cm long Plexiglas horizontal cylinder fed with glass beads of the same size as those used in their earlier studies, revealed axial banding segregation of relatively pure single concentration along the rotational axis (Figure 2-5). They attributed the observed segregation to both radial segregation and to the rotational speed of the drum.

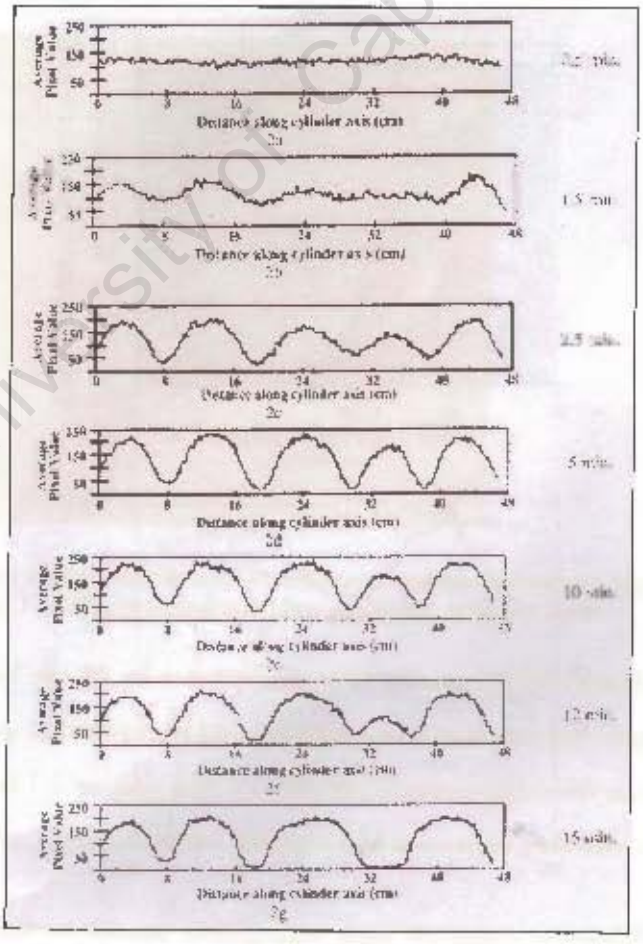

Figure 2-5: Digital image analysis results for binary glass beads mixture, (after Hill *et al.* 1997)

The work of Henein *et al.* revealed that percolation of fines through the voids was responsible for segregation rather than the flow of fines over a particle bed. However, this observation seems to be only valid for dry horizontal rotary cylinder operations. For instance, Hogg (1984) showed that the flow of fines in the carrier fluid was one of the two major transport mechanisms in wet ball mills. In SAG mills, segregation factors are more complicated than those for the dry horizontal drum mixers, in fact, both percolation and the flow mechanism and even other factors like material properties are likely to influence particle segregation along SAG mills.

2.1.2.4 Regained segregation of binary mixtures of granular materials by Hill and Kakalios

Hill and Kakalios (1994) observed segregation in a 12.7 cm diameter by 60 cm long Plexiglas horizontal cylinder rotated by a 1/17 hp motor and fed (50 % material filling) with a binary mixture of 2.85 mm large glass beads and 0.5 – 0.75 mm small glass beads. By varying the rotational speed of the cylinder, axial segregation was observed at higher speeds and once the speed had been reduced, the segregation of particles disappeared but could be restored on increasing the speed again (Figure 2-4).

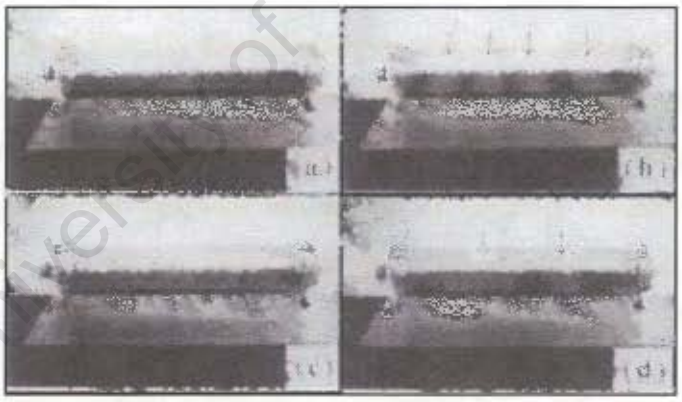

Figure 2-4: Photographs showing homogeneity (a) and (c), and banding segregation (b) and (d) for a binary mixture, (after Hill and Kakalios, 1994)

Figure 2-4 (a) shows a 50 – 50 % mixture of different size sand and beads well mixed, and after a rotation for 13 minutes at the speed of 14 rpm, axial segregation of small and large beads into alternating bands was observed Figure 2-4 (b). When the motor speed was decreased to 5 rpm for one hour, the bands disappeared and a homogenous mixture was restored Figure 2-4 (c), but upon increasing the speed back to 14 rpm for 13 minutes, the bands were reformed even though they were at slightly different locations and with different widths as shown in Figure 2-4 (d).

Hill and Kakalios ascribed the observed regained segregation to the difference of the dynamic angle of repose between the mixed and the segregated phases being zero at very high rotational speeds. They

could not in general be classified into one of the three groups observed by Donald and Roseman. Finally, the granular components that had similar properties still revealed segregation when the particles were blended and did not yield a random mixture.

The findings from the work of Rogers and Clements highlighted the importance of not underestimating the presence of segregation in horizontal rotary devices and also demonstrated that the patterns of the observed segregation are of several variations rather than just the three forms showed by Donald and Roseman.

2.1.2.3 An experimental study of segregation in rotary kilns by Henein et al.

Henein, Brimacombe and Watkinson (1985) performed experiments in two cement rotary kilns, one 40 cm by 40 cm long and the other 40 cm diameter by 86 cm long, with the aim of elucidating the mechanism of radial segregation in a kiln bed. Two sand mixtures and one limestone mixture containing fines were used as experimental materials for the study. They noticed that the fines could not segregate according to the differential flow of particles down the surface of a bed and that the static angle of repose was not influenced by the amount of fines present in the bed and so the flow characteristics of slumping beds were not significantly affected by the presence of fine particles. The flow mechanism therefore, did not contribute to the segregation of the mixtures when slumping. The observed segregation was rather ascribable to percolation of fine particles through the voids. The experimental procedure involved measuring the slumping and rolling characteristics of the bed of particles in the kiln. Slumping and rolling behavior of the bed were used to describe the flow mechanism of the particles.

Henein *et al.* observed that radial segregation occurred in both slumping and rolling beds, but assumed that all fines segregated into a core. However, some fines were also observed on the cylinder walls and this observation suggested that a second zone of fines concentration existed. The second layer of fines seen on cylinder walls were thought to be so small that when set in motion they could percolate through the coarser sizes even when the later were stationary, and would come to rest at the cylinder walls where they accumulated and formed the second segregation zone.

Henein described the percolation mechanism similar to the definition of mixing given by Donald and Roseman in section 2.1.2.1. They claimed that small particles passing over other particles and over void spaces are likely to fall into the central core of the bed and when the fines are sufficiently small, the particles might fall past the central core and trickle through the voids until they reach the cylinder wall to form a segregation zone of very fine particles.

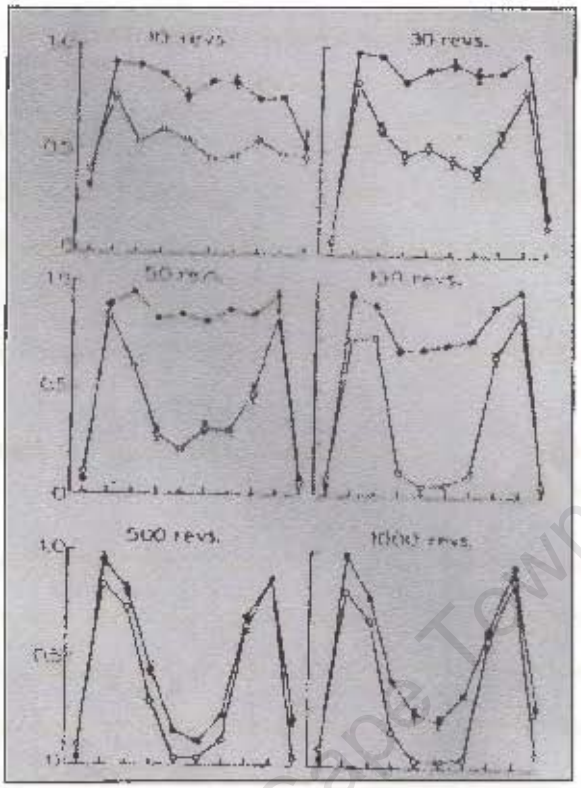

Figure 2-2: Graph of proportion of component 1 in the sample against axial position along the mixer at times of 10, 30, 50,100,500 and 1000 revolutions, (after Rogers and Clements, 1971). Y - axis : fraction of component 1 in sample and X – axis: axial position in the mixer.

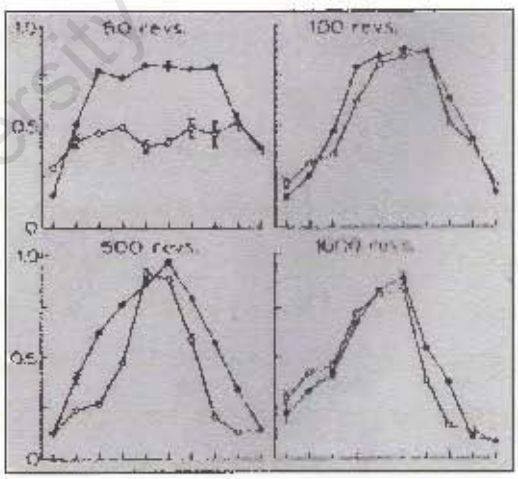

Figure 2-3: Graph of proportion of component 1 in the sample against axial position along the mixer at times of 50,100,500 and 1000 revolutions, (after Rogers and Clements, 1971). Y - axis : fraction of component 1 in sample and X – axis: axial position in the mixer.

Rogers and Clements demonstrated that segregation could exist in a mixture that appeared to be homogeneous when the surfaces were inspected visually and they attributed the observed segregation to the little differences in the physical properties (size and density) of the components fed to the mixer and to the speed of rotation of the horizontal cylindrical mixer. They observed that band formation in a mixture was not always detectable by visual inspection. Also the patterns of segregation noticed

of segregation to SAG mills as the particle size distribution and operational factors assume a more dominant role and the angle of repose is for the whole charge rather than independent angles of repose for smaller and larger particles. The important outcomes from Donald and Roseman's work were the thorough description of mixing and segregation from their definition. Also the three forms of the observed segregation were clearly explained for the first time, which many researchers have used as the benchmark for further segregation studies. The influence of the closed ends of the drum mixer on the observed segregation was identified as the cause for the patterns found.

2.1.2.2 *Examination of segregation of granular materials in a tumbling mixer by Rogers and Clements*

Rogers and Clements (1971) followed up Donald and Roseman's work by using a special sampling scheme to detect segregation of granular solids in a horizontal rotating cylinder. They adopted the same definition of mixing and segregation given by Donald and Roseman for particle movement from the original path of circulation into a void space. However, they claimed that even small differences in the physical characteristics of particles could cause a bias in movement of particles and therefore result in a small amount of segregation.

Two horizontal cylindrical mixers made from Perspex, one 4.6 in. by 6.5 in. and the other 3.5 in. by 5 in. diameter by length, each rotated by a ¼ horse power motor, were used for the tests. The two mixers were each operated in variable speed mode in the speed range 5 – 60 rpm and the mixers were fed with different size ballotini beads, citric acid monohydrate crystals and sucrose crystals. A special sampling thief could collect between 40 and 100 particles. Rogers and Clements performed a series of experiments to investigate the combined effects of mixer speed and composition of the mixture upon the pattern of segregation and they observed both band formation and core formation. Some results obtained are given in Figure 2-2 and Figure 2-3. From the results, it was found that irrespective of the composition of the mixture, the mixer speed influenced the outcome of the pattern of segregation. For low mixer speeds, both core formation and band formation occurred at an early stage and were intensely enriched with the smaller size particles. However, increasing the mixer speeds to about 40 rpm led to a single central band being formed that was less intense and collapsed with further increase in speed to about 60 rpm.

In Figure 2-2 and Figure 2-3 the ends of the mixer had smaller amounts of filling than the middle section of the mill that had banding segregation.

2. End-longitudinal mix where the smaller (or heavier) particles are in two end bands connected by a diminished core.
3. Longitudinal mix where the smaller (or heavier) particles form alternate bands with the larger (or lighter) particles along the length of the mixer.

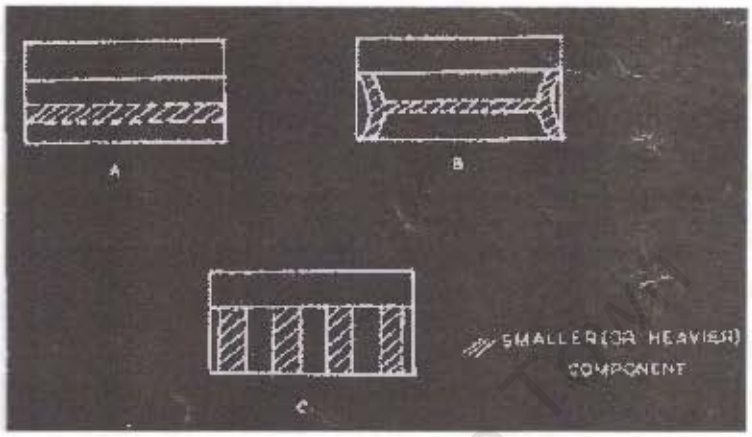

Figure 2-1: Final forms of de-mixing or segregation, (after Donald and Roseman, 1962)

The core formation (type a) of smaller particles was attributable to radial segregation and the stability of this core was dependent on whether "useless" radial movement or axial movement was predominant at the ends of the mixer.

The type b, observed segregation resulted from subjecting the core (type a) to a considerable increase in end friction through high drum speeds and the core at the ends of the mixer became unstable. At the two closed ends, steeper velocity gradients were thought to encourage axial movement and reduced radial motion resulting in a dominant side ways movement that produced two end bands of smaller particles while in the middle, the core remained intact as the velocity gradient over the middle section was unchanged.

The banding (type c) segregation is believed to have resulted from the smaller particles having a higher angle of repose than larger particles which induced the smaller particles with a high velocity down the charge surface. Because of the high velocity, the radial dropping of particles into void spaces was inhibited and axial segregation dominated over the mixer length by forming alternate bands of the binary component in the drum mixer.

The three forms of segregation observed by Donald and Roseman shown in Figure 2-1, have been used by many investigators as the yardstick for segregation along rotary cylindrical devices. However, standardizing the three patterns of observed segregation could prove futile when extending the study

horizontal rotary drum. Besides, other mechanisms of mixing caused by machine and operational parameters such as particle filling, Shoji *et al.* (1973) and mill speed, Cleary (1998) have been found to be additional factors that affect mixing and segregation of particles in horizontal rotary devices.

The definition of mixing and segregation by Donald and Roseman has been hailed by many investigators as an adequate explanation of the mechanism in tumbling devices. Donald and Roseman defined mixing and segregation as follows;

"When a mixer rotates, particles are carried around the mixer until the maximum angle of repose is exceeded at which point the particles will roll down the slope over the rest of the particles. On reaching the end of the surface, the particles are again carried round with the mixer walls to complete a full circuit. Therefore, every particle can be described to have its own "path of circulation." A particle moving in its path of circulation will pass over other particles and over void spaces. Mixing occurs when a particle leaves its path of circulation and drops completely into a void space. However, if a particle leaves its original path of circulation and joins another path or if it drops partially into a void space and is trapped between lower particles, it will remain in its state until this particle collides with another particle resulting in two possibilities. After the collision, the particle will either drop into the void space completely and mix with the rest or it will be freed outward and segregate from the rest. When a particle changes its path and drops into a void space, another particle/s within the charge would change the path of circulation due to the difference in the velocity gradient of the layers and thus mixing is continued."

From the mixing and segregation definition, Donald and Roseman reasoned that gravity is influential for radial mixing mechanism and they attributed axial mixing and segregation to particles changing in the radial plane to move to a corresponding path in an adjacent plane. They termed mixing involving identical particle sizes and density as "useless mixing."

Donald and Roseman also claimed that the axial movement of the smaller particles at any point is facilitated by movement of the larger particles in an opposite direction due to angle flow. This claim however, cannot be consistent in industrial SAG mills as the transport of fines is solely dependent on the amount of voidage between larger particles and on the carrier fluid motion, Hogg (1984) and not necessarily fines movement being aided by opposite transport of the larger particles.

The important findings from Donald and Roseman's work were the observed segregation by size and/or density which they called "final forms of the equilibrium mix." The final mix obtained after long rotation of the mixer could adopt one of the three forms (Figure 2-1).

1. Diametrical mix where the smaller (or heavier) particles form a horizontal core.

Where C = the concentration of the tracer at position x and at time t. x is the distance from the end of the mixer and D is the diffusion or mixing coefficient.

The studies conducted by Shoji et al were inspired by earlier work of Chaudhuri and Fuerstenau (1971), who studied the effect of balls, used as mixing aids, on the rate of axial segregation and found that the addition of balls increased the rate of mixing.

The experiments conducted by Shoji et al involved studying the effect of filling of particles on the diffusion coefficient and the effect of the fractional ball filling on the rate of mixing.

From the experiments, the diffusion coefficient D increased with the fractional ball filling J at various material fillings f_c as shown in Figure 2-8. However, D decreased with increase in the 'true' material filling f_c, attributed to dense packing of particles as the filling increased. This means that ball addition promoted diffusion of particles through more void spaces that arose from the higher ball load. Therefore, a higher ratio of steel balls/true filling would result in a higher Diffusivity D, and consequently increase the rate of diffusion of particles.

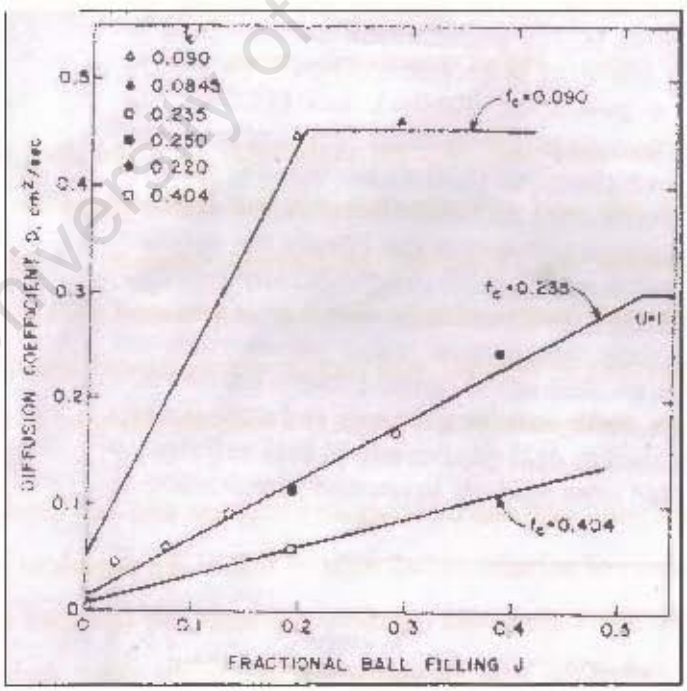

Figure 2-8: The experimental effect of ball filling J on the diffusion coefficient D in a batch ball mill at various material fillings f_c, (after Shoji, Hogg and Austin, 1973)

Shoji, Hogg and Austin also showed that at low material fillings, the segregation potential was high while the balls exhibited uniform mixing and distribution along the length of the mill. Even though these findings were obtained from batch ball mills, the results might be applicable to SAG mill

operations as low material fillings would promote particles to scatter over the length of the mill and therefore promote axial segregation.

The work of Shoji *et al.* was followed by extensive studies in wet overflow ball mills by Richard Hogg and Rogovin at the Pennsylvania State University.

2.2.2 Mass transport in tumbling ball mills by Hogg and Rogovin

The work of Hogg and Rogovin (1982) distinctly tackled the mechanism that causes transport and segregation of particles along wet ball mills. Even though their investigations were restricted to ball mills, which are very different in operation from that of SAG mills, some of their findings could be useful to extending the understanding of segregation in SAG mills and to provide solutions to the problem of the current study.

Hogg and Rogovin stated that the progress of transport and segregation research has fallen behind due to the misconception of describing the transport process through residence time distribution (RTD), and argued that the RTD in a mill is dependent on the particle size. Their argument can be supported as it can be backed by previous study results, for instance Rogers (1979) showed that the residence time for solids is higher than that for water.

An experimental laboratory mill 30.5 cm in diameter by 61 cm long and rotated at 54 rpm (70 % of the critical speed), was used to study transport and axial segregation of particles along the ball mill. The mill feed trunnion was 2.5 cm and the discharge trunnion 7.6 cm in diameter. The samples were collected along the mill using a sampler that was constructed such that it could be fitted through the mill and collect particles in 10 equal axial slices covering the mill length. The mill was fed with 0.95 cm diameter steel balls, solid particles and water at a constant filling of 34 %.

A transport model was proposed by Hogg and Rogovin and they made several assumptions about the transport mechanism of particles in ball mills to reduce the complexity of the problem. The motion of the charge and the slurry along wet overflow ball mills was classified into two regions; the ball charge region, containing all of the grinding media and part of the slurry, and the liquid "pool" containing the remainder of the slurry. The two transport regions are represented schematically in Figure 2-9.

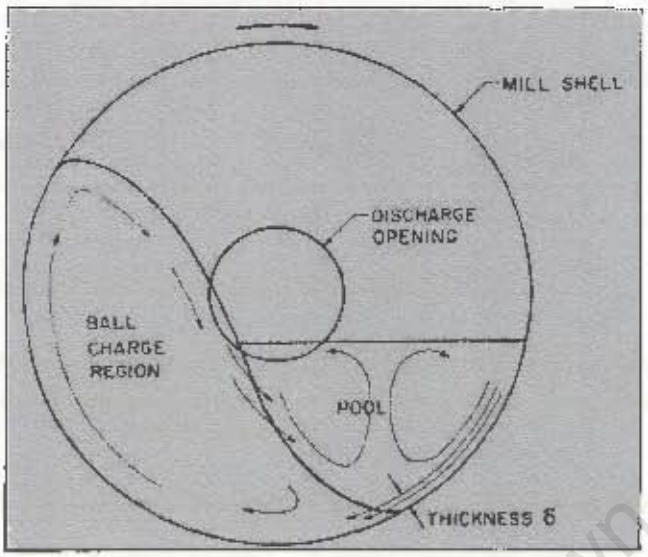

Figure 2-9: Schematic of the transverse motion of slurry in a wet, overflow ball mill. δ is effective thickness of slurry layer carried along the rotating mill shell (after Hogg and Rogovin, 1982)

The basic assumptions made in the transport model are as follows:

- The filling level of grinding media and slurry are uniform along the mill.
- The voids in the tumbling ball charge are completely filled with slurry at all times
- The net axial transport of both solids and liquid occurs only in the pool
- The axial velocities of solids and liquid in the pool are equal
- Solids and liquid are fully mixed in the ball charge region
- Settling of solid particles in the pool leads to preferential transport of solids into the ball charge region
- Material is discharged from the mill by overflowing from the pool.

Hogg and Rogovin's assumption that the net material transport only occurs in the pool is an over simplification because material transport might exist even in the charge region through the interstices. It is believed though, that solids transport principally takes place in the pool.

The physical basis for the model was that the pool acts as a slow flowing "river" of slurry carrying solids and liquid along the mill from the feed to the discharge end. The rotation of the mill causes a layer of slurry, adjacent to the mill shell, to be transported into the ball charge region and at steady state; a balance is maintained by gravity flow of slurry out of the upper part of the ball charge region, and back into the pool. The system is further complicated by the possibility that settling of solids in the pool, particularly the larger particles will cause them to be transported preferentially into the ball charge region. The trajectory of a particle in the axial direction is shown schematically in Figure 2-10

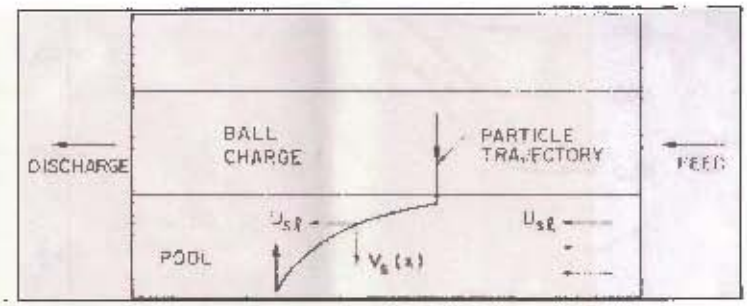

Figure 2-10: Schematic representation of the axial motion of a particle in a wet overflow ball mill. U_{sl} is the mean axial velocity of the slurry in the pool, $V_s(x)$ is the settling velocity of a particle of size x, (after Hogg and Rogovin, 1982)

A number of equations were derived from Figure 2-9 and Figure 2-10 to describe the solids hold-up, axial velocity of solids, and the mean residence time of solid particles.

The net axial velocity $U_s(x)$ of size x was represented by equation (2.8)

$$U_s(x) = \frac{U_o}{[1 + K_B \frac{V_s(x)}{V}]} \tag{2.8}$$

Where

U_o = the velocity of an infinitesimally small (i.e. non-settling) particle

$V_s(x)$ = the settling velocity of particle of size x in the pool

K_B = the fraction of the slurry which is contained in the interstices of the ball charge

V = the characteristic velocity which describes the convective transport of slurry into the ball charge as a result of the rotation of the mill. V is expressed by equation (2.9)

$$V = \frac{\omega\delta}{k} \tag{2.9}$$

Where;

ω = the angular velocity of the mill

δ = the effective thickness of the layer of fluid, carried along with the mill shell

k = the geometrical factor (a constant, typically k≈1)

It was evident from equation (2.8) that given the dependency of the settling velocity V_s on particle size, the axial velocity U_s will also be size dependent. Therefore, equation (2.8) predicted internal classification in the mill due to particle size dependent mass transport. To determine the distribution of axial velocities in the mill, the settling velocities of different sized particles in the pool were estimated (Figure 2-11) on a size by size basis, using equations suggested by Concha and Almendra, (1979).

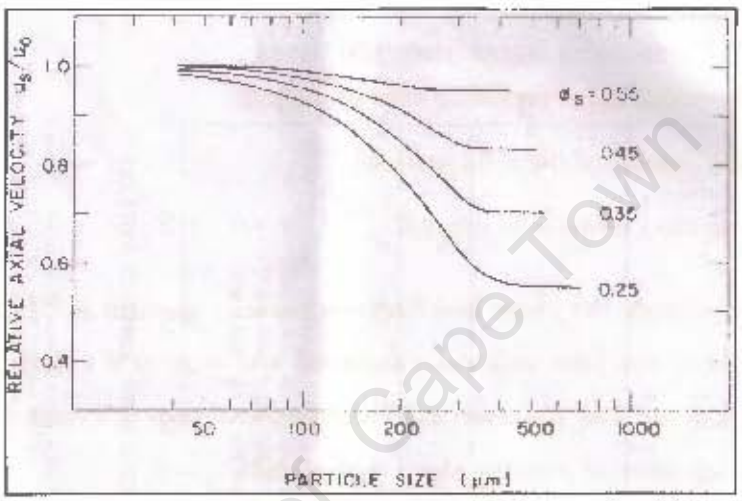

Figure 2-11: Predicted effect of particle size and slurry density (volume fraction of solids) on the axial velocity of particles in a mill. The specific result shown here is for quartz particles in a 30.5 cm diameter mill, (after Hogg and Rogovin, 1982)

From Figure 2-11, size dependence transport especially at low solids concentration was predicted and suggested internal mill classification to be the cause for the observation.

The mill contents were characterized in terms of a single mean hold-up and average particle size distribution approximation represented by equation (2.10)

$$\phi_{sm} = \phi_s[1 + K_B \frac{\bar{V}_s}{V}] \qquad \textbf{(2.10)}$$

Where;

ϕ_{sm} = the fractional solids contents of the slurry in the mill

ϕ_s = the volume fraction of solids in the feed to the mill

$\bar{V}_s$ = the mean volumetric build-up of solids

From equation (2.10), it was observed that the slurry density was generally higher in the mill contents than in the mill feed.

The solids mean residence time in the mill was derived and represented by equation (2.11)

$$\tau_s = \frac{\rho_s \phi_s V_{sc}}{F_s}[1 + K_B \frac{\bar{V}_s}{V}] \qquad (2.11)$$

Where;

τ_s = the solids mean residence time in the mill

ρ_s = the density of the solid particles

F_s = the mass feedrate to the mill.

A comparison between the Hogg and Rogovin model (equation (2.10) and experimental results from the laboratory mill and pilot mill was conducted and there was a very good agreement between the two sets of outcomes. The observed axial segregation shown in Figure 3-3 (chapter 3), was attributed to internal classification of particles along the ball mill.

Hogg and Rogovin have proposed that the axial transport and internal mill classification (axial segregation) could be promoted or suppressed through *"specific liner/lifter design."*, even though their proposal could be true, unfortunately this area of research is still virgin and more work is needed to verify just how the liners/lifters affect segregation. It is believed that segregating liners are in use in dry milling in the cement industry.

The major difference between the mechanism of transport and segregation in ball mill and the SAG mill is the amount of slurry present. Because slurry pools in SAG mills are undesirable, and SAG mills are usually operated with low slurry levels, the solids transport via entrainment within the slurry is minimized compared to that in ball mills. Therefore as good as the Hogg – Rogovin proposed model might be, it still cannot be applied to SAG mill operations.

2.2.3 A sampling procedure validated by Vermeulen and Howat

The influence of shape of particles on segregation was unexpectedly identified through the work of Vermeulen and Howat, (1989) who emptied out and sized all the steel balls at Libanon Gold mine, South Africa. The objective of the work was to prove that a sample is as nearly representative as possible of the whole mass of material from which it is collected.

The steel balls were emptied out from a ball mill 2.75 m diameter and 3.05 m long, which was allowed to grind out all the rock particles until only the steel balls remained in the mill. A comparison was made between the size distribution of the balls obtained from a sample through a sampling device attached to the mill and the size distribution of the entire ball charge emptied out from the mill. The comparison revealed a general correlation of the size distribution between the sampled steel balls and that of the total emptied out steel balls. However, for small irregular shaped steel balls (scats) shown in Figure 2-12, there was a difference in the results of the scats size distribution with those for the total charge. The difference between the results of the scats in the sample and those in the charge was ascribed to the segregation by shape of such components within the body of the charge in the mill.

Figure 2-12: Characteristic irregular shape balls (Scats) that did not match the size distribution of the whole ball charge in the work of Vermeulen and Howat, (1989)

Vermeulen and Howat's results, where the size distribution of the sampled balls generally correlated the size distribution of the entire ball charge emptied from the mill, are expected.

Firstly, the comparison was only restricted to steel balls. Mwansa and Powell (2006) have observed that steel balls do not segregate along the mill in similar work conducted by emptying out the entire mill charge of balls and rocks. Therefore collecting a sample of balls along any position along the mill should give a good representation of the entire ball charge that is perfectly mixed by size. However, including the rocks in the sampling might require dividing the mill into a number of sampling slices, as the rocks have been found to segregate by size along the length of the mill (Hogg, 1984 and Mwansa and Powell, 2004). Thus, drawing just one sample from the mill may not be sufficient to represent the size distribution of the entire rock and steel ball charge.

Secondly, even though the claim that the scats' difference in the size distribution was a result of the segregation by shape was found true, Vermeulen and Howat did not explore the pattern of segregation

exhibited by the scats along the mill. Their claim for the difference in the scats size distribution was simply based on intuitive expectation.

In summary, the scats segregation observed by Vermeulen and Howat is expected but not important as far segregation of rocks along SAG mills is concerned, because the scats are not desirable in mills and should be removed through magnets fitted after the trommel of a mill.

2.2.4 A study of charge motion in rotary mills by Powell and Nurick

A detailed description of balls motion and the radial segregation of balls due to size and mass within the charge of a rotary mill were clearly explained by Powell and Nurick (1996).

Powell and Nurick used a bi-planar angioscope that utilizes high energy X-rays emitted in short pulses to stimulate a scintillating screen, similar to a television screen, and gamma ray filming to plot the variation of the average radial distributions of different ball types in order to illustrate the radial segregation of balls within the charge.

They used a 97 mm long by 190 mm diameter Perspex mill, transparent to X-rays for the studies. Perspex lifter bars of heights from 1.8 mm to 10 mm, and face angles from 45° to 90° (rectangular) were fastened in the mill with plastic bolts. The charge comprised steel balls of 6 mm and 3 mm diameters, and a 3.7 mm diameter glass bead. The mill was operated at 45 % filling and at five different speeds, from 68 to 100 % of the critical speed.

The outcomes from Powell and Nurick's work indicated that larger balls segregate to the periphery of the mill at low speeds, and to the centre at high speeds. At a certain speed they referred to as 'neutral' speed, located at 77 % critical speed, no segregation of balls by size was observed. The radial segregation by mass revealed that the heavy balls resided near the centre at most speeds, and near the periphery of the charge at high speeds, with a 'neutral' speed located at 92 % of the critical. For the speed range of about 80 to 90 % of the critical, small, heavy balls strongly segregated to the periphery of the mill. Powell and Nurick suggest that the behavior of the small heavy balls is directly applicable to steel balls in SAG mills.

Powell and Nurick have explained the radial segregation phenomenon to primarily arise from energy considerations, with the mill charge attempting to assume the lowest available energy state. To achieve the lowest energy state of the charge as a whole, the heaviest balls must segregate to the centre of the mill, where the work done in lifting them per revolution is at a minimum. At a given outer radius, the

centre of mass of the large balls is closer to the centre of the mill than the small balls. Therefore, it is energetically favorable for the larger balls to be located near the periphery of the mill. The counter-segregation at high speeds was asserted to arise from the centrifuging effect of the mill. As the mill begins to act as a centrifuge, the heavier balls move to the outside. The centrifugal force becomes stronger for small particles, as they have a larger displacement at a given radius, so those small particles move to the outside at high speeds.

The extensive work of Powell and Nurick has been supported by recent DEM work whose outcomes also back the speed influence on radial segregation observed by Powell and Nurick using the bi-planar angioscope X-ray detection and gamma ray filming techniques.

2.2.5 Predicting charge motion and speed influence on particle segregation using DEM by Paul Cleary

Paul Cleary (1998) using discrete element modeling (DEM) has supported the work of Powell and Nurick and clarified the position of large particles and that of small particles in the radial core after radial segregation of particles has been attained. He demonstrated that the mill speed determines whether the large particles forms a central core surrounded by small particles or the opposite particle positioning is attained, by varying the mill speed.

The detailed description of DEM is not included in this section; rather the focus is on the DEM outputs relating to segregation of particles in a tumbling mill.

A ball mill 5 m in diameter and 7 m long with 23 symmetrically placed lifter bars, and at a filling of 50 %, was used to simulate the particles (steel balls and rocks) tumbling behavior. The mill was simulated for a charge composition of steel balls uniformly distributed between 50 mm and 200 mm, and rocks uniformly distributed between 5 mm and 50 mm that were ten times more than the steel balls in the charge.

The pattern of segregation of particles is illustrated in Figure 2-13. At N = 50 % critical speed in Figure 2-13 (a), the particles appear to be randomly distributed, but closer inspection reveals that the largest particles are concentrated in the outer regions of the charge. For N = 70% critical speed in Figure 2-13 (b), the particles were observed to be randomly mixed. Increasing the speed to N = 90 % critical speed shown in Figure 2-13 (c), leads to concentrating the large particles in the center of the charge and a slight occupancy of small particles towards the outside. At N = 110 % critical speed in

Figure 2-13 (d), the large particles are in the central core of the charge and the small particles occupy the surrounding regions towards the mill shell.

According to Paul Cleary, two basic mechanisms produce radial size segregation in mills. At low speeds, segregation is produced by percolation of fines through the avalanching layers and causes the large particles to migrate to the outside of the charge. At high speeds, the second segregation mechanism causes the large particles to move against the acceleration field and the smaller particles move in the same direction as the acceleration field, because in mills at a higher speed, the centrifugal force is comparable to gravity and is directed radially outwards from the center of the mill. This centrifugal force causes large particles to move into the center of the charge and the fines to the outside as shown in Figure 2-13 (d). The radial segregation due to centrifugal forces has also been reported and explained in detail by Powell and Nurick (1996). For the intermediate rotational speeds like 77 % critical, these two mechanisms cancel each other out and leave a randomly mixed charge, (Figure 2-13 b).

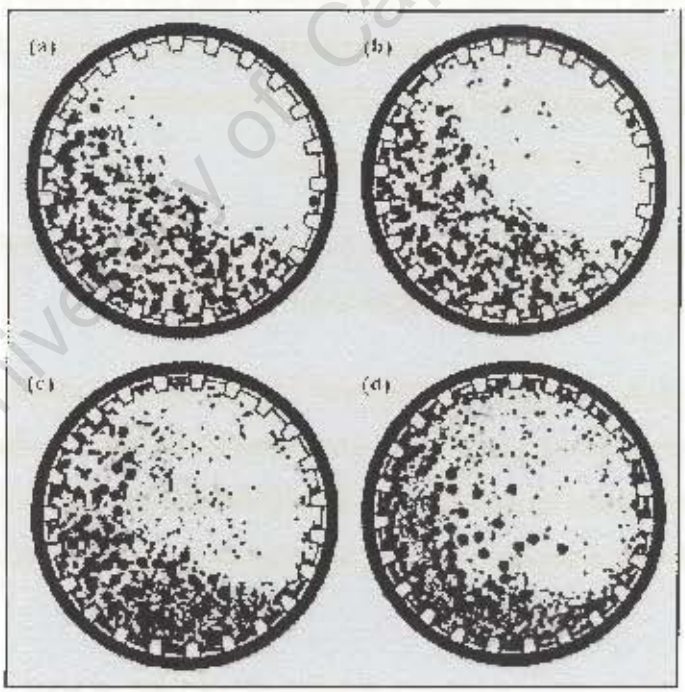

Figure 2-13: Segregation of particles at t = 60 sec for % critical speed of: (a) N = 50 %, (b) N = 70 %, (c) N = 90 % and (d) N = 110 %, (after Cleary, 1998)

For typical milling operations, Cleary proposed that a perfectly mixed charge would be attained at about 77 % of the critical speed. Segregation, with the fines in the core of the charge and large particles outside was predicted at less than 50 % of the critical speed, while that with large particles in the center and fines outside was predicted at 90 % or more of the critical speed

So far as the speed influence on the observed segregation is concerned, the theory of Paul Cleary that the large particles occupy the periphery of the charge at low speeds is supported. This phenomenon has been observed by Powell and Nurick (1996) and has also been observed during slow rotations "barring" or "inching" of the mill on several occasions during comminution sampling surveys involving the author, where the large rocks roll over the charge surface and occupy the mill shell region, while the fine particles trickle through the voids and occupy the central core of the charge.

2.2.6 Simulation of open circuit clinker grinding by Benzer et al.

Benzer *et al.* (2001) have conducted extensive modelling and simulation research work in the cement industry to reduce the energy expenditure of the tube mills employed for dry clinker grinding. They have developed a mathematical model that assumes that the first compartment of a long tube mill may be modelled as three perfectly mixed ball mills in series. This modelling technique is believed to eliminate the complication of the axial segregation that is present in long mills.

Benzer *et al.* used an 11.5 m long by 3.4 m diameter tube mill with two compartments to conduct modelling studies. The length of the first compartment was 4.5 m. The partition between the two compartments of the tube mill had 8 mm aperture with an open area of about 14 %. The mill was operated at 70 % critical speed and with a 32% volume ball load in each compartment. Steel balls 90 – 60 mm diameter where used in the first compartment whilst the second compartment had 50 – 20 mm diameter balls. Samples were collected around the circuit and inside the mill after a crash-stop as shown in Figure 2-14. From each compartment, samples were collected from 8 points with equal intervals along the mill axis. About 3 – 5 kg of sample was collected from each sampling point dug to about 25 cm deep.

The size distribution results of the material inside the mill are shown in Figure 2-15 for the first compartment, and in Figure 2-16 for the second compartment. The size distribution becomes finer along the length going from the feed to the partition (grate) of the first compartment. In the second compartment, the material showed a similar trend of becoming finer towards the mill discharge end but the size distribution at both sides of the end grate was identical (Figure 2-16).

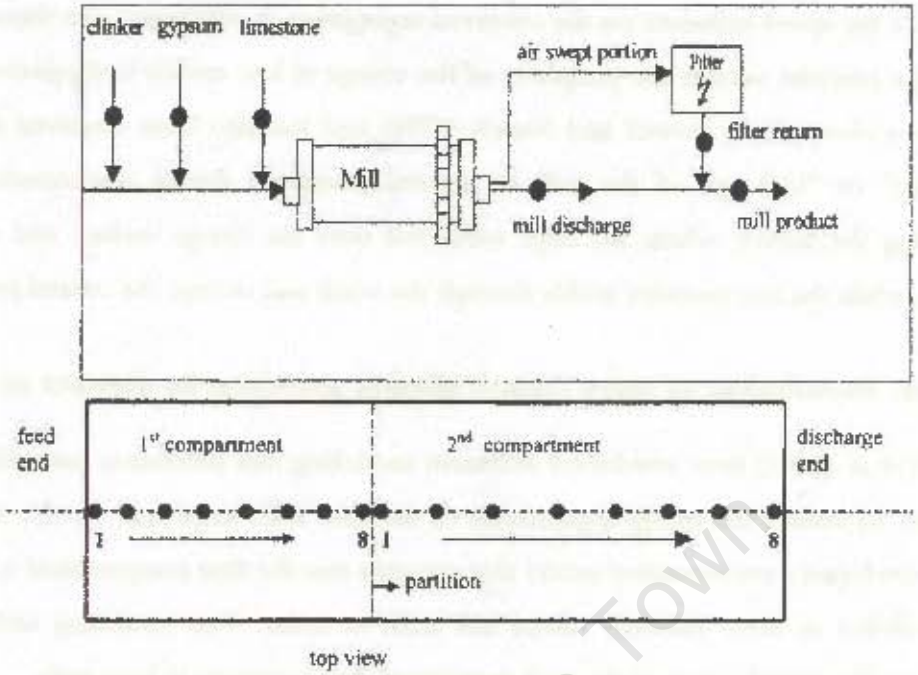

Figure 2-14: Sampling points around the circuit and inside the mill in an open circuit clinker grinding line, (after Benzer *et al.* 2001)

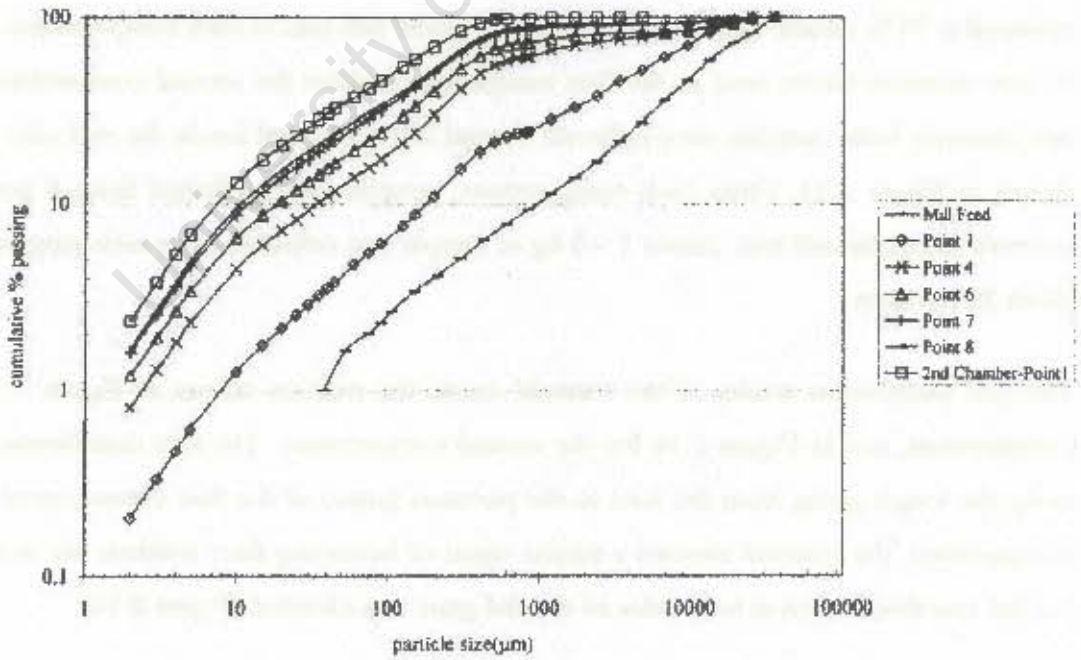

Figure 2-15: The size distributions of the mill feed, samples from inside the first chamber and the first point in the second chamber, (after Benzer *et al.* 2001)

The size distribution results revealed clear axial segregation by size in both compartments of the mill. Benzer and co-researchers observed that the grate opening between the two compartments was 8 mm

but the largest size at the first point of the second compartment was 0.8 mm and it was ascertained that the grate effectively operated as a fine screen.

Benzer *et al.* detected that the coarse particles were broken very rapidly in the first 1.69 m length of the first compartment of the mill. The second 2.25 m length was observed to operate as a conventional mill whilst the particles in the third 0.56 m were deemed to operate in closed circuit with the grate. As a result of the above findings, Benzer *et al.* concluded that the first compartment of the mill can be modelled as three perfectly mixed ball mills in series, whilst the second compartment was considered as a single perfectly mixed ball mill.

Benzer *et al.* felt that the second mill compartment did not show a significant segregation trend to warrant a multi-segment mill model, and From Figure 2-15 and Figure 2-16 it is deduced that axial segregation existed in both compartments but was more pronounce in the first compartment. Benzer *et al.* decided on three perfectly mixed ball mills in series to describe the model of the first compartment of tube mill based on the mechanical interaction of the ore particles.

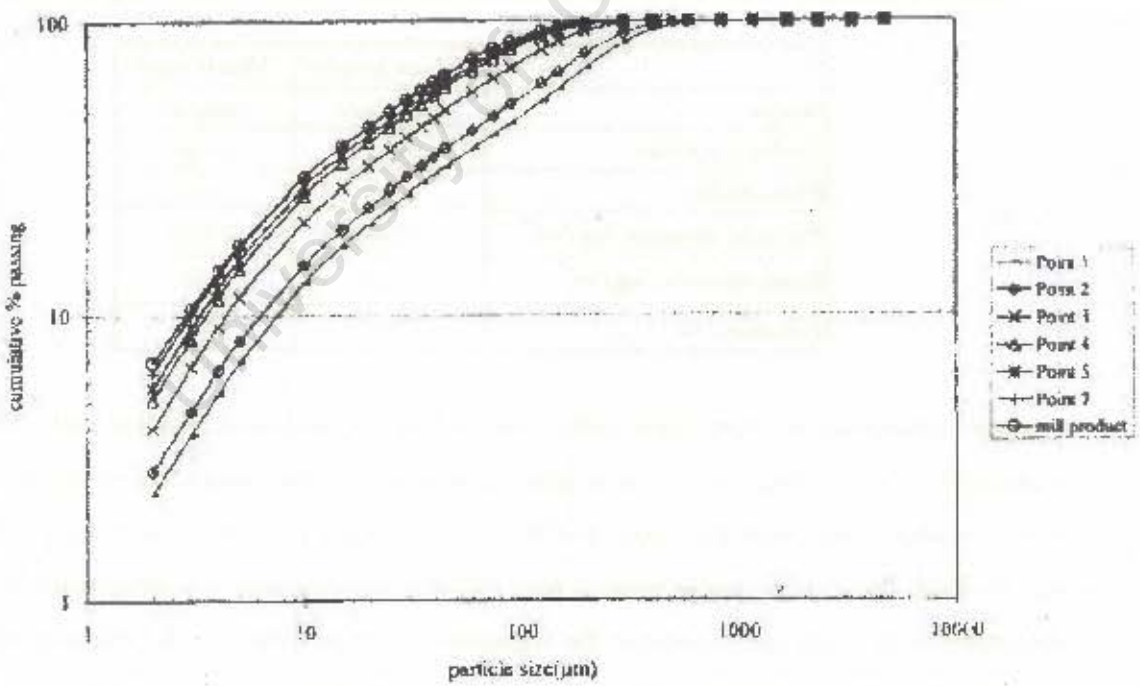

Figure 2-16: Mill samples and mill product size distribution, (after Benzer *et al.* 2001)

It is not reported in literature what criterion should be used to decide the number of perfectly mixed mills (tanks) in series required to model segregated mills. The choice of how many segments (perfectly mixed mills in series) in a long mill might seem to vary from mill to mill and would most probably be influenced by how segregated the particles are along the length of the mill.

The work of Benzer *et al.* reaffirmed the occurrence of axial segregation by size in long mills. Their approach of modelling segregated mills as multi-perfectly mixed mills in series might be a very successful technique of incorporating axial segregation in description of long mills.

2.2.7 Effect of particle characteristics on segregation by Tang and Puri

Tang and Puri (2004) have conducted interesting work recently where they have used a redesigned equipment called the; second generation primary segregation shear cell (PSSC – II) to simulate and quantify particle segregation based on percolation and sieving. Even though this research work is in the agricultural and biological engineering field, the segregation behavior especially that based on particle size ratio has motivated the inclusion of this paper in the literature review for the current study.

A binary mixture of glass beads and poultry mash having distinct physical properties were used for the segregation study. A summary of the key properties for the two materials used are shown in Table 2-1.

Table 2-1: Summary of key physical properties of two study material, (after Tang and Puri, 2004)

	Glass beads	Mash feed
Shape	spherical	irregular
Surface texture	smooth	rough
Flowability	high	low
Particle density, kg/m^3	2,760	1,970
Bulk density, kg/m^3	1,420	520
Porosity, %	50	70

Four binary combinations from glass beads (denoted as G) and from poultry mash (denoted as F) were obtained. The combination of coarse glass beads and fine glass beads was designated as GG, that of coarse poultry mash with fine glass beads was designated FG, the coarse glass beads with fine poultry feed GF and that of coarse poultry feed with fine poultry feed was designated as FF. The four combinations were expected to provide the segregation response such as the relationship of size ratio and absolute size with materials. Also, the segregation difference between the ideal combinations (GG) and real materials (FF) were to be studied, as well as intermediate mixtures FG and GF. The segregation due to density and shape was determined through various comparisons of the four binary combinations as shown in Table 2-2. Tang and Puri assumed that the shape effect of fine particles on segregation was negligible compared to the density effect, and that the density effect of coarse particles was negligible. The assumption for the shape effect of fines having a negligible influence on

segregation compared to fines density effect is supported; however there are reservations on assuming that the density of large particles should be neglected.

Table 2-2: Identification of particle shape and density effect on segregation through comparison of four different binary mixtures - GG, FG, GF, and FF, (after Tang and Puri, 2004)

	GF	FG	FF
GG	Density	Shape	Shape and density
GF		Shape and density	Shape
FG			Density

As shown in Table 2-2, the coarse particle shape effects could be measured through the comparison of GG vs. FG combination and confirmed by FF vs. GF combinations. For instance, the fine particle components are glass beads for both GG and GF but the coarse particles differ in shape, i.e., spherical shaped glass beads and irregular shaped poultry feed. Similarly, the fines density effect was quantified through the GG vs. GF comparisons and verified through the FF vs. GF combinations. In this case, both the GG and GF had glass beads as coarse particles, and the fines differed. Therefore the density effect could be examined since shape was assumed negligible for this combination. The comparison of GG vs. FF and FG vs. GF was used to determine the cumulative effect of particle density and shape on segregation since both the coarse particles and fines are involved. If the segregation potential of GG was higher than that of FF, it was concluded that the density effect was more significant than the particle shape.

Three size ratios 4:1, 6:1, and 8:1 were selected for the PSSC – II test. Tang and Puri claimed that segregation for binary mixtures becomes significant when the size ratio is larger than 3:1, and that increasing the size ratio further results in an even more significant segregation. Three absolute coarse sizes; 1700 – 1400 µm, 1180 – 1000 µm, and 850 – 710 µm were selected for the study. Tang and Puri also claim that the coarse particle size is a key measure for establishing the size range of continuous distribution of mixtures, therefore the coarse particle size would feature prominently in quantifying the segregation potential. The coarse particle size was termed as the absolute particle size in the description of segregation rate.

The PSSC – II was poorly described by Tang and Puri, but it appears that it operated like a screen. Its major component, the shear box, where the study material was fed by gravity through an improvised funnel provided the shear motion for simulation of the percolation and sieving segregation. Four sampling points were aligned along the center line of the shear box. The amount and distribution of the segregated fine particles were measured through a computer data acquisition system. The

segregation (Table 2-3) in the binary mixture was described by a parameter called the "Normalized segregation rate (NSR)". NSR was defined as the ratio of collected fines mass to the feed fines mass divided by the total feed time.

Table 2-3: Normalized segregation rates (NSR) for four binary combinations (GG, FF, FG, and GF) of glass beads and mash poultry feed, (after Tang and Puri, 2004)

Absolute size (μm)	Size ratio	GG		FF		FG		GF	
		Mean	SE	Mean	SE	Mean	SE	Mean	SE
710	-	0.93	0.04	-	-	0.9	0.1	-	-
1,000	-	1.30	0.05	0.81	0.03	2.1	0.1	0.9	1.0
1,400	-	2.83	0.05	1.34	0.03	3.0	0.1	0.3	1.0
	4:1	0.51	0.05	1.05	0.03	0.8	0.1	0.5	1.1
	6:1	1.54	0.05	1.20	0.03	1.8	0.1	0.7	1.1
	8:1	3.01	0.05	0.98	0.03	3.4	0.1	0.5	1.1
710	4:1	0.31	0.08	-	-	0.5	0.1	-	-
710	6:1	0.74	0.08	-	-	1.0	0.2	-	-
710	8:1	1.74	0.07	-	-	1.0	0.2	-	-
1,000	4:1	0.44	0.08	0.87	0.04	0.7	0.2	1.1	1.1
1,000	6:1	0.97	0.08	0.89	0.04	1.4	0.2	1.1	1.1
1,000	8:1	2.48	0.09	0.67	0.04	4.1	0.2	0.7	1.1
1,400	4:1	0.76	0.08	1.24	0.04	1.0	0.2	0.2	1.1
1,400	6:1	2.91	0.08	1.50	0.04	3.0	0.3	0.5	1.1
1,400	8:1	4.81	0.08	1.28	0.04	5.1	0.2	0.4	1.1

Note : units for the Mean and SE are (g/g/ms)

From the results in Table 2-3, the NSR increased with increase in size ratio and increase in absolute size for the GG and FG combinations. Increasing the size ratio two-fold (from 4:1 to 8:1) for the same size e.g. 710 μm, increased the NSR approximately six-fold. The NSR for the FG binary combination was statistically higher than that for GG due to the difference in porosity that was 70 % and 50 % respectively from Table 2-1, between the two combinations. The porosity of the fine particles was attributed to the coarse component characteristics.

The density effect was obtained through comparison of the GG and GF combination whose difference was the fines component. From Table 2-3, the NSR for the GG combination was significantly higher than that for GF. The NSR being higher for GG than for GF was attributed to the higher density (2,760 kg/m^3) of glass beads than the density (1,970 kg/m^3) of poultry feed, the finer component of the GF combination. With gravity being a dominant factor for the percolation and

sieving mechanism, the denser particles (glass beads) influenced the NSR for GG being higher than that for the GF combinations.

The fine particles density effect dominated the coarse particles shape effect as the NSR for GG was significantly higher than that of the FF combinations as shown in Table 2-3. The GF and FG comparison revealed that irregular shaped particles caused a higher NSR than the spherical particles. The higher density smooth surface fine particles were responsible for a higher NSR than the low density roughly shaped particles.

The results of Tang and Puri have shed insight on particle behavior and might be useful in analysis of especially radial segregation in SAG mills when gravity or percolation is a dominant factor. For a binary mixture, the irregular shaped coarse component was observed to promote high porosity while the high density smooth fine component trickled through the voids easily and in both cases segregation was increased. However, these results have revealed that the segregation caused by particle density and shape effects along SAG mills might be negligible as the denser steel balls are usually larger in size than the bulk of the small rocks in the charge. Also, the shape of both the rocks and steel balls is nearly spherical (Steyn and Hinde, 2005) in SAG mills therefore the shape influence is negligible. A smaller size ratio of rocks in the mill feed might reduce the observed size segregation.

2.3 MILL MODELS

The comminution models, including the JK SAG mill model have been developed from the population balance model (PBM) concept. The complication of particle segregation and evaluation of the average residence time of solids in the mill required the PBM to be simplified by assuming that mill contents are perfectly mixed for the SAG mill model. The SAG mill model is therefore termed as the "perfect mixing" model. The perfect mixing assumption is very convenient and valid as long as the mill is of a high aspect ratio (reasonably short length). Moreover, the current SAG model was developed using Australian local mills that are traditionally of short length. However, the work of Powell *et al* (2000) have suggested that modelling low aspect (long) mills using the perfect mixing JK AG/SAG model may not be adequately suited to predicting mill performance of the "long" mills, as the two mill types have a significant difference in the window of operation. Thus, this current study is also intended to research the possible incorporation of axial segregation in the modelling of low aspect mills.

2.3.1 The Population Balance Model (PBM)

The PBM was first introduced to comminution machines by Epstein (1948). Epstein suggested that the result of a comminution operation was the product of the probability of breakage and the size distribution of the broken particles, which seems to be the basic concept of the breakage mechanism of SAG mills. The PBM has since undergone improvements especially by Herbst and Fuerstenau (1968) and by Whiten (1974). The PBM is also referred to as the "first order rate model" due to the assumption that the production of ground material per unit time is only dependent on the mass of material in a size fraction present in the mill contents, characterised by a specific breakage rate. The PBM is given by equation (2.12).

$$f_i' + \lambda \sum_{j=1}^{i-1} b_{ij} k_j s_j' = p_i' + k_i \lambda s_i' \qquad \text{(after Napier-Munn } \textit{et al.} \text{ 1999 a)} \qquad \textbf{(2.12)}$$

Where;

f_i = total flowrate of feed material in size $_i$ (tph)

p_i = total flowrate of discharge material in size $_i$ (tph)

k_i = breakage rate of particles in size $_i$ (h^{-1})

b_{ij} = the appearance function representing breakage from size $_j$ into size $_i$

$\lambda = \sum s_i / \sum f_i$ is the mean solids residence time

The size distribution for each stream is represented by a prime '

From the PBM equation (2.12), the mean residence time λ of the charge (water, and all solids) as well as measurements of p_i, f_i, the experimentally problematic mill contents s_i, and a suitable appearance matrix b_{ij} should be obtained before using the model to predict mill performance. Usually to obtain all the parameters is a very difficult task, and therefore the simpler perfect mixing model is preferable to the PBM when appropriate.

2.3.2 The perfect mixing JK AG/SAG mill Model

The perfect mixing mill model was developed with the same material balance structure as the PBM, but the residence time was omitted as the mill contents are assumed to be perfectly mixed. The development of the mathematical theory of the perfect mixing model was conducted mainly by Alban

Lynch and William Whiten, (1967) at the Julius Kruttschnitt Mineral Research Centre (JKMRC). The AG/SAG mill model is a special form of the perfect mixing model given in equation (9.3) that was first formulated by Whiten, (1974) with lots of input from the pilot and industrial work of Stanley, (1974).

The AG/SAG mill model developed by Leung, (1987) and described in detail in Appendix 1 is popular for its versatility and for its prediction of especially high aspect ratio mills. However, the weakness of this model is that it is semi-empirical and relies on the physical description of the sub-processes on which it depends. Also, it has limitations for applicability to long mills where segregation might exist when the mill contents are not homogenous.

2.4 SAG MILL OPERATIONS AND CHARGE BEHAVIOR

Segregation and transport of material as well as the general behavior of the charge along SAG mills is very much influenced by the dimensions or design of the mill and on how the mill is operated. This section therefore, gives an overview of SAG mill design and how the operations of SAG mills influence segregation and material transport.

2.4.1 SAG Mill design

SAG mills are generally defined by three aspects of design that comprise the mill shell, the discharge mechanism, and the lifters and liners, Napier-Munn et al (1999 c).

2.4.1.1 Aspect Ratio (Shell design)

The Diameter: Length ratio which in Comminution is termed as "aspect ratio" is the major distinguishing feature in categorizing mills. This ratio relates to a continent that historically would favor a particular shell design. Mills fall in three main aspect ratio groups namely;

1. Low aspect mills (aspect ratio is in the range 0.3 to 0.7)
2. Square mills (the diameter is approximately equal to the length)
3. High aspect mills (aspect ratio is in the range 1.5 to 2.5)

The low aspect SAG mills are generally associated with South Africa. They are usually described as South African styled mills and are sometimes referred to as Run of Mine (RoM) ball mills because of the tendency to operate them with high filling and with high ball loads as shown in Table 1-1.

The high aspect SAG mills which are informally referred to as pan cake type mills because of their appearance are associated with Australia and North America. They are often regarded as the North American designed mills.

Segregation seems to be more prevalent in the low aspect South African styled SAG mills. Napier-Munn *et al.* (1999 d), stated that the physical examination of mill contents after a crash-stop always shows a strong gradation from coarse to fine from the feed end to the discharge, even for "well mixed" SAG mills!

2.4.2 Material transport and diffusion within mills (Discharge effect)

Transport of rocks and slurry along SAG mills is not well understood. Material transport along SAG mills is currently modelled using equation (9.7) proposed by Latchireddi, (2002). However, this equation only covers particles less than Xm that flow like water and does not incorporate the classification of larger particles, especially rocks larger than the grate/pebble port size, Xg. It is an intention in this thesis to address transport and segregation of rocks along SAG mills. The transport of slurry along SAG mills and the discharge of slurry out of the mill is being seriously studied in a separate P9 project in the Comminution group of the MPRU at the University of Cape Town.

2.4.3 Liners and lifters

The use of liners and lifters is to protect the mill from being worn away by the impact of balls and rocks. The influence of liners and lifters on the mill charge is to provide a higher amount of lift to the rocks and balls thereby increasing the impact breakage. Hogg (1982) suggested that the lifters and liners might suppress or promote segregation if designed accordingly, but there is no reported work on the influence of lifters/liners on segregation of particles along SAG mills or any other wet mills. It appears that Hogg's postulation might be true and in future tests should be conducted to study the liners/lifters effects on the segregation of particles.

2.4.4 Mill filling effect

The SAG mill filling effect on segregation is hypothesized to follow the same pattern as that observed by Shoji *et al.* (1973) in batch ball mills. Shoji et al observed significant segregation at low material filling, and at a higher filling, the charge was quite well mixed. Also, increasing the ball load promoted mixing but hindered charge segregation of particles. However, for the current studies in chapter 7, segregation was observed in the SAG mill with high filling and therefore mill filling may have less significance on the observed segregation.

2.4.5 Mill speed

The SAG mill speed influence on particle radial segregation has been clearly explained by the work of Powell and Nurick (1996). Also, Paul Cleary (1998) using DEM confirmed the findings of Powell and Nurick that the large particles reside on the outside of the charge whilst the small particles occupy the center, and the trend is reversed at high speeds. The explanation given from the two sets of work seems adequate. However, there seem to be no reported work on the influence of mill speed on axial segregation.

2.5 SUMMARY

The literature review can be summarized as follows:

1. The abundant segregation work research conducted in horizontal drum mixers is not conclusive enough to extend the results obtained to SAG mill operations.
2. The work of Shoji et al to study the material and ball load effects, that by Hogg to explain material transport effects, the work of Powell and Nurick and the DEM work by Cleary to explain mill speed effect on segregation, and that by Benzer *et al.* in the cement industry to model long mills as tanks in series, stand out to have come close to describe and understand axial segregation along mills. It is noted that almost all of the previous research work was not conducted in SAG mills and therefore the findings of the above researchers needs to be tested on SAG mills.
3. The current JK SAG mill model omits segregation of particles along the mill and the transport description of particles, especially larger rocks, along the SAG mill is insufficient.
4. The operation of SAG mills could influence the observed segregation. For instance, low mill speed and very low material filling could promote particle segregation.

The literature shows that axial segregation and transport of particles along SAG mills is poorly understood. The current JK SAG model concept of "perfect mixing" applicability to all SAG mills is not completely supported even by the JKMRC (Napier- Munn *et al.* 1999 d) who developed it.

Chapter 3

3 HYPOTHESES

This chapter firstly explains a brief background to segregation studies and then revisits the causes and the trends of the observed segregation reported in literature. The purpose for the review is to illustrate the predictable axial segregation expected along SAG mills. The thesis hypotheses and the specific objectives for this research work are the main focus of this chapter and are described in the final sections.

3.1 HYPOTHESES PREAMBLE - BACKGROUND

Early researchers considered transport and size reduction of particles as independent and so they modeled transport independent of breakage. The major focus was on transport of material in mineral processing systems and they tackled this subject through residence time studies. The importance of the residence time of particles spent within the tumbling mixers is apparent from the huge amount of literature available on the subject.

In the current study, it is believed that both transport and breakage influences axial segregation of particles along SAG mills.

The transport process is related to the aspect ratio of SAG mills, which had initially been thought to be the major influence of the observed axial segregation of particles. The low aspect ratio mills were thought to exhibit more segregation than the high aspect mills. However, recent observations (Chapter 5) have revealed that the major influence is actually the absolute mill length due to the higher residence time particles spend traveling from the feed to the discharge end of the mill. Segregation is therefore highly likely to be more prevalent in longer mills than in shorter mills due to the higher residence time of particles in longer mills. The residence time of large particles has been found to be longer than that of fine particles, (Chapter 5) and the difference might be the cause of size segregation. Segregation might also be observed due to particles surviving the breakage process.

3.2 CAUSES OF SEGREGATION FROM LITERATURE

From the literature, segregation of particles along tumbling cylinders has been found to exist due to a number of factors which are outlined in the next sections:

3.2.1 Particle characteristics

Particle characteristics here mean the "packing" of particles that is responsible for the transport and consequent segregation of particles due to diffusion and percolation through the void spaces. Particle characteristics also include the effects of size, shape and density of particles on segregation.

- The difference in particle size encourages movement of small particles through voids by axial diffusion along a rotary cylinder thus promoting mixing or segregation, Shoji *et al.* (1973), Hogg and Rogovin (1982), and Ding *et al.* (2002), while particles' percolation due to gravity results in radial segregation, Donald and Roseman (1962) and Henein *et al.* (1985).
- Differences in physical properties of particles reveal small amounts of segregation in a bed of particles that appear to be homogeneous on the outside, Rogers and Clements (1971).
- Vermeulen and Howat, (1989) observed that the amount of small balls (scats) in the sampled stream did not compare with the amount of scats collected from the total charge. They attributed the difference in the observed amount of scats to segregation by particle shape.
- Percolation and sieving based segregation as well as gravity radial segregation due to particle size, shape and density has a high dependence on the "size ratio" of particles within the particle bed, Eskin and Kalman, (2000) Khakhar *et al.* (2002) and Tang and Puri, (2004).

3.2.2 Speed of tumbling drum/mill

The speed of the rotary cylinder is a huge driver in the mixing or radial segregation of the tumbling particles. There is no reported influence of mill speed on the observed axial segregation. However, there are several volumes of literature covering radial segregation.

- Rogers and Clements, (1971) ran their drum mixer at a low speed of 40 rpm and claim that the small amounts of the observed segregation in the particle bed is attributable to the speed.
- Nityanand *et al.* (1986) observed radial segregation of big particles in the drum core region and the fines on the periphery and attributed this observation to higher operating speeds.
- Hill and Kakalios, (1994) attained reversible segregation in a drum mixer, by operating at a low speed of 5 rpm and at higher speed of 14 rpm. Segregation occurred at the speed of 14 rpm but disappeared at low speed (5 rpm), and again reappeared when moved back to a higher speed of 14 rpm. Hill *et al*, (1996) observed that segregated bands stabilized by increasing the rotational time and changed appearance by changing the drum speed. They also claim that radial segregation is responsible for evolution of axial segregation.

- The radial segregation dependency on mill speed was clearly explained by Powell and Nurick (1996) and by Cleary, (1998). In both sets of testwork, it was observed that at low speeds (less than 50 % of critical) segregation of fines in the central core exists and above 50 % critical speed, the charge particles remain reasonably perfectly mixed until around 77 % critical speed (limiting segregation speed) after which segregation of large particles to the central core and fines to the periphery appears.
- Ding *et al.* (2002) showed that axial particle mobility increases with drum rotational speed therefore particle segregation is dependent on the drum speed too.

3.2.3 Particle filling

The charge filling in the mill or material bed filling in a rotating drum has been found to have an influence on the mixing or segregation of particles. Lower material filling has been found to increase the segregation rate of particles within the charge.

- Shoji *et al.* (1973) and Abouzeid (2000) noticed segregation of particles at low material fillings which they attributed to more freedom in individual particles to move in any direction.
- Eskin and Kalman (2000) showed at low material filling, that the greater the size ratio difference within the charge, the higher the segregation potential.
- Cleary (2003) found that increasing mill filling led to a decrease in the diffusion of fine particles along the mill and reduction of the observed axial segregation.
- Djordjevic *et al.* (2004) showed that increasing material filling increased the proportion of energy used for the low energy abrasion breakage.

3.2.4 Mechanical action of particles

The action of particles on each other through collisions, slipping and the vibration of particles with the mill shell, lifters, and liners all result in material segregation.

- Donald and Roseman (1962) and Shoji *et al.* (1973) attributed the observed segregation to collision of a particle by another thereby freeing the particular particle into space and discouraging it from mixing with the rest.
- Hogg and Rogovin (1982) and Hogg (1984) claimed that segregation resulted from vibrations of the small particles onto the mill shell and suggested that lifters and liners promote axial transport and segregation.

- Abouzeid (2000) explained that the mechanical action of particles allows material to be thrown backwards and forwards. In steady state conditions, continuous feeding creates a gradient along the mill responsible for axial transport and segregation.
- Djordjevic (2004) observed that lifters promote particle impacts and consequently increase the segregation potential.

3.3 PATTERNS OF THE OBSERVED SEGREGATION

The patterns of the observed particle segregation along drum mixers and along ball mills from literature in Chapter 2 are summarized in this section.

The observed segregation cited the most in literature was first reported by Donald and Roseman, (1962). They reported the occurrence of segregation in three forms shown in Figure 3-1;

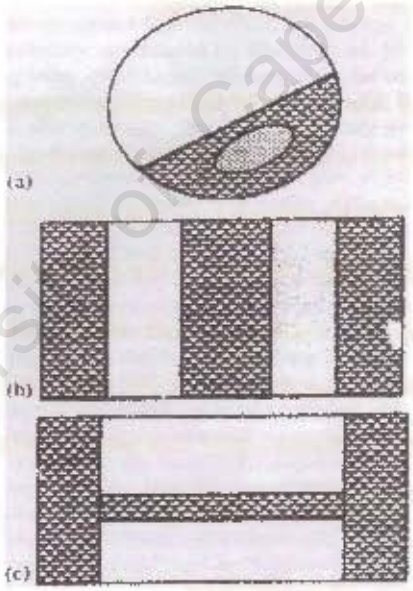

Figure 3-1: Patterns of segregation in a horizontal drum: (a) radial, typified by a central core, (b) axial, where alternative bands of the components develop (c) end longitudinal, which are two bands adjacent to the end wall connected by a thin core, (after Wightman and Muzzio, 1998)

Other forms of segregation patterns have been reported but most of them are variations of either all of the above three or a form of any one of the above three segregation types. Other observed segregation forms reported are;

- Shoji *et al.* (1973) observed axial segregation of particles in a laboratory mill and found that the balls were perfectly mixed along the mill, (Figure 3-2)

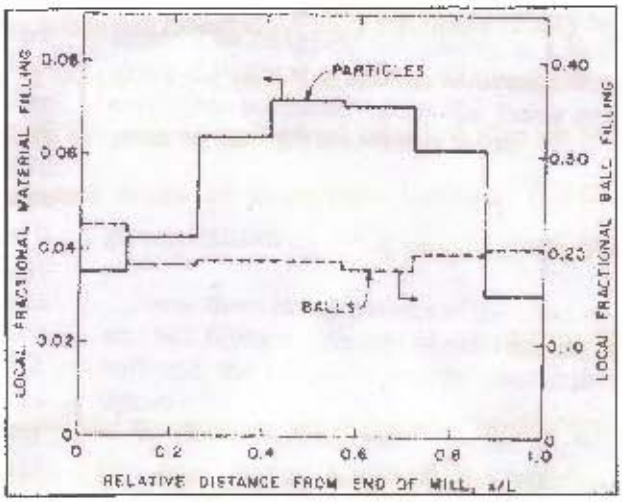

Figure 3-2: Distribution of particles, for particle filling, f_c = 0.055 and ball filling, J = 0.193 showing the tendency for particles to segregate towards the center of the mill (after Shoji et al, 1973)

- Hogg and Rogovin, (1982) and Hogg, (1984) reported observed segregation of particles decreasing by size from the feed position towards the discharge of a laboratory mill. They also showed that small particles had a higher relative axial velocity at low slurry solids concentration. The axial segregation observed by Hogg is shown in Figure 3-3.

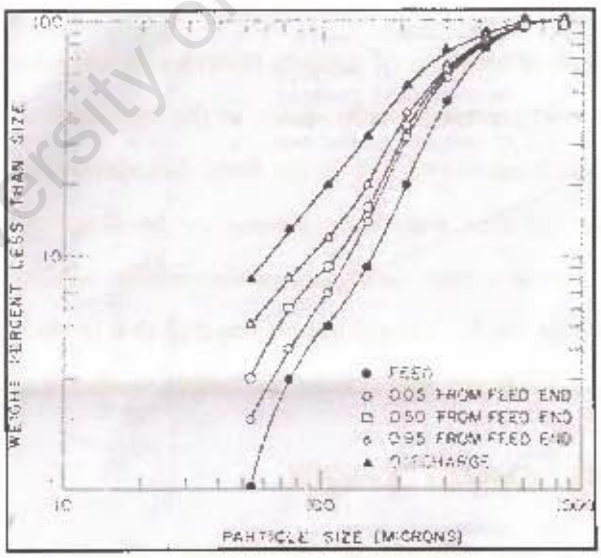

Figure 3-3: Experimental particle size distributions obtained from the continuous grinding of quartz in a 30 cm diameter, wet, overflow ball mill (after Hogg and Rogovin, 1984)

- Hill and Kakalios, (1994) and (1997) observed alternate band formation of large and small particles along the drum, similar to that observed by Donald and Roseman, (1962). They further observed axial segregation of a mixture of split peas and uncooked rice. After a drum rotation of two hours at the speed of 14 rpm, a central band of round peas formed with two side bands of rice.

- Benzer *et al.* (2001) observed axial segregation along the tube mill used for dry grinding in the cement industry. As shown in Figure 2-15 (chapter 2), the particles became finer along the length of the mill from the feed going towards the discharge position.
- Khakhar, (2002) observed segregation by streak formation at low rotational speeds as shown in chapter 2 (Figure 2-7).

3.4 HYPOTHESES

From the observed segregation covered in the literature, it has been shown that axial segregation of particles exists in tumbling cylinders and in long mills. The hypothesis of the current study is summed up in the statement;

"Axial segregation of rocks along SAG mills exists and becomes more significant with increased mill length, due to longer residence times. The observed segregation arises from both the transport and breakage mechanisms of particles within the mill."

The two mechanisms are assumed to influence the observed axial segregation as follows;

1. Different transport rates of distinct particles would result in axial segregation by size, where the bigger rocks preferentially reside at the mill inlet and fines at the discharge, due to the mill feed mechanism and due to the fines diffusional flow along the mill.
2. The distinct particle wear rates during the breakage process results in axial segregation by hardness, where softer rocks are preferentially broken within the mill feed region whilst survivor rocks can be located across the mill due to their competence as they are transported towards the discharge, and due to the longer residence times of harder particles in the mill.

3.5 SPECIFIC OBJECTIVES

Arising from the set out hypotheses, the specific objectives of this thesis designed to fulfill the requirements of the hypotheses statements were to:

1. Collect charge samples in demarcated zones of about one meter each separately, along the mill and size the dry charge to compare the particle size distributions.
2. Collect samples of pre-screened size fractions from the same demarcated zones and subject these particles to the standard JK Drop Weight test procedure to study the impact and abrasion properties of rocks relative to their position along the mill.

Chapter 4

4 PRELIMINARY PLANT TRIALS

This chapter presents the methodology followed during three investigative preliminary plant surveys. The requirements for satisfactory sample collection are outlined followed by a description of the actual sampling technique. The findings from the three preliminary investigations are presented and discussed before concluding the chapter by highlighting some methodology weaknesses and recommendations for improving the sampling technique. It should be stressed here that these tests were merely scoping trials to direct the research work, and no hard conclusions could be drawn from the survey findings. However, an indication of axial segregation along the mills was observed.

4.1 APPROACH AND METHODOLOGY

At the start of this research work, the segregation pattern exhibited along mills was only speculative. For instance it was thought that all particle sizes within the charge would show a consistent segregation propensity along the mill, yet typical results later, in chapter 7 revealed the opposite. With no reported studies along SAG mills in the literature, it was decided that the best starting point for this work was to conduct preliminary plant tests. Industrial trials were chosen over pilot scale tests in order to obtain an insight of axial segregation in real (non-ideal) operating conditions. The opportunity arose at two Concentrators of LonMin Platinum Limited and three distinct tests were performed in Run-of-Mine (RoM) ball mills.

The methodology for collecting samples of the charge along a SAG mill after a crash-stop for the trial surveys is completely novel. The sampling method chosen was restricted by the following:

1. Fixed sampling time - dictated by the duration allowed by the plant for the mill to remain stopped after a crash-stop.
2. Representative sample size, big enough sample comprising a representation of almost all particle species within the charge.
3. Axial distance selected to collect the sample was to be suitable to represent reasonable sizes of slices along the mill.
4. Sample cutter choice, the selected sampling spot was to be demarcated by an open template square used for defining the sampling area boundaries.
5. Repetitive, the chosen sampling technique was to be repeatable or reproducible.

The methodology requirements are explained in detail in the next sections.

4.1.1 Time for sample collection

The samples were to be collected only when the mill was stopped. The plant management allowed two hours as the standard mill down time after a crash-stop, coinciding with mill maintenance, and the segregation samples were to be dug out within that period. The time for collecting axial samples of the charge imposed the limit to the sample size to be dug out from slices along the mill. Owing to limited times allocated to mill stoppage due to loss of production and subsequent loss of income, the samples collected during the stipulated crash-stops could not be very large.

4.1.2 Representative sample size

The sample to be collected was to include all species in the charge, i.e. the fine solids (slurry), medium sized rocks, and big rocks. It was decided not to include the steel balls in the sample because the focus was on the rocks size distribution along the mill. Also, the RoM ball mills where samples were targeted to be collected from, have high ball loads, thus it was feared that the balls might dominate the sample if included and that the rocks in the sample might not be enough to be representative of the mill slice from which those rocks were dug out. A 200 ℓ capacity drum comprising slurry and rocks was selected as sufficient for collecting a representative sample from each slice along the mill.

4.1.3 Axial distance of slices along the mill

The mills targeted for collecting axial segregation samples were generally about 5 m long. Due to the limiting two-hour sample collection time, it was decided that three samples each of about 200 ℓ in capacity were to be collected over the 5 m length of the mill. Thus the 5 m length was to be divided into five 1 m long segments, referred to as "slices" in this thesis. Slices 1 (inlet), 3, and 5 (discharge) were samples while no material was collected at position 2 and 4.

4.1.4 Sample cutter

To collect a sample of the charge, a simple open square metal template was used to define the sampling boundaries. Rocks were dug out with shovels, spades, and by hand and transferred by bucket to labelled drums outside the mill. Balls were placed aside while the slurry at the sampling

spot was collected using smaller buckets by immersing the bucket into the slurry pool and scooping it out.

4.1.5 Sampling reproducibility

It was imperative to collect samples along the mill slices consistently. The adopted sampling technique was applied to all the sampled slices identically. At each slice, an area of 1 m^2 constituted the sampling spot and the rocks were dug out up to a depth of approximately 1 m. The same volume of slurry was collected from each sampling spot.

4.2 PLANT SITES

Two of the preliminary tests were conducted at the K4 Concentrator and the third test was carried out at the C stream of the Eastern platinum Concentrator (EPC) LonMin Platinum Limited. For all of the three tests, the circuit ran at steady-state conditions and then samples were taken around the circuit before crash-stopping the mill. The segregation samples were collected after the circuit sampling survey had finished and after the mill crash-stop.

4.2.1 EPC Concentrator

The EPC primary milling circuit comprises a RoM ball mill fed with open cast UG2 ore at a feedrate of around 180 tph and closed with a 0.6 mm linear screen. The mill discharge stream is classified on a 6 mm aperture vibrating screen and the oversize is conveyed back to the mill, passing by a scats removal belt magnet. A schematic of the milling circuit is shown in Figure 4-1.

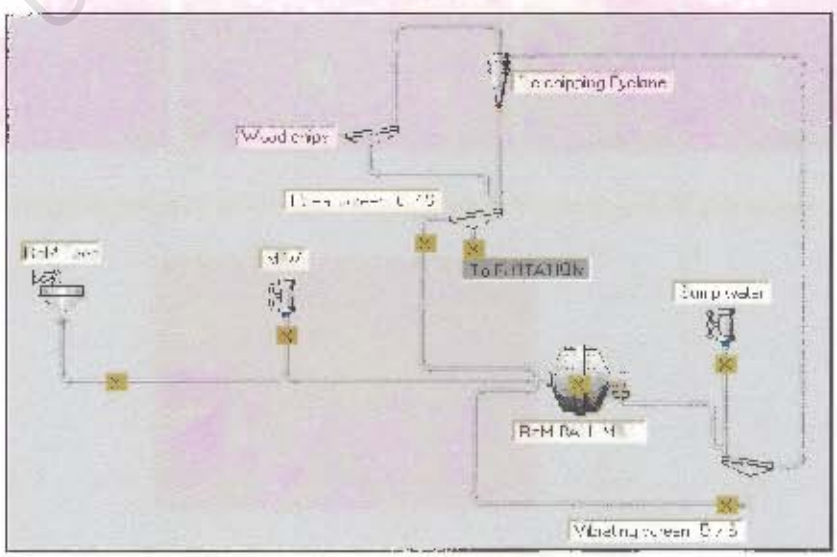

Figure 4-1: Schematic of the EPC primary mill circuit

4.2.2 K4 Concentrator

The K4 milling circuit is identical to the EPC circuit schematically shown in Figure 4-1. The RoM ball mill also treats around 180 tph open pit UG2 ore. Therefore the sampling procedure followed at EPC was repeated for the K4 milling circuit.

4.3 EXPERIMENTAL PROCEDURE

The RoM ball mill was operated under steady-state conditions for about two hours before starting the collection of samples for an hour milling circuit survey.

4.3.1 Sampling the mill charge

After a crash-stop, the mill inlet trunnion cover was moved backwards to allow access to the mill. Inside the mill, the charge surface was demarcated into five equal 1 m slices along the mill length. For the three slices chosen for sampling, the square template was placed in the central spot of the slice to define the sampling boundaries. The samples were dug out and taken out of the mill as explained in section 4.1.4.

Photographs were taken of the surface of the charge before digging out the samples for each slice and are shown in Figure 4-2. The appearance of a sampling spot after the material had been dug out along the mill is illustrated in Figure 4-3.

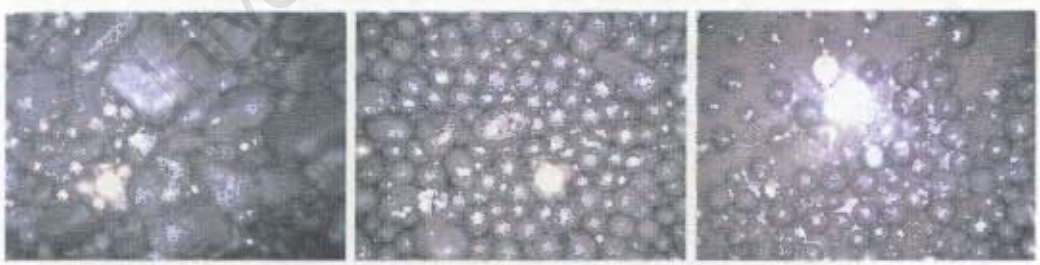

Figure 4-2: Photographs of sampling spots, slices 1 to 3 before collection of samples

Figure 4-3: Sampling the inlet (slice 1) spot at EPC

4.3.1.1 Size ratio sampling Bias concern

During the sampling process, it was easier to collect the rock samples than to scoop the slurry from the sampling spot with buckets. Thus, the final sample from the slice had a size ratio bias towards more rocks but less fine particles. It was unavoidable to remove the size ratio bias completely with the sampling technique used, and to minimize this bias as much slurry as was possible to collect was scooped out of the sampling spot.

4.3.1.2 Size ratio bias Correction

After processing the mill charge samples, it was found as expected that the amount of fines in each slice sample were less than the coarse particles. The sampling technique did not extract a 'full' sample of fines from the same volume where the coarse material was extracted, so the ratio of fines to the coarse rock is expected to be incorrect. It was, however, hoped that the size distribution of the fines sample would be representative of the total fines in the sampling zone.

The mass of fines (-1 mm) was corrected through calculation to a value of fines that should have been obtained in relation to the amount of rocks picked from a sampling slice. In the calculation, it was assumed that slurry filled a voidage of 0.4 in the mill, based on charge voidage reported by Napier-Munn *et al.* 1999 and on that measured independently in a SAG mill (Chapter 7). It was also assumed that the density of slurry in the mill was equal to the density of the mill discharge (product), as found in the slurry segregation study (Chapter 7).

4.3.1.2.1 Derivation of slurry mass calculation at every sample position

The slurry mass in each sample is derived in equations (4.1) to (4.5).

Then, at every slice (sample position);

$$Slurry\ volume = 0.4 * (Sample\ volume) \tag{4.1}$$

And at that sample position

$$Sample\ volume = \frac{Rocks\ volume + Balls\ volume}{0.6} \tag{4.2}$$

Also, at each sample position, let the balls volume : rock volume ratio be;

$$R_{br} = Balls\ volume / Rocks\ volume \tag{4.3}$$

Substituting the balls volume in equation (4.3) into equation (4.2), and then substituting the resulting sample volume into equation (4.1), the slurry volume becomes;

$$Slurry\ volume = \tfrac{2}{3} * [1 + R_{br}] * rock\ volume \qquad (4.4)$$

Therefore, the mass of the slurry expected to have been collected at each sample position is;

$$Mass\ of\ slurry = Specific\ gravity\ of\ mill\ product * \tfrac{2}{3}\left[\frac{rock\ sample\ mass}{density\ of\ rocks}(1 + R_{br})\right] \qquad (4.5)$$

The experimental value of R_{br} is expected to be different for every sample since the rocks reduce in size, into fine particles towards the mill discharge. However, the average value of R_{br} in the mill was approximated by the ratio [mill ball load / + 1 mm rock volume filling], and the + 1 mm rock volume in the mill is equal to the (total mill filling – ball load).

Even though the correction was not totally perfect, applying equation (4.5) to the measured slurry mass, ensured that the particle size distributions calculated were close to that which might have been obtained in an ideal (perfect) sampling of the charge. The raw data and converted full size distribution data is presented in Appendix A2.

4.4 PRELIMINARY FINDINGS

The key measurements from the three circuit surveys are summarized in Table 4-1.

From Table 4-1, it is observed that the three mills in which the tests were conducted have similar length and the aspect ratio (AR) of 0.8 for EPC and 0.9 for K4 is within long mills classified as low aspect South African style RoM ball mills. It is observed that K4 test 2 had a higher F80 and thus the coarsest mill feed size distribution. The linear screen oversize streams were run very dilute in order to wash off all the oversize solid particles back to the mill. Both the vibrating screen oversize and the linear screen oversize flowrates were very low and so the re-circulating loads from the classifiers were less than 1 %. The EPC primary RoM mill had a relatively higher filling and a higher steel ball load (top size - 100 mm) resulting in a coarser product shown by the higher P80. As a result of the coarser product, the calculated Operating work index (OWI) for EPC was low. Had the actual Bond ball Mill Work Index been conducted and found to be in agreement with the calculated OWI, this would have suggested that EPC mill had better usage of the drawn power.

Table 4-1: Key (mill) test measurements

Mill measurements	EPC	K4 Test 1	K4 Test 2
Mill length, m	5.0	5.0	5.0
Mill diameter, m	4.2	4.7	4.7
Mill speed, % critical	73.6	72.7	72.7
Fractional mill filling, %	43.3	32.2	35.6
Ball load, %	38	27.5	27.5
Mill power, kW	1635.4	2073.3	2275.1
Mill feed F80, mm	87.9	67.3	93.4
Circuit product[#] P80, µm	181.0	153.0	163.0
Calculated OWI (kWh/t)	12.5	13.9	15.9
Flowrates			
Circuit feedrate, tph	176.3	184.9	183.7
Mill product, tph	177.8	186.0	184.0
Vibrating Screen O/S, tph	0.13	0.11	0.06
Linear screen O/S, tph	1.5	1.0	0.2
Mill inlet water, m^3/h	14.6	15.0	18.0
Sump dilution water, m^3/h	133.3	114.1	119.3
Percent solids			
ROM Feed	99.1	99.1	99.4
Vibrating Screen O/S	97.7	97.1	96.3
Linear Screen O/S	3.2	3.9	2.3
Circuit product[#]	49.2	49.2	48.0
Average Ore SG	3.2		

[#] Primary circuit product is the Linear screen U/S

The mill charge findings from the three Scoping tests are presented independently. The rocks size distribution are expressed in specific size ranges between the top size and the finest sub mesh rocks, and compared amongst the three tests. Three size ranges chosen are; big rocks (+ 63 mm), small (1 – 63 mm) and fine particles less than 1 mm which have been classified as slurry in this thesis. Particles less than 1 mm have generally been referred to as slurry by other researchers. For instance, Napier-Munn *et al.* (1999) and Morrell (2004) claim that particles less than 1 mm flow like water and can therefore be classified as slurry.

The particle size distributions (PSD) of samples around and inside the mill for each of the three tests are shown in Figure 4-4.

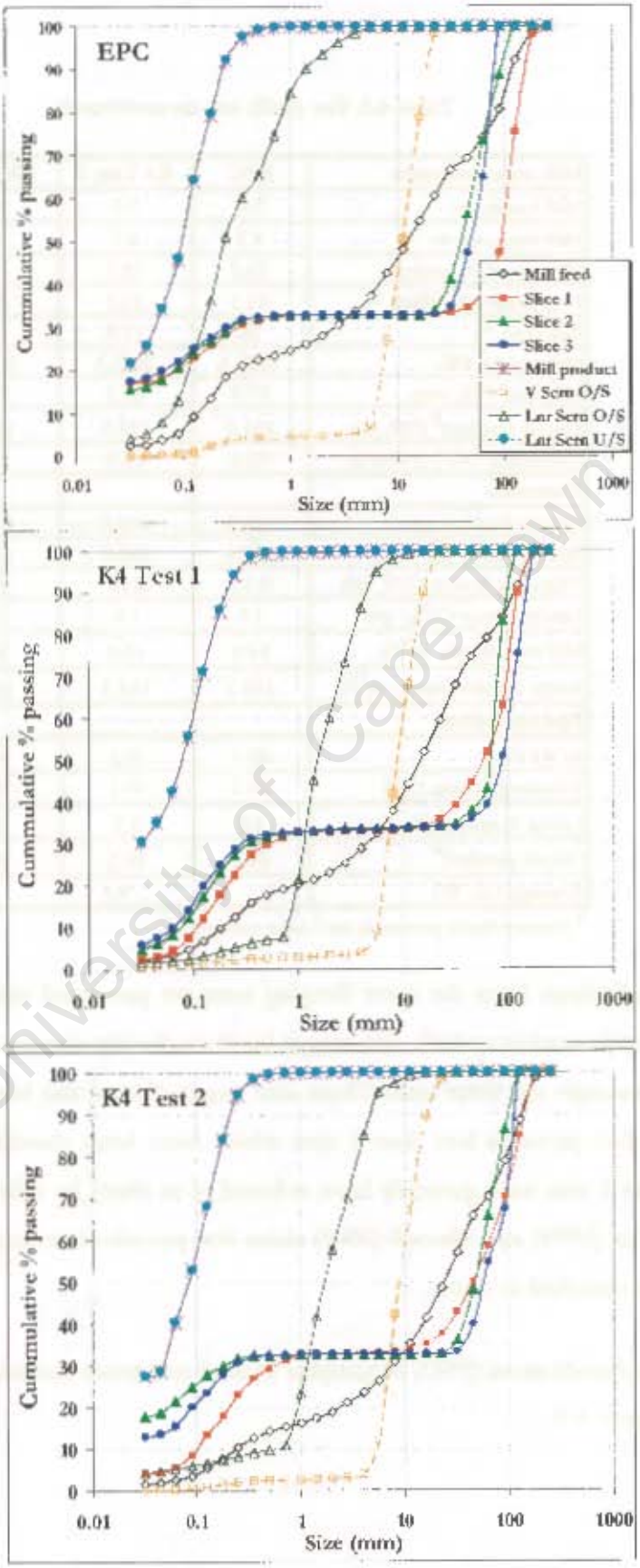

Figure 4-4: EPC full circuit particle size distributions

From Figure 4-4, it is observed that the linear screen undersize and the mill product curves lie on top of each other because these are essentially the same stream, with an exception of less than one percent of oversize particles recycled back to the mill after being screened from the mill product. There is a small difference among the size distribution trends of particles from the three slices along the mill. All the three slices depict a step in the curves from about 1 mm to 31.5 mm in between the coarser and the fine particles indicating presence of fewer rocks in this size range. Powell (2004) suggests that the particles fewest in the mill, as given by the flat step in Figure 4-5, are of the size equivalent to the interstices between the packed charge such that these particles receive very high pressure on all fronts and get squashed to fines. Additionally, the discharge rate of this size class is high as it falls within the slot size (18 mm to 40 mm) at the mill discharge, and thus the 1 to 31.5 mm rocks should be deficient in the mill. The sampling representativeness may also add to this artifact.

A detailed analysis of PSD trends within narrow size ranges is given in section 4.4.1

4.4.1 Comparison of size distribution within defined size ranges

A comprehensive comparison of the size distribution of the particles amongst the three preliminary tests is presented by segmenting the slice PSD curves into three defined size ranges; slurry (-1 mm), small rocks (1 – 63.5 mm), and big rocks (+ 63 mm). The complete PSD of the three individual scoping tests is given in Appendix A2.

The segmented rock graphs from the three preliminary tests are compared as size distributions (Figure 4-5) and as plots of S80 – the 80 % passing size (Figure 4-6).

From Figure 4-5, the big rocks from the EPC test shows an anticipated trend of particles decreasing in size from the feed (slice 1) towards the discharge (slice 4). The K4 tests do not show a clear segregation trend. The small rocks for all the three tests reveal no segregation. Slurry on the other hand shows that the inlet position (slice 1) had a coarser size distribution than the other two slices.

Both the size distribution and S80 data show that there is minimal segregation. The small rocks graphs include the 'critical size' smooth rounded rocks in the size range 25 – 50 mm, which are thought to be competent and might inhibit particle segregation in SAG mills.

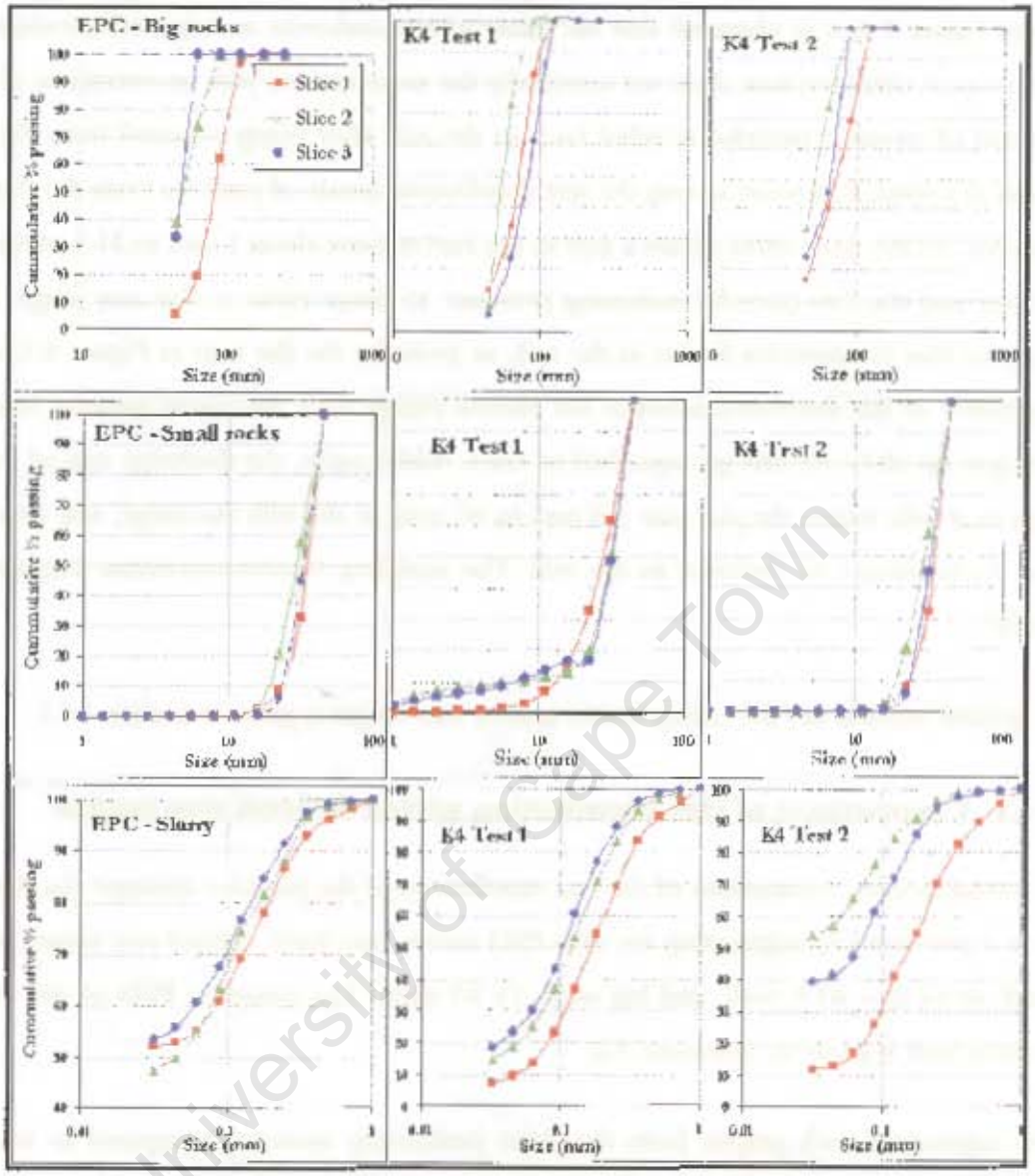

Figure 4-5: Size distribution comparison of big rocks, medium rocks and slurry from trial tests

The S80 data plotted in Figure 4-6, shows axial segregation of big rocks for the EPC test with decrease in size towards the discharge of the mill. The K4 tests indicate on average a finer middle section and possible accumulation of coarser rocks at the discharge. This may be related to ore competence, but this aspect was not tested in these preliminary trials. The number of + 63 mm rocks sampled and mass bias between the coarse rocks and fine solids is shown in Table 4-2.

Table 4-2: comparison of numbers and mass of + 63 mm rocks and – 63 small rocks for the trial tests

	Number of +63 mm rocks			Mass of + 63 mm rocks, kg			Mass of - 63 mm rocks		
EPC	99	36	12	2465	223	49	720	334	56
K4 test 1	16	16	6	309	225	113	121	40	12
K4 test 2	180	29	6	2306	271	250	1432	260	110
	Slice 1	Slice 2	Slice 3	Slice 1	Slice 2	Slice 3	Slice 1	Slice 2	Slice 3

The slurry size distribution for the three tests reveals a trend of particles becoming finer towards the discharge. The S80 curves also show a significant decrease from about 340 µm to around 180 µm along the mill.

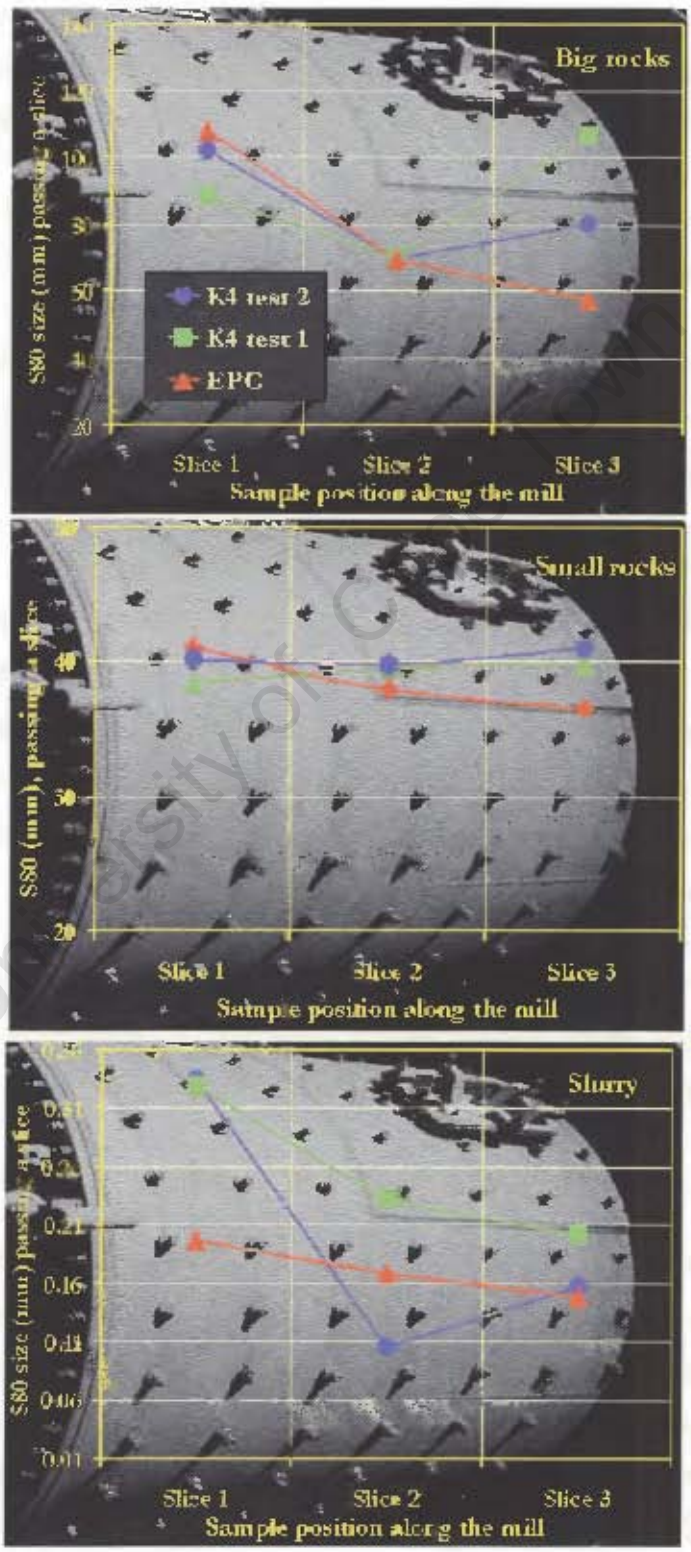

Figure 4-6: Comparison of the S80-size at which 80% rocks passes a slice, for the three trial tests

4.5 DISCUSSION OF FINDINGS

The particle size distribution curves for the sampled slices shown in Figure 4-5 and Figure 4-6 did not reveal a clear indication of the segregation trend along the mill. However, truncating the charge size distribution curves into three narrow size bands showed that big rocks (+63 mm) and slurry (-1 mm particles) indicated size segregation. On the other hand, the small rocks (1 – 63 mm) showed an inconsistent or irregular tendency that appeared as a mixed axial distribution phenomenon.

The segregation exhibited by slurry is what was expected along the mill with size reduction towards the mill discharge.

The three preliminary tests bore some similarity when the sampled charge size distributions were expressed within three defined narrow size ranges. The similarity in the defined size ranges suggests that the sampling technique was reasonably reproducible.

The second more consistent size range with a recognizable segregation trend was the big rocks size range shown. The EPC and K4 test 1 big rocks distribution showed that the discharge -slice 3 was coarser than the central -slice 2 and even the inlet -slice 1. For the big rocks, it is possible that fewer rocks picked from the sampling spot might not have been enough to represent the true number present at a slice. However the indication that axial segregation existed along the mills was adequate during the preliminary trials as the objective was to obtain an impression of axial segregation for future rigorous surveys.

The small rocks shown in Figure 4-5 and in Figure 4-6 did not show any segregation trend. The size distribution pattern observed from this size range was not definitive and the S80 plots shows that the particles in this size range were quite well mixed along the mill.

4.6 SOME METHODOLOGY WEAKNESSES

The major weakness of the trial sampling methodology encountered was the bias towards collecting more rocks than fine particles. The sampling technique used for the preliminary studies imposed a limitation on collecting a sufficient component of the fine particles as the sample collection perimeter narrowed deep down into the sampling slice. Therefore, it was difficult to scoop out enough fines at the narrow tip of the sampling spot. The slurry filling up the dug out empty void at the sampling collection spot of each slice also made it difficult to pick up fines.

The other weakness was that some size fractions in the samples collected from the slices might not have been sufficient. The problem was not necessarily the entire sampling technique used, but rather the amount of fines (sample size) collected at each sampling slice was inadequate. The overall slice samples then contained fewer fine particles. Equation (4.5) was used to correct the slurry mass deficiency. However this correction had a limitation of only increasing the slurry size distribution by a factor and could not correct the problem created from collecting a non-representative sample.

The samples collected were quite representative of the medium size rocks, but the fines were inadequate and not completely representative of the slurry along the mill. The big particles were also few in numbers and might not have been representative of the slices from which they were picked.

4.7 SUMMARY AND RECOMMENDATIONS

The preliminary tests revealed two findings:

1. Axial segregation does exist to some extent along low-aspect tumbling mills.
2. The observed segregation is strong at the fine and coarse sizes whilst it's weaker or not present for mid size ranges.

Slurry revealed strong segregation whilst the big rocks showed weak segregation. The small rocks showed no segregation trends and implied a well mixed size distribution. The observed segregation and the mixed size distribution patterns should be verified with further tests.

The results have indicated that distinct size distribution might arise from different flow rates of particles along the mill that tends to result in segregation of fine particles towards the mill discharge and the big rocks being preferentially retained in the mill inlet region.

It is recommended that sampling the entire charge in separate discrete slices along the mill would be the best way to obtain adequate data to investigate the axial size distribution of solid particles. This way the results would be completely reliable as the testwork sample would be the entire mill charge. Additionally, the bias of collecting more medium sized rocks than the fines component of the sample would be avoided.

From the scoping tests, the presence of big rocks located at the discharge position of the mill suggested that those rocks located at the discharge might be harder than the ones at the inlet and center slices. It is therefore highly recommended that ore hardness tests be performed on rocks sampled from the charge to ascertain the influence of rock hardness on the observed segregation.

Chapter 5

5 MILL LENGTH EFFECT SURVEYS

This chapter reviews the significance of mill length and the aspect ratio influence on the observed axial segregation. To consolidate the claim that mill length significantly affects the observed segregation, the size distribution obtained by use of Split software, of the charge surface photographed from five distinct style SAG mills is presented. Additionally, residence time study results revealing transport rates of rocks and slurry along an AG mill are reported.

5.1 MILL LENGTH AND ASPECT RATIO

The influence of mill length and aspect ratio on the observed segregation is highlighted in a collection of charge surface shots taken from different mill types and different Concentrators. The surface shots were taken during several comminution surveys conducted by the Comminution research group of the MPRU at the University of Cape Town. A marker of known dimensions used for scaling was placed on the spot selected for taking a picture and when taking photographs, the camera was held to point vertically down at the charge. In almost all the sampling campaigns, the author was involved in the sampling surveys, and when not present particularly at Los Bronces, photographs were taken by other members of the Comminution group. The charge surface shots were taken after a mill crash-stop and using Split Desktop software[1], the size distribution of the particles on the surface of the charge has been plotted. The imperial root two sieve series is used. The Split data is truncated at 10 mm as the quantitative analysis is imprecise below this size.

5.1.1 Low aspect (long) mills

The load in the Eastern Platinum Concentrator (EPC), LonMin Platinum mill, sampled in the preliminary trials was photographed. This mill is operated as a run of mine ball mill receiving open pit primary crushed UG2 platinum ore.

[1] Split – Desktop Software Academic Version 2.0, developed by Split Engineering LLC, 110 South Church Avenue number 8312, Tucson, Arizona, USA 85701. Website: www.spliteng.com

Snap surveys in SAG mills with distinct mill length

A summary of the plants and mill descriptions is given in Table 5-1 whilst the charge surface photographs are shown in Figure 5-1. The five mills whose charge surface was photographed at crash-stop were operated at similar speeds of about 75 percent of the critical speed and therefore the charge surface size distribution can be compared despite some distinct operational variables.

Table 5-1: Plant sites and SAG mills with different dimensions

	Site/ Plant	Mill description	Ore type	Ore competence	L (m)	D (m)	AR	Comment
1	EPC	Long low aspect	UG2	Low	5	4.1	0.82	Segregation
2	Waterval	Long low aspect	UG2	Low	9	7.2	0.80	Seg & accumulation
3	Target	Square aspect	Vaal reef with Quartzite	High	5.6	5.5	0.95	quite mixed
4	South Deep	Short high aspect	Conglomerate with Quartzite	High	4.4	7.8	1.77	quite mixed
5	Los Bronces	Long high aspect	Porphyry Copper ore	Medium	5.2	10.4	2.00	Segregation

The scale maker in all photographs is either a 64 mm disc or a 65 mm measuring tape.

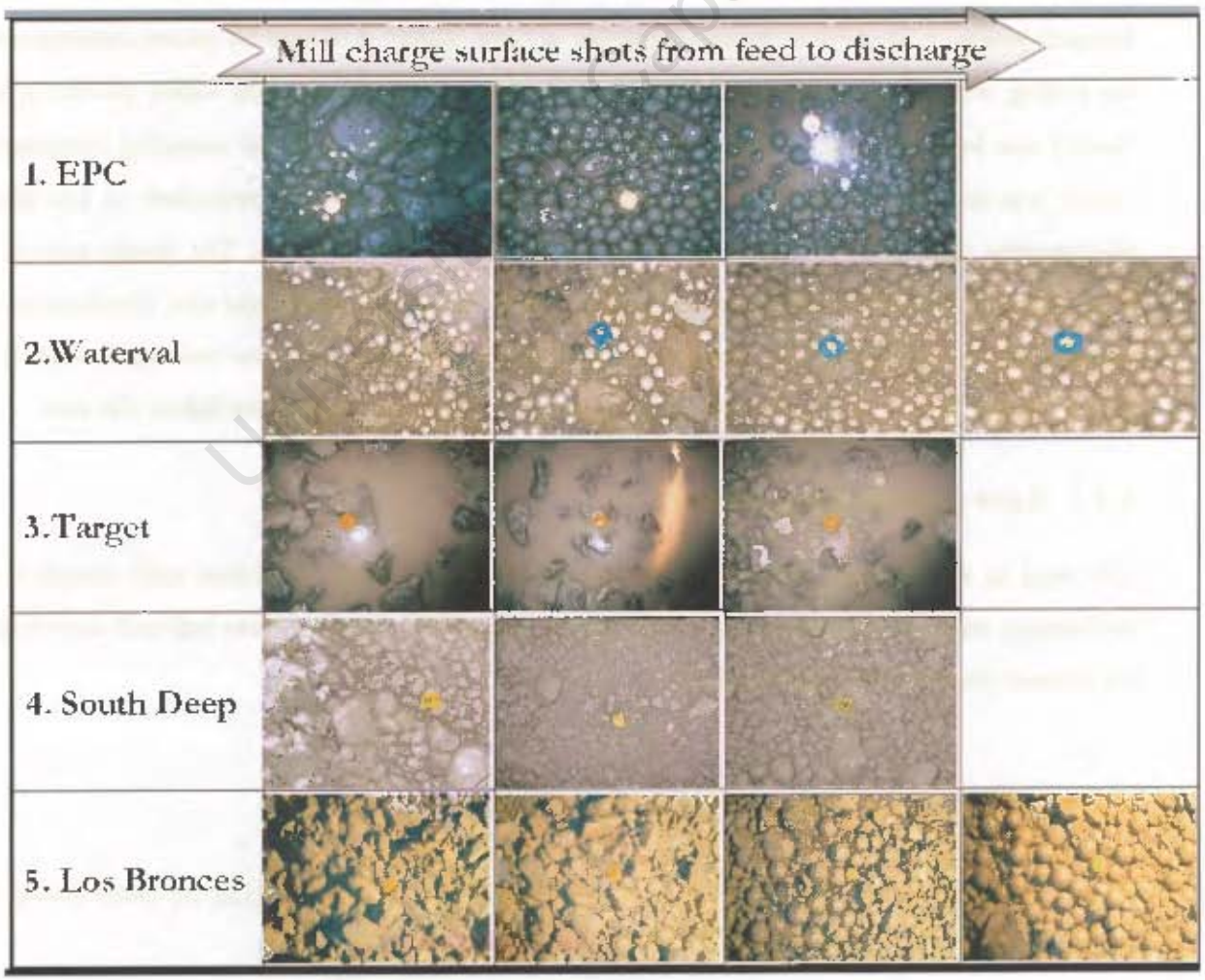

Figure 5-1: Charge surface photographs from five different plants

The images in Figure 5-1 show that there is visual charge surface size segregation of rocks from the inlet to the discharge end of the mill for EPC, Waterval and Los Bronces mills whilst Target and South Deep to be appear mixed.

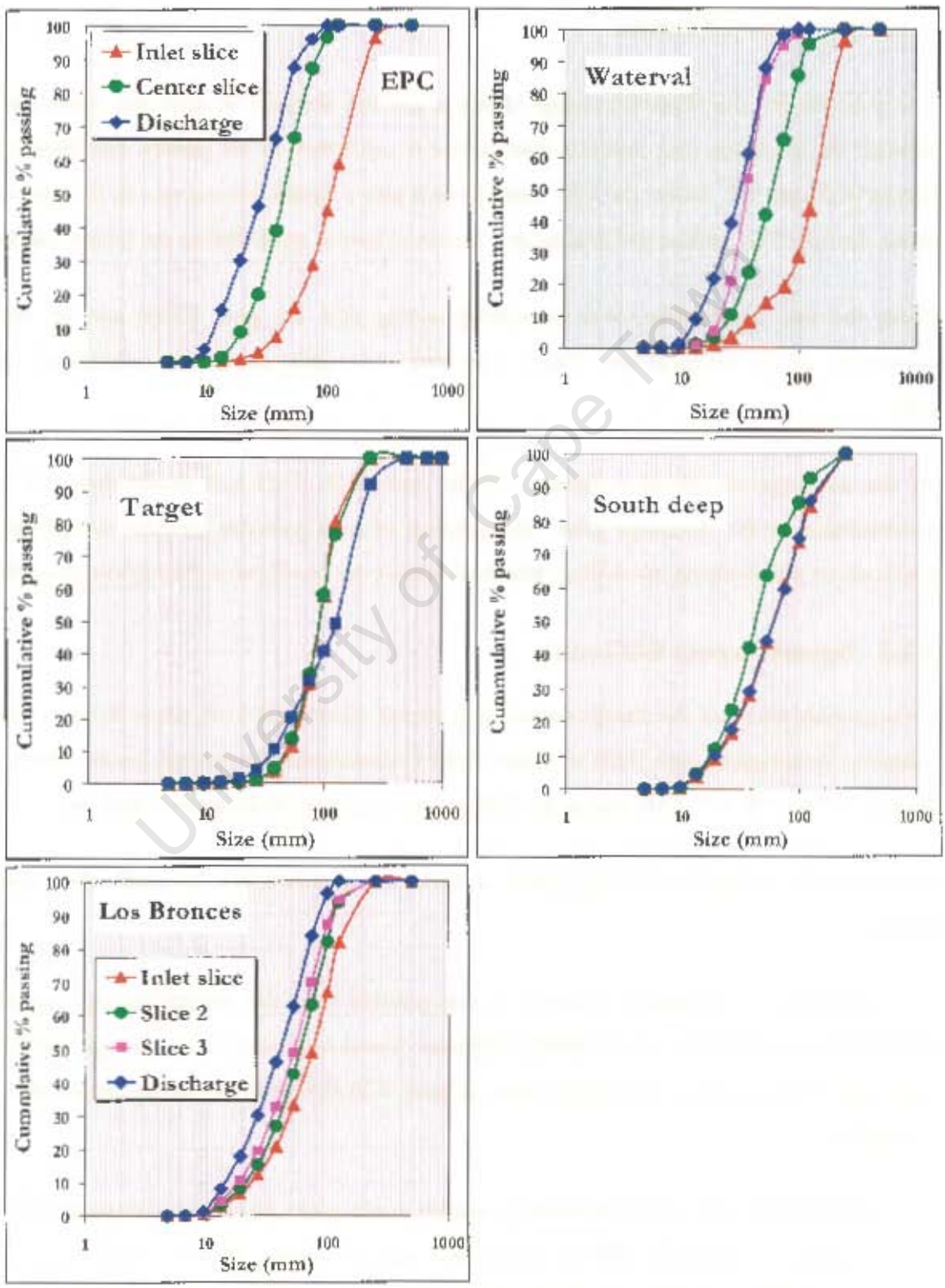

Figure 5-2: Charge surface particle size distribution plotted using split software

The particle size distribution in Figure 5-2 confirms this observation. There is a progressive reduction in rock size from the inlet to the discharge slice. This observation was ascribed to the mill length being greater than the diameter (low aspect ratio), for EPC and Waterval, and due to the mill length being long (5 m) for Los Bronces. The size distribution for EPC correlates with the trends obtained from the mill samples.

The pictures for the Waterval charge shows a gradual decrease in rock size from the inlet slice towards the discharge slice and this observation is confirmed in the particle size distribution graph shown in Figure 5-2. As for the EPC data, there is also a significant increase in the ball to rock ratio along the mill. The surface size segregation observed here is attributed to the longer mill length.

From the size distribution, it is interesting noting that the plus 10mm sub 20 mm particles accumulate at the discharge end. This is expected, as the grate aperture is only about 15mm in this mill.

As the discharge classification function of the current JK SAG mill model does not account for accumulation at the discharge grate, the build-up of near gate-size particles would have negative implications for discharge modelling, which assumes even distribution throughout the mill

5.1.2 Square aspect SAG mill

Photographic shots of the charge surface in a square aspect mill were taken during a comminution sampling campaign in June 2003 at Target Gold Concentrator, AngloVaal, South Africa. The 5.6 m long by 5.3 m (AR ≈ 1) SAG mill is fed with primary crushed underground gold ore.

A 64 mm disc was placed in the center of each second meter spot to mark slices along the mill length axis.

The water in the photographs (Figure 5-1) was omitted from the analysis during computing of the particle size boundaries in Split desktop software. Visual inspection of the charge surface shots and the plotted Split particle size distribution, (Figure 5-2) does not reveal significant rock size axial segregation.

It is hypothesized that ore competence enables some rocks to survive breakage and be located almost anywhere along the mill as shown in chapter 7 where the steel balls were found to be uniformly distributed along the mill. Coincidentally, the gold ore fed to Target Concentrator is

classified as hard (A*b = 45.7, ta = 0.32) and thus good mixing of the rocks across the mill should be expected in a mill fed with competent ore especially if the mill is short. The large rocks do appear to be accumulating at the discharge end of the mill, a function of the grate classification and slurry discharge causing a slight accumulation of these coarse rocks.

5.1.3 High aspect (short) SAG mill

Charge surface pictures in a short mill were taken in July 2005 during a comminution site survey at South Deep Gold Concentrator, Placer Dome and Western Areas, South Africa.

The South Deep SAG mill is a typical high aspect "pan cake" mill 4.4 m long and 7.8 m diameter, (AR = 1.8) and is fed with primary crushed gold ore from the second deepest underground mine in the world, (at the time of writing this thesis).

This charge surface size composition depicts a "perfectly mixed" SAG mill. The particle size distribution plotted using Split software from the three central positions along the mill in Figure 5-2 reveals no significant segregation.

It was expected to observe no segregation in a high aspect ratio SAG mill at South Deep due to the short residence time particles take to reach the mill discharge and also due to the high competence of the feed gold ore, allowing even bigger particles to be found at the discharge slice, and these particles may move back and fourth for further breakage. The observation of a lower segregation rate or minimal segregation in high aspect ratio SAG mills seems to be the reason why the current JK SAG model assumes "perfect mixing" of particles within the mill.

5.1.4 High aspect but still "long" SAG mills

The charge surface photographs taken in September 2004 at Los Bronces Copper Concentrator, Anglo base metals – Chile by Dr. Malcolm Powell and Mr. Percy Condori during a massive collaborative sampling campaign involving the Comminution Research group of the University of Cape Town, has revealed interesting, unforeseen, but not surprising segregation of rocks gradually reducing in size towards the discharge slice.

The Los Bronces SAG mill from where the pictures were taken is 5.2 m long by 10.4 m diameter, (AR = 2) and these charge surface shots are shown in Figure 5-2.

The observed segregation of rocks by size along the mill is attributable to the mill being long even though this SAG mill is high aspect.

The analysis includes balls, and a lot of balls are visible in the discharge end images, so these will bias the results to a coarser distribution than the pure rocks size distribution, this implies that the real rock segregation is grater than that given by the Split analysis.

From the particle size segregation, (Figure 5-2), it is believed that increasing the mill length of the SAG mill would increase the potential of the observed particle size segregation. The limiting mill length that would initiate an increased segregation rate is not known at the moment as this would require a huge data bank of charge surface photographs along several high aspect ratio SAG mills. However, since the Los Bronces SAG mill where segregation by size was observed is 5.2 m long, it seems logical to assume that high aspect mills of length greater than 5.2 m would exhibit particle size segregation. The ore type (hard or soft) could also play a role for the limiting mill length that would initiate significant size segregation.

5.2 PARTICLES RESIDENCE TIME ALONG AN AG MILL

The residence time distribution (RTD) studies were conducted jointly for the current study and for a separate project of slurry transport along SAG mills coordinated by AMIRA P9N. The input of the work of Mr. Percy Condori in this section is very highly acknowledged, Condori and Powell (2005).

5.2.1 RTD Methodology

Pebbles of different sizes of an open cast platinum ore were used to conduct residence time distribution (RTD) experiments. A low aspect (AR = 0.8) autogenous (AG) mill, 5.8m long and 4.5m in diameter with exceptionally large pebble ports was used for the RTD study. The pebble products of the autogenous mill are very competent and it was believed that some of them could survive the milling action.

The pebbles were classified into three size classes: small (32 – 63 mm), medium (63 - 90 mm) and big pebbles (90 – 125 mm). Three fast drying paint brands of bright colors; yellow, red, and green were used to paint the distinct pebble size classes. Additionally a salt tracer experiment was conducted to determine the residence time of liquid.

A good number of painted (tracer) pebbles were found at the mill discharge. This was only possible due to the extreme competence of the rock that was tested, and that the paint soaks into the rock.

The pebbles discharging from the mill were recorded by a video camera and counted visually to obtain the residence time distribution.

5.2.2 RTD findings

The experimental RTD data was characterized conveniently by the mixers-in-series model using the method of Levenspiel (1962).

Generally pebble sizing data obtained from inside the mill (after a crash-stop) or from the mill product is a combination of transport and grinding processes, and the two phenomena cannot be directly separated. However, in this testwork, pebbles of the same size as those fed into the mill were collected - as was clear from the painted surfaces still being visible - so the transport time could be independently derived. It is therefore possible to deduce the differences in RTD of different sizes in the feed as shown in Figure 5-3. Table 5-2 gives the data fitted to the tanks in series model. The liquid was modelled with a 0.7 minute delay.

Table 5-2: Mean residence time and RTD modelling results, (Mwansa, Condori, and Powell, 2006)

Tracer	Size, mm	Mean residence time (τ), min	Variance $G^2(t)$
Water	-	6.5	15
Small	32 - 63	9.1	12
Medium	63 - 90	11.2	17
Big rocks	90 - 125	9.9	9

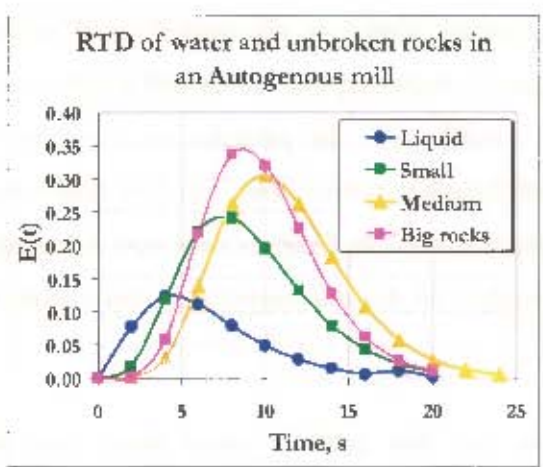

Figure 5-3: RTD of the solids and liquid fitted to N tanks in series model.

As expected, experimental data in Table 5-2 and Figure 5-3 shows progressive increments of the mean residence time with pebble size. However, the mean residence time of the biggest rocks used

in the experiment is slightly lower than the medium size rocks. The drop in the mean residence time for the biggest rocks may be attributed to the fact that most of the painted larger rocks in the feed could not survive breakage compared to small and medium rocks and therefore the detectable survivor big rocks with paint still on the surface after passing through the mill were narrower. The larger rocks with a higher breakage probability can thus not be useful tracers. The mean residence time of medium and bigger size pebbles were in the range of 34 - 42% greater than that of the liquid.

From Table 5-2, it is observed that the mean residence time of solids in the mill increases proportionally with increase in particle size, and therefore the *transport rate* of fine solids (slurry) below the grate aperture size is near to that of water, and is higher than the rocks transport.

5.3 SUMMARY

This chapter has shown that axial transport of particles in mills results in size segregation. The residence time is directly proportional to the mill length; the longer the mill, the higher the residence time. The RTD tests have confirmed that the mean residence time is a function of particle size.

Arising from the interpretation of the charge surface pictures, the effect of mill length and aspect ratio on the observed segregation is summarized as follows:

1. In low aspect ratio SAG mills, segregation of rocks by a gradual decrease in size towards the mill discharge slice, (Figure 5-2) is expected due to the mills being *longer*.
2. In square aspect mills, the particles would be expected to be reasonably "mixed" for shorter mill lengths, e.g. greater than 6 m, segregation could be prevalent and the significance of the observed segregation might depend on the mill length and the ore hardness.
3. In high aspect (short) mills, the particles are expected to be reasonably perfectly mixed provided the mill length is not too long (say less than 5 m as in Figure 5-2). For longer high aspect SAG mills as in the Los Bronces case, size segregation is expected to exist.
4. Mill length, regardless of the mill aspect ratio has a huge influence on the observed particle size segregation.

The RTD results show that fine particles travel faster than bigger rocks along the mill. This observation implies that the difference in particles transport favors the fine particles to be preferentially segregated and located towards the mill discharge position. It can then be deduced that axial segregation is influenced by the *transport* mechanism of particles along a mill as observed from both the mill length surveys and the RTD studies.

Chapter 6

6 AMANDELBULT METHODOLOGY

This chapter describes the improved methodology followed during the main sampling campaign for this thesis that involved emptying out the entire mill charge and sizing it into four separate slices along the mill length. The methodology described in this chapter is an advanced version of the earlier sampling technique used when conducting the preliminary plant trials. The planning before conducting the major survey is presented followed by the methodology for emptying out the entire mill contents. Sample preparation and processing are then described in detail. The chapter is concluded by the summary and recommendations of improving the sampling technique in future.

The charge of SAG mills has been emptied out before at the JKMRC, Stanley (1974) and Morrell (1993). However, emptying out the entire charge from industrial mills in separate axial slices has not been reported in literature; the sampling technique followed in this study is a novel methodology.

6.1 PLANNING

Because the amount of samples involved in the testwork was in the magnitude of tons and the difficulty of collecting the charge samples, planning constituted an important aspect of the sampling technique.

Planning included producing a detailed testwork proposal that was sent to the contact Process Metallurgist representing the plant Management. The testwork proposal outlined the testwork objectives, sampling schedule and a list of equipment among other sampling details. Planning also included arranging preferentially coarser mill feed for the test, checking flowrates, preparing collection of slurry from the mill, and organizing sampling equipment.

6.1.1 Testwork objectives

The three major objectives for the Amandelbult project were:

1. To conduct a full sampling survey around the old open cast plant milling circuit.
2. To drain slurry along the mill shell after a crash-stop, measure and size the solids.
3. To empty out the charge in separate axial slices and size the particles independently.

6.1.2 Milling circuit

The Amandelbult old open cast plant aerial photo is shown in Figure 6-1 and a schematic of the milling circuit where the test was conducted is shown in Figure 6-2.

Figure 6-1: Amandelbult old open cast plant aerial photograph

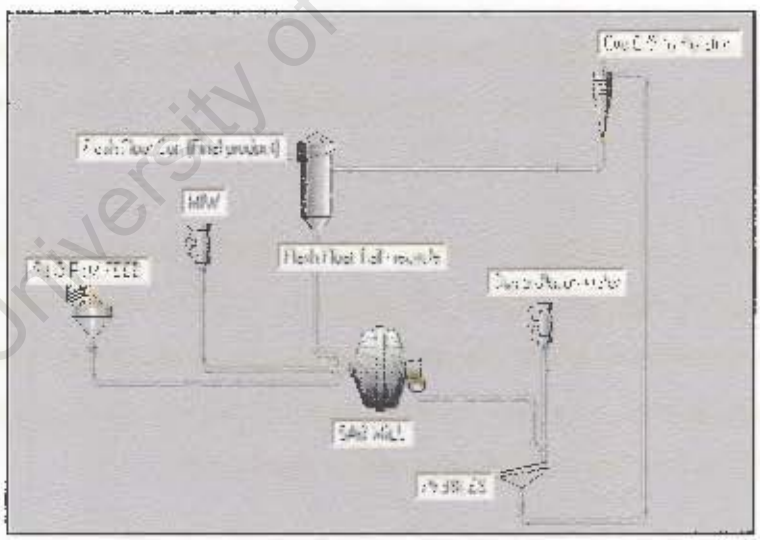

Figure 6-2: Amandelbult old open cast circuit diagram

The milling circuit shown schematically in Figure 6-2 comprises a single-stage RoM overflow SAG mill in closed circuit with a cyclone and a flash float cell with a re-circulating load of 130 %. The SAG mill receives open cast UG2 ore. The mill speed is 71 % of the critical. For this sampling survey, the total mill filling was 43 % and the calculated ball load was 22%.

Four circuit streams around the SAG mill; run of mine mill feed, trommel screen oversize pebbles, cyclone overflow, and cyclone underflow were sampled. The mill charge samples were sampled separately after the mill crash-stop.

6.1.3 SAG mill axial slices

The SAG mill of 3.5m diameter and 4.7m long is low aspect (0.7) classified as a South African style mill. The mill length was to be divided into four separate slices of 1.2m each from the inlet to the discharge. The four different slices were named 1 from the inlet to 4 for the last segment at the discharge end of the mill as schematically illustrated in Figure 6-3. During sampling, the mill slices were to be separated out and it was ensured that they remained separated as the charge was dug out. The charge was separated according to slices during sampling as described in detail in section 6.4.2.

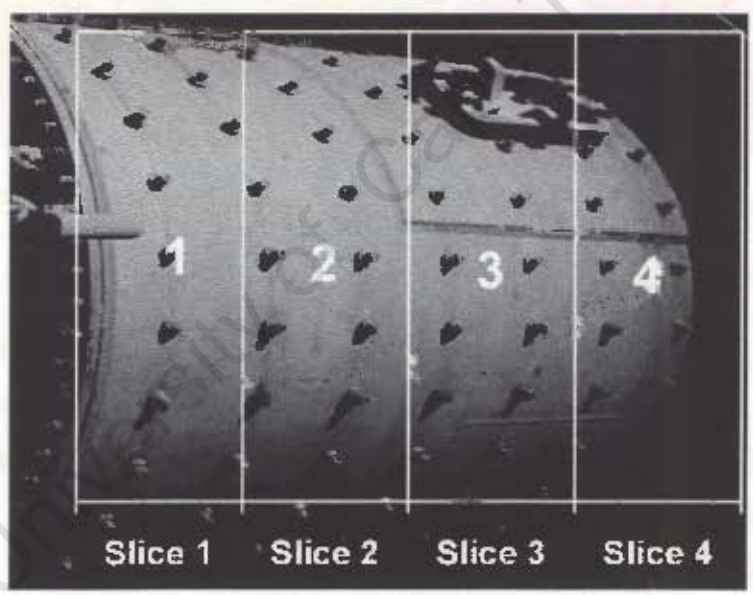

Figure 6-3: Schematic of axial slices divided along the Amandelbult SAG mill

6.1.4 Preferential coarse SAG feed

The original steady-state mill feed shown in Figure 6-4 was dominated by fines and did not comprise sufficient big rocks needed for an investigative segregation study. Therefore, for the purpose of observing a marked rock size distribution along the mill after the crash-stop, the mill feed with a coarser size distribution shown in Figure 6-5 was sourced from the open-pit, with great help from the resident open-pit Mining Engineer.

Figure 6-4: Original steady-state fine SAG mill feed

Figure 6-5: Specially arranged coarse SAG mill feed

6.1.5 Flowrates

The flowrate of the mill inlet water has a separate control panel near the mill while the make-up water to the sump, gland service water and trommel water have a common control valve. The flowrates were checked and stabilized three hours before the test. The Flash float wash water and the bond area spillage pump were to be switched off during the sampling campaign in order to restrict and control flowrates around the mill.

6.1.6 Mill slurry flow samples

Wood plugs shown in Figure 6-6 for use in blocking bolt holes prior to collection of slurry from the mill shell were arranged from the plant workshop. The plant relining crew was notified in advance to assist the investigators in removing bolts from the mill shell.

Figure 6-6: Wooden plugs used for blocking off bolt holes before collection of slurry

6.1.7 Mill charge coarse samples

Old used filter cloths were arranged and spread on a cleaned dry spot next to the mill for drying samples. Large plastic sheets were organized for covering samples at night.

6.1.8 Equipment and manpower resources

Appendix A4 summarizes the equipment used in the survey and the 21 personnel involved in the testwork.

6.2 STEADY-STATE TEST PROCEDURE

To obtain the necessary data on the significance of particle and slurry segregation in the mill, the sampling campaign conducted on the circuit was done at chosen operating conditions. This required careful planning of how the sample at each point around the circuit was to be taken, so as to ensure that it was representative of the stream from which it was taken. To achieve an optimum cut of the stream flow and a statistically adequate sample size it was necessary to construct customized sample cutters for some of the points on the circuit. A series of 5 samples of every stream were taken over a period of approximately 1 hour, during which the mill was held as close as possible to steady state operation. It was important to operate the mill under steady-state conditions as any fluctuations in the mill operation could be reflected in the components of each stream, and this would introduce errors into the samples resulting in poor modelling of the circuit characteristics.

The Amandelbult open cast plant circuit has no control room for online measurement of the flowrates and process data, the plant has local isolated panels situated near the plant equipment and the process data can be obtained manually from these panels. The other general plant data such as silo levels and mill feedrate can be accessed online from the Concentrator central control room at the

instrumentation department. The flowrates and general plant data, power draw, mill speed etc, were closely monitored from the instrument panels for about three hours before conducting the test. The observed process data from the panels was used to assess the stability of the plant before the test. During the test, the plant operating data was constantly checked and logged by hand from the local panels to ensure that the circuit was operating under sufficiently steady-state conditions for the sampling team to continue taking survey samples. The plant stability data is given in Figure 7-1, in chapter 7 and shows that the plant was in a steady-state condition during the survey. Had the operating conditions exhibited a significant variation from the set points, the samples would have been discarded and the test restarted at a later suitable period.

At the end of the test period the entire circuit was 'crash stopped', to provide an opportunity to measure the filling of the mill at the time of the test. This stop was also used to collect an adequate sample from the feed belt, which was used for a full feed sizing and ore characterisation. Emptying out of the mill charge in four slices was done after the crash-stop.

With the reliable set of samples obtained from the test, they were each sized into a full set of standard √2 screen sizes. The sizing data was then analysed by using JKSimMet to derive a full mass balance around the circuit. When found to be self-consistent the data was used to model the circuit. The mass balancing of data helped to check the integrity of the data before using it to model the circuit so as to avoid the consequences of "garbage in garbage out." The model fitted from the experimental data is useful for predicting the performance of the milling circuit under a range of conditions. By varying the conditions about the modelled circuit; such as coarse ore to fine ore ratio, water additions, mill filling, and feed size distribution an optimum circuit configuration and set of operating conditions can be derived.

6.3 GENERAL SAMPLING PROCEDURE

The procedure followed after the circuit survey sampling is outlined in the next sections.

6.3.1 Post crash-stop procedure

When the survey was completed, the SAG mill was crash stopped. This was done by simultaneously stopping the mill, the RoM feed, the mill inlet water, and the sump dilution water. At the same time, the mill sump pump was stopped (and the pump stop-cock opened to allow slurry to drain out). The spillage pump which had been running was also stopped.

The charge level was measured using the dip stick by inserting a long thin steel pipe from the top of the mill through an open hatch, marking the height on the pipe corresponding to the inside mill shell on the hatch opening and then checking the slurry level mark, when the pipe has been removed from the dip. Figure 6-7 shows the position were the measurements were taken. A schematic of the vertical cross section of the mill after a crash stop is shown in Figure 6-8. The heights from the inner edge of the hatch opening to the solid charge surface (H) as well as to the slurry surface (h_s) represent the measurements of the charge taken during the crash-stop. These were noted on the thin steel pipe using a marking pen.

Figure 6-7: Measuring slurry level using the dip stick method.

6.3.2 Mill load

The mill load constitutes the fractional filling (rocks and steel balls only) and the slurry filling. For the Amandelbult SAG mill being overflow, the slurry pool above the charge was determined before entering the mill through the "dip-stick" method and the value was virtually the same as that from the mill shell to the bottom level of the discharge trunnion.

6.3.2.1 Total charge filling

This vital piece of data was obtained from a physical measurement of the charge in the mill. The hatch of the mill was opened and the physical measurements taken inside the mill.

The charge load was measured from the average of a number of chords (S) taken across the surface of the charge. The internal mill diameter (D) and length (L) were measured. The measurements were onto the inside of the surface of the grid, not onto a lifter bar.

Another height (H) measurement for the charge level was obtained from inside the mill to act as a check for the data obtained using the steel pipe.

For the charge load close to 50%, as is common in most South African mills and as was in the Amandelbult old open cast SAG mill, it was important to measure the vertical height to the liner. The combination of chord length, height, and mill diameter gave a good measure of charge load. These measurements were carried out in 3 positions along the mill, to provide a reasonable average, and to allow for a variation in liner thickness and load level. The internal mill length was also measured in 2 points, from the end shell plates, and against the mill shell.

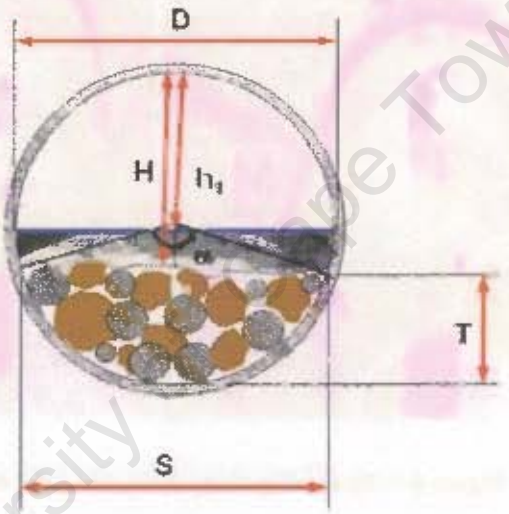

Figure 6-8: Schematic vertical cross-section of the mill after a crash stop

6.3.2.2 Mill filling equations

From Figure 6-8, the angle α and charge thickness T are given by equations (6.1) and (6.2).

$$\alpha = 2\arcsin\left(\frac{S}{D}\right) \tag{6.1}$$

$$T = \frac{D}{2}\left(1 - \cos\frac{\alpha}{2}\right) \tag{6.2}$$

Where;

S = chord across charge

D = internal diameter of the mill;

T = thickness (depth) of charge

H = vertical height from charge to liner

h_1 = vertical height from the slurry surface to the liner.

Also, $H = D - T$ and the two must be checked to correlate, if not then the measured H is used to derive T. The mill filling can then be calculated from equation (6.3)

$$\text{Percentage mill filling} = 100\left(\frac{D\arcsin(S/D) - 2HS/D + S}{\pi D}\right) \qquad (6.3)$$

Details of the measurements and survey techniques are contained in Appendix 4.

6.4 EMPTYING OUT THE MILL CONTENTS

The charge was emptied out in phases. Slurry was drained out first followed by demarcating four slices along the mill and then removing the particles separately from the mill.

6.4.1 Slurry

A novel method for collecting slurry from a standing industrial mill is described in this section. Slurry was collected from the mill through bolt holes on the mill shell.

Transport of slurry along the mill length has been assumed to be different from that of rocks due to factors such as the slurry rheology/viscosity as well as solids concentration in the slurry. The aim of collecting the slurry sample was to investigate the segregation of solids contained in the slurry along the SAG mill. The second objective was to quantify how much of the slurry was in the mill in relation to the charge and thus calculate the voidage (space occupied by slurry in the charge). Although care was exercised in collecting this sample, spillage occurred and an estimate of the voidage was made through back-calculations. Slurry spilled was calculated to be half (50%) of the total drained slurry.

The method was designed to minimise mixing of the fine particles along the mill length while the slurry was being collected from the mill shell. Immediately after the crash stop a row of bolts would be removed, and the holes plugged. The mill would then be rotated until the holes were at the base, then plugs would be knocked out simultaneously and the slurry drained out via hoses into drums that were positioned underneath the mill.

Unfortunately in the test work the relining crew were not available to remove the bolts, so the slurry drainage could not be conducted immediately and it had to be delayed until the next morning. The

mill was barred into a position where the slurry could not spill from the bolt holes. The relining crew helped removing bolts from the mill shell and all of the eight bolts in the row along the mill length were removed. When the bolts had been removed, wood plugs were used to block out bolt holes to prevent the slurry from spilling while the mill was barred in position to collect slurry samples underneath. Plastic was wrapped around the wood plugs before they were inserted into the bolt holes, in order to prevent any leaks while barring the mill into position for slurry collection. The plugging of the mill is shown in Figure 6-9.

Figure 6-9: Knocking off bolts, inserting wood plugs into bolt holes & wrapping plugs with plastic

The mill as shown in Figure 6-10, was carefully barred into a position were the slurry could be drained through hoses into the 210 ℓ labelled drums. Four people were placed to handle each bolt hole; one person was responsible for removing the wood plug and later help in filling slurry into the correctly labelled drums while two people were immediately to insert the hose onto the surface edge of the bolt hole and the last person was responsible for directing the hose into the drum being filled.

Figure 6-10: SAG mill barred into a position ready for slurry draining

Hoses of 50mm diameter were used to direct the slurry from the bolt holes into the drums. Of the eight wood plugs along the mill shell roll, four plugs - from positions 2, 4, 6, and 8 - were simultaneously and carefully removed and immediately the hoses were inserted at the bolt holes. As each drum filled, the hose was immediately placed into the next drum, minimising spillage. The slurry was drained until there was no flow from the mill, so it was hoped that all the slurry was collected. Later, when the mill was dug out, it was observed that the charge was damp, but not wet, so it is concluded that this technique does successfully drain the mill of slurry.

Figure 6-11: Slurry collection from four bolt holes

Draining slurry from bolt holes along the mill shell is illustrated in Figure 6-11 whilst the slurry collected into labelled drums is shown in Figure 6-12. As shown by the researchers' shower in Figure 6-13, sampling of slurry presented some difficulty! Due to high discharge flows, spillages were experienced, especially at position 3. This section had the strongest flow of the four positions sampled.

Figure 6-12: Drained slurry from four bolt holes along the SAG mill

An estimated 8600 ℓ of slurry was drained out from the mill - including that which was lost through spillages. The processed slurry weighed 1.5 tons dry mass.

As this was the first trial of the slurry collection method. It was a worthwhile experiment, and shed light on challenges and improved techniques of slurry sampling in future projects.

Figure 6-13: Sampling the slurry rewarded the researchers with a shower!

6.4.2 Solid particles

Removal of the charge commenced after all the slurry had been drained from the mill. Figure 6-14 shows shovelling out of the charge from a position (slice) along the mill into a bucket.

Figure 6-14: Collection of the charge from the SAG mill

The investigators marked out the slices using mill liners and ensured the slices remained separated as the charge was dug out. The charge from each slice was separately emptied out from the mill using colour coded buckets and deposited on a specific corresponding slice at the drying spot. Figure 6-15

shows the sample collection zones inside the mill whilst the corresponding slices at the drying spot are shown in Figure 6-16.

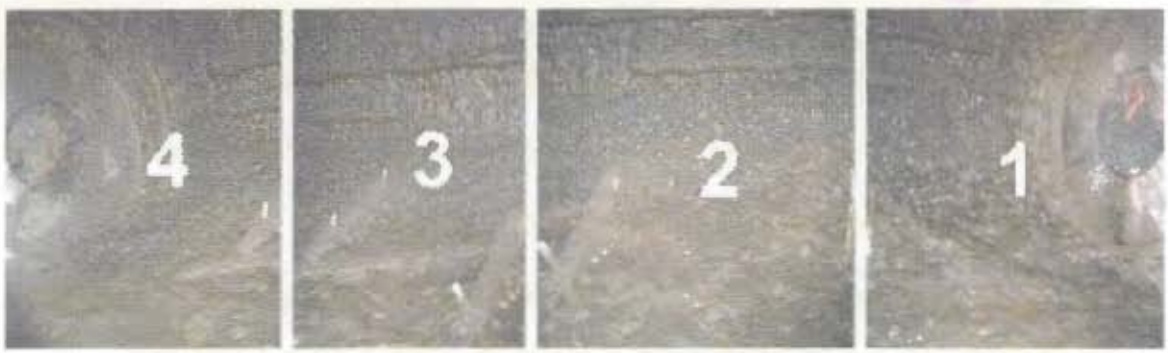

Figure 6-15: Sample collection slices inside the Amandelbult old open cast SAG mill

Figure 6-16: Drying spot corresponding to the slices inside the SAG mill

Collection of charge samples took four days to completely empty the mill. In the initial two days of digging out the charge, the charge was removed simultaneously from all the four slices with slow occasional barring of the mill once the charge got very compacted. When the charge layer inside the mill was low, several strategies were employed to quicken the removal of the charge from the mill and allow for the mill to start running again.

6.4.3 Color coding of buckets according to the slices

Each slice had a different bucket color used to pack the charge and taking it out of the mill to the drying spot. Orange buckets were used for slice 1 (inlet), blue for slice 2, green for slice 3, and yellow for slice 4 (discharge).

Figure 6-17: Color coded buckets used to transfer the charge from4 mill slices to the drying spot

6.4.4 Sorting samples to respective drying spot

To avoid mixing samples, two people were assigned to check that the color coding was adhered to, one inside the mill and the other during dumping the samples at the drying spot.

6.4.5 Covering samples

To prevent samples getting soaked in case of rain, samples were covered before leaving the site at the end of each working day as shown in Figure 6-18.

Figure 6-18: Covering segregation samples after each working day

Figure 6-19 shows a technique employed to remove the charge from a specific zone inside the mill via a custom-designed iron sheet launder followed by team effort of removing the emptied out charge to the respective drying zone. In this technique, slice 2 which was directly opposite the open hatch was removed first followed by slice 1 before dumping slice 3. When the three zones had been completely emptied, the remaining particles of slice 4 were removed by continuously barring the mill, forcing particles to move towards the hatch. The particles were then removed once the hatch was at the bottom position of the mill. The emptied out charge was then transferred to the respective drying spot.

Figure 6-19: Dumping charge through iron sheet followed by transfer to the drying spot

Figure 6-20 shows the inside of the SAG mill and three jubilant UCT researchers after emptying out the entire mill contents on the fourth night of charge removal.

Figure 6-20: Jubilant investigators after emptying out the entire mill charge!

6.4.6 Mill charge samples

The mill charge samples were processed in four phases. The slurry collected from the mill was processed separately from the rest of the charge. Since balls were required for the mill start–up, they were screened first and returned to the mill. Then the remaining solids from the charge were processed. Figure 6 25, illustrates the screening of the solids mill charge.

6.4.6.1 Mill slurry samples

The volume of the collected slurry was measured and the spillage was estimated after careful analysis and consultation with all the members of the sampling team. The clear water from each drum was decanted off and the remaining solids were sun dried on clean filter cloths. The slurry cake in the drums from each slice were mixed and dried together. The dried slurry fines were screened on a 1mm

screen. The oversize was screened from the topsize down to 1mm using the procedure for coarse screening. The sub 1mm material was processed following the standard procedure for fine screening.

6.4.6.2 Steel Balls

The balls were screened using hand sizers and then at sub 45mm, the 450mm diameter screens were used with the standard technique for sizing coarse material. These balls were screened down to 4mm and filled in drums that were placed on pallets, (Figure 6-21) before being returned back into the SAG mill.

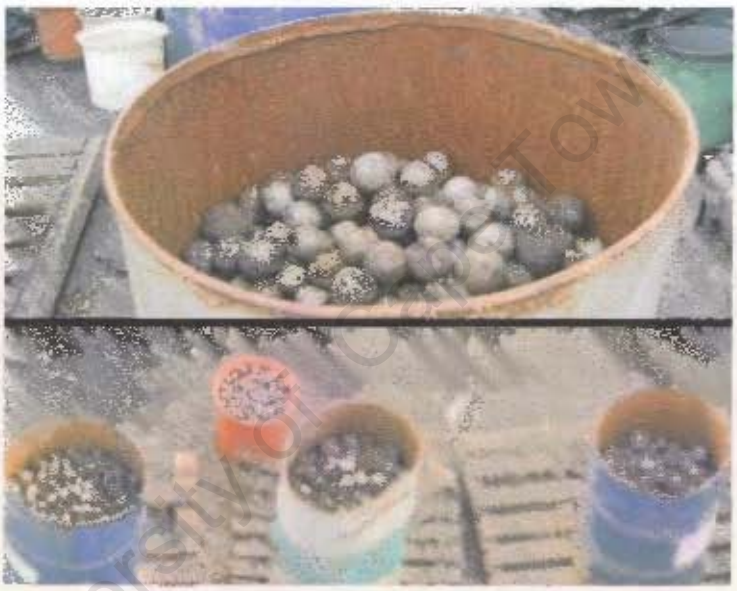

Figure 6-21: Screened steel balls

Balls less than 22.4mm shown in Figure 6-22 were classified as scats and were not returned to the mill. The + 22.4mm balls were returned to the mill via the RoM feed conveyor belt.

Figure 6-22: Steel ball Scats

Other pieces of metal scrap were found within the charge. The metal scrap from the charge shown in Figure 6-23 were isolated from the rest of the charge, weighed and then discarded.

Figure 6-23: Scrap metal found in the charge

6.4.6.3 Rocks

The rock particles were screened separately for each slice. The samples from each slice were weighed, dried, and screened separately in the same manner as the RoM belt cut sample. The rocks were picked out from the fines and heaped in one area (Figure 6-24) after which they were sized and counted if they were in the hand sizing magnitude.

Figure 6-24: Coarse rocks from slice 1

6.4.6.4 Fines from dried charge slices

The fines (minus 1mm particles) from the four separate zones were split separately using the coning and quartering method to produce two bins from approximately a ton of fines per slice. The resulting fines were further split on the rotary splitter to produce samples of about 300g which were suitable for

the standatd wet and dry fine screening procedures. Sizing of the dry emptied out charge is shown in Figure 6-25.

Figure 6-25: Sizing of mill coarse charge

6.4.7 Screening of coarse + 1 mm material.

For the bulky charge and RoM feed samples, it was important to follow a systematic and consistent procedure to obtain good results. The general procedure is laid out stepwise:

- The + 1 mm material should be moved to a chosen clean screening spot.
- Tare at least 20 buckets, and write the tare on each bucket.
- Line up the screens and hand sizers in a long row on top of buckets or drums. Label each bucket as sub (screen size) plus (next screen size down), e.g. below the 63mm screen the bucket must be labelled – 63 mm +45 mm. This is to avoid confusion as with this technique the contents of each bucket are the size passing the screen, not retained on it – as is normal ptactice. Figure 6-26 shows screening of coarse rocks.

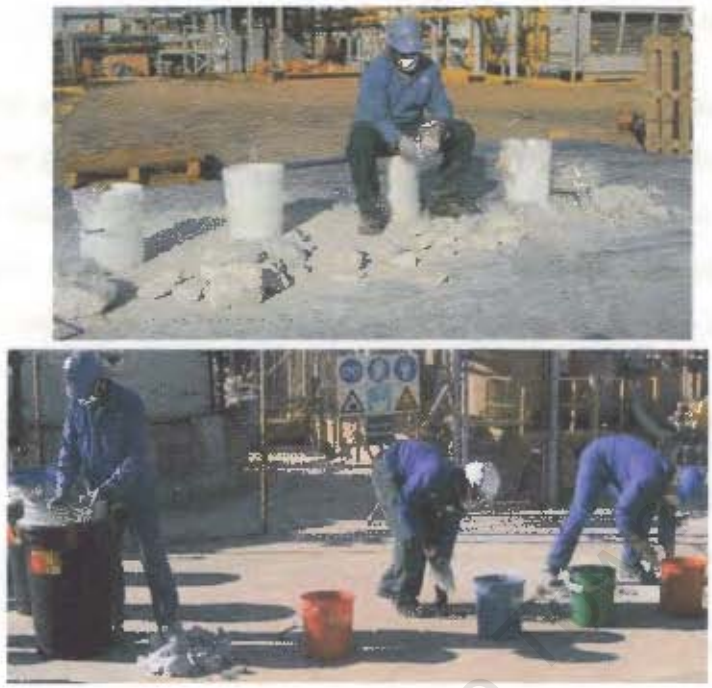

Figure 6-26: Hand screening of coarse rocks

- Remove larger rocks by hand, immediately brushing off any fines into the bucket, and pass along the row of screens. A rock must always be tested on the screen size below the final one it passes through, so as to ensure it is in the correct size fraction.
- If a bucket fills up then place an empty one in front and continue screening into that.
- Do not remove any buckets until the entire sample has been screened.
- Then start from one end and work your way along, weighing each size fraction at a time. This prevents the samples from being mixed up. If the samples are not required for further analysis or breakage testing then as you finish weighing each sample, decant back into the original drum for discarding. Weigh the minus 1mm bucket and remove the sample for fine screening. Figure 6-27 shows screened coarse rocks.

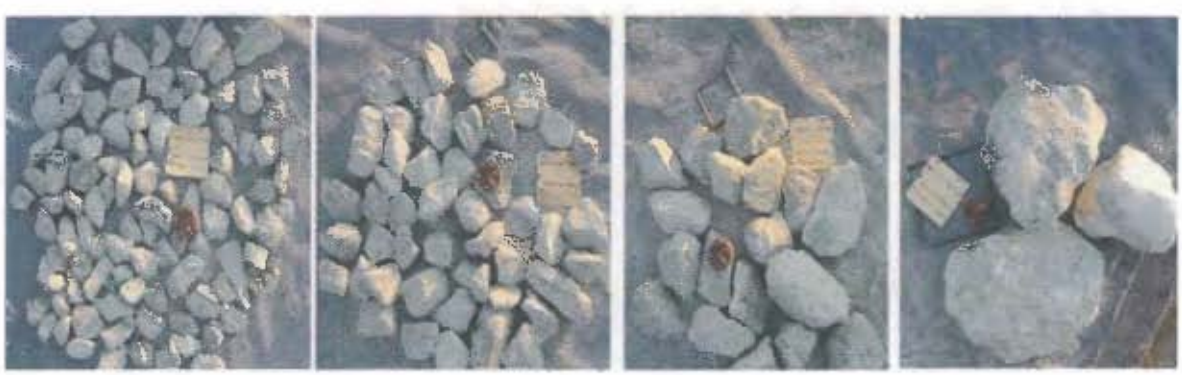

Figure 6-27: Coarse screening routine showing screened large rocks

6.5 DROP WEIGHT TESTS METHODOLOGY

Five samples, one from the screened Rom SAG mill feed, and four samples from screened rocks at mill positions of slice 1 (inlet), slice 2, slice 3 and slice 4 (discharge) were subjected to a drop weight test procedure to study the impact and abrasion properties of the rocks relative to their position along the mill. The drop weight tests for this testwork were conducted at Anglo Platinum Research Centre (ARC) in South Africa. The JK drop weight test is described in detailed in Appendix A3.

6.6 SUMMARY AND RECOMMENDATIONS

This section presents a summary to the methodology for emptying out the mill charge and also highlights the recommendations to improving the sampling technique.

6.6.1 Summary

The schedule for the mill charge emptying out testwork from start to finish is summarized in Table A4 - 2 in Appendix 4. The actual duration for emptying out the charge was 4 days, the entire campaign, including preparation, a trial survey, ore sourcing, and sample processing took 37 days.

As far as the emptying out of the charge from the mill in four slices along the mill is concerned, the technique used was quite adequate even though it clearly could be improved. For instance, the method to use color coded buckets to remove the charge from the four slices and dump the material onto the matching slices at the drying spot was most successful.

6.6.2 Recommendations

The recommendations suggested to improving the current methodology of emptying out the charge from SAG mills cover slurry draining and quicker axial removal of particles.

6.6.2.1 Draining the slurry from the mill shell

Issues to be addressed:

1. If the opportunity exists, it would be advantageous to trial the fitting of the stoppers prior to the test.
2. Larger diameter hoses would be required, at least 100mm, preferably 150mm.

3. Since there was uneven flow from the holes, it is concluded that this was a function of the mill standing overnight prior to draining - causing settling and partial blocking of some holes. So the mill must be drained as soon as possible after the crash stop.
4. The axial distance of one hole every 1.2m was sufficient.
5. Collection drums should be new with proper lids, so that they can be transported without spillage for weighing and processing.
6. The volume in each drum should be measured.
7. The drums from each segment should be weighed together, the plant weighbridge would be the most convenient.

6.6.2.2 Emptying out the mill charge

1. Separate samples of about one and half drums must be collected from the central spot of the axial slices by digging out particles to about 1 m deep before emptying out the rest of particles at each slice. The collected particles will be required to check if a sample would be representative of the slice from which that charge is dug out.
2. Custom-made sampling boxes to be used for loading the charge along the mill length.
3. The sampling boxes to be placed along the mill, each at a specific slice and then the mill would be barred to allow the charge to be filled into the boxes. The mill would again be barred back to its original position to allow removal of the sample boxes out of the mill.
4. Relining machine to aid collection of samples in the filled boxes from inside the mill.
5. Mechanical mobile screening to be used to quicken the coarse screening process.

Chapter 7

7 AMANDELBULT RESULTS

This chapter reports the findings from sampling the milling circuit of the Amandelbult old open cast plant and also reports the results from emptying out and sizing the entire mill charge into four different slices along the mill. The findings from the sampling survey around the SAG mill are presented first followed by the results from sizing of the slurry, rocks, and the steel balls. The ore characterization of the rocks selected from the RoM mill feed and from the four positions (slices) along the mill are presented and analyzed before the chapter is concluded by presenting a summary on the results from emptying out the whole mill charge.

7.1 CIRCUIT SURVEY RESULTS

The circuit survey results comprised the plant steady-state trends and the general circuit data. The test was conducted on 15th March 2004 between 12:50 and 13:50 hours after which the SAG mill was crash stopped and the whole plant was shut down.

7.1.1 Steady-state plant data

The plant operating data monitored and logged by hand within the test period is shown in Table 7-1 and is graphically represented by the process variable trends in Figure 7-1. There was instability in the mill inlet water addition (Figure 7-1) and the cyclone feed pressure that fluctuated a bit, which could be attributed to inconsistent feed. This was due to the coarse feed to the mill, whilst the throughput had been maintained constant and this allowed lapses and empty spaces on the feed belt conveyor each time very big rocks entered the belt. However, the fluctuations in the mill inlet water were not too high to affect the overall stability of the circuit. The plant was therefore operating at reasonably steady-state during the test period.

Table 7-1: Summary of plant operating data of the circuit before the test

Process variable	Average value	S D
Power draw, kW	898	3
Mill discharge flow, m^3/h	147	23
Sump water, m^3/h	50	19
MIW Flow, m^3/h	12.5	3.6
Cyclone pressure, kPa	16.4	3.5
Mill discharge SG, kg/m^3	1.6	0.1

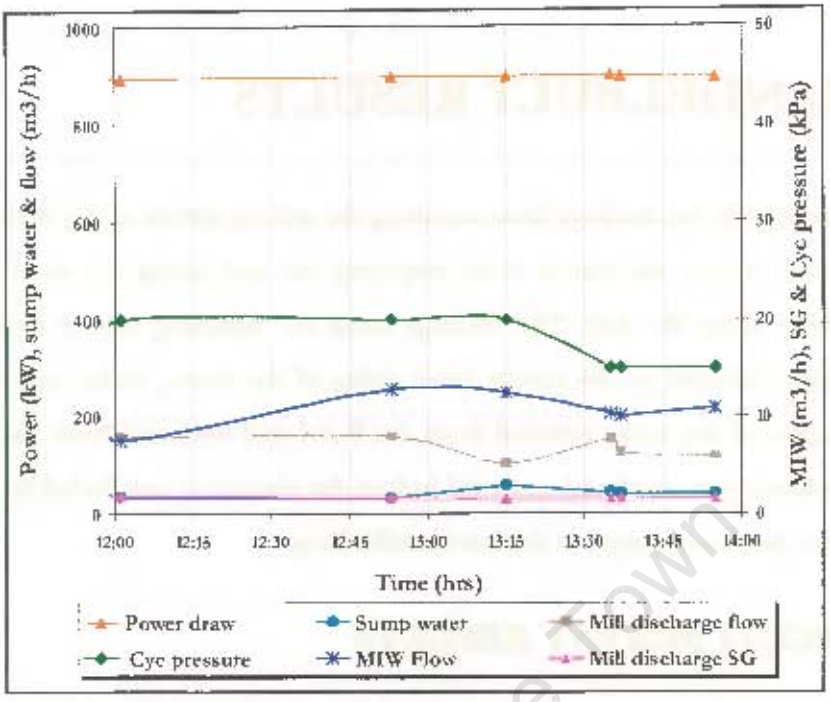

Figure 7-1: Steady-state Amandelbult plant trends

7.1.2 General Plant survey results

The plant data detailing how the circuit streams were obtained is given in Table 7-2.

Table 7-2: Summary of plant circuit data

Sampled streams	Flowrate	% solids
RoM feedrate, tph	34.2	95.7
Trommel pebbles, tph	0.01	98.9
Cyclone U/F, tph	44.8	64.3
Cyclone O/F, tph	-	33.6
Instrument measured		
RoM feedrate, tph	34.2	95.7
Mill inlet water, m^3/h	12.2	-
Mill discharge sump water, m^3/h	49.5	-
Mill discharge flow, m^3/h	145.0	-
Calculated/mass balanced		
Mill discharge, tph	78.94	67.1
Trommel screen U/S, tph	78.93	47.1
Cyclone O/F, tph	34.2	-

The flowrates and percent solids of the circuit were within the acceptable range. The pebbles flowrate is very low so they are not immediately recycled back to the mill. The pebbles are allowed

to accumulate below the head pulley of the pebble belt conveyor over a long period and are only fed back to the mill after about one week.

The particle size distributions of streams around the SAG mill are shown in Figure 7-2. The entire particles (steel balls and all rock solids) emptied out from the mill are represented by the 'total mill contents' size distribution. The cyclone overflow has the finest size distribution as expected, since it is the final product of the circuit while the mill contents and trommel pebbles are the coarser streams. The total mill contents (Figure 7-2) reveal that there is little material between 16 mm and 500 µm, which is known to be typical of the size distribution of the mill charge. This is similar to the size distributions obtained from the full mill contents sizings conducted by Stanley (1974) and Morrell (1989). This form of size distribution is also derived from JKSimMet SAG mill model fitting, based on this being the standard form of the mill charge size distribution.

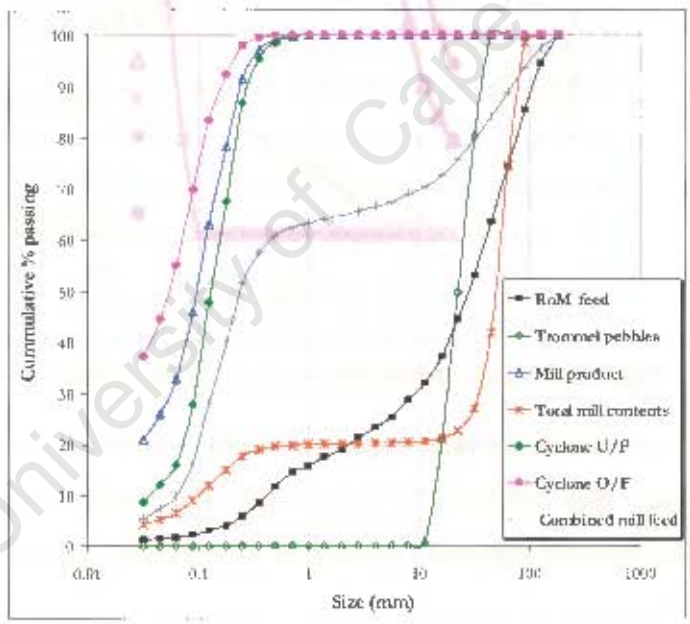

Figure 7-2 Full circuit particle size distribution

7.1.3 Mass balancing and model fitting

The data was mass balanced using JKMBal, the mass balancing software contained in the mineral processing simulator JKSimMet.

The stream experimental and mass balanced values matched closely, as shown in Table 7-3 and in Figure 7-3. The experimental data is represented by points whilst the balanced data is given by the solid lines. Since the experimental curves lie on top of the mass balanced curves, it can be deduced that the sampling technique followed during the sampling period was suitable.

Table 7-3: Summary of Experimental versus mass balanced stream data

Stream	TPH Solids		% Solids		P80 (mm)		% Passing 75 µm	
	Exp	Bal	Exp	Bal	Exp	Bal	Exp	Bal
RoM SAG feed	34.2		95.7	-	74.9		1.9	-
SAG mill product		78.9	-	67.1		0.2	-	39.3
Trommel pebbles	0.01	0.01	98.9	98.9	31.4	31.4	0.6	0.6
Trommel U/S	-	78.9		47.1	-	0.2	-	39.3
Cyclone U/F	44.8	44.8	64.3	64.3	0.2	0.2	21.6	21.6
Cyclone O/F	34.2	34.2	33.6	33.6	0.1	0.1	62.6	62.6

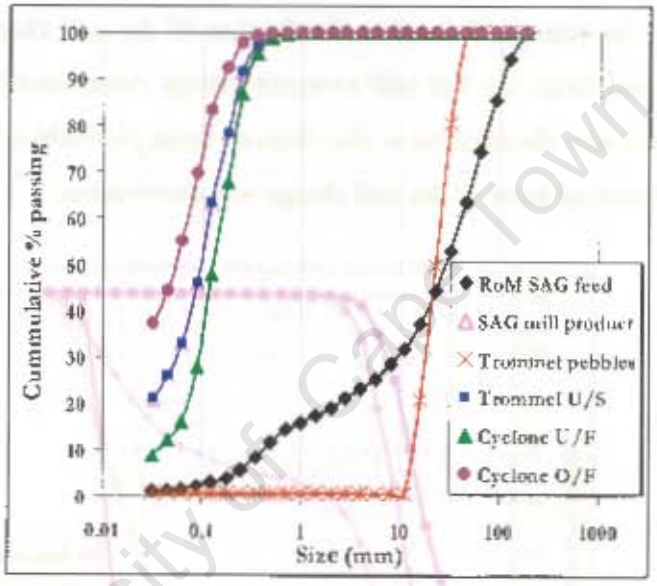

Figure 7-3: Graph of Experimental versus mass balanced stream data

The Amandelbult mill, which the plant regard as "SAG", could not be modelled as a SAG mill as it is overflow, carrying a high ball load (21.65 %) and is what locally known as a run of mine ball mill. Thus, the mill characteristics imposed a restriction on modelling options.

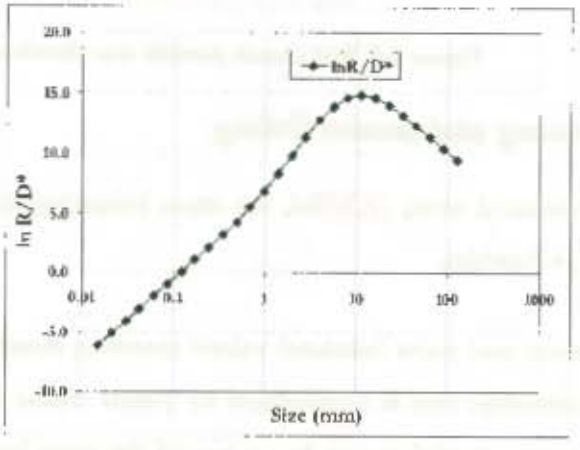

Figure 7-4: Breakage rate in the Amandelbult mill

The breakage rate curve for the mill obtained using the perfect mixing ball mill model is shown in Figure 7-4 and follows a typical ball mill breakage, increasing with particle size.

From Figure 7-4, the highest breakage occurs for particles about 10 mm in size 11.2 – 8 mm. The breakage rate at 10mm would be commensurate with a ball/rock top size of 150 mm as per the JK rule of thumb model, which is consistent with the feed and ball size data. The rate of breakage drops for particles less than this especially for the small particles where the rate drops more rapidly. The breakage rate is low for the rocks in the coarse size range. The typical pick up of breakage rate at the coarse end for SAG mills is not observed, but as this is fitted with 4 knots and is ln (R/D), it is most likely masked.

7.2 RESULTS FROM EMPTYING OUT THE CHARGE

The ore for running the test was specially arranged from the open pit by selectively picking bigger rocks from the heaps at the pit and monitoring the transport of the ore from the pit to the old open cast plant feed silo.

7.2.1 Full mill measurements and particles axial distribution

A summary of the measured particle masses of the charge emptied out from the SAG mill and the key testwork data is given in Table 7-4. The total weight of the emptied out charge was 62.2 tons making up a total mill (slurry) filling of 43 % and a high ball load of 22 %. The volume of charge could not be cross-checked by summing all solids and slurry volumes, because of the slurry spillage during sampling. The JK power model calculated to be 885 kW when compared with the power of 897 kW drawn during the sampling period are quite close.

The calculated voidage of the mill charge was 0.38, which closely matches the accepted standard voidage of 0.4. The ball load could not be calculated using the chords and height method that is usually applied after a grind out as it was not possible for this study because the rock particles would be ground, so the ball filling was calculated from the absolute steel ball volume using a 40% voidage.

Table 7-4 also gives the mill measurements and calculations of residence time of the charge and liquid using the mass and volume flowrate of the mill product i.e. (residence time = mill hold-up/flowrate). The calculated residence times show that liquid travels faster than rocks and it can

therefore be inferred that slurry (fine particles which are completely entrained in the liquid) must also have short residence times through the mill.

Table 7-4: Key test work data

Emptied out Charge masses		
	Weight, tons	Volume, m^3
Steel balls	46.6	5.95
Rock particles	14.1	3.6
Drained slurry	1.5	3.9
Total	**62.2**	**13.4**
Mill measurements		
Mill power, kW	897.8	
Mill Length, m	4.7	
Mill diameter, m	3.5	
Mill volume, m^3	45.8	
Mill Speed, % critical	70.9	
Slurry filling, %	43.2	
Fractional mill filling, %	23.0	
Ball load, %	21.6	
Fresh feed (RoM), tph	34.2	
Mill product, tph	78.9	
F80, mm	74.9	
P80, µm	115.0	
Calculated OWI (kWh/t)	29.3	
Steel balls top size, mm	90	
Voidage	**0.38**	
Charge properties and calculations		
Average Ore SG	3.96	
Steel balls SG	7.80	
Water residence time, min	11.8	
Solids residence time, min	13.5	

7.2.1.1 Mass distribution of particles along the mill

The dry mass distribution of the different particle species along the mill is summarized in Table 7-5 and shown graphically in Figure 7-5. From Table 7-5 and Figure 7-5, it is evident that steel balls and the total mill contents are generally uniformly distributed along the mill except for slice 3 where there is a low ball charge. As expected, slice 1 has a higher rock loading than the other slices. The solids content is dominated by the fine particles (slurry).

Table 7-5: Breakdown of the dry weight (tons) distribution along the mill

	Slice 1	Slice 2	Slice 3	Slice 4	total
Steel balls	12.4	12.5	9.2	12.3	46.4
Mill rock particles	6.0	3.1	3.3	3.3	15.7
Metal scraps	0.03	0.03	0.04	0.06	0.15
Slurry, - 1 mm	4.1	2.5	2.9	3.0	12.4
Big rocks, + 45 mm	1.1	0.3	0.1	0.2	1.7
Steel scats	0.24	0.03	0.14	0.54	1.0
Total mill contents	18.4	15.6	12.5	15.7	62.2

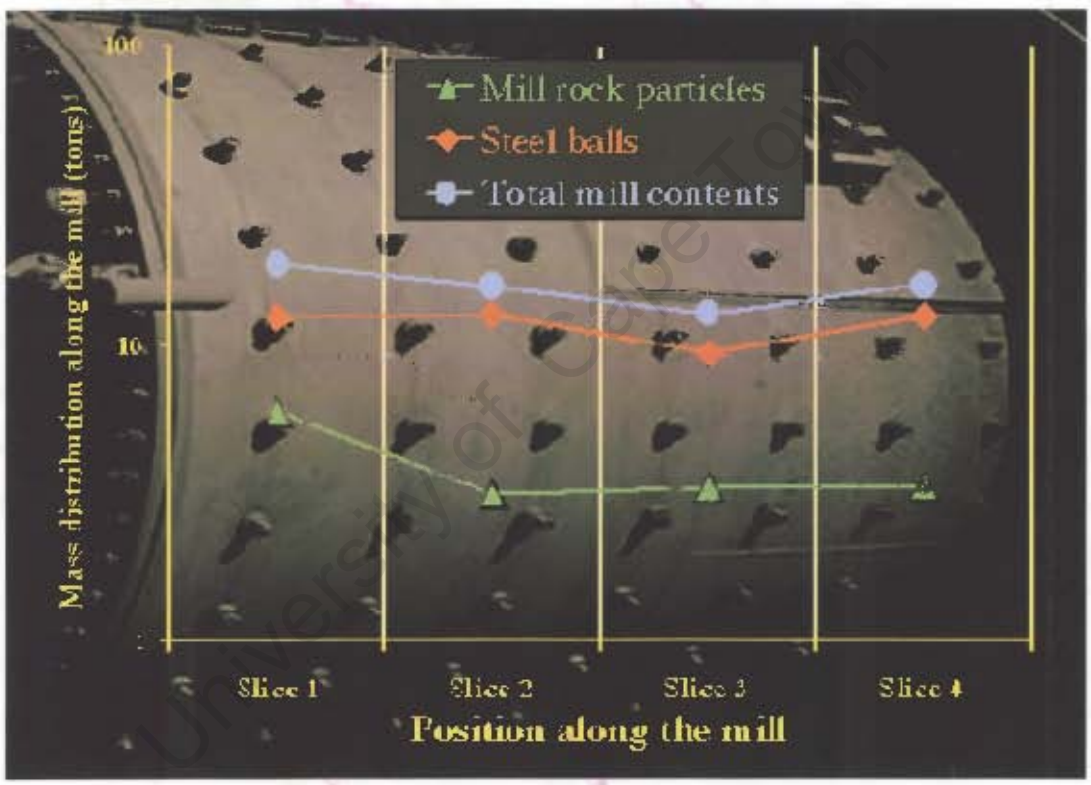

Figure 7-5: Mass distribution of rock particles and steel balls along the mill

7.2.1.2 Size distribution along the mill

The full size distribution of particles along the mill is shown in Figure 7-6. The full mill size distribution shows that the steel balls were coarsest. The mill slurry, lying on top of the mill product (Figure 7-6), and which is essentially the same stream, was the finest sample. As the solids removed from the mill contained a considerable mass of fines, the total slurry and the rock masses were added together to give the 'mill rock particles' size distribution shown in Figure 7-6.

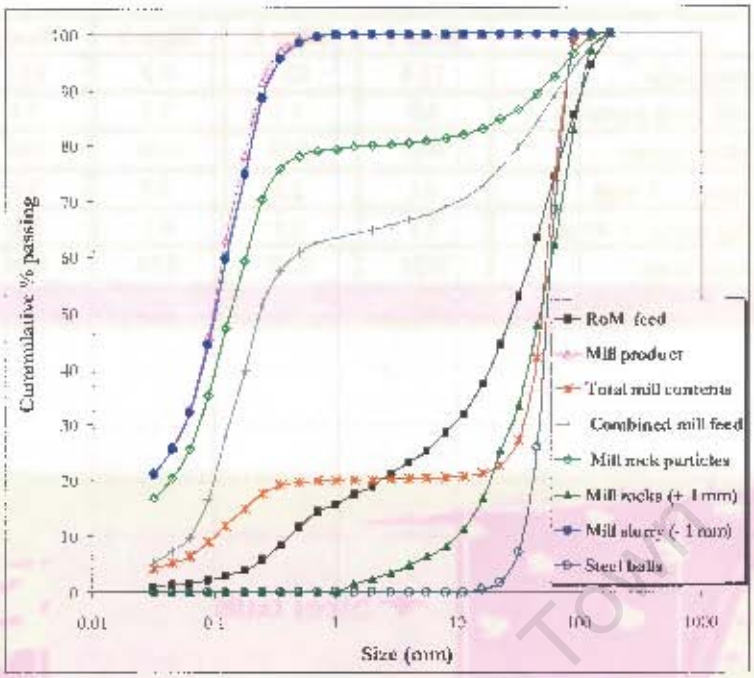

Figure 7-6: Full mill size distribution

The circuit has a considerable re circulating load of cyclone underflow (180 %), so the feed to the mill is considerably different to the RoM feed. This real mill feed is shown as the combined feed in Figure 7-7. It is in fact finer than the inlet (slice 1) size distribution above 20 mm, illustrating distinct segregation as it enters the mill. It is slightly coarser for the sub 20 mm particles. This stream and its flowrate represent the feed material that should be used to assess segregation in the mill.

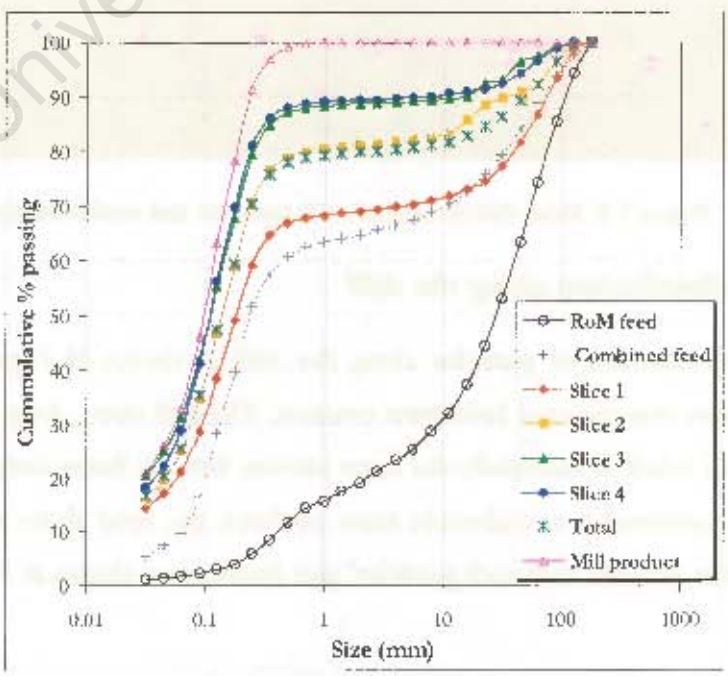

Figure 7-7: Mill rock particles size distribution

From Figure 7-7, a strong progressive segregation is revealed where the solid particles become substantially finer towards slice 4. The observed large difference in the size distribution between slice 4 and the mill product can be attributed to the discharge classification function and faster transport rates of small particles to reach the discharge end.

To give a clearer indication of the particle segregation, the material above 1mm, (the topsize in the product stream) was separated out and called rocks whilst the fines less than 1 mm were classified as slurry. These distributions for each zone are also illustrated in Figure 7-9 and in Figure 7-11. The size distribution along the mill can be illustrated further by a size at which 80 % of mill rock particles pass a slice along the mill referred to as "S80" in this thesis and shown in Figure 7-8. The S80 reveal a drastic drop in size from slice 1 to slice 2 from where the size reduction continues but not very strongly. The apparent weak size reduction towards the mill discharge is due to the fact that smaller particles become increasingly harder to break.

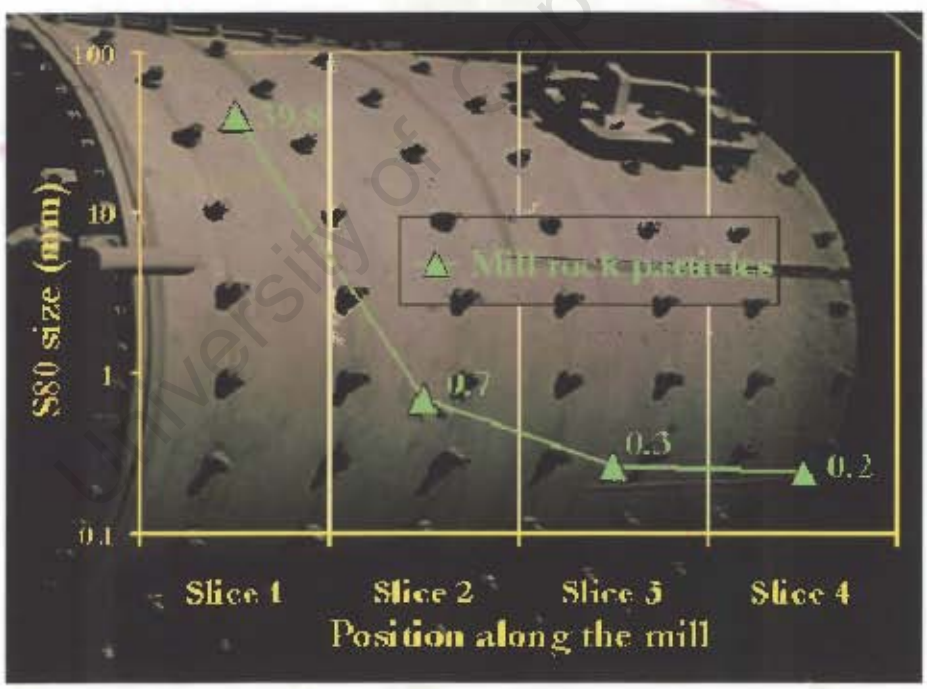

Figure 7-8: S80 size of mill rock particles passing a given slice along the mill

From Figure 7-7 and Figure 7-8, the full mill solids show distinct segregation from coarse particles at the feed towards fine particles at the discharge. The observed trend is however biased considering the high amount of fines present in each slice. Plotting the size distribution of the + 1 mm rocks independently (Figure 7-9) reveal a mixed size distribution. However, truncating the + 1 mm rocks into three distinct size classes; small rocks (1 – 16 mm), Critical size rocks (16 – 45), and big rocks

(+45 mm) and plotting their size distributions separately reveal that only the big rocks show segregation (Figure 7-9).

7.2.2 Rocks (+1 mm) axial distribution

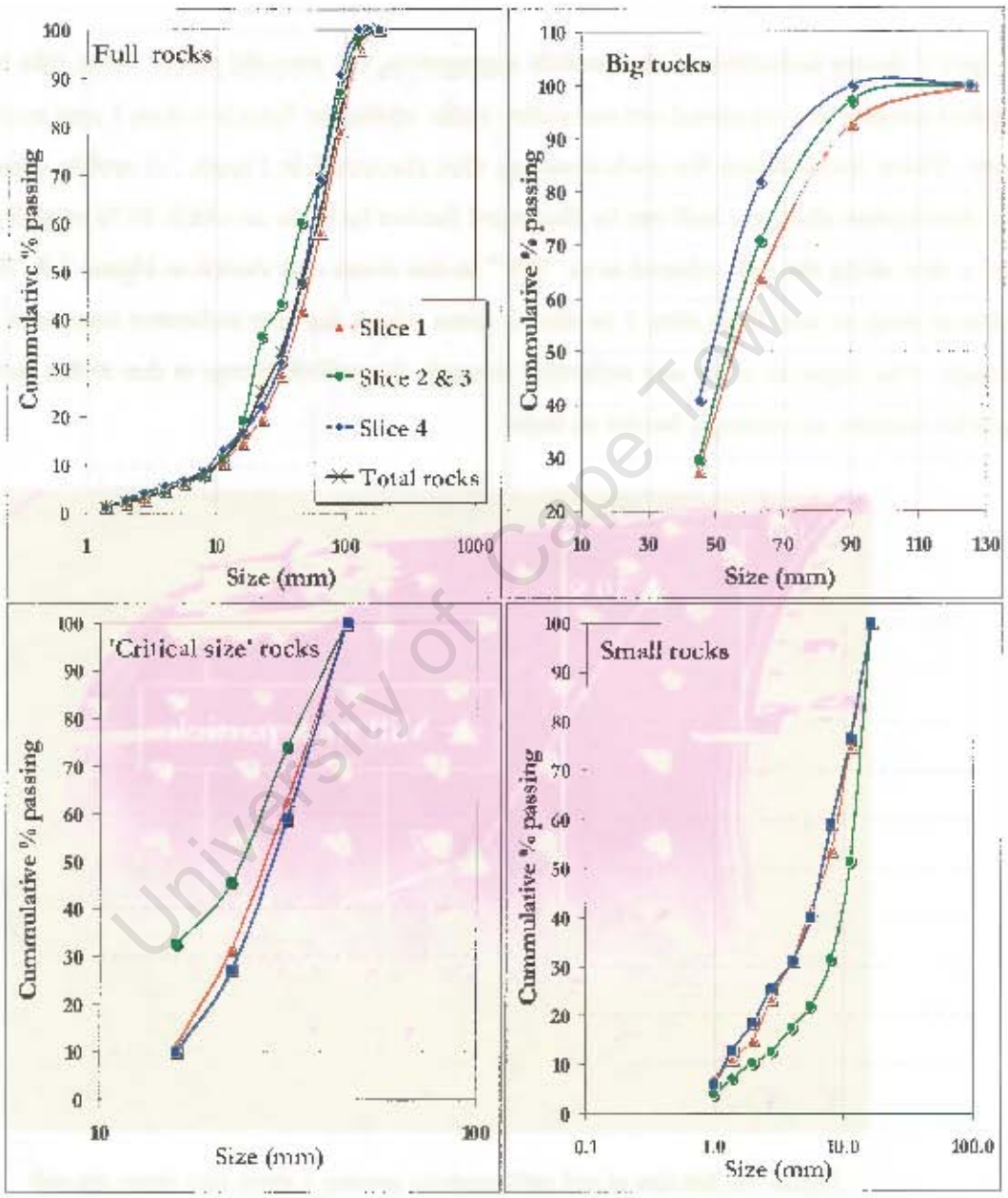

Figure 7-9: Size distribution of defined size classes for + 1 mm rocks

The S80 for the + 1 mm rocks is given in Figure 7-10 and shows that both the small and critical size rocks are reasonably mixed across the mill. Interestingly, this corresponds to the averaged critical size range for SAG mills, given as 25-50 mm by Napier-Munn et *al.* (1999). The S80 of the big rocks and full + 1 mm rocks depicts a weak axial segregation.

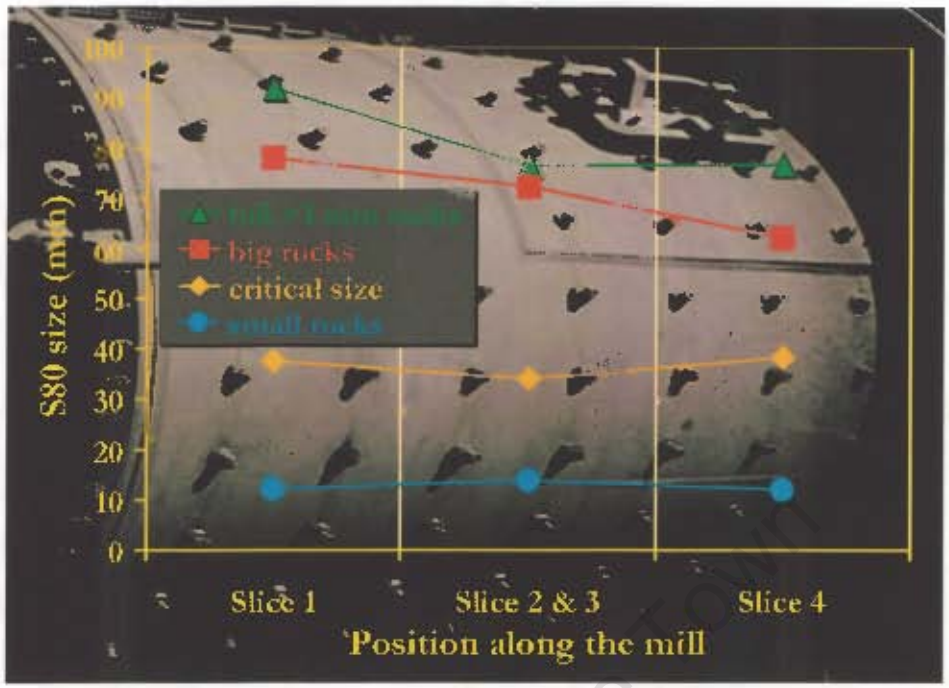

Figure 7-10: S80 size at which 80 % of the + 1 mm rocks passes each slice along the mill

Table 7-6 gives the detailed properties of big rocks for the four sampled mill slices. The average rock mass for each size range in a given slice and the ore density have been used to compute the spherical diameter of rocks in the hand sizing range. The spherical diameters are quite consistent for a given size in all slices which implies that a consistent or precise sizing procedure of the coarse rocks was conducted. The exception is in the plus 125 mm size range, where slice 2 is distinctly finer than the inlet zone, showing that the coarse rocks are reduced in size. Additionally there is no material in the plus 125 mm size after slice 2, so there is distinct segregation at the very coarse end.

Table 7-6: Big rocks specific properties

Size fraction, mm	Slice 1	Slice 2	Slice 3	Slice 4	
125 - 250	78.9	18.2		–	Mass, kg
90 -125	315.4	86.8	30.8	34.2	
63 - 90	397.7	128.3	51.2	77.6	
45 65	303.1	94.2	35.7	77.2	
125 - 250	12.0	4.0	–		No. of rocks
90 -125	109.0	31.0	12.0	12.0	
63 - 90	387.0	127.0	62.0	90.0	
45 - 65	920.0	273.0	108.0	232.0	
125 - 250	6.58	4.55	–	–	Mean mass, kg
90 -125	2.89	2.80	2.57	2.85	
63 - 90	1.03	1.01	0.83	0.86	
45 - 65	0.33	0.34	0.33	0.33	
125 - 250	1.66	1.15	–	–	Volume, ℓ
90 -125	0.73	0.71	0.65	0.72	
63 - 90	0.26	0.26	0.21	0.22	
45 - 65	0.08	0.09	0.08	0.08	
125 - 250	146.9	129.9	–	–	Spherical dia, mm
90 -125	111.8	110.6	107.4	111.2	
63 - 90	79.1	78.7	73.6	74.6	
45 - 65	54.2	55.0	54.2	54.3	
Ore density, g/cm^3	3.96				

7.2.3 Slurry distribution along the mill

Since the finer material dominated the charge (Figure 7-7), forming 80% of the solids content, the mass of slurry drained out from the mill slices and the mass of the fines from the screened charge were combined to produce the total slurry. Slurry was considered to be solid particles less than 1 mm in size because this was the maximum size in the discharge (Figure 7-11). Also, Napier-Munn et

al. (1999) refers to slurry as particles less than 1 mm. The slurry samples as drained from the mill are compared with the full -1 mm slurry samples. Clearly the slurry samples drained from the mill are extremely biased, giving a much finer size distribution than the real -1 mm slurry size distribution in the mill.

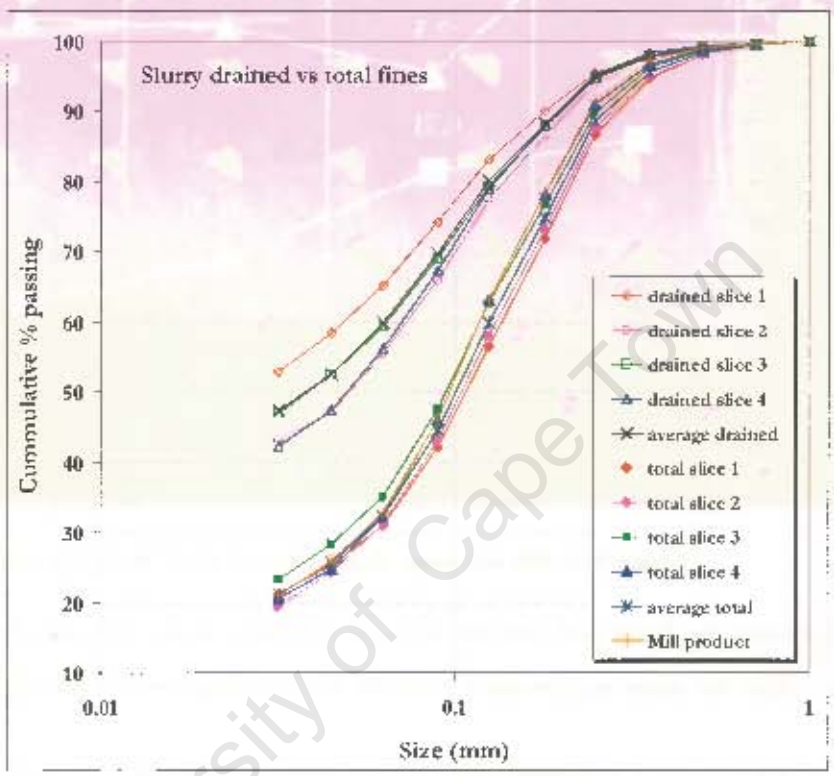

Figure 7-11: Comparison of drained slurry and the combined fines distribution along the mill

Figure 7-11 and Figure 7-12 both show progressive segregation of solids in the slurry, other than at the very fine end of the 3rd segment (Figure 7-11). The S80 sizes at which 80 % of solids in the slurry passes each slice (Figure 7-12) show fine segregation for total slurry and is similar to that of rocks where the inlet slice is coarser, the center slices finer and the discharge slice with the finest solid particles.

What is of particular interest is that the slurry in the discharge (slice 4) has the same size distribution as the mill slurry product. The mill discharge stream is not representative of the average slurry in the mill, however, the difference is small. It thus appears that the mill product slurry is a good approximation of the slurry size distribution in the mill, and certainly of the discharge end of the mill.

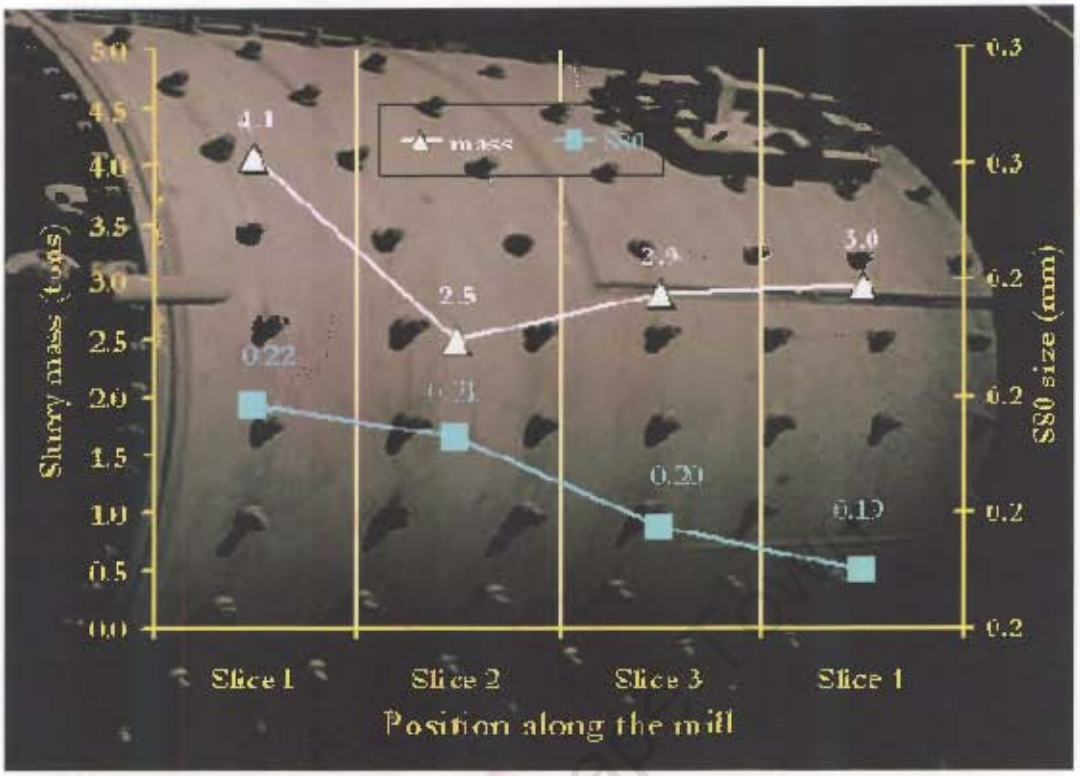

Figure 7-12: S80 and mass distribution of slurry along the mill

Figure 7-12 shows the mass and S80 distribution of slurry along the mill. As expected, the size of slurry drops whilst the mass accumulates towards the discharge end of the mill.

7.2.4 Steel balls axial distribution

The size and mass distribution of steel balls along the mill showed uniform mixing.

7.2.4.1 Steel balls size distribution along the mill

Figure 7-13 and Figure 7-14 show no significant segregation along the length of the mill for the steel balls and this implies that hardness or wear rate of material is a major factor on the observed segregation. While these steel balls have a low wear rate and survive rigorous breakage as they travel along the mill, the rocks have a relatively faster wear rate and might not survive travelling to the mill discharge end without being broken to smaller fragments.

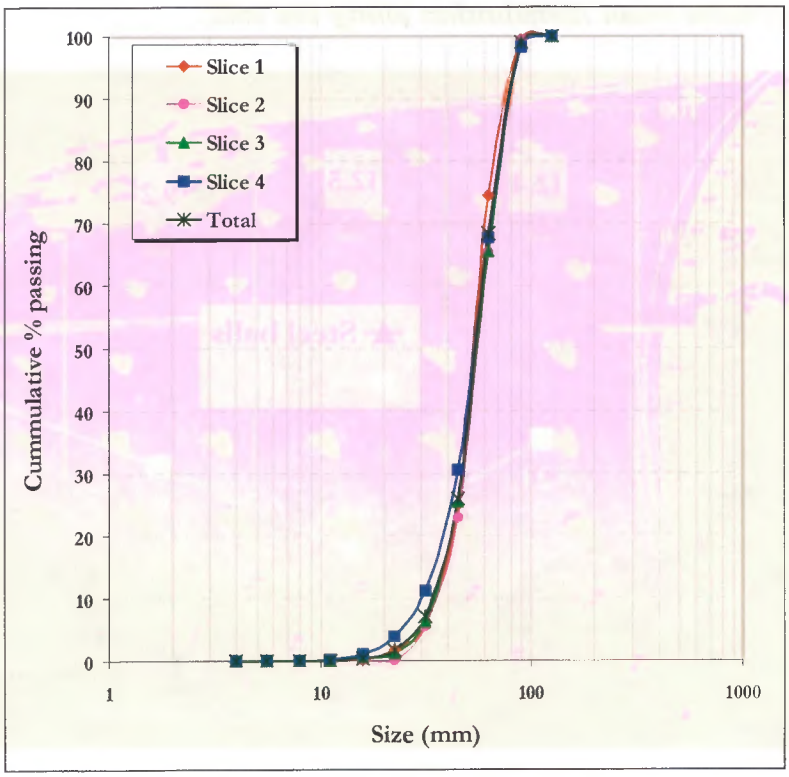

Figure 7-13: Steel balls size distribution along the mill

Both Figure 7-13 and Figure 7-14 show uniform size distribution of steel balls along the mill.

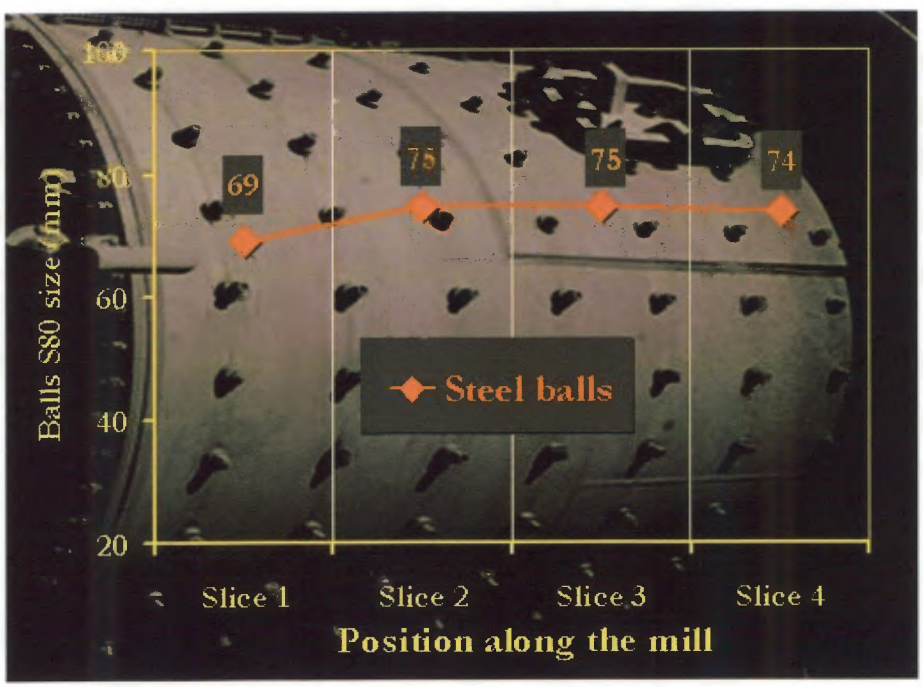

Figure 7-14: S80 size distribution of steel balls along the mill

7.2.4.2 Steel balls mass distribution along the mill

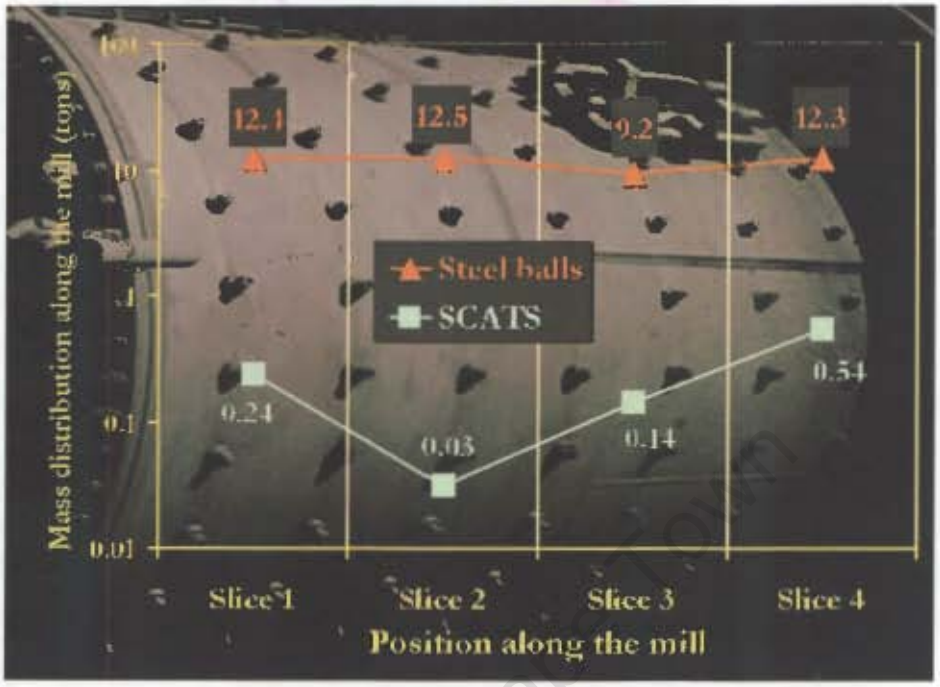

Figure 7-15: Mass distribution of steel balls and scats along the mill

The distribution of steel balls by mass across the mill is shown in Figure 7-15 and the specific size classes of balls emptied out of the mill is shown in Figure 7-16.

The mass distribution of steel balls and of the scats (small misshaped balls) shown in Figure 7-15 reveal that the balls were uniformly distributed along the mill whilst the scats mass increased towards the mill discharge end. The observed difference in the mass distribution between the balls and scats can be attributed to segregation by shape, which favors the scats whose shape is plate-like to have higher transport rates through the charge and reach the discharge of the mill were they accumulate.

The fractions of the entire steel balls removed from the mill and sized using the root two screen series is shown in Figure 7-16.

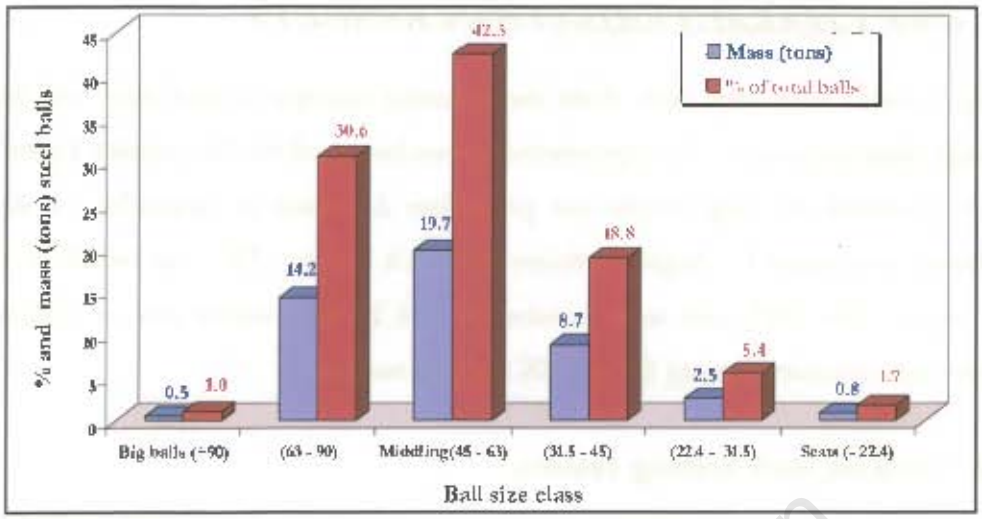

Figure 7-16: Steel balls size classes within the mill depicting a Gaussian normal distribution

The majority of the balls found in the mill were in the size range of 45 - 63mm and constituted 42.5 percent of the total collected balls. This is a normal seasoned ball charge size distribution that exists in the mill due to wear – with new balls replacing worn balls; thus a seasoned charged in the mill is maintained. Close to 2 % of the total ball load in the mill was below 22.4 mm and were classified as scats. When the mill was recharged after the test, the scats were not returned back into the mill as they only increase the mill load and power draw but do not take part in meaningful grinding.

A standard ball size distribution has been developed through earlier mill charge sizings, and this is used in the JK mill models. This compared with the measured distribution is presented in Table 7-7. There is a considerable difference in the first root two screen sizes, with much more in the standard size distribution. This is in contrast to data collected from a full ball sizing conducted on a SAG mill at Amandelbult, and also shown on the table. The reason for such differences in size distribution is not known.

Table 7-7 Comparisons of measured and standard ball size distributions

ball size, mm	experimental	Std distribution	Std	Merensky SAG
125			0	0
90	1	0	54	58.9
63	30.6	54	27	31.8
45	42.5	27	13	7.1
31.5	18.8	13	6	2.2
22.4	5.4	6	0	0
- 22.4	1.7	0		

7.3 ORE CHARACTERISATION RESULTS

100 kg of rocks were kept aside from the screened material of each slice, and from the feed, for breakage characterisation. The experimental procedure used on the samples for ore characterisation was the standard JK drop weight test procedure described in Appendix A3, and the work was generously performed by Anglo Platinum Research Centre (ARC) on behalf of the University of Cape Town. The BWI tests were conducted at a limiting screen size of 106um and the DWT analyses were conducted using the new JK analysis method.

7.3.1 General rock testing results

Five sizes as in the standard JK drop weight test methodology were used in performing ore characterisation tests on each of the five (Belt feed, zone 1, zone 2, zone 3 and zone 4) supplied samples. Three tests were conducted for each size range using three different nominal input energies. 10 rocks were used for 53 – 63 size range, 15 for the 45 – 37.5 mm range and 30 rocks for the other three size ranges. The rock hardness is clearly defined by the abrasion parameter (ta) and the impact parameter (A*b) - which is the slope of "zero" input energy for the t_{10} versus specific comminution energy plot. Lower A*b or ta values indicate that there is low percentage of material passing a given fraction of the original particle size and this means greater resistance to abrasion and impact breakage, therefore hard ores have lower A*b and ta parameters.

A summary of the overall breakage parameters for the full samples is given in Table 7-8 and the interpretations of the results are presented in Table 7-9.

Table 7-8: Summary of Drop weight test parameters

	A	b	A * b	ta	Average ore SG
Mill feed	65.59	2.94	192.65	1.94	4.10
Slice 1	64.46	1.98	127.93	1.75	3.96
Slice 2	64.53	1.59	102.64	1.51	4.10
Slice 3	60.33	1.60	96.68	0.85	3.78
Slice 4	63.86	1.33	84.96	0.59	3.87
Average	**63.75**	**1.89**	**120.97**	**1.33**	**3.96**

Table 7-9: Typical JK Drop Weight test parameters and their interpretations

Property	Very hard	hard	Moderately hard	Medium	Moderately soft	Soft	Very Soft
A * b	< 30	30 - 38	38 - 43	43 - 56	56 67	67 - 127	>127
ta	< 0.24	0.24 - 0.35	0.35 - 0.41	0.41 - 0.54	0.54 - 0.65	0.65 1.38	>1.38

From Table 7-9, the ta and A*b parameters shows that the UG2 ore fed to the mill during the test period is classified as soft according to the JK data base.

7.3.2 Breakage effect along the mill

Breakage within the mill is classified into high energy (impact) breakage and low energy (abrasion) breakage. Both types of breakage have an influence on the transport and segregation of broken particles along the mill.

Table 7-10 shows t_{10} values obtained through a minimization of error squared routine for specific input energy values.

Table 7-10: Minimisation of error squared energy (Ecs) and breakage index (t_{10}) data

	Minimisation of error squared t_{10} values				
Ecs	Feed	Slice 1	Slice 2	Slice 3	Slice 4
0.00	0.0	0.0	0.0	0.0	0.0
0.25	34.7	25.2	21.2	19.3	18.1
0.50	51.3	40.6	35.4	32.5	31.0
1.00	62.9	55.6	51.4	48.0	47.0
1.50	65.5	61.2	58.6	55.4	55.2
2.00	66.1	63.2	61.8	58.9	59.4
2.50	66.2	64.0	63.3	60.5	61.6
3.00	66.2	64.3	64.0	61.3	62.7
3.50	66.2	64.4	64.3	61.7	63.3
4.00	66.2	64.4	64.4	61.9	63.5

A plot of the percentage of material passing one tenth of the original feed size (t_{10}) also referred to as the 'amount of breakage', versus the specific comminution energy (Ecs) is given in Figure 7-17. There is a consistent increase in ore competence along the mill, as shown by the curves shifting downwards indicated by the arrow in Figure 7-17.

The large scatter in the mill feed sample which gave a poor fit of the t10 – Ecs curve may be attributed to a high variability in the ore hardness.

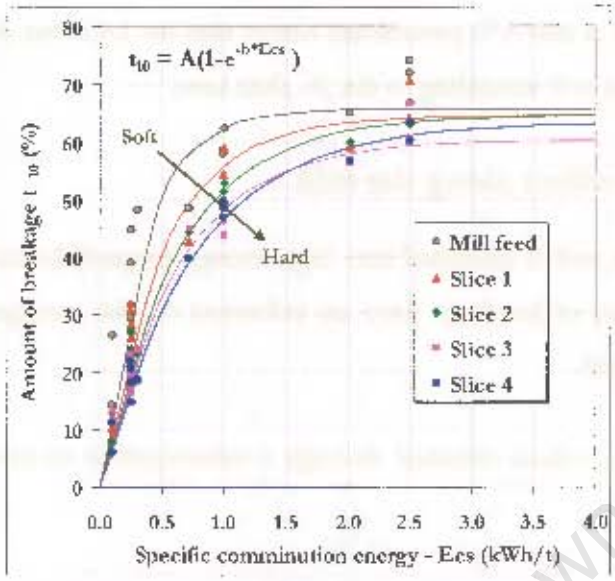

Figure 7-17: Breakage index t_{10} (%) versus Specific comminution energy - Ecs (kWh/t) per slice

7.3.2.1 Impact breakage along the mill

The relationship of the overall impact parameter (A*b) to the relative sample collection point is illustrated in Figure 7-18. There is a significant and consistent decrease in the A*b value, representing an increase in ore competency, along the mill. From Figure 7-18, it is evident that there is a higher resistance to rock breakage down the length of the mill, revealing that it becomes increasingly harder to break particles towards the discharge of the mill. Since the particles tested were of the same size, the higher resistance to impact breakage for rocks picked near the discharge of the mill is attributed to these particles being more competent than those from the inlet position.

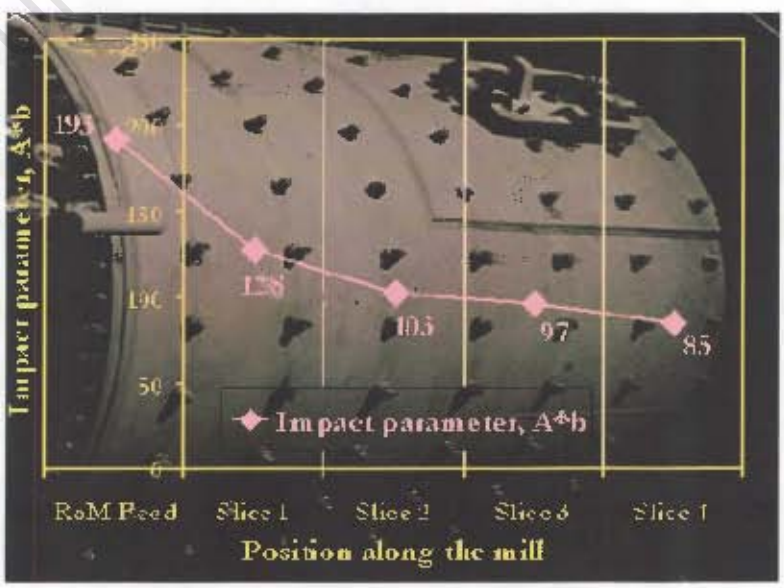

Figure 7-18: Impact breakage (A*b) effect along the mill

Amandelbult results

The size distributions of the progeny broken particles from the five different parent rock sizes produced from an Ecs (comminution energy) of 0.25 kWh/t are shown in Figure 7-19. Since the impact specific comminution energy to break the rocks was maintained at 0.25 kWh/t, the product size distribution is expected to be identical for the same parent rock size. However, Figure 7-19 reveals a general trend where particles at the mill inlet position have a finer size distribution than those at the mill discharge, which are coarser. The distinctive gradual coarser distribution towards the mill discharge is more apparent at the size of 57.8 mm (Figure 7-19). The observed difference in the size distribution of the product particles is attributed to axial segregation of rocks due to *hardness* as these resulted from identical sizes.

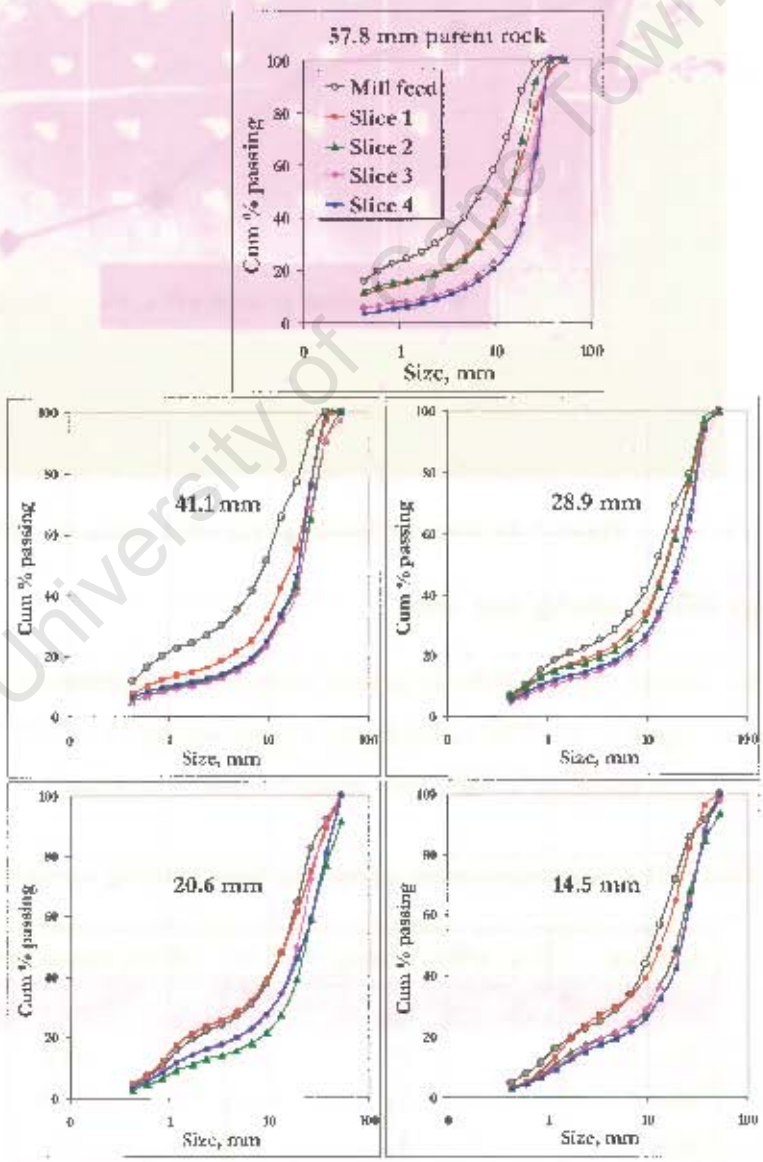

Figure 7-19: Impact breakage product size distribution at different sizes for 0.25 kWh/t Ecs

7.3.2.2 Abrasion breakage along the mill

Figure 7-20 illustrates the plot of the low energy (abrasion) breakage parameter (t_a) against position from which the rocks were picked. Again, the breakage parameter (t_a) decreases in value, representing an increase in the abrasion resistance, along the mill. The higher increase in the abrasion resistance along the mill is expected and since rocks of the same size were tested, ore hardness was responsible for the observed ta difference.

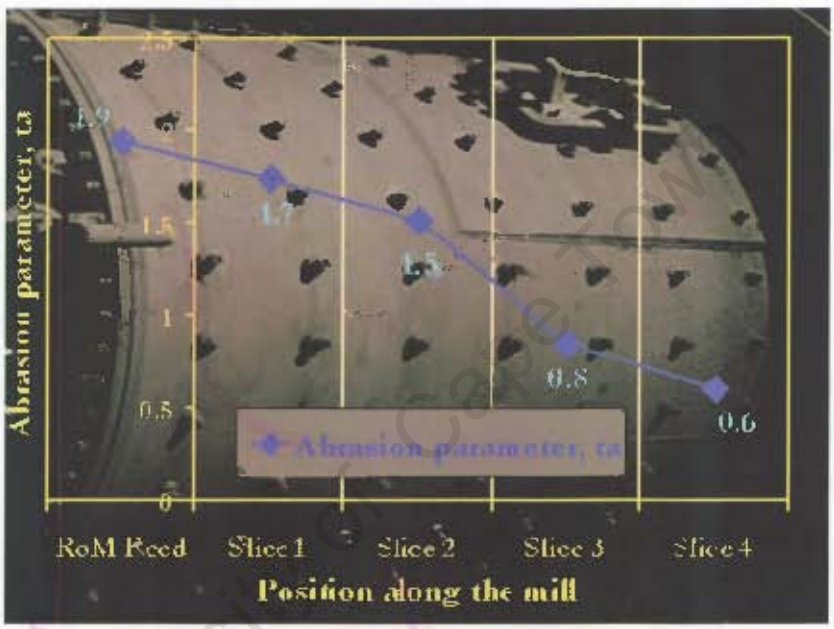

Figure 7-20: Abrasion breakage (t_a) effect along the mill

7.3.3 Energy effect along the mill

The effect of the applied energy on rocks picked from different positions along the mill is shown in Table 7-11 and in Figure 7-21. The comminution input energy at t10 of 50 % and the bond work index required for rock breakage at each slice along the mill is presented.

Table 7-11: Comminution input energy and bond grinding energy along the mill

Sample	Ecs, kWh/t at t_{10} = 50 %	Work index, kWh/t
Mill Feed	0.5	15.1
Slice 1	0.8	16.6
Slice 2	1.0	16.3
Slice 3	1.1	17.0
Slice 4	1.2	18.2

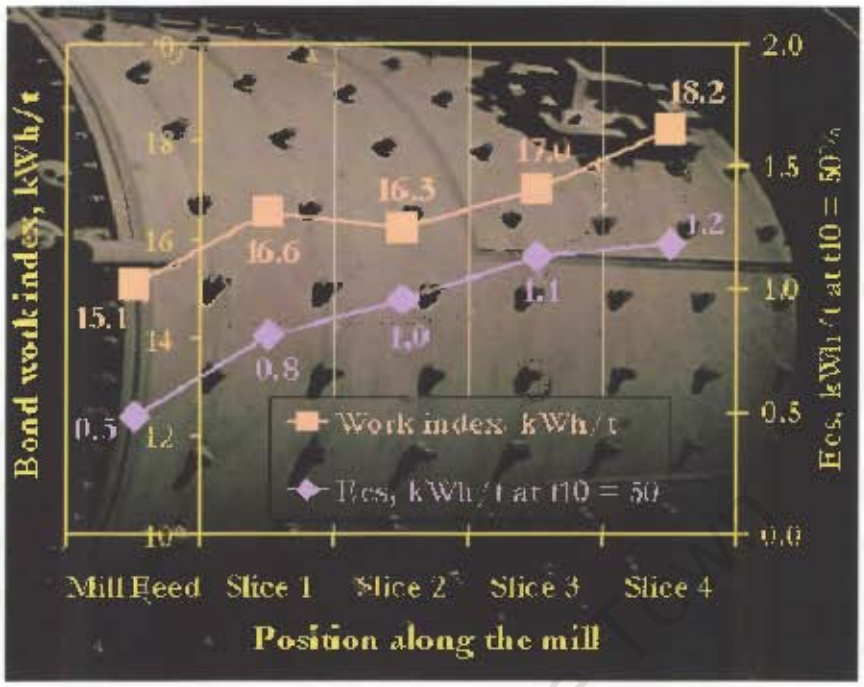

Figure 7-21: Energy effect along the length of the mill

From Figure 7-21, it is apparent that a higher amount of energy is required for breakage of particles located at the discharge region of the mill. This observation is in agreement with the high breakage resistance revealed by parameters A*b and ta in Figure 7-18 and Figure 7-20.

7.4 DISCUSSION OF RESULTS

This testwork showed that the total solids emptied out from the mill revealed clear segregation along the mill. However, when the charge was separated into rocks and slurry (fine particles), slurry showed segregation while the rocks had only a slight segregation trend. This behaviour implies that it is misleading to draw conclusions based on the size distribution of the total mill rock particles because of the bias of more fines present. Separating the material into distinct size ranges gives a broader picture of the rocks and fine solids distribution and hence the segregation of material along the mill. The coarser, plus 45mm, rocks do show some segregation.

The balls had no segregation, which implies that wear rate is critical to the observed segregation.

The ore characterization results revealed segregation due to the difference in energy required for breakage and due to hardness (resistance to both impact and abrasion breakage) of the rocks relative to their position along the mill.

The rock breakage tests reveal a progressive and significant increase in ore competency from mill feed to the discharge zone, the A*b drops from 129 to 85 (Figure 7-18), and the ta from 1.7 to 0.6 (Figure 7-20) along the mill. It is evident that significantly more energy is required for the same degree of breakage at the discharge end of the mill than at the feed end. This is logically due to the preferential breakage of the softer particles at the feed end of the mill and the survival of the more competent material along the mill.

Segregation is a function of rate of breakage, or survival, of particles, and the transport function along the mill. As the 'very competent' balls were found to not be segregated, it is tentatively deduced that segregation is a function of ore competency, and more particularly a function of the range of competency within the ore – as reflected by the significant increase in ore competency along the mill. It is also tentatively deduced that segregation by ore competency may be more significant than segregation by size.

The mechanisms causing segregation observed from this testwork have been identified as *transport* of particles along the mill and *breakage* or resistance to breakage of particles within the charge. From Table 7-4, the residence time of liquid (slurry) was calculated to be shorter than that of rocks, in agreement with the RTD results (chapter 5) and this shows that distinct transport rate of particles determines where certain *sizes* of rocks are located. On the other hand, breakage or non-breakage of particles also influences the location of the same size particles along the mill, leading to segregation due to rock *hardness*. For instance, the high resistance to breakage of the steel balls results in their uniform distribution along the mill as they survive breakage and can therefore be found anywhere along the mill. The difference in the energy utilized for breaking rocks of the same size confirmed that the rocks under test had distinct levels of competence. The results from this testwork have satisfied the hypotheses of the present study.

7.5 SUMMARY

The results of the Amandelbult testwork have revealed that segregation of full mill rock particles, slurry and big rocks (Figure 7-7, Figure 7-8, and Figure 7-12) was present along the mill. The screening of the mill contents revealed segregation by size and by mass of the particles distributed along the mill.

Slurry drained out of the mill (Figure 7-11) was found to not be representative of the fines in the mill. The full combined slurry (drained out slurry and fines from the charge) showed distinct

segregation along the mill, becoming finer at the discharge end. From the slurry size distribution (Figure 7-11), it is tentatively concluded that the mill product slurry is a good approximation of the slurry size distribution in the mill, and certainly of the discharge end of the mill.

Figure 7-22 summarizes the observed particles distribution along the mill. The big rocks (+45 mm) and slurry reveal progressive segregation along the mill whilst the steel balls show uniform mixing across the mill. It can be concluded that the fine particles that are segregated at the discharge end of the mill are *transported* with the help of the carrier fluid and their small *size* help in percolating through the interstices of the bigger particles. Figure 7-23 is a summary of the ore characterization results and reveals segregation trends. The comminution input energy (Ecs) and the bond work index required for breaking rocks of the same size increases along the mill towards the discharge. Also, the resistance to impact (A*b) and to abrasion (ta) breakage for rocks of the same size collected along the mill increases towards the discharge end. It is apparent that the *breakage* mechanism influences axial segregation by rock competence (*hardness*).

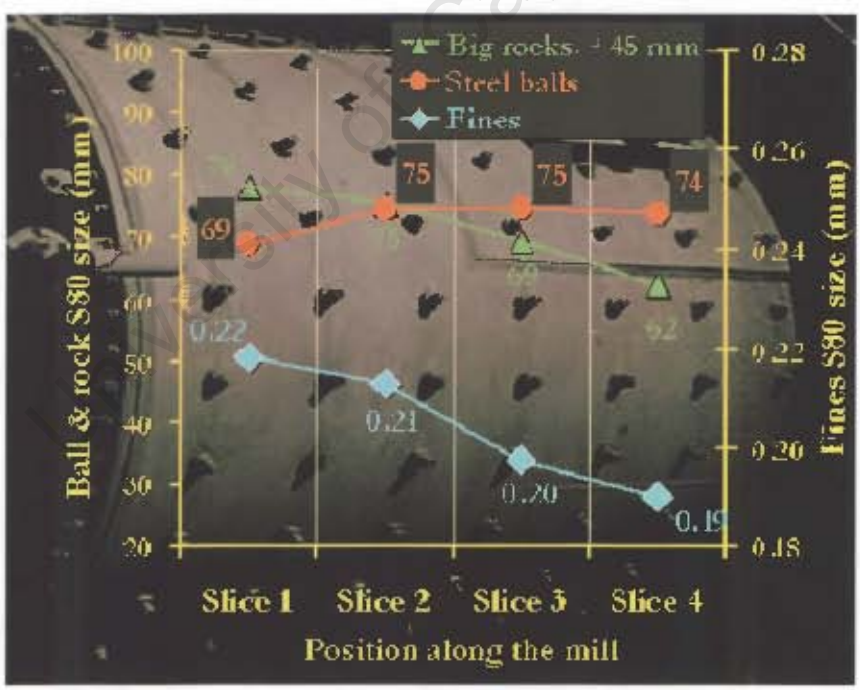

Figure 7-22: Axial size segregation of slurry and big rocks, and uniform distribution of balls

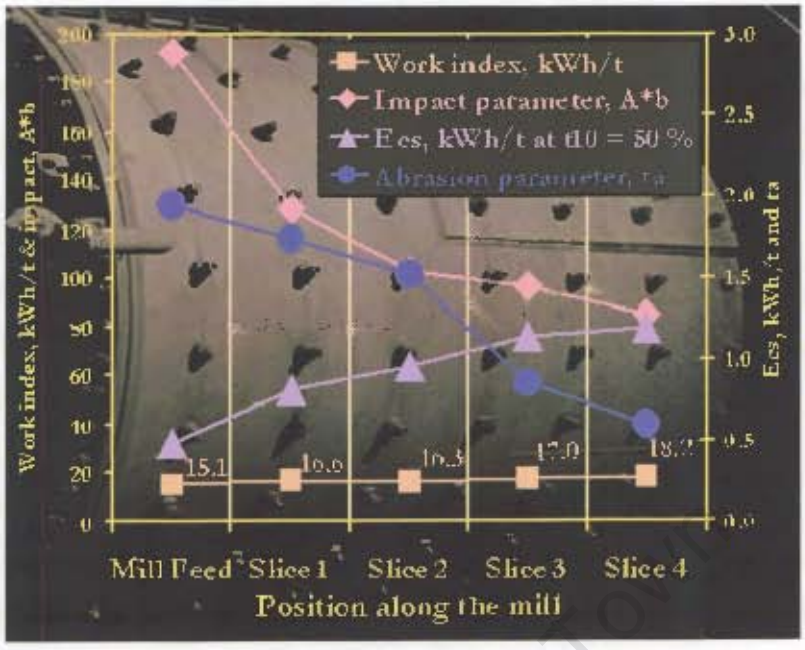

Figure 7-23: Summary of ore characterisation results

Chapter 8

8 DEM SIMULATIONS

This chapter reports the results of simulating impact events of particles that were located at the inlet (slice 1) and discharge (slice 4) positions of the Amandelbult SAG mill, using the discrete element modeling (DEM) technique. An introduction to the particles DEM simulations at the two mill positions is covered in the background and the objectives sections. The DEM procedure is briefly described followed by an overview of the expected DEM simulation outputs. The general simulation outcomes are then presented. A comparison between the specific impact energy at the inlet and the discharge mill positions utilized in the drop weight tests (DWTs), and that of the DEM impact energy spectra for slice 1 and slice 4 of five rock sizes are described in detail. Finally, the DEM simulation outputs from the two mill slices are used to predict the product size distribution and the mass, subject to an assumed proportionality of the rocks degree of breakage to the DEM collision frequency. The mass calculated at the two slices is used to assess the endeavor of modelling a long mill as perfectly mixed.

8.1 BACKGROUND

In current comminution studies, both DEM simulations and ore characterization (impact and abrasion tests) have been found to be useful tools for predicting the behavior of rocks in the full scale industrial SAG mills. In this chapter, a comparison is drawn between the inlet and discharge slices of the mill for both the collision rates from the DEM energy spectra and for the amount of breakage predicted from multiple impacts.

Axial segregation due to impact *breakage* of rocks has been found to exist in an industrial SAG mill from the DWT results, (chapter 7). The DWT results also revealed that particles at the inlet position of the mill required lower input energies (Ecs), than those at the discharge position, to achieve the same degree of breakage (t_{10}). Additionally, the DWT results showed that for the same size and same Ecs value of 0.25 kWh/t, rocks at slice 4 had a coarser size distribution than those at slice 1 and thus indicating axial segregation by ore *hardness*.

Even though there is no breakage from particle interactions in the DEM simulations, the multiple collisions among particles from impact events in a given energy range over a fixed simulation time (collision rate), may produce some degree of breakage, provided the impact energy absorbed by the rock is greater than a threshold energy, E_{cs} that can generate fracture with cyclic impacts. Despite

some limitations, DEM is still regarded as a future solution to accurate modelling of SAG mills. This is because it gives a broader picture of the motion of particles in mills. In a DEM simulation, all collision events and the energy lost per impact in a fixed time is recorded to give a full description of charge behavior for every revolution.

8.2 OBJECTIVES

The objectives of running DEM simulations of particles with similar specifications to those particles emptied out from the two end slices of the Amandelbult SAG mill are as follows:

1. To provide extra information on the collision frequency per energy range (energy spectra) of particles in relation to their axial position along the mill.
2. To compare between slice 1 and slice 4, the DWTs specific input (impact) energy and the peak DEM impact energy for five rock sizes.
3. To use the DEM simulation outputs from the two mill positions to predict the product size distribution and the mass, subject to an assumed proportionality of the rocks degree of breakage to the DEM collision frequency.
4. To assess the modelling implications from the predicted progeny particles mass at the two mill positions.

The modelling of breakage and production rate in a mill from DEM simulations is at the forefront of comminution research and beyond the scope of this thesis. The DEM with a simple link to breakage data is used to indicate a comparative breakage rate between the inlet and discharge ends of the mill, and thus indicate the need, or otherwise, of allowing for segregation when modelling breakage in a mill.

8.3 DEM EXPERIMENTAL METHOD

The detailed DEM procedure has been given in papers such as Cleary 1998 and 2001, thus only a brief description is given here.

The DEM mill was simulated as 1 m slices (at the feed and discharge end) enclosed by periodic boundary conditions. The particles were considered dry and were assumed to be perfectly mixed within each 1 m slice at the start of the DEM simulations. A narrow energy range was chosen for binning the detected collisions and after four revolutions spanning 15 seconds, the detected

collisions per energy range were used to compute the collision rate (number of collisions per second), r_c in that duration.

The particle numbers obtained from the two mill end slices of the SAG mill were used for the DEM simulations performed at CSIRO[2], Australia on behalf of the University of Cape Town (UCT).

Except for the analysis and the evolution of the product size distribution and subsequent mass prediction, the DEM simulation outputs presented in this chapter are those given by CSIRO, Owen 2005a, in CMIS Technical report: 05/127 (*webGF - UCT 002*) for the inlet slice and Owen 2005b, in CMIS Technical report 05/151 (*webGF - UCT 003*) for the discharge slice.

The particle data (mass and numbers obtained from the SAG mill sizings) of slice 1 and slice 4 were each entered separately to run the DEM simulations for several weeks and the energy spectra were calculated.

8.4 GENERAL DATA EXPECTED FROM SIMULATIONS

The bulk shoulder and toe positions of particles in DEM simulations can be calculated from the radial images that show the instantaneous particle positions and particle trajectories respectively.

The mill torque and power draw can be obtained from respective graphs obtained for the mill during running of the simulations.

The most important output from the DEM simulations energy spectra is the energy lost or the energy available during collision of particles with each other and collisions with the mill liners. The impact energy that results during the collision of two particles or from a particle colliding with the liner can be resolved into two components called the normal and shear energies. This representation is commonly referred to as the "energy spectra", Cleary (2001).

There are five classes of collision interactions within the mill that are considered:

1. Rock – Rock

[2] CSIRO Mathematical and Information Sciences, Locked bag 10, Clayton VIC 3168, Australia. Website: www.cmis.csiro.au

2. Rock – Steel balls
3. Rock – Liners
4. Steel balls – Steel balls
5. Steel balls – Liners

The collision interactions within the mill are best described by the energy spectra (plot of the collisions frequency against the energy range). In this chapter, the energy spectra is presented for each of the above five collision types, and for each of the sizes between the top size of 125 mm and bottom size of 16 mm for steel balls and between 180 mm and 8 mm for rocks.

The outputs from the DEM simulations in this case were simply a *calculation* of the energy spectra resulting from the original data entered for the particles emptied out from the inlet (slice 1) and the discharge positions (slice 4) of the Amandelbult SAG mill.

8.5 GENERAL DEM SIMULATION RESULTS

The DEM simulation outputs for both slice 1 and slice 4 are given in this section. The results also include general conditions and specifications for the simulations.

8.5.1 Mill specification

The specifications for the mill used for the DEM simulations are given in Table 8-1. Both slices had identical mill specifications, as the length of the original slices in the SAG mill had approximately the same length.

Table 8-1: Identical mill specification, (*webGF- UCT 002*)

Mill diameter, m	3.157
Slice length, m	1.1787
Mill speed, rpm	16.014
Duration of simulation, revs (S)	4 (15)
Geometric type	3D
Lifter configuration	28 lifter rows

8.5.2 Collision parameters

Both slices were subjected to identical collision parameters as given in Table 8-2.

Table 8-2: Identical collision parameters, (*webGF- UCT 002*)

Steel-Steel interactions	
Spring constant	7.5 MN/m
Co-efficient of restitution	0.75
Friction co-efficient	0.40
Steel-Rock interactions	
Spring constant	7.5 MN/m
Co-efficient of restitution	0.5
Friction co-efficient	0.50
Rock-Rock interactions	
Spring constant	7.5 MN/m
Co-efficient of restitution	0.3
Friction co-efficient	0.60

8.5.3 Particle specifications

Table 8-3 gives the specifications of particles obtained from slice 1 and slice 4.

Table 8-3: Particle specification

		Slice 1	Slice 4
Mill filling Level (% v/v)		23	23
Ball load (%v/v)		16.6	21.7
Number of particle size groups		15	13
Number of total	- balls	27, 544	36,188
	- rocks	58, 952	16, 417
	- total	86, 496	52, 605
Charge mass	- balls	9, 414	12, 202
	- rocks	1, 851	388
	- total	11, 265	12, 590
Number rocks by size	- 106 mm	109	12
	-53 mm	757	198
	- 38 mm	1, 779	428
	- 26.6 mm	3, 325	661
	- 19 mm	5, 136	1, 066
	- 13.4 mm	12, 402	2, 202
	- 9 mm	25, 607	9, 050

From Table 8-3, it is observed that the mill filling is the same for both slices. However; the ball load is higher in slice 4 implying that this slice has more balls and fewer rocks as confirmed by the

numbers in Table 8-3. The number of particles for the rock size groups is higher at slice 1 than at slice 4. The rocks mass is also less at slice 4 than at slice 1. The - 11.2 mm particles are excluded from the simulations due to computational limitations. However, the total charge mass is more in slice 4 than in slice 1 due to a higher proportion of the heavy steel balls at the mill discharge.

8.5.4 Ball size classes

Table 8-4 shows the ball sizes for the two slices and gives the proportion of each size class. Because it was observed that steel balls did not reveal segregation, the steel ball sizes and proportions were identical for both slices. As shown, the steel balls density was 7800 kg/m^3.

From Table 8-4, it is observed that the majority of the balls in both slices was of middling size of 45 mm and accounted for 42 % of the total balls.

Table 8-4: Identical ball size class, (*webGF - UCT 002*)

Class ID	Minimum Diameter (mm)	Maximum Diameter (mm)	Minimum Density (kg/m^3)	Maximum Density (kg/m^3)	Class Proportion
1	90	125	7800	7800	0.0098
2	63	90	7800	7800	0.3061
3	45	63	7800	7800	0.4249
4	31.5	45	7800	7800	0.1878
5	22.4	31.5	7800	7800	0.0542
6	16	22.4	7800	7800	0.0173

8.5.5 Rock size classes

The size classes for the rocks and the proportions in each size class for the two slices are given in Table 8-5. Slice 4 has a smaller size rock range and has no big (+125 mm) rocks and the small 8 mm rocks. It is observed here that slice 4 has more small (11.2 – 16 mm) rocks which accounts for about 17 % of the total rocks as compared to only 7% of small (8 – 11.2 mm) rocks in slice 1.

Table 8-5: Rock size classes, (*webGF - UCT 002 and UCT 003*)

Class ID	Minimum Diameter (mm)	Maximum Diameter (mm)	Minimum Density (kg/m^3)	Maximum Density (kg/m^3)	Class Proportion
8	125	180	3960	3960	0.045
9	90	125	3960	3960	0.182
10	63	90	3960	3960	0.229
11	45	63	3960	3960	0.175
12	31.5	45	3960	3960	0.147
13	22.4	31.5	3960	3960	0.096
14	16	22.4	3960	3960	0.054
15	11.2	16	3960	3960	0.046
16	8.0	11.2	3960	3960	0.026

Slice 1

Class ID	Minimum Diameter (mm)	Maximum Diameter (mm)	Minimum Density (kg/m^3)	Maximum Density (kg/m^3)	Class Proportion
8	90	125	3960	3960	0.0946
9	63	90	3960	3960	0. 2145
10	45	63	3960	3960	0. 2134
11	31.5	45	3960	3960	0. 1663
12	22.4	31.5	3960	3960	0. 0892
13	16	22.4	3960	3960	0. 0530
14	11.2	16	3960	3960	0.1690

Slice 4

8.5.6 Torque and power draw predictions

The estimated torque and power drawn by slice 1 and slice 4 are given in Table 8-6. It is observed here that slice 4 drew more torque and power than slice 1 and this could be attributed to the presence of a higher ball load at slice 4.

Table 8-6: Power draw and Torque comparison

	Slice 1	Sice 4
Torque, kNm	83.8	93.4
Power draw, kW	149	166

8.5.7 Shoulder and toe positions

A comparison of predicted traces of particles during the final simulated mill revolution providing an indication of particle trajectories is given in Figure 8-1 showing four snapshots for each slice. The color of the traces indicates the speed of the particles, where yellow-orange indicates high speed particles whilst blue indicates low speeds or stationary particles. The traces reveal a distinctive

equilibrium surface (dark blue curve) where the particles move with the lowest speed, and also show the highest speed (yellow-orange) particles that are located just near the toe region.

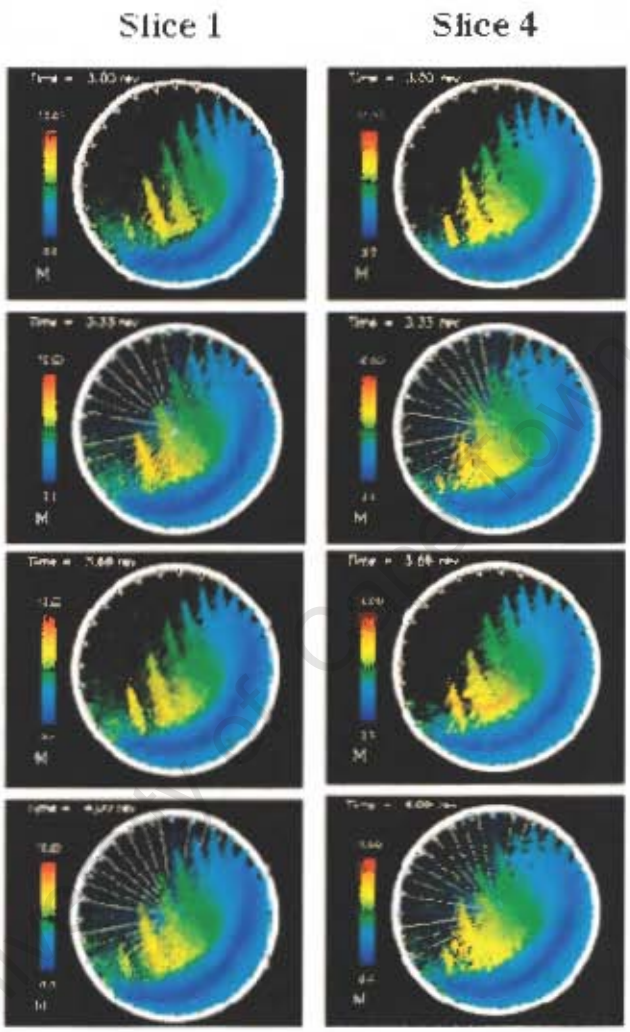

Figure 8-1: DEM predicted particle trajectories, (*webGF- UCT 002 and UCT 003*)

From Figure 8-1, the images of slice 1 show some scatter of particles and the mill appears to have a higher filling compared to slice 4. This visualization can be attributed to presence of more coarse particles in slice 1 and smaller particles in slice 4. The images also show a higher toe position in slice 1 compared to slice 4.

Figure 8-2 shows the two slices comparison of still images of the predicted particle position during the final simulated mill revolution.

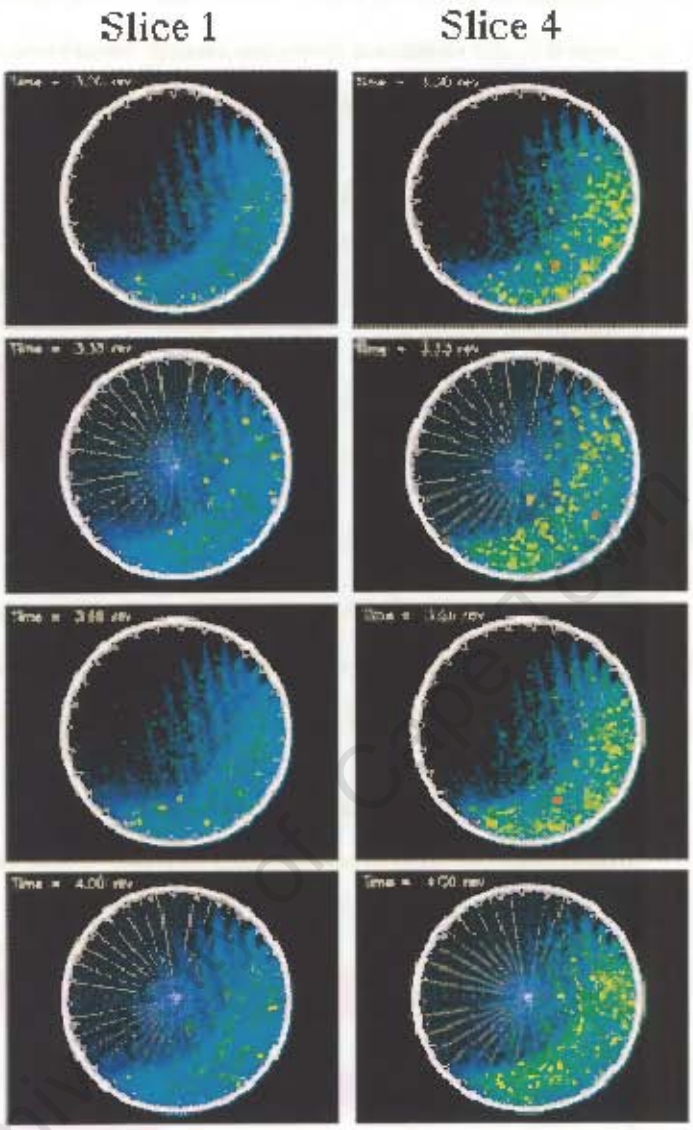

Figure 8-2: Predicted particle positions, (*webGF - UCT 002 and UCT 003*)

From Figure 8-2, the still images shows a higher toe position at slice 1 and the visual appearance of bigger (yellow) particles at slice 4 suggests a higher presence of fine particles that cannot obscure large particles completely.

From the stationary particle position images, estimates of the bulk toe and shoulder positions have been obtained as per definiton given by Powell and McBride, 2004. The impact toe positions were estimated from the particles trajectories. The angles were measured counter-clockwise relative to the 3 o'clock position.

A summary of the comparison between slice 1 and slice 4 shoulders, bulk toe, and impact toe positions is given in Table 8-7. As observed from the charge visualization (Figure 8-2), the images of slice 4 has lower toe positions and this implies large toe angles at slice 4.

Table 8-7: Toe and shoulder positions

	Slice 1	Slice 4
Shoulder position	38°	32°
Bulk toe position	220°	230°
Impact toe position	220°	228°

8.5.8 Impact energy distribution

The distribution of the impact energy amongst the different collision types (i.e. Rock – Rock, Rock – Balls, Rock – Liner, Ball – Ball, and Ball – Liner) is given in Table 8-8. The given percentages of the impact energy are relative to the total dissipated energy during one full revolution.

Table 8-8: Distribution of impact energy

	Percent of total impact energy	
Collision type	Slice 1	Slice 4
Rock - Rock	6.59	0.4
Rock - Liner	1.23	0.4
Rock - Balls	34.35	9.62
Ball - Ball	55.88	86.59
Ball - Liner	1.95	2.99

From Table 8-8, it is observed that the Rock – Rock percent input energy is higher at slice 1 than at slice 4; this is due to a higher number of rocks (more than number of steel balls) compared to fewer rocks in slice 4, (Table 8-3). This also applies to Rock – Ball input energies where the higher numbers of rocks in slice 1 lead to higher energy inputs. The high ball load and fewer rocks in slice 4 are reflected by the higher percentage of Ball – Ball and Ball - Liner energy inputs.

It should be borne in mind that the limitation of DEM simulations not including the fine material means that only the breakage of + 11.2 mm material (in this instance) is simulated. The high ball – ball impact ratio does not account for the fine slurry between the balls, so the apparent massive waste of energy indicated by the simulations is not the case in reality.

8.5.9 Energy spectra comparison

The energy spectra of collisions detected by the DEM calculation (Appendix 5) showed that overall; particles at slice 1 produced higher energy spectra than those at Slice 4.

8.5.9.1 Modal peaks from energy spectra

Table 8-9 shows the highest energy loss, (modal peak) detected for each collision interaction during the simulation period, and the corresponding collision rate for each modal peak.

Table 8-9: Energy spectra modal peaks

Collision type	Slice 1		Slice 4	
	Collision rate (s-)	*Peak energy loss, J , X 10^{-6}*	*Collision rate (s-)*	*Peak energy loss, J , X 10^{-6}*
Total collisions	3, 333	1, 810	30, 000	8, 770
Rock - Rock	667	601	1, 320	258
Rock - Liner	400	0.5	1, 667	2
Rock Balls	1, 667	1, 440	7, 000	1, 590
Ball - Ball	1, 327	12, 000	30, 000	12, 100
Ball Liner	33	141	1, 000	68.1
Balls collisions by size				
All surfaces - 106	7	2, 570	133	9, 570
All surfaces - 75	400	4, 590	6, 667	10, 400
All surfaces - 53	1, 333	6, 320	21, 333	9, 290
All surfaces - 38	1, 000	4, 590	20, 000	6, 200
All surfaces - 27	667	2, 350	12, 000	3, 680
All surfaces - 19	467	1, 520	6, 667	1, 890
Rocks collision by size				
All surfaces - 150	12	1, 280		-
All surfaces - 106	53	1, 710	67	10, 700
All surfaces - 75	127	3, 640	267	11, 100
All surfaces - 53	200	4, 730	667	8, 280
All surfaces - 38	267	2, 720	1, 200	4, 640
All surfaces - 27	467	1, 660	1, 333	2, 320
All surfaces - 19	600	903	1, 267	1, 160
All surfaces - 13.4	800	378	6, 667	354
All surfaces - 9.5	900	2.15		-
Rocks number	58, 952		36, 188	
Steel balls number	27, 544		16, 417	
Total number particles	86, 496		52, 605	

Even though the modal peak is a point that corresponds to the *energy* at the highest number of collisions detected, a comparison of this peak for different collision types and then for each size at slice 1 and slice 4, gives a reasonably good indication of the energy spectra.

From Table 8-9, the modal peak energies are generally higher at slice 4 than at slice 1, even though the highest peak of 1.2 * 10^{-2} J was the same for both slices and recorded for the Ball – Ball collisions. This is expected as at each slice, the grinding media which is harder than rocks should give out more collision energy. The modal peaks for the Rock – Liner and for the small rocks (9.5 mm at slice 1 and 13.4 mm at slice 4) show that these collision events resulted in the least impact energy loss. The modal peaks reveal that the maximum energy for both the rocks and the balls was consistent, each 53 mm at slice 1 and 75 mm at slice 4.

The collision rate peaks from Table 8-9 were determined by dividing the peak number of collisions of the energy spectra by the total simulation time (15 seconds). Table 8-9 also reveals that peak collision rates at slice 4 are higher than those at slice 1 due to a higher proportion of small particles and a higher ball load at slice 4. The collision rate peaks were driven by the particles' number, size and surface properties; friction resistance and coefficient of restitution of particles at each slice. The Ball – Liner interactions and the biggest (top-size) rocks' contacts produced the lowest collision peaks at both slices, since the two contact types had the least collision probability within the mill. The highest collision rate peaks were Rock – Ball at slice 1 and Ball – Ball at slice 4 due to the respective high number of rocks, and balls at the two slices. Unexpectedly, the Rock – Liner collision peak was higher at slice 4. This could be explained from visual inspection of the particle traces (Figure 8-2), where it is apparent that the smallest size particles (dominant at slice 4) colored blue, were closest to the shell in the en-masse zone. Additionally, this visual observation is reinforced by the fact that the same small (blue) particles (Figure 8-2), form the outer most trajectory in the mill because they are thrown further than the big particles which are obscured (at slice 1) and resides in the central region of the charge. The 53 mm balls (class 3 in Table 8-4) had the highest collision rates since they were the largest fraction amongst the steel balls. The smallest size rocks produced the highest collision rates amongst rocks.

8.6 ROCKS IMPACT ENERGY SLICE COMPARISON

This section describes the comparison of the impact energy absorbed by the rocks during the DEM simulations at the inlet and discharge mill positions. To highlight how low the DEM impact energies are, the impact energies applied to the rocks in the drop weight tests (DWTs) are also included in this analysis. The huge difference in the impact energies both in joules and kWh/t applied to the rocks in the DWTs and in DEM is illustrated in Table 8-10. It is observed from Table 8-10 that most of the energies produced from particle collisions in DEM are not large enough to cause severe breakage on a single impact. For the chosen DEM range, breakage on a single impact could only be

attained at the largest energy range (2.25 J), for the 14.5 mm rock size at 0.1 kWh/t, and this is equivalent to the minimum specific comminution energy used in the drop weight tests.

Table 8-10: Difference in applied impact energy range between DWTs and DEM simulations

	DWT energy range, ore mean SG = 3.934					
Size, mm	*2.5*	*1.0*	*0.4*	*0.25*	*0.10*	kWh/t
57.8	3577	1431	572	358	143	Joules
41.1	1285	514	206	129	51	
28.9	447	179	72	45	18	
20.6	163	65	26	16	6.5	
14.5	57	23	9	6	2.3	
	DEM energy range selected for analysis					
	2.25	**0.9**	**0.1**	**0.03**	**Joules**	
57.8	*0.002*	*0.001*	*0.0001*	*0.00002*	kWh/t	
41.1	*0.004*	*0.002*	*0.0002*	*0.00005*		
28.9	*0.01*	*0.01*	*0.0005*	*0.0001*		
20.6	*0.03*	*0.01*	*0.0014*	*0.0004*		
14.5	*0.10*	*0.04*	*0.0040*	*0.0011*		

The geometric mean size of rocks for the DWT was slightly different to the mean size of the rocks used in the DEM simulations as shown in Table 8-11. However, the difference between the mean sizes is small and at selected energy ranges the response (collision frequency for DEM and amount of breakage for DWTs) can reasonably be analyzed at these mean sizes. As a way of simplification, the geometric mean size of rocks from the DEM simulations are generally quoted in the assessment between the DEM and DWT results.

Table 8-11: Geometric mean size (mm) of experimental rocks

	1	2	3	4	5
DWT	57.8	41.1	28.9	20.6	14.5
DEM	53	38	26.6	19	13.4

The amount of breakage (t_{10}) versus the comminution specific energy (Ecs) curves from DWTs and the energy spectra (the collision frequency versus impact energy) from the DEM simulations at the five mean rock sizes are illustrated in Figure 8-3 to Figure 8-7.

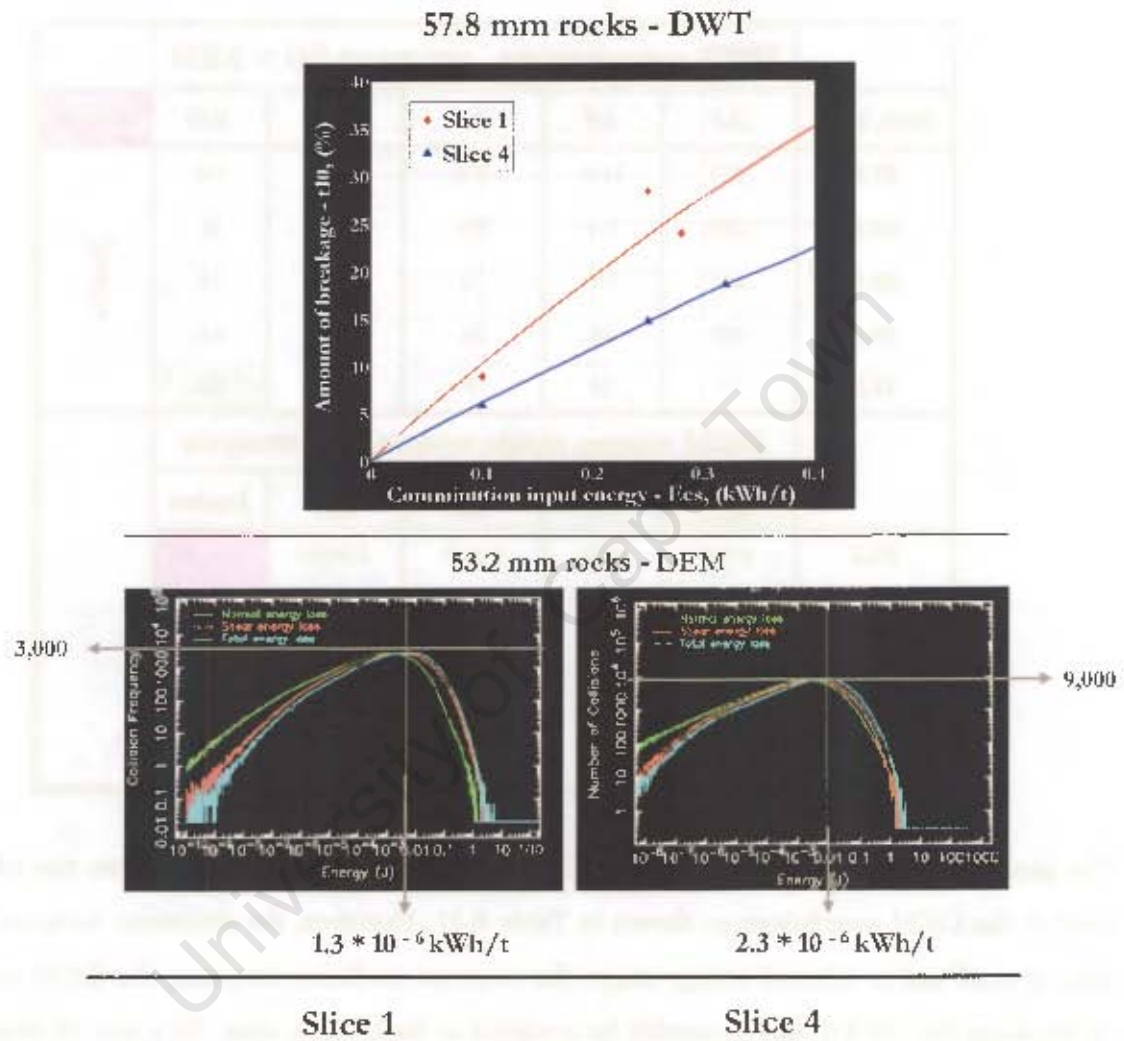

Figure 8-3: Impact energy comparison for the 53.2 mm rocks

From Figure 8-3, the amount of breakage (t_{10}) was lower at slice 4 for varying energy (Ecs) values, and for the DEM results, slice 4 had a higher energy spectra. The DWTs lower amount of breakage at slice 4 is attributed to the competence (hardness) of rocks picked from slice 4. The DEM energy spectra of the 53.2 mm rocks being higher at slice 4 is attributable to a high proportion of steel balls relative to the amount of rocks within slice 4.

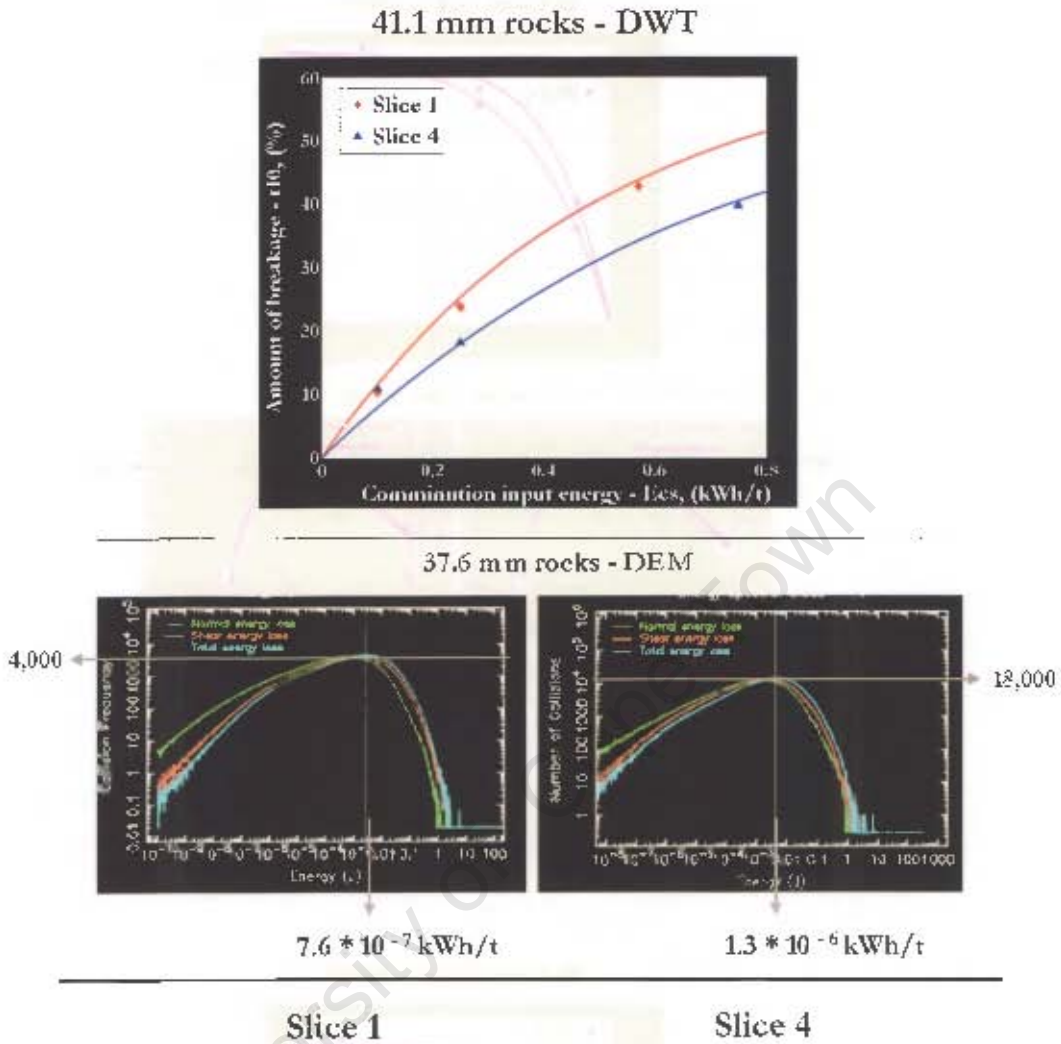

Figure 8-4: Comparison of impact energy for the 37.6 mm rocks

From Figure 8-4, at any given Ecs for the DWT graph, slice 1 has a higher t_{10} implying that the 37.6 mm rocks were softer at slice 1 and thus more breakage could be achieved at slice 1. Similarly, at any given t_{10} (amount of breakage) greater than zero, the energy required to achieve breakage of these rocks is lower at slice 1. The DEM energy spectra at slice 4 reveal a higher number of collisions and a higher impact energy modal peak for the 37.6 mm rocks. Similar conclusions can be drawn for the three smaller sizes as shown in Figure 8-5 to Figure 8-7.

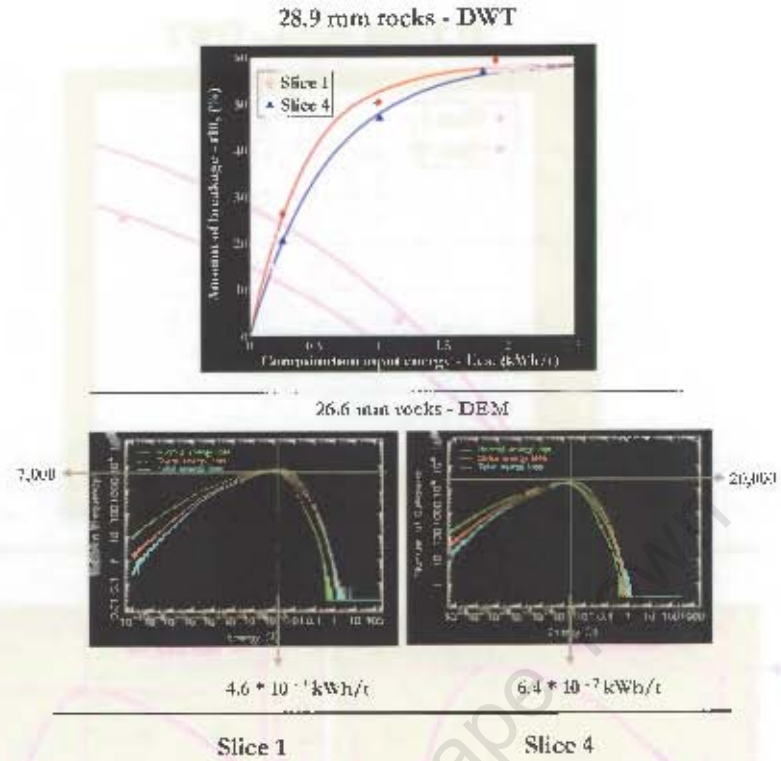

Figure 8-5: Energy comparison for 26.6 mm rocks

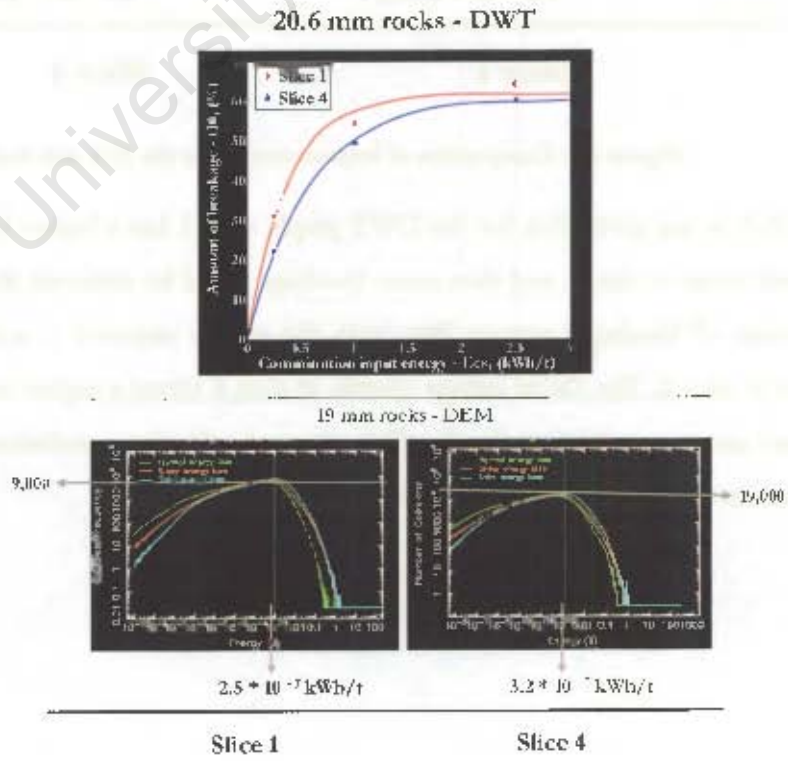

Figure 8-6: Energy comparison for the 19 mm rocks

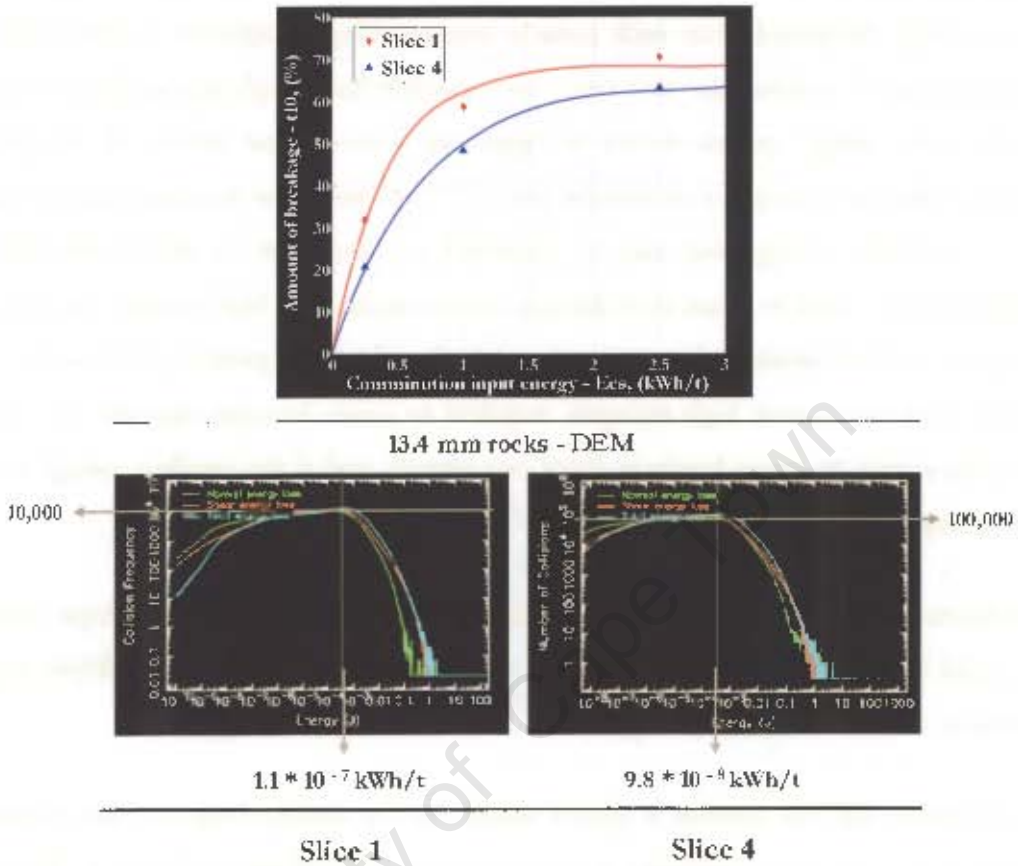

Figure 8-7: Energy comparison for 13.4 mm rocks

As shown in Figure 8-7, the smallest 13.4 mm rocks DWTs specific input comminution energy was higher at slice 4 like the rest of the bigger size rocks. However, for the DEM simulations, even though the 13.4 mm rocks had a higher collisions frequency at slice 4 than at slice 1, these collisions only resulted in lower energies as these particles had smaller mass.

8.7 USING DEM TO PREDICT PRODUCT PSD

This section describes a novel technique employed to use the DEM energies absorbed by the same rock repetitively from multiple impacts, to predict the size distribution of the fines that might be produced after breakage has been attained from the cyclic impacts.

The premise for using small collision energies to achieve breakage after cyclic impacts is described in an elementary approach.

The DEM energy spectra give all detected collisions of particles during a simulated mill revolution. During the simulation time, the detected collisions are binned (allocated) according to the magnitude of the energy dissipated from each particle impact. After completion of the DEM simulation (4 revolutions in 15 seconds for this case), each particle has a high probability of receiving multiple impacts. The energy spectra shown in Appendix 5 reveal that almost all the particles received multiple collisions during the simulation time of 15 seconds. The multiple impacts that each particle receive dissipates energy that may be classified as either low or moderately high. Low impact energies are too small to cause bulk damage, whilst moderately high energies are those that are high enough to achieve breakage if repetitively applied to the same particle. The number (frequency) of impacts with moderately high energies, required to cause fracture can only be determined if the minimum energy to cause breakage from one impact, and if the smallest energy to break particles from multiple impacts are known.

In industrial mills, rocks are expected to receive moderately high energy multiple impacts. Although this could be after longer mill revolutions, the breakage achieved from multiple impacts might be significant towards the final milling.

The emphasis for this analysis is placed mainly on the multiple impacts that generate moderately high energies. Also, the assessment in this section is restricted only to breakage that results from the impact mechanism, assessing the rate of production of fines from attrition and abrasion is beyond the scope of this work.

8.7.1 Assumptions

The following assumptions were made when using the DEM impact energies to predict the size distribution and the mass of fine rock particles generated per unit time (second) from repeated absorption of moderately high DEM energies;

1. Multiple (cyclic) impacts of moderately high magnitude energies on rocks may have a significant contribution towards total impact breakage in SAG mills.
2. The DWT comminution specific energy (E_{cs}) can be equated to the collision impact energy in the DEM simulations. In both cases the energy results from impact events between two particles/surfaces.
3. The rocks rate of breakage is proportional to the DEM collision rate (number of impacts per fixed simulation time) that would cause breakage.

4. The impact energy resulting from each collision during the DEM simulations is shared equally (50/50) between the interacting particles/surfaces.
5. According to Split-Hopkinson Pressure Bar experiments by Bbosa (2006), the energy absorbed to rocks is only about 20 % of the input energy. Since the DWTs measures the input energy whilst DEM gives the absorbed energy, multiplying the DEM energy by 5 gives an effective impact energy that correlates with the DWTs energy.
6. From the work of Ryan Whyte (2005), the minimum energy to achieve breakage from one impact (E_{cdi}) may be taken to be 0.05 kWh/t (Figure 8-8) and the minimum energy (E_{ci}) that can cause breakage after several repeated impacts, is estimated to be 0.001 kWh/t in the current study.
7. The size distribution of progeny rocks broken from moderately high energy multiple impacts would be identical to the size distribution of rocks broken from the single impact energy, E_{cdi}. This assumption follows from Griffith's[3] theory of brittle fracture and Dieter's (1988) description of the breakage process of brittle materials.
8. According to Griffith, brittle materials have a population of fine cracks that create points of high stress concentrations, and if energy is applied to the high stress concentration points, fracture is attained at levels below the theoretical predictions. The theory of Griffith in its entirety is stated below:

"A brittle material contains a population of fine cracks which produce a stress concentration of sufficient magnitude so that the theoretical cohesive strength is reached in localized regions at a nominal stress which is well below the theoretical value."

The theoretical cohesive strength is a point at which the repulsive and the attractive forces between two neighboring atoms in a crystal become negligible due to increased distance of separation between the two atoms, due to actions such as tensile loading.

Griffith's theory is popular in brittle metals fracture mechanics and among physical Metallurgists. According to Dieter (1988), even though Griffith's cracks have not been observed up to magnifications of the electron microscope, there is a considerable amount of experimental evidence

[3] A. A. Griffith, *Philos. Trans. R. Soc. London*, Vol. 221A, pp. 163 – 198, 1920; *First Int. Congr. Appl. Mech.*, Delft, 1924, p. 55; this paper has been reprinted with annotations in *Trans. Am. Soc. Met.*, Vol. 61, pp 871-906, 1968.

to show that micro-cracks can be produced from plastic deformation. Dieter further describes the process of breakage to be comprised of three stages. (1) Dislocation pile-ups are produced from plastic deformation. (2) Crack initiation then starts. (3) With cyclic application of stress, the produced crack propagates. Finally breakage occurs.

In the current analysis, both Griffith's theory and Dieter's description of the breakage process are used to support the argument that the breakage distribution from multiple impacts is identical to that broken from the E_{cet} single impact energy. It is assumed that for the multiple impacts on rocks, cracks are always initiated on application of moderately high energies that are less than E_{cet} in magnitude. Additionally, the micro-cracks are assumed to define the boundaries of the breakage product (progeny particles) such that for energies between E_a and E_{crit}, the progeny particles will have the same size distribution as that originally outlined by micro-cracks. When the absorbed impact energy is greater than E_{crit}, severe breakage is achieved and the original outline of the micro-cracks is disturbed. Thus the energies greater than E_{crit} are expected to create distinct progeny rocks' size distributions.

8.7.2 Procedure for predicting the progeny fines size distribution

Four DEM energy ranges were chosen for comparison of multiple impacts achieved during the simulations and for predicting the PSD and fines produced from the calculated breakage.

- The impact energy from the energy spectra was first multiplied by 0.5 (to allocate to a single rock) and then by 5 to convert it to the effective impact energy that correlates with the DWTs energy. To obtain the specific energy (J/kg) absorbed by a rock, this equivalent DWT energy is divided by the average mass of the rock at any given size. The specific energy is then converted to kWh/t by dividing by 3600 (since 3600 J/kg = 1 kWh/t).
- The impact energy (kWh/t) is assessed and checked against the degree of breakage versus comminution energy curve (Figure 8-8). If the energy is less than E_a, no breakage occurs, if the energy lies in the $E_a \leq E_b < E_{crit}$ range, breakage may occur from multiple impacts/hits and for higher energies greater than E_{crit} severe breakage is achieved from a single impact (Figure 8-8).

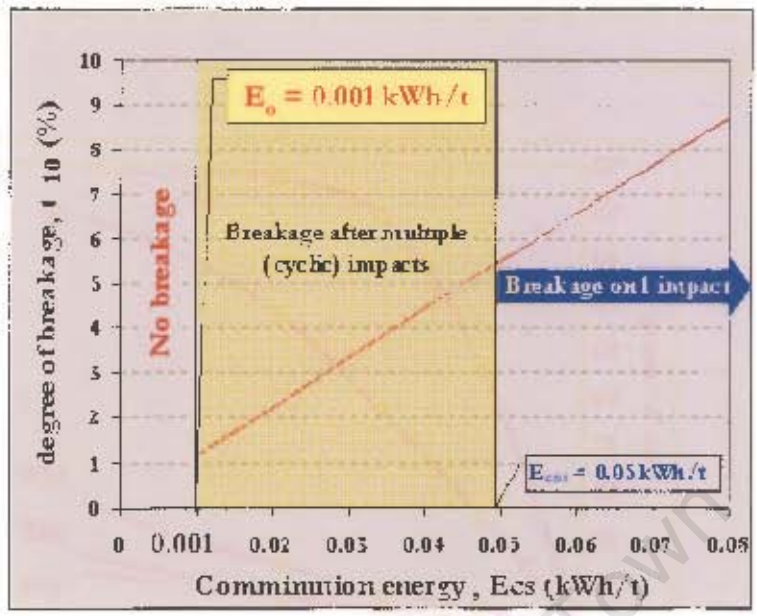

Figure 8-8: Effect of the specific comminution energy on the degree of breakage, t_{10}

- The evaluated moderately high energies (E_h) that were greater than 0.001 kWh/t but less than 0.05 kWh/t are those that require several hits to achieve breakage. As shown in Table 8-12, the numbers of collisions from the energy spectra were divided by the total simulation time (15 seconds) to obtain the collision rate (r_c) per second for four selected energy ranges.
- To calculate the number of collisions required to cause breakage from multiple hits, the single impact breakage energy E_{crit} is divided by multiple hits breakage energy E_h (i.e. number of hits to cause breakage, $n = E_{crit} / E_h$).
- The number of breakage events from multiple impacts is calculated by dividing the collision rate r_c by the number of hits to cause breakage, n (breakage events = r_c / n).
- The product size distribution for the minimum breakage energy E_{crit} and of larger energies were determined by first calculating the standard breakage index t_{10}, the percent passing one tenth of the original rock size, from the $t_{10} = A\,(1 - e^{-bEcs})$ equation using the A and b impact parameter values for each of the five rock sizes.
- After the degree of breakage t_{10} had been calculated at the four selected Ecs energies, the appearance function (degrees of breakage – t values, at different levels) were read off from the plot of the normalised relative size distribution against the standard breakage index t_{10} (Figure 8-9) for both mill positions.

The routine for obtaining the progeny size distribution points (t – values) relative to the initial particle size to construct the predicted product size distribution has been proposed before by

Morrison and Cleary (2004) although no typical predicted mill product size distributions has been reported in the literature.

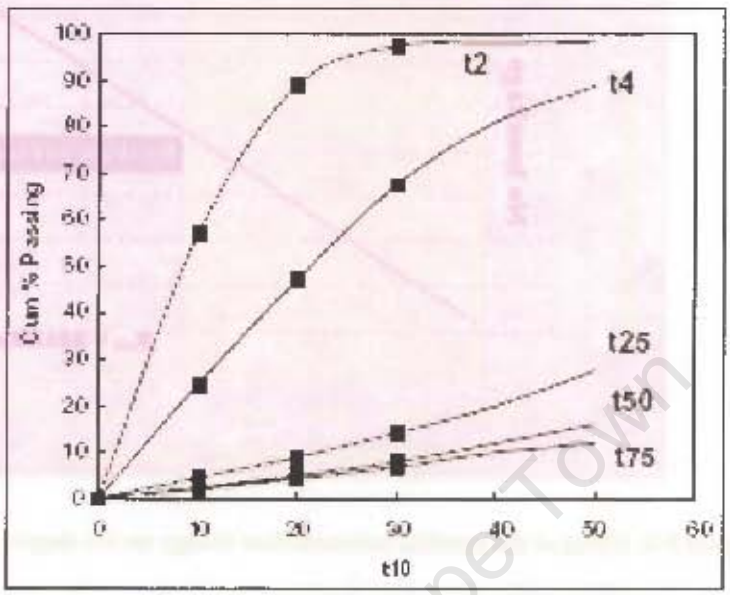

Figure 8-9: Normalised relative size distributions plotted against degree of breakage (t_{10}), after Napier-Munn *et al*, (1999)

Figure 8-10, shows the appearance of the predicted product size distribution constructed from a set of degrees of breakage (the appearance function t_ns, – percentage passing one nth of the original rock size, Y).

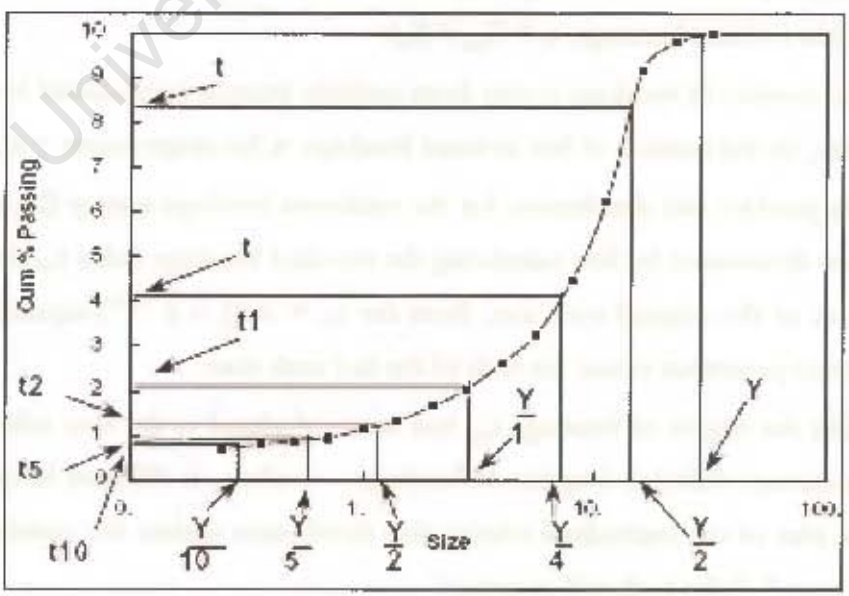

Figure 8-10: Relative cumulative size distribution predicted from the appearance function (t) after Napier-Munn *et al*, (1999)

8.7.3 Comparison of impacts at four selected DEM energy ranges

Four energy ranges from the DEM energy spectra were chosen and used to compare the collision rates between the inlet slice and the discharge slice for the different impact interactions encountered during the simulation period.

The selected effective impact energies chosen for comparison of the collision rates, as obtained from the energy spectra were 2.25 J, 0.9 J, 0.1 J and 0.03 J, Table 8-12.

Table 8-12, gives a summary of the DEM collision rates detected at the four chosen impact energy ranges, shown to be higher at slice 4 than at slice 1.

Table 8-12: DEM collision rates (S^{-1}) at four selected energy ranges for distinct impacts

DEM Energy range	2.25 J		0.9 J		0.1 J		0.03 J	
Collision type	Slice 1	Slice 4	Slice 1	Slice 2	Slice 1	Slice 4	Slice 1	Slice 4
Rock - Rock	1.3	1.2	5	4	100	100	267	333
Rock - Liner	0.7	2.0	2	7	13	80	40	133
All surfaces - 106 mm rocks	0.7	1.8	5	7	40	47	53	67
All surfaces - 75 mm rocks	0.3	4.7	3	20	120	400	200	667
All surfaces - 53 mm rocks	0.1	1.3	1.3	7	100	333	267	1, 267
All surfaces - 38 mm rocks	0.03	0.07	0.2	0.7	67	200	267	1, 000
All surfaces - 27 mm rocks	0.01	0.01	0.1	0.5	27	100	133	400
All surfaces - 19 mm rocks	0.004	0.1	0.1	0.7	13	200	100	1, 333
All surfaces - 13.4 mm rocks	6.7	26.7	7	200	533	2, 667	1, 333	4, 667
	Collision rate (S^{-1})							

From Table 8-12, the lowest collision rates were detected at the maximum impact energy (2.25 J) during the entire simulation period. As expected the highest collision rates were at the lower 0.03 J energy range.

Figure 8-11 also shows the collision rates of the four selected DEM energies and reveal that the collision rates at slice 4 are generally higher than those at slice 1.

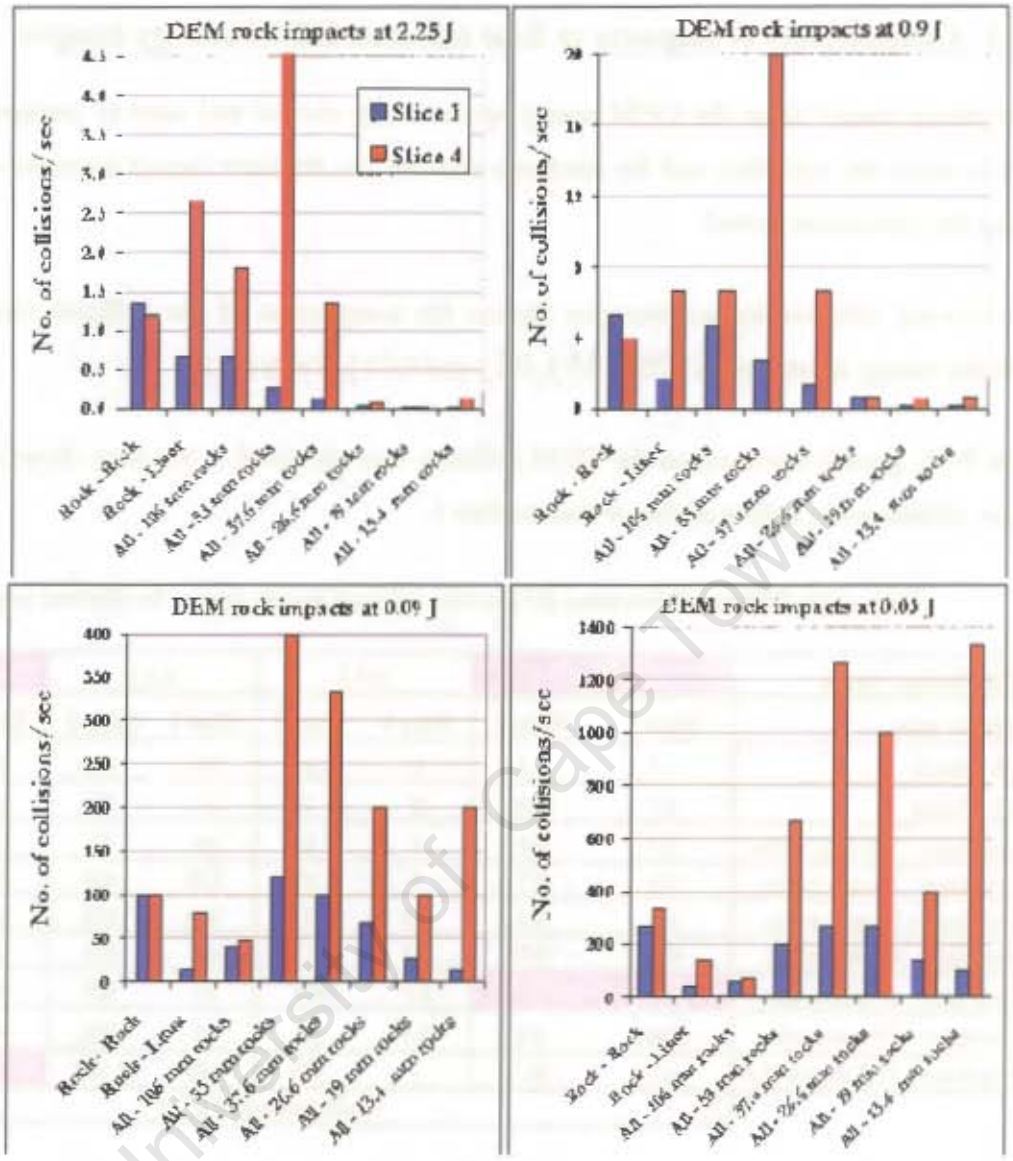

Figure 8-11: DEM collision rate comparison at four different energy ranges

Figure 8-12 shows the degree of breakage (t_{10}) correlation between the two mill positions for fracture attained from the single impact breakage energy E_{cs} and from 0.1 kWh/t. The degree of breakage drops at the discharge (slice 4), and the decrease in the t_{10} is more pronounced for the largest rock size (53 mm). The drop in the amount of breakage at the mill discharge is expected as the rocks were more competent at this position (Chapter 7).

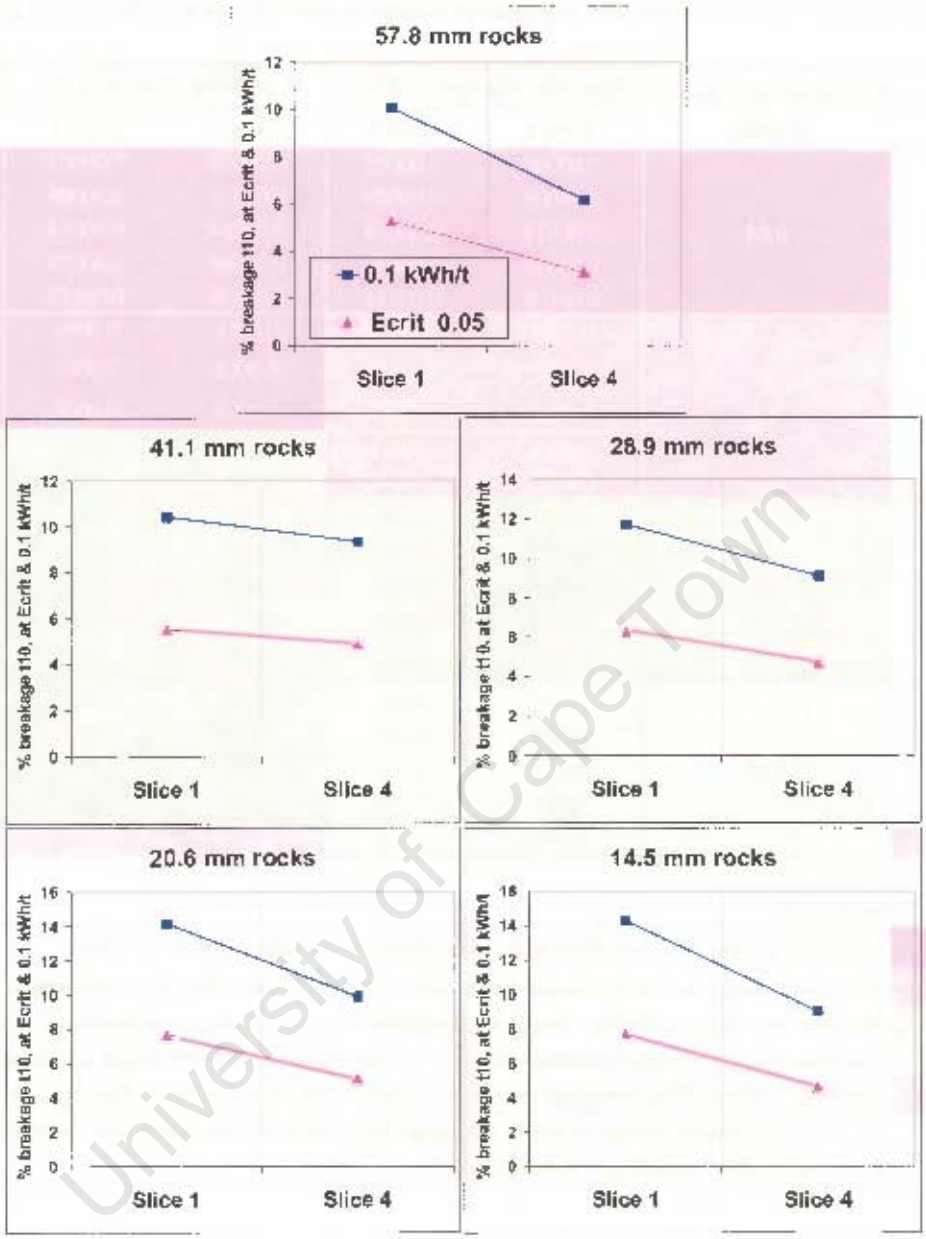

Figure 8-12: Predicted DWT impact breakage (t_{10}) at four energy ranges for inlet & discharge.

8.7.4 Product size distribution at four selected DEM energy ranges

A summary of specific energies and breakage events from multiple impacts for four DEM energies is given in the color coded Table 8-13. The rose color shows low energies that could not generate breakage regardless of applying multiple impacts to a rock. Yellow is for the fairly high energies that could achieve breakage only on several hits whilst blue is for single impact breakage energies.

Table 8-13 shows that more breakage events occur at slice 4.

Table 8-13: Collision rates and cumulative energy at specific sizes for four DEM energy ranges

Size, mm	DEM energy range Joules	Specific energy, kWh/t		# of brkg hits, E_b/E_{crit}		Breakage events	
		Slice 1	Slice 4	Slice 1	Slice 4	Slice 1	Slice 4
57.8	0.03	0.00002	0.00002	0.00002	0.00002	0	0
41.1		0.00005	0.00005	0.00005	0.00005	0	0
28.9		0.00014	0.00014	0.00014	0.00014	0	0
20.6		0.00038	0.00039	0.00038	0.00039	0	0
14.5		0.00109	0.00112	0.00109	0.00112	0	0
57.8	0.1	0.0001	0.0001	0.0001	0.0001	0	0
41.1		0.0002	0.0002	0.0002	0.0002	0	0
28.9		0.0005	0.0005	0.0005	0.0005	0	0
20.6		0.0014	0.0014	0.03	0.03	0.7	2.8
14.5		0.0039	0.0040	0.08	0.08	1.0	16.1
57.8	0.9	0.001	0.001	0.01	0.01	0.03	0.3
41.1		0.002	0.002	0.03	0.04	0.05	0.2
28.9		0.005	0.005	0.10	0.10	0.07	0.07
20.6		0.014	0.014	0.27	0.28	0.04	0.15
14.5		0.039	0.040	0.79	0.80	0.10	0.54
57.8	2.25	0.002	0.002	0.03	0.03	0.01	0.15
41.1		0.004	0.004	0.09	0.1	0.01	0.12
28.9		0.012	0.013	0.25	0.3	0.01	0.02
20.6		0.034	0.035	0.69	0.7	0.005	0.009
14.5		0.098	0.101			0.004	0.133

Energy colour code	
	Absorbed energy very low (below E_o) and therefore no breakage occurs at all
	Absorbed energy is low, breakage might not occur & occurs only on several hits at some sizes
	Medium repetitive collision energy, E_b, Requires several hits to attain breakage. Lies in E_o - E_{crit} range
	Collision energy is high, breakage occur by either several hits or by single hit depending on rock size
	Breakage energy, Ecs, breakage achieved by single hit. Ecs is greater than E_{crit}, & used in DWTs
	E_o, is the minimum energy to cause breakage regardless of how many hits are applied to a rock E_o = 0.001 kWh/t and E_{crit} = 0.05 kWh/t

From Table 8-13, it is apparent that there was no breakage attained from the tiny 0.03 J DEM energy range at all rock sizes. Breakage after cyclic impacts were achieved from the 0.1 J energy range at rock sizes 20.6 and 14.3 mm, from the 0.9 energy at all rock sizes, and from the 2.25 energy range at all sizes except the smallest 14.3 mm rock size. The single impact breakage being achieved only at one size (2.25 J energy range at 14.3 mm rock size) from the full simulations, highlights how small the energies obtained from DEM simulations may be.

Table 8-14 gives the degrees of breakage (t_{10}) calculated from the specific impact parameters (A and b) for the single impact breakage energy E_{crit} at slice 1 and slice 4.

Table 8-14: Degree of breakage and impact parameters for E_{cri} energy at slice 1 and slice 4

E_{cri} = 0. 05 kWh/t				
	A	b	Energy, kWh/t	t_{10}
Slice 1	64.46	1.98	0.05	6.1
Slice 4	63.86	1.33	0.05	4.1

From Table 8-14, it is shown that the t_{10} is greater at slice 1 than at slice 4 which implies that breakage yielded more progeny particles at the inlet slice than at the discharge slice. The amount of breakage being higher at slice 1 than at slice 4 is expected as was established from the drop weight tests results presented in chapter 7.

The size distribution from the single hit breakage energy E_{cri}, shown in Figure 8-13 , obtained from the procedure described in section 8.7.2, reveal a finer size distribution for rocks at slice 1. The observed finer distribution at slice 1 also implies that at a given impact energy, more breakage is attained at slice 1 than at slice 4.

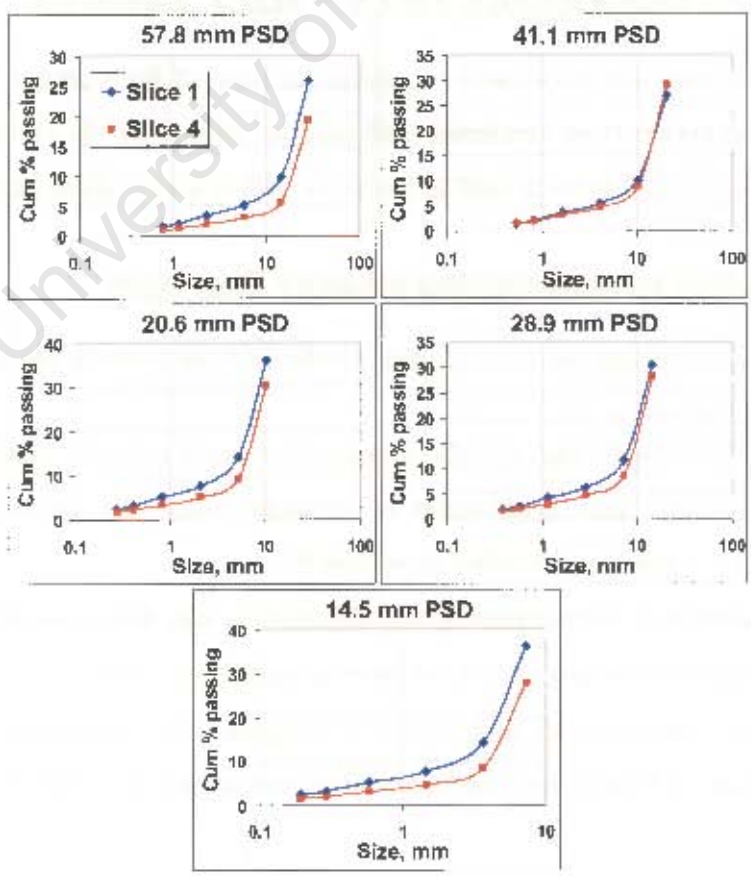

Figure 8-13: Single hit breakage product size distribution for E_{cri} , 0.05 kWh/t

Figure 8-14 shows the PSD obtained from the only energy (0.098 kWh/t at slice 1 and 0.101 kWh/t at slice 4) that achieved breakage from a single impact, for the 14.3 mm rock size.

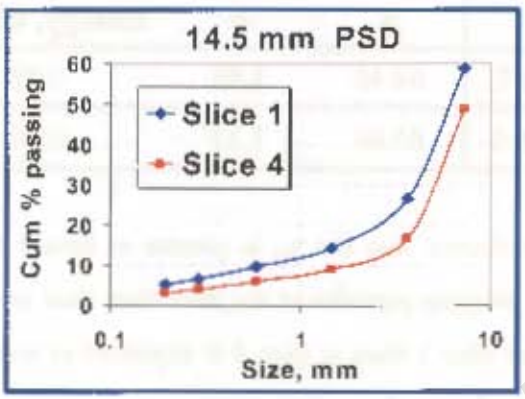

Figure 8-14: Product size distribution for the 14.5 mm rock at an absorbed energy of 0.1 kWh/t

From Figure 8-14, the PSD of the rocks at slice 1 is finer than that at slice 4 which is coarser. The coarser PSD of progeny rocks at slice 4 is derived from the 14.3 mm parent rock being harder than that at slice 1, as given by the drop weight tests results in Chapter 7.

8.8 DEM FINES PREDICTION – MILL PRODUCT MASS

This section describes a method used to predict the mass of fines produced from multiple impacts, and presents the results from simulating mill product mass from the cyclic impacts. The total mass calculated at the two mill slices is used to assess modelling long mills as perfectly mixed.

8.8.1 Procedure for determining progeny fines mass

The method for calculating the mass of fines produced from multiple impacts is as follows;

- For the moderately high specific energies that could generate breakage on repeated impacts, the cumulative size distribution of progeny rocks was obtained from the appearance function (t values) as described in section 8.7.2.
- The cumulative percent passing size distribution was then converted to the percent passing size to indicate the amount (%) of fines in each broken size.
- The mass produced in each size was computed by multiplying the percent passing, the individual rock mass and the breakage events shown in Table 8-13 for each specific rock size.

- The total mass produced at each slice is the sum of all the fines mass calculated from all the rock sizes.

8.8.2 Predicted mass of progeny rocks from multiple impacts

The calculated mass produced from multiple impacts is shown from Figure 8-15 to Figure 8-19 and shows a higher mass production at slice 4 which can be attributed to a higher number of breakage events at the mill discharge slice.

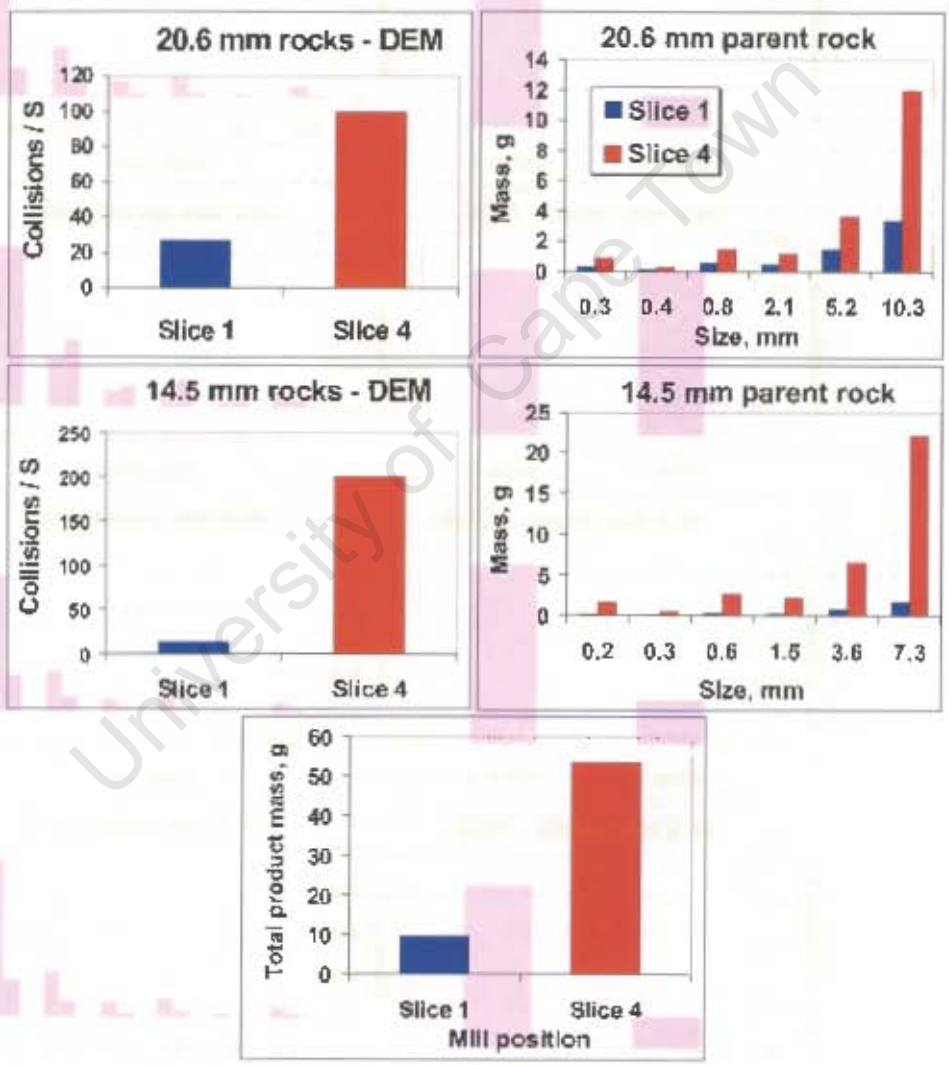

Figure 8-15: DEM collision rate and the predicted product mass at 0.1 J energy range

Figure 8-15 shows the individual progeny mass and the total mass predicted from collision rates per second for the 0.1 J energy range. Both the total and specific masses predicted are more at slice 1 than at slice 4.

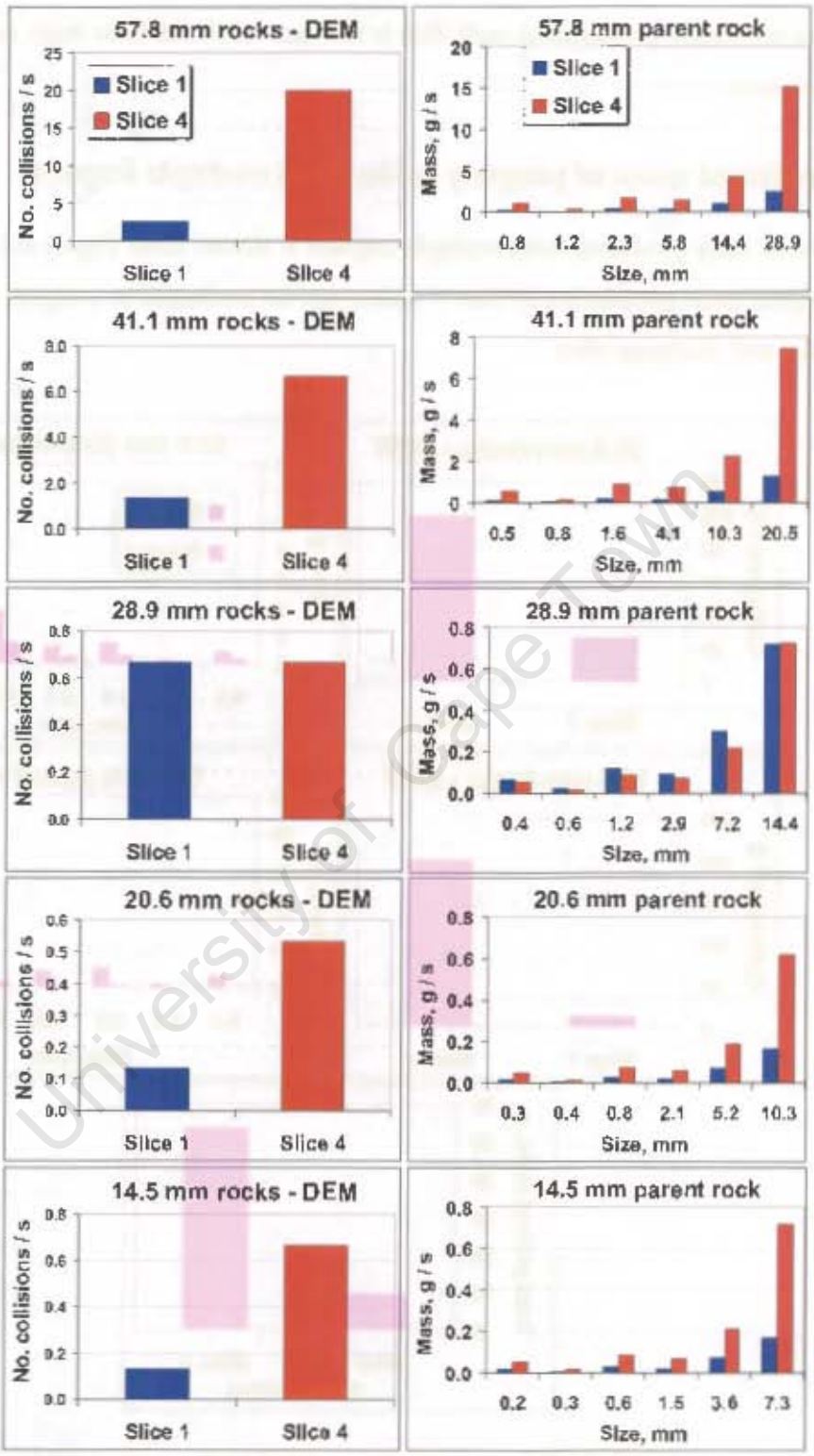

Figure 8-16: DEM collision rate and the predicted product mass at 0.9 J energy range

Figure 8-16 shows the specific masses of progeny rocks predicted from multiple impacts of the 0.9 J energy magnitude, whilst Figure 8-17 shows the calculated total mass. Both graphs show a higher mass prediction at slice 4 than at slice 1.

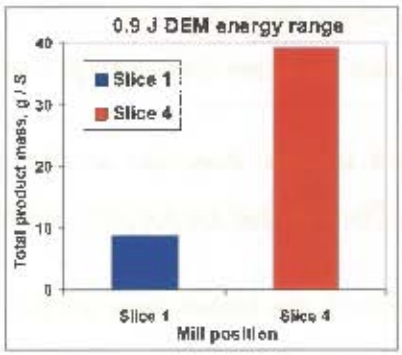

Figure 8-17: Total predicted product mass at for the 0.9 energy range

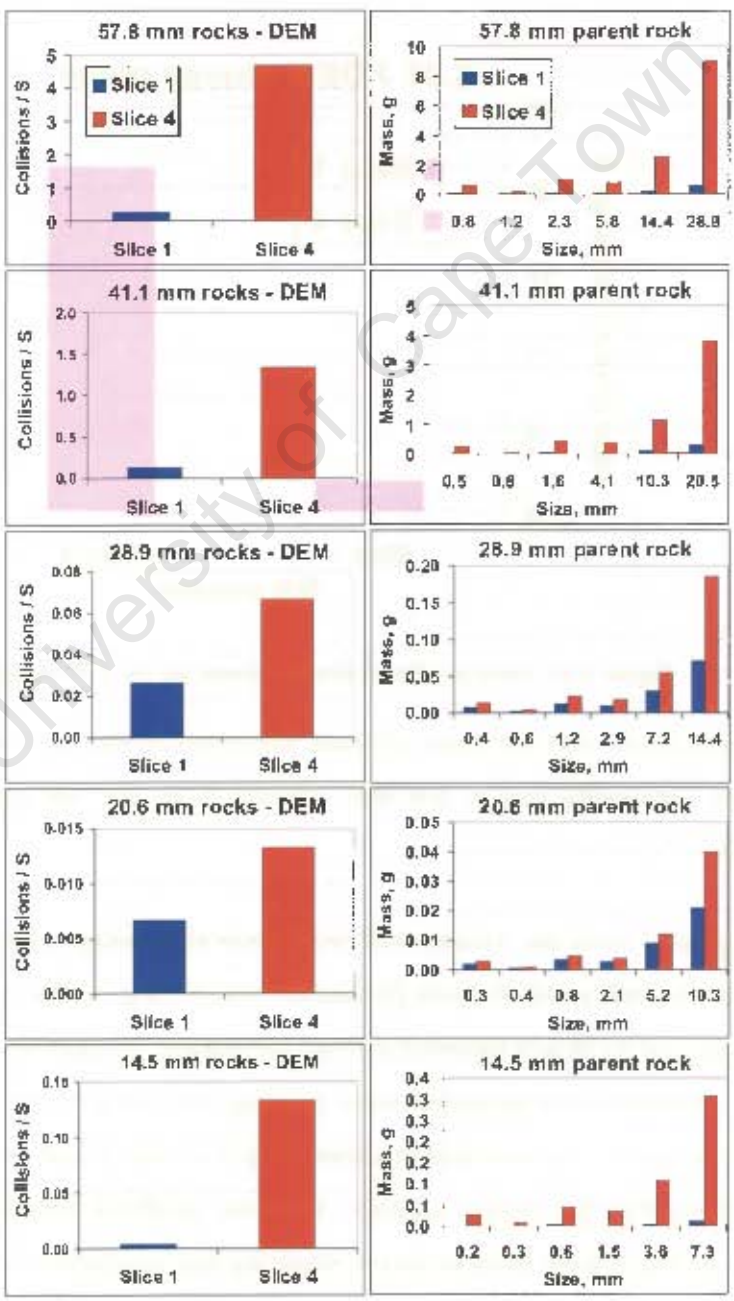

Figure 8-18: DEM collision rate and the predicted product mass at 2.25 J energy range

The mass predicted from repetitive impacts of the 2.25 J DEM energy is shown in Figure 8-18 for the individual progeny sizes, and the entire fines mass is shown in Figure 8-19.

The predicted mass at slice 4 is more than that at slice 1 mainly due to the higher number of collisions recorded at slice 4. The high ball load at slice 4 is attributed for this observation.

From Figure 8-18 and Figure 8-19, the higher mass prediction at slice 4 than at slice 1 suggests that multiple impact breakage may be more pronounced at the discharge end of the mill than at the inlet due to a higher proportion of steel balls at the discharge.

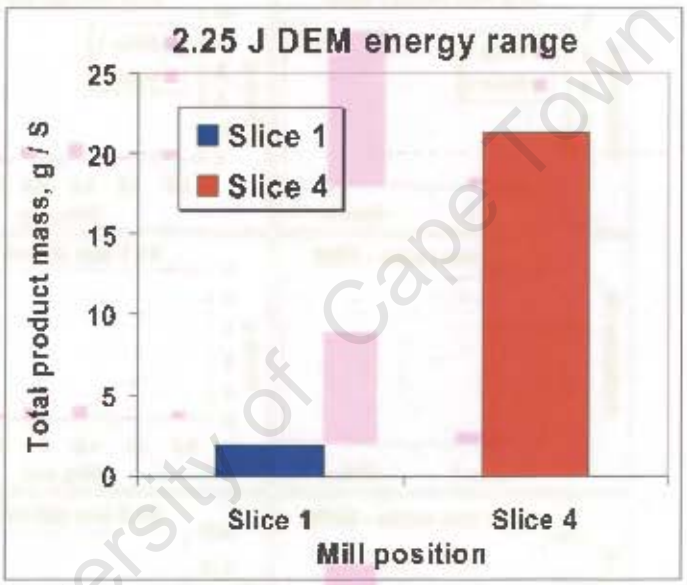

Figure 8-19: Total predicted product mass for the 2.25 energy range

It should be emphasized that the mass of fines presented in this section is that *predicted* from the multiple impacts hypothesis and is not that attained from the full grinding action in industrial production mills.

The total fines ground from the Amandelbult mill, from all breakage processes as determined by the net % - 8 mm of the mill product, from JKSimMet was 6778 g/s. Since fine milling is usually from abrasion breakage, the 6778 g/s included a small proportion of fines that were milled from impact breakage. The combined total predicted mass passing one tenth of the original "parent" rock, t_{10} widely accepted as useful comminution is about 30 g/s at slice 1 and 90 g/s at slice 4 for the four energy ranges selected in the current analysis. Thus the predicted fines mass only gives the impact breakage products which were more at slice 4, implying that production of fines along the mill is not uniform but increases towards the discharge. The actual % passing 8 mm of progeny rocks from

multiple impacts may be calculated only if all the detected collisions and associated DEM energies are incorporated in the computation. The ratio of abrasion at slices 1 and 4 is likely to be in the same proportion to the impact, as the same rate and force of impacts will be responsible for the abrasion. Even though the total % - 8 mm from DEM simulations were not calculated due to computational restrictions, the input of multiple impacts towards final milling is deduced to be slightly significant.

8.9 SUMMARY

A summary for simulating particles impact interactions at the inlet and discharge positions of the Amandelbult mill is as follows;

1. The vital DEM outputs (the toque, power, impact energies, and the collision frequency) were found to be generally higher at slice 4 than at slice 1.
2. The DEM energy spectra were influenced by the particles' numbers, size and surface properties; friction resistance and coefficient of restitution of particles at each slice.
3. The smaller particles, and a higher particle population at a slice generally resulted in a higher number of collisions. However, for the same number of particles, the higher coefficient of restitution and lower friction (*hard* steel balls) produced higher energy impacts than those with high friction and low restitution coefficients.
4. Due to the lower competence of the rocks at slice 1, they produced a finer progeny size distribution.
5. The mass predicted from multiple impacts of moderately high energies were higher at slice 4 than at slice 1. This indicates that impact breakage is not uniform along the mill but increases towards the discharge, due to a higher proportion of steel balls.
6. Provided the assumptions set out in the prediction of progeny rocks size distribution and mass are upheld, the huge difference in the predicted rate of fines production at the mill inlet and at the discharge suggests that long SAG mills should not be modelled as perfectly mixed.

Chapter 9

9 CONCLUSIONS AND FUTURE WORK

The current study has shown that axial segregation is present, at least in the *long* South African style SAG mills. In a way this study has provided an extended understanding of particle segregation in industrial scale mills as this subject was previously almost entirely restricted to laboratory scale investigations. The highlight of this study was the emptying out of the entire mill contents and sizing the particles in four separate slices along the mill, as this gave a lots of confidence in the results obtained from taking the entire sample population. It had initially been planned to empty at least another mill to provide sufficient data comparison on axial particle size distribution in distinct SAG mills, but unfortunately mill down-time concerns from the plants limited the study opportunities. As such, further axial segregation studies along SAG mills, especially on ways of accurately modelling significantly segregated mills should be conducted in the future.

Generally, the results from this study have shown that axial segregation of material along the mill is caused principally by the *transport* and *breakage* mechanisms of particles along the mill. The distinct transport rates of particles are responsible for the observed *size* segregation whilst the particles resistance to breakage reveals axial segregation due to rock *hardness*.

The conclusions on the specific industrial sampling surveys are presented below.

9.1 TRIAL TESTS AND MILL LENGTH SNAP FINDINGS

It can be concluded from the three trial surveys (Chapter 4) conducted at EPC and K4 LonMin Concentrators that collecting samples along the mill after a crash-stop requires gathering enough material to represent different size species in the charge. Taking one set of samples along the mill may not be enough to draw strong conclusions on the particles axial segregation. It is deduced from the trial tests that the slurry sample is the most difficult and challenging sample to collect along the SAG mill. However, the slurry sample if taken correctly should give the best indication of axial segregation of fines in the mill and can therefore be used to assess whether a specific SAG mill being studied has a significantly segregated charge or not.

From the results of the snap surveys along SAG mills of different mill lengths (Chapter 5), it is evident that axial segregation is prevalent in *long* South African style SAG mills. It can be concluded from these results that modelling the mills that have a segregated charge, using the current SAG mill

model would have adverse implications as it was found that modelling can even be complicated further by particle accumulation of "hard" rocks, at the mill discharge due to exit classification.

9.2 AXIAL SEGREGATION FINDINGS

The results from emptying out the entire mill charge and sizing the particles in four axial slices, the DWTs results and the DEM simulations have revealed three primary conclusions.

9.2.1 Segregation of rocks by particle size

From the observed size segregation of the big rocks and slurry (fine rock particles), it can be concluded that the different *transport rates* of the particles is a primary cause of the observed segregation. This is confirmed by the RTD of particles (Chapter 5) where it was found that the smaller particles have shorter residence times than the larger particles. The fine particles (slurry) are preferentially segregated towards the mill discharge due to the ease of transport with which they are entrained in the carrier fluid and can also be easily transported through the interstices between larger particles, whilst the big rocks have longer residence times due to lower transport freedom and preferentially reside within the inlet position of mills. The *breakage* mechanism allows for the disappearance of large rocks so that the broken fine particles (slurry) are concentrated at the mill discharge except when the large particles can survive breakage and migrate to the discharge before they are reduced into small rocks.

9.2.2 Segregation of rocks by ore hardness

The comminution input energy (Ecs) and the Bond work index required for breaking rocks of the same size increased along the mill towards the discharge. Also, the resistance to impact (A*b) and to abrasion (ta) breakage for rocks of the same size collected along the mill increased towards the discharge end. The mass and size distribution of the steel balls was found to be uniform across the mill, attributed to their high wear resistance and could therefore be found anywhere along the mill. The even distribution of balls along the mill and the drop weight test results revealing lower degrees of breakage and requiring more energy for breakage of rocks located towards the discharge, at identical sizes, imply that particle *hardness* affects the axial distribution of the charge along the mill. The hard particles can survive breakage and be transported back and forth and thus can be positioned anywhere along the mill. On the other hand, the softer rocks are not expected to survive breakage and reach the mill discharge as big rocks. Therefore for identical size rocks, the softer

rocks tend to have a higher occupancy at the inlet position of the mill whilst the harder particles can be located anywhere and can also preferentially migrate towards the discharge.

9.2.3 DEM prediction of non-uniform breakage along the mill

The DEM simulations of particles impact events at the inlet and discharge positions of the Amandelbult mill revealed that the collision frequency of particles were different for the two positions, being higher at the discharge than at the inlet. The size distribution of progeny rocks were predicted to have a finer distribution at the inlet position than at the discharge, demonstrating a higher degree of breakage at the inlet than at the discharge, which was concluded from the drop weight test results. The mass of fines predicted from multiple impacts were found to be significantly higher at the discharge than at the inlet position of the mill. The disparity in the predicted mass and size distribution of progeny rocks indicates that impact breakage is not uniform along the mill but increases towards the discharge position. Therefore, it can be concluded that these results suggest that long SAG mills may not be modelled as perfectly mixed mills due to the significant differences in the competence of the particles and the breakage environment along the mill.

9.3 FUTURE WORK

The present work findings have identified rocks transport and breakage mechanisms as the causes of axial segregation in long mills. The implication of the current findings is that modelling of long South African style SAG mills should incorporate rocks axial segregation. The next big challenge, which lies beyond the scope of the current study, is to either find a simplified scheme of incorporating rocks axial segregation in modelling long mills, or to isolate axial segregation in the milling process and then use the current perfect mixing model. Thus future work could make a strong contribution to improving the generic applicability of the SAG mill model.

There is also a potential of modeling the four slices along the mill as perfectly mixed tanks and to calculate the independent discharge and breakage rates for each slice in order to assess the extent to which the size effect has on strongly segregated SAG mills. The Modeling the four slices along the mill is a challenging task with great benefits towards accurately modeling 'long' industrial SAG mills.

9.3.1 Model

The observed gradual segregation in chapter 7, showed that the upper coarse size fractions diminishes (and in some cases the top size fraction is completely absent) in slices towards the mill

discharge. This trend means that certain coarse size fractions will be absent in slices near the mill discharge. There is also classification within the charge, (chapter 5), where the fines are transported preferentially through the voids of large particles, and also at the discharge grate, where the sub grate fine particles are screened out of the mill and the large particles recycled back into the mill. With the observed axial segregation, it is proposed that;

1. The future model may include the gradual axial segregation effect along the SAG mill, a factor in reduction of coarse material and factor in increase of fine particles.
2. Alternatively, tanks in series modeling (multi-segment model) may be applied to long South African style SAG mills.

9.3.2 Hardness inconsistency along the mill

The reason for the observed hardness difference between rocks located at the inlet and those at the discharge could not be conclusively assessed in this work. It is speculated that the ore mineralogy might have an effect; hard rocks might have been predominantly gangue whilst soft rocks could have been rich with the reef. To isolate axial segregation in long mills, the pertinent segregation root cause identified to be the particle competence, should be further interrogated.

Bibliography

Abouzeid, A. M., 2000. *Material transport in Mineral Processing Systems.* Mineral Processing on the verge of the 21 st Century conference proceedings, 2000. Rotterdam, ISBN 90 5809 1724. pp 11 – 17.

Ahlberg, J. H., Nilson, E. N. and Walsh, J. L., 1967. *The theory of splines and their applications.* Mathematics in Science and Engineering, Volume 38, Academic press, New York and London

Bbosa, L. Powell, M.S., Cloete, T. J. 2006. *An investigation of impact breakage of rocks using the Split Hopkinson Pressure Bar.* In SAIMM Journal, 2006, vol.106 no4. pp.291-296.

Benzer, H., Ergun, L. Oner, M. and Lynch A. J., 2001. *Simulation of open circuit clinker grinding.* Minerals Engineering, Volume 14, No. 7, pp 701 – 710, 2001.

Bond, F. C., 1961. *Additions and revisions to "Crushing and grinding calculations"* British Chemical Engineering, August 1961. Vol. 6, No. 8. pp 378-385

Carley-Macauly, K. W., 1954. Ph.D. Thesis, University College, London. 1954.

Chaudhuri, P. K. and Fuerstenau, D. W., 1971. *The effect of mixing aids on the kinetics of mixing in a rotating drum.* Powder Technology, Volume 4, 1970/71. pp 146

Choo, K., Baker, W. M., Molteno, T. C. A. and Morris, W. S., 1998. *Dynamics of granular segregation patterns in a long drum mixer.* Physical Review E, Volume 58, No. 5, pp 6115 – 6123

Cleary, P., 1998. *Predicting charge motion, power draw, segregation and wear in ball mills using discrete element methods.* Minerals Engineering, 1998. Volume 11, no. 11, pp 1061 – 1080.

Cleary, P., 2001. *Recent advances in DEM modelling of tumbling mills.* Minerals Engineering, 2001. Volume 14, no. 10, pp 1295 – 1319.

Concha, F. and Almendra, E. R., 1979. *Settling velocities of particulate systems, 2. Settling velocities of suspensions of spherical particles.* International Journal of Mineral processing, 6. 1979. pp 31 – 41.

Condori, P., and Powell, M.S., 2005. *RTD of solids in an industrial Autogenous mill.* In abstracts, Mineral Processing conference, SAIMM, Somerset West, South Africa, pp 67-68 (2005).

Ding, L. Y., Forster, R., Seville, J. P. K. and Parker, D. J., 2001. *Segregation of granular flow in the transverse plane of a rolling mode rotating drum.* Int. journal of multiphase flow, 28 (2002), pp 635 – 663.

Dieter E. G., 1988. *Mechanical metallurgy.* McGraw-Hill Series in Materials Science and Metallurgy, SI Metric Edition, 1988. pp 348 – 374.

Donald, M. B. and Roseman, B., 1962. *Mixing and de-mixing of solid particles. I. Mechanisms in a horizontal drum mixer.* British Chemical Engineering, October 1962, Volume 7. No. 10 pp 749 – 753

Epstein, B., 1948. *Logarithmic normal distribution in the breakage of solids.* Ind. Eng. Chem. 40, pp 2289 - 2291

Eskin, D. and Kalman, H., 2000. *A numerical parametric study of size segregation in a rotating drum.* Chemical Engineering and processing, Volume 39 (2000), pp 539 – 545

Henein, H., Brimacombe, J. K. and Watkinson, A. P., 1985. *An experimental study of segregation in Rotary kilns.* Metallurgical Transactions B, Volume 16B, December 1985, pp 763-774.

Herbst, J. A., and Fuerstenau, D. W., 1968. *The zero order production of fines in comminution and its implication in simulation.* Trans SME/AIME, pp 254 – 348.

Hill, K. M., and Kakalios, J., 1994. *Reversible axial segregation of granular material.* Physical Review E, May 1994, Volume 49. No. 5 pp R3610 – R3613

Hill, K. M., Caprihan, A. and Kakalios, J., 1997. *Axial segregation of granular media rotated in a drum mixer: Pattern evolution.* Physical Review E, October 1997, Volume 56. No. 4 pp 4386 – 4393

Hogg, R. and Rogovin, Z., 1982. *Mass transport in wet overflow ball mills.* Canadian Institute of Mining and Metallurgy (CIM) XIV International Mineral Processing Congress (IMPC), October 17 – 23, 1982, Toronto, Canada, pp I-7.1 – I-7.19

Hogg, R., 1984. *Mass transport models for tumbling ball mills.* Control '84. Metallurgical Society of AIME. Int. Symposium on Automatic Control in Min. Processing and Process Metallurgy, 1984. pp 55 – 61.

Hogg, R., 2005. - *Personal communication.* Prof. Emeritus of Min. Proc. and Geo-Environmental Eng. Dept of Energy and Geo-Environmental Engineering. The Pennsylvania State University.

Hukki, R. T., 1961. *Proposal for the solomonic settlement between the theories of von Rittinger, Kick, and Bond.* Transactions of the SME/AIME (220), pp 403 – 408

Khakhar, D.V., McCarthy, J. J., Shinbrot, T, and Ottino, J. M., 1996. *Transverse flow and mixing of granular material in a rotating cylinder.* Physics Fluids, Volume 9. No.1, January 1997, pp 31-43.

Khakhar, D. V., Orpe, A. V. and Hajra, S. K., 2002. *Segregation of granular materials in rotating cylinders.* Elsevier Science B. V. In Physica A 318 (2003) pp 129 – 136.

Kick, F., 1883. *The law of proportional resistance and its application to sand and explosions.* Dinglers j., Volume 245. pp 1 – 5.

Lacey, P. M., 1954. Journal of Applied Chem., 1954, Volume 4, p257.

Latchireddi, S. R., 2002. *Modelling the performance of grates and pulp lifters* in *autogenous and semi-autogenous mills.* Ph.D. Thesis, University of Queensland (JKMRC), Australia

Leung, K., 1987. *An energy-based ore specific model for autogenous and semi-autogenous grinding.* Ph.D. Thesis, University of Queensland (JKMRC), Australia

Levenspiel, O., 1962. *Chemical Reaction Engineering.* John Wiley, New York (1962)

Lynch, A. J., Whiten, W. J. and Draper, N. 1967. *Time dependent equations for comminution machines.* 34 th Annual Chemical Engineering Symposium, M.I.T.

Morrell, S. 1989. *Simulation of bauxite grinding in a semi-autogenous mill and DSM screen circuit.* M. Eng. Thesis, University of Queensland, Australia.

Morrell, S. 1993. *The prediction of power draw in tumbling mills.* PhD. Thesis, University of Queensland.

Morrell, S., Finch, W. M., Kojovic, T., Delboni Jr., H., 1996. *Modelling and simulation of larger autogenous and semi-autogenous mills.* Julius Kruttschnitt Mineral Research Centre, University of Queensland, Brisbane, Australia. International Journal of Mineral Processing, 44-45, 1996. pp 289 – 300.

Morrell, S. 2004. *A new autogenous and semi-autogenous mill model for scale-up, design and optimisation.* Minerals Engineering Volume 17 (2004), pp 437 – 445.

Mwansa, S., and Powell M. S., 2004. *Measuring particle segregation along SAG mills.* Abstracts, Mineral Processing 2004. SAIMM, Somerset West, South Africa, pp 101-102, 2004.

Napier-Munn, T.J., Morrell, S., Morrison, R. D. and Kojovic, T., 1999. *Mineral Comminution circuits: their operation and optimisation* Text book. JKMRC, University of Queensland, Australia.

Napier-Munn, T.J., Morrell, S., Morrison, R. D. and Kojovic, T., 1999a. *Mineral Comminution circuits: their operation and optimisation* Text book. JKMRC, University of Queensland, Australia. p25

Napier-Munn, T.J., Morrell, S., Morrison, R. D. and Kojovic, T., 1999b. *Mineral Comminution circuits: their operation and optimisation* Text book. JKMRC, University of Queensland, Australia. pp 162 - 163

Napier-Munn, T.J., Morrell, S., Morrison, R. D. and Kojovic, T., 1999c. *Mineral Comminution circuits: their operation and optimisation* Text book. JKMRC, University of Queensland, Australia. pp 154 – 229

Napier-Munn, T.J., Morrell, S., Morrison, R. D. and Kojovic, T., 1999d. *Mineral Comminution circuits: their operation and optimisation* Text book JKMRC, University of Queensland, Australia. p20

Narayanan, S. S., and Whiten, W. J. 1988. *Determination of comminution characteristics from single particle breakage tests and its application to ball mill scale-up.* Trans. Inst. Min. Met., 97, pp C115 – C124

Nityanand, N., Manley, B. and Henein, H., 1986. *An analysis of radial segregation for different sized spherical solids in rotary cylinders.* Metallurgical Transaction B, 17 B (1986), pp 247 – 257.

Owen, P., 2005a *UCT002 report on computational services requested via webGF-MILL.* CMIS Technical report: 05/127. CSIRO Mathematical and Information Sciences, Australia.

Owen, P., 2005b *UCT003 report on computational services requested via webGF-MILL.* CMIS Technical report: 05/151. CSIRO Mathematical and Information Sciences, Australia

Oyama, Y., 1933. The Bulletin of Institute of Physical and Chemical Research 12 (12) pp 63 – 69.

Oyama, Y., 1939. The Bulletin of Institute of Physical and Chemical Research. (Tokyo) Rep. 5, 600.

Pickering, R. W., Feakes, F. and Fitzgerald, M. L., 1951. *Journal. appl. Chem.1.* pp 13 - 19

Powell, M. S. and Nurick, G. N., 1996. *A study of charge motion in rotary mills part 3- Analysis of results.* Minerals Engineering, Volume 9, No. 4, pp 399 – 418.

Powell, M. S., Morrell, S. and Latchireddi, S. 2000. *Developments in the understanding of South African styled SAG mills.* Minerals Engineering 2001 Volume.14, pp 1099-1109

Powell, M. S. and McBride, A. T., 2004. *A three-dimensional analysis of media motion and grinding regions in the mill.* Minerals Engineering 2004 Volume.17., No. 10., pp 1143-1153

Powell, M. S. 2006. – *Personal communication.* Head Comminution Group, Mineral Processing Research Unit (MPRU). Department of Chemical Engineering. The University of Cape Town.

Rittinger, R. P. 1867. *Textbook of mineral dressing.* Ernst and Koln, Berlin.

Rogers, A. R. and Clements, J. A.., 1971. *The Examination of Granular Materials in a Tumbling Mixer.* Powder Technology 5 (1971/1972) pp 167 – 178.

Rogers, R. S. C., 1979. *Application of the segregated flow concept to the analysis and simulation of continuous ball mills by the mechanistic approach.*, Ph.D. thesis, North Carolina State University, 1979.

Saeman, W. C., 1951. *Passage of Solids through Rotary Kilns. Factors affecting time of passage.* Chemical Engineering Progress 1951 Volume 47 No.10, pp 508 – 514.

Shoji, K., Hogg R. and Austin, G. L., 1973. *Axial Mixing of Particles in Batch Ball mills.* Proceedings of the international conference on particle Technology. Powder Technology, 7 1973. pp 331-336.

Stanley, G. G., 1974. *The autogenous mill – a mathematical model derived from pilot and industrial scale experiment.* PhD Thesis, JKMRC, The University of Queensland, Brisbane, Australia.

Steyn, B. and Hinde, A. 2005. *Direct Measurement of specific Breakage Rate and Breakage Distribution functions for large Rocks in Pilot SAG/AG Mills.* Min. Proc. Abstracts, Cape Town, 2005, pp 45-46.

Sullivan, J. D., Maier, C. G. and Ralston, O. C., 1927. *Passage of Solid Particles through Rotary Cylindrical Kilns.* United States Bureau of Mines (USBM) Technical paper No. 384

Tang, P. and Puri, V. M., 2004. *Effect of particle characteristics on Segregation.* The Canadian Society for Engineering in agricultural, food, and Biological Systems. 2004 ASAE/CSAE Annual International Meeting, paper No. 044148. St. Joseph, Michigan: ASAE.

Vermeulen, L. A. and Howat, D. D., 1989. *A sampling procedure validated.* Journal of the South African Institute of Mining and Metallurgy. Volume 89, No. 12. December 1989. pp 365 – 370.

Weidenbaum, S. S., 1958. *Advances in Chemical Engineering,* edited by Drew, T. B., and Hoopes, J. W., Academic, New York, 1958, Volume 2, p 211.

Whiten, W. J., 1974. *A matrix theory of comminution machines.* Chemical Engineering Science, 1974, Volume 29, pp 589 – 599

Whyte, R., 2005. *Measuring Incremental Damage in Rock Breakage by Impact.* Final year engineering thesis, University of Queensland, 2005

Wightman, C. and Muzzio, J. F., 1998. *Mixing of granular material in a drum mixer undergoing rotational and rocking motions II. Segregating particles.* Powder Technology 98 (1998), pp 125 – 134

Appendix 1

A1 THE SAG MILL MODEL

Appendix A1 describes the current JK AG/SAG mill model.

A1.1 MATHEMATICAL DESCRIPTION OF THE MODEL

A schematic of the mechanism of operation in a SAG mill is shown in Figure A1- 1 and the perfect mixing SAG model material balance is given in equation (9.1).

Feed in + Appearance from breakage into size $_i$ = Product out + Breakage out **(9.1)**

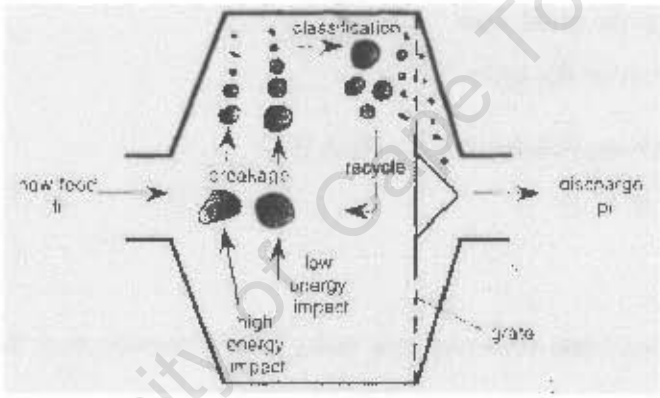

Figure A1- 1 : Schematic of SAG mill operation, (after Morrell *et al*, 1996)

The SAG mill model also includes a classification function for particle transport out of the mill, proposed by Leung (1987) and improved by Latchireddi (2002)

For perfectly mixed mill contents s_i, the relationship with the product of discharge rate d_i is

$$p_i = d_i s_i \text{ or } s_i = p_i / d_i \qquad (9.2)$$

The mass balance of the perfect mixing SAG model is given by equation (9.3).

$$0 = f_i - p_i + \sum_{j=1}^{i} r_j s_j a_{ij} - r_i s_i \quad \text{(after Napier-Muno et al, 1999 b)} \qquad (9.3)$$

Where;

r_i = the breakage rate of particles of size $_i$ (hr^{-1})

a_{ij} = the appearance function representing particle breakage from size $_j$ into size $_i$

Substituting the experimentally difficult mill contents s_i into equation (9.3) gives;

$$f_i + \sum_{j=1}^{i}\left[\frac{a_{ij} r_j p_j}{d_j}\right] = p_i + \frac{r_i p_i}{d_i} \qquad (9.4)$$

To use the model, besides the mill feed f_i, and mill product p_i, measurements, of three modelling descriptions must be determined as described in the next sections.

A1.2 SLURRY TRANSPORT OUT OF THE SAG MILL (d_i)

The transport of slurry out of the mill is described by the discharge rate d_i, which is considered to be a product of two mechanisms namely;

i. transport to the grate, and
ii. Classification by the grate.

The discharge rate is modeled using equation (9.5)

$$d_i = dc_i \qquad (9.5)$$

Where;

d = the maximum discharge rate and c_i is the classification function in size $_i$.

The maximum discharge rate is determined iteratively within the model using an empirical relationship that relates slurry hold-up to the volumetric flowrate that is discharged from the mill, while the classification function is based on a simple classifier model shown in Figure A1- 2. From Figure A1- 2, the value of Xg is the effective grate aperture, whilst Xm is the largest/maximum particle size that flows "like water" without subject to grate classification. For practical purposes, Xm is assigned the value of 0.3 to 1.0 mm.

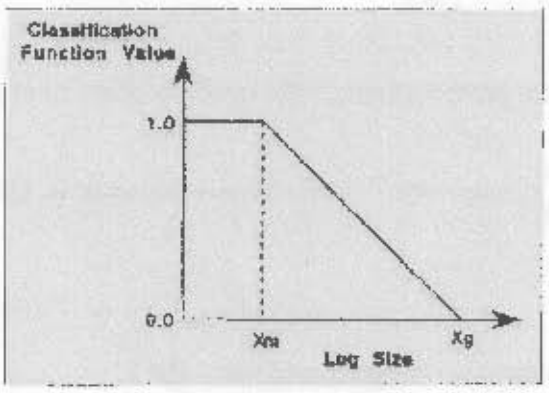

Figure A1- 2 : Grate classification function, (after Morrell et al, 1996)

From Figure A1- 2, the region with a constant discharge rate (d_m) is directly related to the slurry flow out of the mill and the slurry hold-up in the mill, which can be expressed as:

$$d_m = \frac{\sum_m p_i}{\sum_m s_i} \tag{9.6}$$

Where $\sum_m p_i$ and $\sum_m s_i$ are the slurry discharge and hold-up respectively. To determine d_m, equation (9.7) involving the slurry hold-up by Latchireddi, (2002) is employed.

$$J_s = \eta\gamma^{n1} A^{n2} J_t^{n3} \phi^{n4} Q^{n5} D^{n6} \tag{9.7}$$

Where; J_s = the net fractional slurry hold-up inside the mill.

A = fractional open area

J_t = fractional grinding media volume

ϕ = fraction of mill critical speed

Q = slurry discharge flowrate

γ = mean relative radial position of grate holes

η = coefficient of resistance which varied depending on weather flow was via the grinding media voids or through slurry pool (if present)

$n1 - n6$ = model parameters

The value of γ is a weighted radial position expressed as fraction of mill radius calculated from equation (9.8).

$$\gamma = \frac{\sum r_i a_i}{r_m \sum a_i} \tag{9.8}$$

Where; a_i is the open area of all holes at radial position r_i and r_m is mill radius inside liners.

The parameter values $n1 - n6$ and η were found to be functions of pulp lifter size and have been modeled in equation (9.9) proposed by Latchireddi (2002)

$$n_i = n_g - k_i e^{(-k_j \lambda)} \tag{9.9}$$

Where; n_g = the parameter values for grate-only discharge condition

k_i, k_j = constants, and

λ = depth of the pulp lifter expressed as a fraction of the mill diameter

The constant discharge rate d_m for particles less than Xm can therefore be expressed as;

$$d_m = \frac{Q}{J_s} \qquad \text{(after Morrell, 2002)} \qquad \textbf{(9.10)}$$

For the particles less than Xm, d_m is equal to d_i.The discharge function values for particle sizes greater than Xm (1mm), d_m is predicted using the Leung (1987) approach of using a log-linear relationship that goes to zero at the grate/pebble port size, Xg (Figure A1- 2). The solution for the classification function C_i in equation (9.5) is resolved by equation (9.11).

$$C_i = \frac{\ln(x_i) - \ln(x_g)}{\ln(x_m) - \ln(x_g)} \qquad \text{for } x_g > x_i > x_m \qquad \textbf{(9.11)}$$

Where; $C_i = 1$, for $x_i < x_m$ and $C_i = 0$, when $x_i > x_g$

A1.3 THE APPEARANCE FUNCTION (a_{ij})

The appearance function a_{ij} shows the size distribution of progeny particles when the original rock undergoes breakage. It describes how an ore particle breaks when imparted with energy and is obtained separately from laboratory techniques through drop weight tests for the high energy breakage using the Narayanan and Whiten (1988) approach and through a tumbling test for low energy breakage following the Leung (1987) approach.

The t_{10} is related to two ore specific parameters A and b and to the specific comminution energy E_{cs} to describe rock breakage under high impact energy as shown in equation (9.12).

$$t_{10} = A\left(1 - e^{-bE_{cs}}\right) \qquad \textbf{(9.12)}$$

Where t_{10} is the percentage of material passing one tenth of the original parent rock size.

For low abrasion energy, the parameter t_a is used to describe the ore resistance to breakage and is shown in equation (9.13).

$$t_a = t_{10}/10 \qquad \textbf{(9.13)}$$

A1.4 THE BREAKAGE RATE (r_i)

From the perfect mixing model expressed in the form of equation (9.4), the breakage rate r_i can be back-calculated for each size fraction from a set of actual feed and product measurements, subject to

reasonable appearance function a_{ij} obtained separately from laboratory ore drop weight tests and the tumbling test. An example of characteristic breakage rate curves obtained through back-calculation from SAG mill modelling is shown in Figure A1- 3. The breakage rate distribution shown in Figure A1- 3 can conveniently be represented by a cubic spline function through the method of Ahlberg *et al.* (1967). Five spline knots at particle sizes of 0.25, 4, 16, 45, and 128 mm are used to obtain the corresponding five breakage rates (R1 – R5) on the spline function represented by the example in Figure A1- 3.

Through a collection of over 150 pilot and full scale AG/SAG mill data sets accumulated by the JKMRC, breakage rates obtained from two full scale AG/SAG mills by Stanley, (1974) and by Morrell, (1989), and breakage rates from 11 pilot scale tests have been compared by the JKMRC.

Comparison of breakage rates for SAG mill data and pilot scale tests revealed the following;

i. Increasing SAG mill speed increased the rate of breakage for the coarser (10 – 100 mm) size particles and reduced the rate of breakage for the smaller particles. The observed trend was attributed to promotion of impact breakage due to the high amount of lift imparted on to the charge with increased mill speed.
ii. Steel balls size distribution (volume) increase in the mill charge, resulted in an increase in the breakage rate. Addition of large balls increased the kinetic energy imparted to the rocks and increased the breakage rate at coarse rock sizes, but at the same time there was a reduction of the ball surface area and thus abrasion breakage of small size particles was discouraged (low breakage rate at small particle sizes).
iii. Generally, coarser feed size distribution resulted in increased breakage rates, however, a reverse of increased breakage rate from coarser feed was also observed.

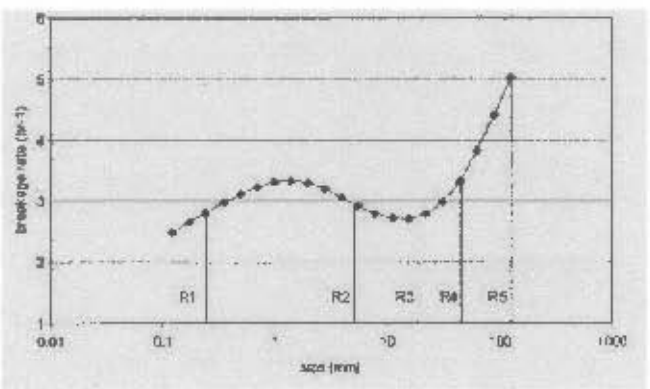

Figure A1- 3: Example of a SAG mill breakage function, (after Morrell et al, 1996)

Appendix 2

A2 PRELIMINARY TRIALS DATA

Appendix A2 gives the raw data and the size distribution of particles collected from three positions along mills of the trial surveys (chapter 4). For each survey, the PSD is presented in four defined size ranges; slurry (-1 mm), small rocks (1 – 22.4 mm), 'critical size' rocks (22.4 – 63.5 mm) and big rocks (+ 63 mm).

A2.1 EXPERIMENTAL PROCEDURE

Samples were taken at 15 minutes intervals over a period of one hour at the vibrating screen oversize stream, the linear screen oversize and linear screen undersize stream. Additionally, the water flowrates were recorded from the installed flow meters during the full circuit survey.

Full mill circuit survey sampling technique

Two samples, the "A" sample and "B" sample were taken at each sampling interval. The "A" sample constituted the primary sample, and the "B" sample was taken as a back-up to be used in the event of an error in the processing of the samples, or uncertainty in the outcomes. The primary and back-up samples had separate buckets

Vibrating screen Oversize

This sample was taken at the vibrating screen discharge chute. The screen was divided into six equal sections and the sample was taken by placing the sample cutter under each section for approximately 10 seconds. A composite of the cuts from the six sections were placed into the same bucket. Stream flowrate, percentage solids and size distribution data were obtained from the same sample. The cuts from each interval were kept in separate buckets and the solids flowrate were calculated for each sample taken to determine if the flow rate changed during the sampling campaign. The solids flowrate was determined by dividing the total sample mass by the total time per stream section, an average flowrate per section was the computed and multiplied by six to obtain the stream flowrate. The sample was then combined and screened to obtain size distributions.

Linear screen oversize

The linear screen oversize sample was taken at the primary mill feed chute by placing a bucket under the screen oversize discharge line. Flowrate samples were taken at the beginning, in the middle and

at the end of the survey. Due to the high water flowrates of that stream, only solids flowrates were taken, water was allowed to overflow from the bucket during the timed sample collection. The flowrates were determined by dividing the dry mass of the sample by the time.

Linear Screen Undersize

This sample was taken using an automatic sample cutter located underneath the linear screen. The sample cutter was operated manually from the control room and the sample was collected from the reject line, which gave sufficient volume of sample per cut. Two cuts (A and B) were taken resulting in two separate composite samples.

RoM Belt cut sample

The RoM mill feed sample was taken after the mill crash-stop. The RoM feed sample was obtained from a 14m belt cut, divided into 8m and 6m sections. Both the rocks and fines were collected from the 8m belt section. Fines were brushed off the belt into collecting buckets to ensure that no material was left on the sampled belt section. Only rocks larger than 45mm were collected from the other 6m belt section. The 6m belt section was obtained to provide sufficient large rocks for a statistically meaningful sample, and to provide sufficient rocks for ore characterization.

A2.2 PROCESSING PRELIMINARY SAMPLES

Samples were categorized into three classes during processing – circuit stream samples, RoM belt cut sample and the mill charge samples. All the samples were weighed wet immediately after the test using a hanging scale. The circuit stream samples were separated and classified either as slurry or coarse and were stored accordingly before processing.

Coarse samples

These were samples taken from the vibrating screen oversize and the linear screen oversize. They were dried directly in ovens at about 90°C. The linear screen oversize sample had a lot of water which had to be syphoned out before drying. The dry masses of the samples were recorded and the percentage solids calculated.

Slurry samples

The Linear screen Undersize and the slurry component of the mill charge samples were processed independently. These slurry samples were pressure filtered separately with filter paper on top of a

filter cloth. Care was taken not to loose fines during the filtration process as these are an essential constituent of every sample. The filtered samples were dried in the oven and the dry samples were weighed to determine the percentage solids of each sample.

RoM feed

The processing of the belt cut mill feed is as given in Appendix 4.

Mill Charge

The rocks from the mill charge samples were weighed and dried in the same manner as that of the rocks from the RoM mill feed sample. The amount of rocks in the +45 mm rocks size distribution were weighed and counted after screening.

A2.3 RAW MASS DATA

The raw data from the three preliminary tests are given from Table A2- 1 to Table A2- 8.

Table A2- 1 : Raw rock mass from three positions along the EPC RoM ball mill

EPC raw mass (g)						
Size (mm)	Slice 1	Rock #	Slice 2	Rock #	Slice 3	Rock #
180	0.0	0	0.0	0	0.0	0
125	92830.0	12	0.0	0	0.0	0
90	88530.0	27	11860.0	4	18140.0	6
63	71230.0	60	17780.0	16	7040.0	6
45	50680.4	144	15120.0	37	8070.0	20
31.5	45611.3		10370.0		3610.0	
22.4	31079.4		2850.0		248.4	
16.0	13947.9		50.0		0.0	
11.2	7426.0		14.3		14.2	
8.0	3191.1		8.3		7.0	
5.6	1788.1		7.2		14.9	
4.0	861.6		6.5		11.2	
2.8	828.5		5.2		19.0	
2.0	584.8		4.4		18.0	
1.4	454.8		3.1		18.5	
1.0	367.9		2.7		15.2	
0.710	377.4		3.1		23.4	
0.500	442.7		14.3		31.5	
0.355	558.3		28.3		58.6	
0.250	946.5		82.1		157.8	
0.180	1232.1		252.3		397.2	
0.125	1062.3		230.4		607.1	
0.090	1168.8		310.9		457.3	
0.063	719.9		387.3		616.9	
0.045	299.8		311.4		269.5	
0.032	51.4		108.7		76.7	
- 0.032	941.1		1974.2		1735.1	

Table A2- 2 : Raw rock mass from three positions along the K4 test 1 RoM ball mill

K4 test 1 raw mass (g)						
Size (mm)	Slice 1	Rock #	Slice 2	Rock #	Slice 3	Rock #
180	0.0	0	0.0	0	0.0	0
125	8106.0	1	0.0	0	5920.0	2
90	7254.0	3	8380.0	2	7800.0	2
63	9540.0	8	20430.0	14	7290.0	2
45	6100.0	17	3650.0	5	790.0	2
31.5	4480.0		1576.2		185.9	
22.4	2740.0		367.6		0.0	
16.0	1350.0		82.0		45.4	
11.2	584.3		44.5		32.8	
8.0	256.8		35.3		37.0	
5.6	109.7		44.3		23.4	
4.0	43.3		32.6		15.1	
2.8	30.0		60.2		15.1	
2.0	28.6		88.5		16.5	
1.4	33.4		115.7		24.2	
1.0	30.0		175.3		39.4	
0.710	15.8		21.0		7.0	
0.500	47.6		38.9		12.1	
0.355	43.0		98.5		29.8	
0.250	144.0		195.3		86.9	
0.160	149.9		256.9		125.9	
0.125	174.6		312.2		128.0	
0.090	138.6		327.0		161.7	
0.063	97.4		242.6		146.7	
0.045	49.3		127.2		75.4	
0.032	27.9		85.0		55.0	
- 0.032	72.5		290.7		201.8	

Table A2- 3: Raw rock mass from three positions along the K4 test 2 RoM ball mill

K4 test 2 raw mass (g)						
Size (mm)	Slice 1	Rock #	Slice 2	Rock #	Slice 3	Rock #
250	0.0	0	0.0	0	0.0	0
180	17180.0	1	0.0	0	0.0	0
125	191380.0	27	0.0	0	0.0	0
90	236690.0	79	19190.0	5	0.0	0
63	76060.0	73	257490.0	24	81000	6
45	30446.0	77	28752.0	79	4049.6	10
31.5	10853.2		25220.0		2816.3	
22.4	2636.4		12170.0		398.2	
16.0	877.4		1674.2		50.2	
11.2	102.5		26.8		2.1	
8.0	38.5		14.3		0.8	
5.6	19.6		8.2		0.0	
4.0	17.8		5.8		0.0	
2.8	16.7		5.9		1.1	
2.0	10.4		5.6		1.5	
1.4	11.1		1.6		3.4	
1.0	12.9		2.1		5.9	
0.710	5.8		21.0		2.0	
0.500	5.0		23.8		1.7	
0.355	8.3		64.9		2.3	
0.250	18.2		30.2		4.0	
0.180	24.9		22.2		4.3	
0.125	26.3		24.6		4.0	
0.090	23.7		37.2		2.6	
0.063	16.8		30.4		1.3	
0.045	6.3		17.4		0.2	
0.032	2.1		8.5		0.0	
- 0.032	14.2		16.4.0		59.3	

Table A2- 4 : Initial cumulative % passing for the three preliminary tests

Cummulative % passing									
	EPC			K4 test 1			K4 test 2		
Size (mm)	Slice 1	Slice 2	Slice 3	Slice 1	Slice 2	Slice 3	Slice 1	Slice 2	Slice 3
250	100.0	100.0	100.0	100.0	100.0	100.0	100.0	100.0	100.0
180	100.0	100.0	100.0	100.0	100.0	100.0	97.0	100.0	100.0
125	77.7	100.0	100.0	85.8	100.0	65.5	63.4	100.0	100.0
90	56.5	80.8	56.4	46.2	76.3	31.7	31.8	83.5	100.0
63	39.5	52.0	39.5	29.4	20.0	15.4	8.4	61.4	49.5
45	27.3	27.5	20.1	18.7	12.8	10.3	3.1	36.7	24.3
31.5	16.4	10.7	11.5	10.9	8.5	7.9	1.1	15.0	6.5
22.4	8.9	6.1	10.9	6.1	7.5	7.9	0.7	4.5	4.0
16.0	5.6	6.0	10.9	3.7	7.3	7.8	0.5	3.1	4.0
11.2	3.8	6.0	10.8	2.7	7.0	7.6	0.5	3.0	3.9
8.0	3.0	6.0	10.8	2.3	7.0	7.2	0.5	3.0	3.9
5.6	2.6	6.0	10.8	2.1	6.8	7.1	0.5	3.0	3.9
4.0	2.4	5.9	10.7	2.0	6.8	7.0	0.5	3.0	3.9
2.8	2.2	5.9	10.7	1.9	6.6	6.9	0.5	3.0	3.9
2.0	2.1	5.9	10.7	1.9	6.4	6.8	0.5	3.0	3.9
1.4	2.0	5.9	10.6	1.8	6.0	6.7	0.5	3.0	3.9
1.0	1.9	5.9	10.6	1.8	5.5	6.4	0.5	3.0	3.8
0.710	1.8	5.9	10.5	1.7	5.5	6.4	0.5	3.0	3.8
0.500	1.7	5.9	10.4	1.6	5.4	6.4	0.5	2.9	3.8
0.355	1.5	5.8	10.3	1.5	5.2	6.2	0.5	2.9	3.8
0.250	1.3	5.7	9.9	1.2	4.6	5.7	0.4	2.6	3.8
0.180	1.0	5.4	9.0	1.0	3.9	4.9	0.1	2.4	3.8
0.125	0.8	5.0	7.6	0.7	3.0	3.9	0.3	2.2	3.7
0.090	0.5	4.5	6.5	0.4	2.1	2.8	0.3	1.9	3.7
0.063	0.3	3.9	5.0	0.2	1.4	1.9	0.3	1.6	3.7
0.045	0.2	3.4	4.4	0.2	1.1	1.5	0.3	1.5	3.7
0.032	0.2	3.2	4.2	0.1	0.8	1.2	0.3	1.4	3.7

Table A2- 5 : Original mass distribution (percent) at each position for each test

Size Fraction (mm)	Inlet slice mass (%)	Centre slice mass (%)	Discharge slice mass (%)
K4 test 1			
180	0	0	0
125	14.4	0	36.2
90	40.2	24.8	35.1
63	16.9	59.1	17.0
45	10.8	7.3	4.8
16.0	15.2	5.9	3.2
1.00	1.9	1.8	1.3
0.32	0.6	0.8	1.2
0.23	0.1	0.3	0.38
Total sample mass	3634.7	3435.3	1658.7
K4 test 2			
250	0	0	0
180	3.0	0	0
125	33.8	0	0
90	41.8	16.9	0
63	13.1	22.7	51.9
45	5.4	25.4	25.9
16	2.5	34.5	20.8
1.00	0.04	0.15	0.12
0.32	0.05	0.15	0.04
0.23	0.05	0.35	1.15
Total sample mass	5666.12	11135.3	15609
EPC test			
180	0	0	0
125	22.3	0	5
90	21.2	49.2	43.6
63	17.1	28.8	16.9
45	12.2	35.9	19.4
16	3.7	21.9	9.3
1.00	1.7	0.1	0.3
0.32	1.5	2.7	6.4
0.23	0.2	1.1	4.2
Total sample mass	11121.3	61,743.5	116,76.1

Table A2- 6 : Converted full mass axial distribution for the three tests

Converted full mass distribution data									
	EPC			K4 test 1			K4 test 2		
Size (mm)	Slice 1	Slice 2	Slice 3	Slice 1	Slice 2	Slice 3	Slice 1	Slice 2	Slice 3
250	0.0	0.0	0.0	0.0	0.0	0.0	0.0	0.0	0.0
180	0.0	0.0	0.0	0.0	0.0	0.0	61031.0	0.0	0.0
125	570033.3	0.0	0.0	41636.2	0.0	30430.4	679877.4	0.0	0.0
90	543628.7	728277	1113990.8	1160159	44105.5	29813.6	8406280	68030.4	0.0
63	437396.0	1091830.4	43229.9	19038.2	1050157	14341.3	2702951	91299.2	28775.2
45	311208.8	92846.1	49554.8	31356.6	13416.1	4060.8	1081381	102134.4	14386.5
31.5	280081.4	63678.2	22167.6	23028.4	8102.1	2497.7	38544.6	89594.0	10111.5
22.4	190846.6	17560.8	1525.3	14084.3	1879.5	0.0	9272.0	43233.9	1414.4
16.0	85648.7	307.0	0.0	6939.4	471.5	253.4	3118.1	5947.6	36.1
11.2	45600.2	87.9	87.2	3003.5	383.0	194.3	357.0	272.9	14.9
8.0	19595.3	51.0	43.0	1165.8	181.5	190.2	136.6	50.7	7.5
5.6	10980.0	44.0	91.5	563.9	227.7	120.3	69.6	29.1	2.8
4.0	5290.8	40.2	68.8	233.6	141.9	77.6	45.5	17.1	0.4
2.8	5087.5	32.0	116.7	93.6	309.4	79.2	59.3	21.0	4.6
2.0	3591.0	27.0	110.5	147.0	439.5	84.8	36.9	10.7	16.0
1.4	2792.8	18.8	113.6	171.7	594.7	124.4	39.4	3.7	12.1
1.0	2359.1	16.1	93.3	154.2	501.1	202.5	45.8	7.5	13.9
0.710	8102.3	138.0	777.6	8368.6	1399.8	348.6	25961.0	1627.4	187.2
0.500	95118.3	932.6	1091.3	9091.8	2279.0	602.2	25590.1	1839.6	204.7
0.355	119957.9	1843.5	2028.9	14102.6	4577.8	1378.7	42279.3	4952.9	588.1
0.250	203384.5	5342.6	5465.6	27482.0	11387.8	4310.5	86783.8	23773.9	2218.1
0.180	264755.3	13172.1	13718.2	28618.5	14981.9	6243.9	114599.1	17193.6	2436.3
0.125	228466.9	15001.3	10025.7	33319.4	20278.5	8827.0	119049.5	19174.8	2044.7
0.090	251136.4	20242.6	15837.5	36448.9	19067.9	9508.5	109777.8	28726.8	3268.8
0.063	154690.4	25216.5	21366.7	18596.9	14149.6	7274.0	77141.1	23632.4	2823.5
0.045	64411.5	20291.5	9535.2	7697.0	7415.3	3740.0	34524.0	13160.6	1817.7
0.032	11049.3	7077.7	2655.5	4184.3	4956.1	2725.8	10013.5	6580.3	819.4
- 0.032	202228.2	128533.2	67094.2	13911.5	16926.5	10007.7	698549.8	126440.4	19511.5

Table A2- 7 : Corrected cumulative percent passing mass for the three tests

Corrected cumulative % passing									
	EPC			K4 test 1			K4 test 2		
Size (mm)	Slice 1	Slice 2	Slice 3	Slice 1	Slice 2	Slice 3	Slice 1	Slice 2	Slice 3
250	100.0	100.0	100.0	100.0	100.0	100.0	100.0	100.0	100.0
180	100.0	100.0	100.0	100.0	100.0	100.0	98.2	100.0	100.0
125	86.1	100.0	100.0	91.3	100.0	97.3	77.9	100.0	100.0
90	73.4	87.7	70.8	67.1	85.0	96.9	52.8	89.8	100.0
63	63.0	69.4	59.1	56.7	49.2	66.7	34.8	76.1	68.5
45	55.6	53.8	46.4	50.4	41.6	52.6	41.5	60.8	52.7
31.5	48.9	43.0	40.6	15.6	11.9	41.9	40.4	47.4	41.7
22.4	44.3	40.1	40.2	42.6	41.2	41.0	10.1	41.0	40.1
16.0	42.3	40.1	40.2	41.2	41.1	40.8	40.0	40.1	40.1
11.2	41.2	40.0	40.2	40.5	41.0	40.6	40.0	40.0	40.1
8.0	40.7	40.0	40.2	40.3	40.9	40.5	40.0	40.0	40.1
5.6	40.5	40.0	40.1	40.2	40.8	40.4	40.0	40.0	40.1
4.0	40.3	40.0	40.1	40	40.8	40.4	40.0	40.0	40.1
2.8	40.2	40.0	40.1	40.1	40.7	40.3	40.0	40.0	40.0
2.0	40.1	40.0	40.1	40.1	40.5	40.2	40.0	40.0	40.0
1.4	40.1	40.0	40.0	40.0	40.3	40.1	40.0	40.0	40.0
1.0	40.0	40.0	40.0	40.0	40.0	40.0	40.0	40.0	40.0
0.710	38.1	40.0	39.8	38.3	39.5	39.7	39.2	39.8	39.8
0.500	35.8	39.8	39.5	36.1	38.7	39.5	38.5	39.5	39.6
0.355	32.9	39.5	39.0	33.1	37.2	38.7	37.2	38.7	38.9
0.250	28.1	38.6	37.5	27.7	33.3	35.2	14.6	35.3	36.5
0.180	21.8	36.4	34.2	21.7	28.2	30.6	21.2	32.6	33.8
0.125	16.5	33.9	28.7	14.8	21.3	24.2	22.6	29.7	30.6
0.090	10.3	30.5	24.5	9.3	14.8	17.3	24.4	25.4	27.0
0.063	6.6	26.2	18.9	5.1	10.0	12.6	22.1	21.9	24.2
0.045	5.1	22.8	16.5	3.8	7.5	9.3	21.1	19.9	22.3
0.032	4.8	21.6	15.8	2.9	5.8	7.3	20.8	18.9	21.4

Table A2- 8: Preliminary tests defined sizes cumulative percent passing

	EPC			K4 test 1			K4 test 2		
	Slice 1	Slice 2	Slice 3	Slice 1	Slice 2	Slice 3	Slice 1	Slice 2	Slice 3
Big rocks									
250	100.0	100.0	100.0	100.0	100.0	100.0	100.0	100.0	100.0
180	100.0	100.0	100.0	100.0	100.0	100.0	100.0	100.0	100.0
125	100.0	100.0	100.0	100.0	100.0	100.0	96.9	100.0	100.0
90	69.4	100.0	100.0	82.5	100.0	61.3	62.2	100.0	100.0
63	40.2	73.5	45.4	33.8	72.9	23.4	19.3	74.0	100.0
45	16.7	33.8	24.3	13.2	8.3	5.2	5.5	39.1	33.3
S80	102.1	69.6	89.1	88.6	70.1	106.9	108.0	69.2	57.6
Critical size rocks									
63.0	100.0	100.0	100.0	100.0	100.0	100.0	100.0	100.0	100.0
45.0	64.1	61.4	62.9	58.3	18.2	31.4	36.6	72.0	42.4
31.5	38.6	28.7	20.3	31.6	7.8	12.0	11.2	40.7	31.3
22.4	15.6	6.2	1.3	12.0	1.5	0.0	2.2	13.3	2.6
S80	53.0	53.7	53.3	54.4	58.6	57.8	57.3	50.1	56.7
Small rocks									
22.4	100.0	100.0	100.0	100.0	100.0	100.0	100.0	100.0	100.0
16.0	48.7	3.4	32.3	47.2	60.7	100.0	29.7	12.8	7.7
11.2	25.6	1.7	32.2	21.1	58.0	82.1	6.0	0.8	5.4
8.0	13.3	1.3	28.3	9.9	51.0	67.3	3.3	0.3	4.4
5.6	8.1	1.0	26.4	5.5	47.7	52.7	2.3	0.2	3.9
4.0	5.1	0.7	22.4	3.4	43.6	43.5	1.7	0.1	3.7
2.8	3.7	0.5	19.3	2.5	41.0	37.6	1.4	0.1	3.7
2.0	2.3	0.3	14.1	1.8	35.3	31.5	0.9	0.0	2.7
1.4	1.4	0.2	9.2	1.2	27.3	25.0	0.6	0.0	1.7
1.0	0.6	0.1	4.1	0.6	16.4	15.5	0.3	0.0	0.9
S80	19.9	21.1	20.5	20.0	18.7	10.7	20.6	20.9	21.0
Slurry									
1.0	100.0	100.0	100.0	100.0	100.0	100.0	100.0	100.0	100.0
0.710	99.2	99.9	99.5	95.6	98.8	99.4	98.1	99.4	99.5
0.500	89.5	99.5	98.8	90.9	96.9	98.3	96.2	98.7	98.9
0.355	82.3	98.8	97.4	83.5	93.0	95.8	93.0	96.8	97.3
0.250	70.2	96.5	93.9	69.2	83.3	87.9	86.5	87.9	91.3
0.180	54.4	91.0	85.5	54.3	70.5	76.6	78.0	81.5	84.6
0.125	40.8	84.7	71.7	36.9	53.2	60.5	69.1	74.3	76.5
0.090	25.8	76.2	61.3	23.1	37.0	43.2	60.9	63.6	67.5
0.063	16.6	65.6	47.3	13.4	25.0	30.0	55.2	54.7	60.6
0.045	12.7	57.0	41.2	9.4	18.6	23.2	52.8	49.8	55.6
0.032	12.1	54.1	39.4	7.3	14.4	18.2	52.1	47.3	53.4
S80	0.3	0.1	0.2	0.3	0.2	0.2	0.2	0.2	0.1

A2.4 CALCULATION OF S80 AT EACH MILL SLICE

The S80 calculated in this thesis was approximated to a linear interpolation evaluation. Even though it is believed that the cubic spline interpolation Ahlberg *et al.* (1967) is the best estimation of solving mid-points on a curve, the difference between the solution of a direct linear interpolation and that

from a spline interpolation is not so large especially when the mid-point is between points of a narrow range. Thus the S80, the size lying between S1 (a larger size) and S3 (a smaller size), and equivalent to 80 % cumulative percent rocks, where 80 % lies between X1 (larger than 80%) and X3 (smaller than 80 %) was calculated as shown in Table A2- 9. It is recommended to apply a natural logarithm to the √2 sizes before interpolation as this helps to linearise the cumulative percent curve intervals.

Table A2- 9 : Linear interpolation calculation of S80

Linear interpolation derivation	
Percent	Size
X1	S1
80	**S80**
X3	S3
(X1-80)/(X1-X3) = (S1-**S80**)/(S1-S3)	
S80 = S1-[(X1-80)(S1-S3)/(X1-X3)]	

Table A2- 10 : S80 (mm) comparison for truncated sizes along the mill length

	Slice 1	Slice 2	Slice 3
Big rocks			
EPC	102	70	80
K4 test 1	89	70	107
K4 test 2	108	69	58
Critical size			
EPC	53.0	53.7	53.3
K4 test 1	54.4	58.6	57.8
K4 test 2	57.3	50.1	56.2
Small rocks			
EPC	19.9	21.1	20.5
K4 test 1	20.0	18.7	10.7
K4 test 2	20.6	20.9	21.0
Slurry			
EPC	0.33	0.11	0.16
K4 test 1	0.33	0.23	0.20
K4 test 2	0.20	0.17	0.15

A2.5 EPC DEFINED PARTICLE SIZE DISTRIBUTION

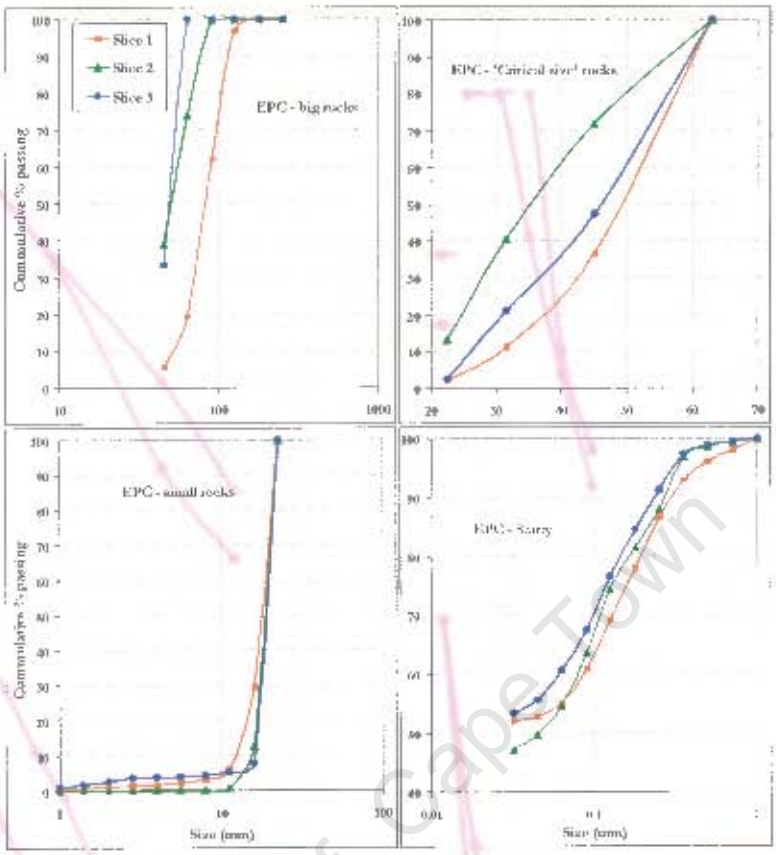

A2.6 K4 T 1 DEFINED PARTICLE SIZE DISTRIBUTION

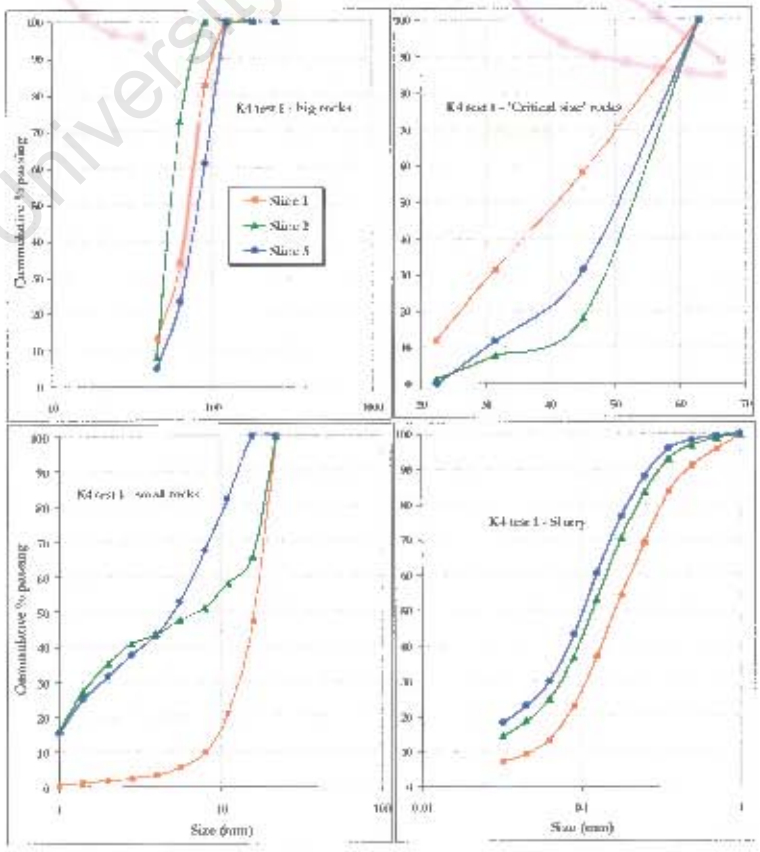

A2.7 K4 T 2 DEFINED PARTICLE SIZE DISTRIBUTION

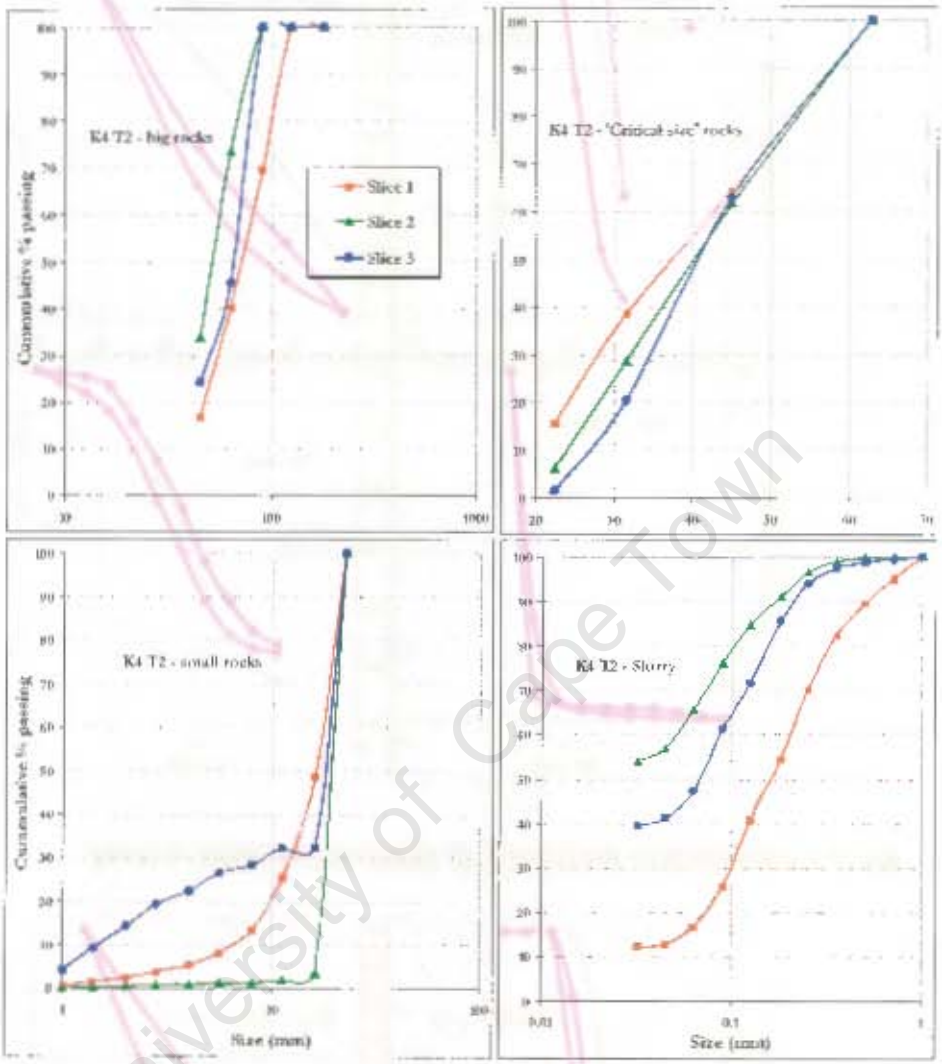

Appendix 3

A3 ORE CHARACTERISATION TESTS

Appendix A3 describes the JK drop weight test procedure used for ore characterisation.

A3.1 THE JK DROP WEIGHT TEST METHODOLOGY

The drop weight test procedure reported in this thesis was developed by the JKMRC and is used by licensed institutions worldwide that perform drop weight tests. The JKMRC uses two complimentary techniques to characterize ore breakage

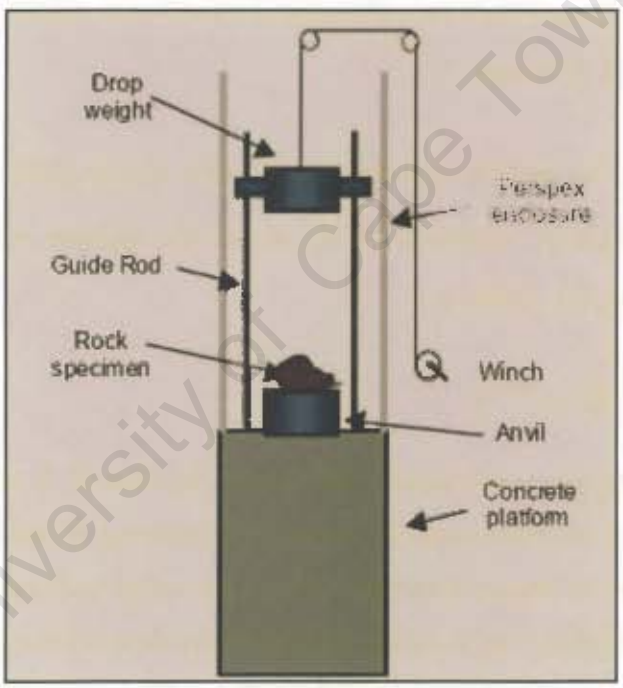

Figure A3- 1 : Schematic of the JK drop-weight tester

Impact breakage is characterized for moderate to high energy levels through drop weight tests conducted in a drop weight tester schematically shown in Figure A3- 1. Abrasion breakage at low energy inputs is characterized through a tumbling test in a laboratory mill.

A3.2 IMPACT BREAKAGE TESTING

For each sample from the four mill slices and from the RoM feed, rocks were sized into five size fractions: -63 + 53 mm, -45 +37.5 mm, -31.5 + 26.5 mm, -22.4 +19 mm, -16 + 13.2 mm. For each size fraction, between 10 and 30 particles were broken at each of the three energy levels, giving fifteen (15) size/energy combinations.

From Figure A3- 1, the JK drop weight tester comprises a steel drop weight that can be raised to known height using a winch. A pneumatic switch is pressed to release the drop-weight that falls under gravity and impacts on a rock particle that is positioned on the steel anvil. For operator safety and avoiding particle scatter, the device is placed in Perspex enclosure.

The breakage products of all particles for each size/energy combination are collected and sized. The size distribution produced is normalised with respect to the original particle size. For a wide range of energy inputs, particle sizes and ore types, the relative size distributions remain similar in shape and can be described by a single point on the distribution. The JKMRC convention is to use the percentage passing one-tenth of the original particle size. This is referred to as the "t_{10}". For the size fractions in the JK Drop Weight test, the original particle size equals the geometric mean of the size range e.g. $\sqrt{63 * 53}$ = 57.8 mm.

In this way, a set of t_{10} and the specific comminution energy (Ecs) values are produced for the 15 energy/size combinations. Equation (9.14) relates the amount of breakage t_{10}, to the specific comminution energy, Ecs (kWh/t):

$$t_{10} = A\left(1 - e^{-bEcs}\right) \qquad (9.14)$$

Using the 15 energy/size combination data values the best fit A and b parameters are calculated using a minimisation of error squared routine. The resulting A and b parameters are related to the resistance of the ore to impact breakage, with lower values indicating hard ore in terms of impact breakage. The product of A by b, which represents the slope of the curve at an Ecs of 0 kWh/t, is a measure of the ore impact breakage resistance and is used for comparison with other samples.

A3.3 ABRASION BREAKAGE TESTING

Low energy (abrasion) breakage is characterised using a tumbling test of selected single size fractions.

The standard abrasion test tumbles 3 kg of -55 +38 mm particles for 10 minutes at 70% critical speed in a 305 mm by 305 mm laboratory mill fitted with 4 x 6 mm lifter bars. The resulting product is then sized and the t_{10} value for the product is determined. The geometric mean particle size of the original size fraction 55 x 38 mm is 45.7 mm. The t_{10} size is therefore 1/10 *45.7 = 4.57 mm

The abrasion parameter, t_a is then defined by equation (9.15) as:

$$t_a = t_{10}/10 \tag{9.15}$$

A3.4 MEANING OF JK DROP WEIGHT PARAMETERS

The three Drop Weight parameters relevant to AG/SAG milling are A, b and t_a. A and b are used to characterise the impact breakage of the ore. The t_a parameter is a measure of the resistance of the ore to abrasion. In both cases the lower the value of the parameter, the greater the resistance of the ore to that type of breakage.

A and b are the high energy impact breakage parameters in the equation which relates t_{10} (the % of broken product passing one tenth of the original particle size) to Ecs (the specific energy of comminution), as expressed in equation (9.14).

Typically, the curve looks like Figure A3- 2. A is the maximum t_{10} value achieved. This is significant for higher energy breakages. The absolute value of A on its own is not that critical in a SAG mill because it is a measure of the breakage of the ore at energy levels higher than those that are usually achieved in a SAG mill. A is important in the part it plays in characterising the overall breakage curve. The parameter b is related to the overall slope of the t_{10} vs Ecs curve at the lower energies. A and b are interdependent, since the value of one will directly affect the other. Since A and b are related, it is usual to report A*b as the single value indicating the hardness of the ore in terms of impact breakage. The A*b parameter is the slope of the t_{10} vs Ecs curve at its origin and it is a measure of breakage of the ore at lower energy levels. This is particularly applicable to SAG mill breakage, which mostly occurs at lower energy levels.

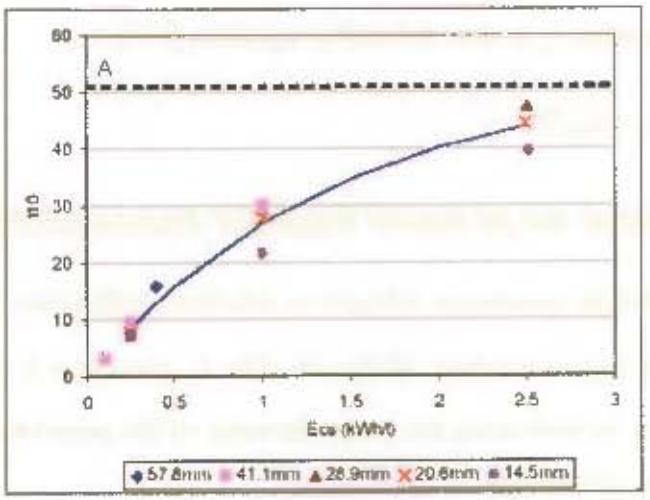

Figure A3- 2 : Example of a typical t_{10} versus Ecs plot

Since the abrasion parameter t_a is defined as $t_a = t_{10}/10$, a lower value of t_{10} (and thus t_a) indicates that there is a lower percentage of material passing one tenth of the original particle size, or there is greater resistance to abrasion breakage.

A summary of the size intervals, nominal input energies, size ranges and geometric mean used for each DWT test of a given sample from the Amandelbult mill emptying out is given in Table 9-1

Table 9-1: Size intervals and nominal input energy (kWh/t) used in the DWTs per sample

Size ranges	63 - 53 mm	45 - 37.5 mm	31.5 - 26.5 mm	22.4 - 19 mm	16 - 13.2 mm
Test /G mean	**57.8**	**41.1**	**28.9**	**20.6**	**14.5**
1	0.40	1.00	2.50	2.50	2.50
2	0.25	0.25	1.00	1.00	1.00
3	0.10	0.10	0.25	0.25	0.25

Appendix 4

A4 AMANDELBULT RESULTS DATA

Appendix 4 presents raw data from the main sampling survey of this thesis that included emptying out the entire mill contents at Amandelbult.

A4.1 PLANT MEASUREMENTS

The plant measurements included power draw, circuit feedrates and flow rates.

Power Draw

The power draw to the mill was monitored from the power meter panel shown in Figure A4- 1. The power is obtained from the panel in two forms. One form is a digital display (on a p-meter) of three readings from a three phase electrical power supply and presented as a percentage of the 1250 kW motor power rating. The other form is a kV meter display with a three phase meter presentation of amperes (p-Amps meter). The power at a particular time is calculated by substituting the digital readings from the p-Amps meter into equation (9.16).

$$Power\ draw = \sqrt{3} * \left(\frac{A_1 + A_2 + A_3}{3} \right) * V \qquad (9.16)$$

Where;

A_1, A_2, *and* A_3 = the three currents readings from the Amp-meter in amperes

V = the voltage to the mill at a fixed supply of 6.75 kV

Figure A4- 1 : SAG mill power meter panel

Feedrate

The totaliser reading gives an accurate feedrate measurement, and the reading was taken at the beginning and at the end of the test noting the exact times of the readings. The feedrate is calculated from the difference in the weights of the totaliser readings and the time measurement. During the test, instantaneous readings were monitored to check for variations in the feed.

Water Addition and flowrates

The water flowrate at every water addition point to the circuit was accurately measured. The flowrates were obtained from the available flow meters and in case of those with no flow meters, the bucket and stopwatch method, (Figure A4- 2) was used. The buckets used for flowrates and sample collection were 25ℓ while the drums used for slurry collection were 210ℓ capacity.

Figure A4- 2 : Collection of flowrate sample using the bucket and stop watch method

Stabilizing the plant for steady-state measurements

All measurable data, such as flowrates, densities, mill speed, and sump levels were taken and recorded. The steps taken to stabilize the circuit for steady-state included by-passing the flash float cell because the discharge pipe kept choking and thus providing an inconsistent flow to the mill. The bond area spillage pump was also switched off.

A4.2 MILLING CIRCUIT SAMPLING

Samples were collected around the SAG mill; run of mine mill feed, trommel screen oversize, cyclone overflow and cyclone underflow sample streams.

Run-of-Mine Mill Feed

This sample was taken after the crash-stop. A section of the belt cut sample after the mill had been crash-stopped is shown in Figure A4- 3. The low feedrate of 35 tph prompted taking the sample

from the whole 24m belt length. The fines were brushed off the belt into collecting buckets to ensure that no material was left on the sampled belt.

Sample size: Four 100 ℓ bins of both the coarse rocks and fine particles.

Figure A4- 3 : Section of the RoM SAG mill feed belt cut sample

Trommel screen oversize (Pebbles)

The pebbles from the trommel screen are discharged through the chute onto the transfer belt for collection into a drum. The pebbles flowrate is vital for mass balancing purposes and enables reconstitution of the inaccessible mill discharge stream. The pebbles sample was collected by placing an empty drum at the head pulley of the pebbles belt conveyor at the beginning of the test campaign and removing the drum and the pebbles at the end of the test. The trommel pebbles sample collection point is shown in Figure A4- 4. The pebbles were weighed and the time for the test campaign was recorded to calculate the pebbles flowrate in tph.

Sample size: About 7 kg dry sample.

Figure A4- 4 : Trommel pebbles sample collection point

Cyclone Overflow

This sample was cut as the overflow stream discharged into the distribution box shown in Figure A4- 5 , but before the stream proceeded to the tank cell. This sample was difficult to cut due to limited and insufficient space within the mixing box. The sample was cut by pushing the sample cutter across the flow. To ensure that a representative sample was obtained from the cyclone overflow stream, the sampling person swung the main body of the sample cutter swiftly across the flow at a constant speed from one end of the pipe to the other. This action required practice to give a smooth swing through the flow of the stream. A number of trial samples were taken to practice the technique.

Care was taken to ensure that the distribution box in which the overflow stream discharges, was not flooding when cutting this sample.

Once the actual sample was taken the sample was rapidly decanted into the sample bucket to avoid settling. The bucket lid was replaced to prevent slurry and other particles splashing into it.

Figure A4- 5 : Distribution box for the cyclone overflow stream

Sample cutter: Pelican Stainless Steel sample cutter.

Sample cutter dimensions: 10mm width by 350mm length.

Sample size: About 8 kg wet mass per sample

Cyclone underflow

The cyclone underflow sample was cut at the point were the stream discharges into a collection box before draining down to the Flash float cell.

Figure A4- 6 : Cyclone underflow sampling point

Figure A4- 6 shows the position where cutting of the cyclone underflow sample was conducted. The cyclone underflow stream was only accessible by the sampling person after removing the cover of the collection box with the help of Q20 lubricant; no modifications were made to the sample cutter.

Prior to cutting each sample a dummy sample was cut to keep the cutter consistently "dirty" with the underflow material. The sampling person swung the inclined cyclone sample cutter across the flow to cut the whole stream. After cutting the sample, the material was decanted rapidly by tipping the sample cutter upside down to empty it and then turning it up to free coarse particles from under the lid and tapped on the side of the bucket, ensuring that loose grit was dislodged from the spout.

Sample cutter: Custom made Stainless Steel Cutter with an inclined edge, (Figure A4- 6).

Sample cutter dimensions: 60mm width by 300mm length.

Sample size: About 13 Kg wet sample.

A4.3 SAMPLE PREPARATION

After a lot of time and effort has been spent on the sampling campaign, the samples are often treated casually and the results of the sampling campaign could be destroyed by poor sample preparation and processing.

Labelling

The Labels were tied on the bucket, and the sample ID written on the side. Good clean lids for slurry samples were used to avoid sample spillages.

The samples were properly labelled and the number of pans for each sample was indicated on each label as shown in the example below:

UCT –AMD-S campaign

Cyclone U/F – A, Test 2

Pan 2 of 3

A 1 of 3

Taring of buckets

Before weighing the samples, all the buckets were tared; i.e. weighing the empty bucket and writing the weight and sample name on opposite sides of the bucket. The bucket lids were also tared. The bucket weight was subtracted from the total to obtain the sample weight.

Weighing

The mass of each sample was obtained to the best available accuracy. Thus smaller samples were weighed on smaller more accurate scales than large samples. It is totally inadequate to weigh a 1kg screen size fraction on a scale accurate to 0.5kg! In general one is looking for a better than 0.1% accuracy. Thus if a sample weighs about 10kg, the scale must be accurate to at least 0,01kg. The general accuracy selection for a given sample mass is shown in Table A4- 1.

Table A4- 1 : General accuracy selection according to sample mass

	Mass range	Accuracy
RoM feed	>50kg	0.1kg
Slurry samples	50kg> Mass > 10kg	0.01kg
Upper end of coarse fractions	10kg> Mass > 1kg	0.001kg
Coarse fractions	1kg > Mass > 100g	0.1g
Fine screen fractions	100g > Mass	0.01g

Circuit stream samples were weighed wet immediately after the survey to give the wet mass, which is essential. Use of a good scale as the one shown in Figure A4- 7 accurate to 0.001kg was appropriate. To avoid loss of data, weights were recorded in a test data book and not on a loose paper.

Figure A4- 7 : Weighing steel balls

Drying

Coarse samples were dried directly in an oven. The slurry samples were filtered with filter paper on top of filter cloth. Care was taken not to lose fines in the sample as they are essential component of final data. The top liquid layer from the bucket was decanted and the settled solids were scraped directly onto drying pans. Samples were dried overnight in an oven at temperatures of about 70°C.

A4.4 SAMPLE PROCESSING

Sample processing is a vital part of the campaign, and inevitably if procedures and checks are not put in place and followed major errors might arise in this phase, and such errors could easily compromise the entire campaign. To ensure a meticulous sample processing, the UCT personnel responsible of the sampling campaign supervised and processed the data.

Stream samples

The four stream samples were processed separately from the mill charge samples. The coarse trommel pebbles, the slurry samples and the mill feed sample were further treated distinctly.

Coarse sample

The tronimel pebbles did not require drying as they had negligible moisture content. The pebbles collected over a known time were weighed to determine the pebbles flowrate, and then screened.

Slurry samples

The cyclone overflow and cyclone underflow constituted the slurry samples. For these streams, both the A and B samples were pressure filtered separately in filter pots, (Figure A4- 8). Care was taken not to lose fines during the filtration process as they are essential to the data. The filtered samples were dried in the oven at about 70 °C and the dry samples were weighed to determine the percentage solids of each sample.

Figure A4- 8 : Filtering slurry samples

RoM mill feed sample

The entire 24m belt cut sample was weighed wet. It was then screened on a 45mm screen to remove the coarse rocks. The plus 45mm rocks were sun dried. After drying, the fines on the plus 45mm rocks were brushed off and added to the sub-45mm material. The sub-45mm material was put into trays with proper labels, (Figure A4- 9) and dried in the oven. After drying all the material (both plus 45mm and sub-45mm) was weighed to determine the moisture content of the feed.

Figure A4- 9 : Oven dried RoM mill feed belt cut sample

Splitting

The splitting procedure was conducted by first thoroughly cleaning dust off the splitter and all the cups before use. The dry sub 1 mm sample was then added slowly into the cone of the rotary splitter shown in Figure A4- 10. When the cone was full with the sample, the motor was started first and followed by the feeder that was set at moderate vibration. Starting the motor first before the feeder was crucial as this ensured that there was no bias of feeding more sample in one cup. When stopping the splitter, the feeder was stopped first before the motor to avoid the feeder supplying material into one stationary cup and biasing the split.

At the end of the first split, cups which were directly opposite to each other were combined. Sets of cups at opposite sides were put together to make half of the sample and it was put back into the cone.

The same process of combing opposite cups and retaining half of the original sample was repeated until each cup had about half of the required mass. Three sub-split samples each of at least 300 g were collected; a screening sample and two back up samples. The splitting equipment is shown in Figure A4- 10.

Figure A4- 10 : Splitting sub 1 mm samples

Screening of finer material, sub 1mm

Fine screening is conducted on the sub-1 mm split samples of, at least 300 g. The total weight of the sub 1 mm fraction must be recorded and is very important because it provides a check for the material loss during the coarse screening process and also gives a scaling factor used to recombine the size distribution of the sub-1mm to the + 1mm material.

The split sample is re-weighed and then wet screened on the finest screen (32 μm). The sample is placed on a screen that is firmly attached onto a vibratory sieve shaker. Water is introduced onto the screen continuously during the wet screening process, and the undersize is collected in a clean bucket (Figure A4- 11). The sieving process continues until only clear water is discharged from the undersize. The undersize is kept in a labelled bucket with an additional tag kept in the slurry. The oversize material is placed on a 125 μm screen firmly attached onto the vibratory sieve shaker and the screening is conducted just as described for the 32 μm screen. The undersize is collected in a clean bucket. When only clear water is discharged at the bottom of the screen, the 125μm screen oversize is placed on a pan and oven dried at about 80 °C. The dried material is then weighed and packed in a labelled plastic bag and stored for further screening at screen sizes above 125 μm. The undersize is wet screened on the 90 μm screen, and the procedure used on the 125 μm screening is repeated for all size fractions from 90 μm down to 32 μm. The minus 32μm from the second pass is combined with the original – 32 μm fraction, then filtered and finally dried.

Figure A4- 11 : wet screening technique.

The dried oversize is weighed and dry screened on standard 200 mm laboratory sieve screens from a 710 µm sieve screen down to 125 µm. A dried sample is placed into the 710 µm sieve and the stack is vibrated by a standard laboratory vibratory sieve shaker for a sieving time of 20 minutes. The equipment used in the dry sieving process is shown in Figure A4- 12.

Figure A4- 12 : A dry screening sieve shaker

The resulting fractions from both wet and dry screening are weighed and kept separately in well labelled plastic bags for further analysis. The integrity of the screening and weighing process is checked by immediately adding up all the screen fraction masses and the total sub 32µm fraction, and checking that it nearly equals the total sub-sample mass. Errors can be checked on the spot before the sample is analysed further or disposed of.

The individual screen size fractions are discarded after their masses have been recorded. However, the back-up split samples are stored long after the sample processing has been finished. The back-up sample can easily be processed to check or confirm the particle size distribution when ever there are doubts about the integrity of the stream in question.

The detailed schedule for the Amandelbult test work activities is summarized in Table A4- 2.

Table A4- 2 : Amandelbult testwork schedule

Task	Start date	Duration
Moving to site	29-Feb-04	-
On-site test preparations	1-Mar-04	1 week
Trial survey	9 Mar-04	1 hour
Main Sampling campaign	15 Mar 04	1 hour
Emptying out charge samples from the mill	16-Mar-04	4 days
Steel balls screening and mill start up	20-Mar-04	4 days
Total mill down-time	15 20 -Mar-04	6 days
Screening rocks and fine samples	26-Mar-04	8 days
Screening fine samples and packing	3 Apr 04	3 days
Leaving site	6 Apr 04	-
Total project duration	**37 days**	

A4.5 RAW MASS DATA

The raw mass data for the fine particles (slurry), rocks, steel balls and metal scrap emptied out from the mill are given in Table A4- 3 to Table A4- 11.

Table A4- 3 : Summary of equipment and personnel involved in the Amandelbult survey

General sampling tools	Qty	Workshop	Qty
Sample cutters	3	Welding equipment	
Handsizer (63 - 250 mm) sets	4	Tool box	1
10 m measuring tapes	2	Screw drivers	5
20 ℓ buckets	60	Clippers	3
25 ℓ buckets	40	Pliers	3
100 ℓ bins	15	Shifting spanners	2
210 ℓ drums	25	2 lb hammers	2
Hanging scales	2	wooden plugs	12
1000 kg Flatbed scale	1	**Mobile**	
Extension light	1	Flat deck crane	1
Torches	2	Fork lifters	2
shovels	15	Wheelbarrows	1
Gwalas	5	Trolleys	3
Wooden pallets	20	**Electronic**	
Old filter cloth sheets	6	Video Camera & accessories	1
Filter pots	3	Digital camera	2
Filter paper	100	Water proof camera	1
Drying pans/trays	15	**Manpower Resources**	
Ovens	2	UCT researchers	6
Rotary splitters	2	Plant personnel	3
Medium sample bags	200	Casual assistants	15

Table A4- 4 : Manually logged Plant control data

Mill power										
Time	KV	Amp 1	Amp 2	Amp 3	AMP Power	Time	V1	V2	V3	P Power
10:10	6.8	72.5	70	70	834.3	9:30	72.08	72.24	72.07	901.6
10:12	6.8	72.5	70	70	834.3	10:09	72.17	72.13	72.06	901.5
11:21	6.8	72.5	70	70	834.3	11:21	71.42	72.06	71.62	896.3
11:53	6.8	72.5	70	70	834.3	11:52	71.44	71.78	71.67	895.4
12:01	6.8	72.5	70	70	834.3	12:01	71.32	71.85	71.82	895.6
12:53	6.8	72.5	70	70	834.3	12:52	71.72	72.05	71.75	897.9
13:15	6.8	72.5	70	70	834.3	13:14	71.8	72.27	71.22	897.0
13:35	6.8	72.5	70	70	834.3	13:26	71.34	72.63	72.12	900.4
13:37	6.8	72.5	70	70	834.3	13:36	71.2	72.23	71.97	897.5
13:48	6.8	72.5	70	70	834.3	13:48	71.27	71.81	71.54	894.3
Average					834.3					897.8

Mill discharge flow		Mill discharge			Cyc Feed pressure		Mill inlet water		Sump water	
Time	flow (m³/h)	Time	SG (sg/m³)	% Solids	Time	(a)	Time	Flow (m³/h)	Time	Flow (m³/h)
9:50	163.4	10:05	1.56	55.8	9:47	20	9:53	19.2	10:10	83.7
10:05	167.2	11:56	1.52	52.6	10:07	20	10:02	18.3	10:12	83.0
11:57	165.6	12:05	1.45	45.1	10:30	15	11:54	12.1	11:20	33.5
12:06	160.5	13:18	1.84	82.7	11:55	12	12:03	11.2	11:50	52.9
13:18	158.4	13:22	1.76	75.2	11:58	15	12:53	7.5	12:02	33.9
13:26	157.2	13:30	1.66	65.3	12:07	20	13:16	12.8	12:53	31.9
13:32	103.4	13:33	1.60	59.5	12:47	20	13:28	12.4	13:15	58.3
13:42	154.1	13:42	1.55	55.5	13:19	20	13:35	10.3	13:26	43.5
13:45	124.3	13:44	1.53	55.4	13:31	12	13:40	10.0	13:38	40.3
13:52	118.2	13:55	1.55	55.5	13:43	15	13:46	10.9	13:39	40.6
13:54	122.3				13:53	15	13:50	10.0	13:49	43.4
Average	145.0		1.60	60.3		17		12		49.5

Table A4- 5 : Circuit raw mass (kg) data

Size (mm)	RoM feed	Total mill charge	Pebbles	Cyclone O/F	Cyclone U/F
180	0.0	0.00	0.0	0.0	0.0
125	27458.0	97.10	0.0	0.0	0.0
90	43208.0	467.32	0.0	0.0	0.0
63	53392.0	654.75	0.0	0.0	0.0
45	52595.0	470.48	0.0	0.0	0.0
31.5	50100.0	458.21	1356.0	0.0	0.0
22.4	42086.0	262.48	2100.0	0.0	0.0
16.0	34294.0	275.75	1984.0	0.0	0.0
11.2	25746.0	176.31	1396.0	0.0	0.0
8.0	15868.0	96.07	40.0	0.0	0.0
5.6	15846.0	61.38	0.0	0.0	0.0
4.0	9946.0	54.99	0.0	0.0	0.0
2.8	10810.0	49.22	0.0	0.0	0.0
2.0	10520.0	33.13	0.0	0.0	0.0
1.4	6580.0	33.32	0.0	0.0	0.0
1.0	8910.0	57.20	0.0	0.0	0.0
0.710	6485.8	57.98	0.0	2.2	16.4
0.500	13450.3	143.05	0.0	5.0	49.0
0.355	15691.6	355.11	0.0	16.5	143.2
0.250	12897.7	857.51	0.0	65.0	391.8
0.180	8951.0	1720.19	0.0	217.6	870.5
0.125	4532.6	1862.26	0.0	359.8	899.5
0.090	3887.2	1901.81	0.0	542.1	903.6
0.063	2551.0	1515.99	0.0	590.3	535.6
0.045	1207.6	814.80	0.0	423.7	183.5
0.032	1393.4	560.73	0.0	284.6	151.4
- 0.0320	5252.0	2633.35	0.0	1485.2	396.6
Total	482959.0	15670.5	6876.0	3992.0	4541.0

Table A4- 6 : Raw mass (kg) of slurry drained out from bolt holes along the SAG mill

Size (mm)	Slice 1	Slice 2	Slice 3	Slice 4
11.2	0.00	0.00	0.00	0.00
8.0	0.02	0.00	0.00	0.00
5.6	0.05	0.00	0.00	0.00
4.0	0.07	4.19	1.19	0.00
2.8	0.11	1.63	0.63	0.00
2.0	0.09	1.29	0.54	0.00
1.4	0.61	1.38	0.50	
1.0	2.90	4.63	3.88	0.17
0.710	1.9	1.5	1.2	0.6
0.500	2.5	1.9	2.9	1.0
0.355	5.5	4.4	6.5	2.6
0.250	12.1	10.8	15.2	7.8
0.180	25.8	23.5	32.7	17.9
0.125	32.8	28.6	40.2	22.6
0.090	42.7	36.0	49.2	29.2
0.063	43.4	32.9	46.5	27.6
0.045	32.2	26.1	32.6	21.8
0,032	26.2	13.0	26.3	13.0
- 0 .032	253.4	134.8	225.2	105.4
Totals	*482.3*	*326.7*	*485.2*	*249.5*
Tons	*0.5*	*0.3*	*0.5*	*0.2*
Total mass	*1543.7*	*1.5*		
	kg	*tons*		

Table A4- 7 : Raw mass of fines (slurry) emptied out with rocks from the mill

Size (mm)	Slice 1	Slice 2	Slice 3	Slice 4	total
1.0	0.0	0.0	0.0	0.0	0.0
0.7	21.6	13.0	8.5	9.7	52.8
0.5	53.4	31.2	25.5	24.8	134.8
0.4	132.8	74.5	66.6	62.3	336.1
0.3	312.4	172.3	167.8	159.2	811.6
0.2	578.9	336.4	346.1	359.8	1620.3
0.1	594.8	352.9	366.9	423.6	1738.1
0.1	545.0	339.7	388.1	472.0	1744.8
0,1	405.0	263.0	315.0	382.5	1365.5
0.0	199.3	140.3	163.5	198.9	702.0
0.0	138.3	112.6	119.0	112.4	482.3
- 0.0320	612.0	359.7	449.9	503.0	1914.6
Total	3592.5	2185.5	2416.7	2708.2	10903.0

Table A4- 8 : Combined raw mass (kg) of fine particles (slurry) collected from the mill

Size (mm)	Slice 1	Slice 2	Slice 3	Slice 4	Total slurry
1.0					0.0
0.7	23.5	14.5	9.7	10.3	58.0
0.5	55.9	33.1	28.3	25.8	143.1
0.4	138.3	78.9	73.1	64.9	355.1
0.3	324.5	185.1	183.0	166.9	857.5
0.2	603.8	359.9	378.8	377.7	1720.2
0.1	627.5	381.4	407.1	446.2	1862.3
0.1	587.7	375.7	437.2	501.2	1901.8
0.1	448.4	295.9	361.5	410.1	1516.0
0.0	231.5	166.5	196.1	220.7	814.8
0.0	164.5	125.6	145.2	125.4	560.7
- 0,032	865.4	484.5	675.1	608.2	2633.3
Totals	*4070.9*	*2499.1*	*2895.1*	*2957.6*	*12422.8*
Tons	*4.1*	*2.5*	*2.9*	*3.0*	*12.4*

Table A4- 9 : Raw mass (kg) of all rock particles emptied out from the mill

Size (mm)	Slice 1	Slice 2	Slice 3	Slice 4	total
180.0	0.0	0.0	0.0	0.0	0.0
125.0	78.9	18.2	0.0	0.0	97.1
90.0	315.4	86.8	30.8	34.2	467.3
63.0	397.7	128.3	51.2	77.6	654.8
45.0	303.1	54.5	35.7	77.2	470.5
31.5	255.9	35.7	106.5	60.1	458.2
22.4	166.4	37.2	26.7	32.3	262.5
16.0	93.6	85.2	78.1	19.0	275.8
11.2	79.0	71.4	12.2	13.7	176.3
8.0	45.1	24.2	11.3	15.5	96.0
5.6	38.2	11.5	4.5	7.1	61.3
4.0	28.9	7.8	8.4	4.5	49.5
2.8	30.8	10.0	0.5	5.6	46.9
2.0	15.1	8.3	3.3	4.6	31.2
1.4	14.1	5.7	5.5	5.6	30.8
1.0	27.6	7.0	6.3	4.7	45.6
0.7	21.6	13.0	8.5	9.7	52.8
0.5	53.4	31.2	25.5	24.8	134.8
0.4	132.8	74.5	66.6	62.3	336.1
0.3	312.4	172.3	167.8	159.2	811.6
0.2	578.0	336.4	346.1	359.8	1620.3
0.1	594.8	352.9	366.9	423.6	1738.1
0.1	545.0	339.7	388.1	472.0	1744.8
0.1	405.0	263.0	345.0	382.5	1365.5
0.0	199.3	140.3	163.5	198.9	702.0
0.0	138.3	112.6	119.0	112.4	482.3
- 0.0320	612.0	349.7	449.9	503.0	1914.6
Total	*5482.2*	*2777.1*	*2797.6*	*3069.8*	*14126.8*
Tons	*5.5*	*2.8*	*2.8*	*3.1*	*14.1*

Table A4- 10 : Raw mass (kg) of + 1 mm rocks emptied out from the SAG mill

Size (mm)	Slice 1	Slice 2	Slice 3	Slice 4	Total
180	0.0	0.0	0.0	0.0	0.0
125	78.9	18.2	0.0	0.0	97.1
90	315.4	86.8	30.8	34.2	467.3
63	397.7	128.3	51.2	77.6	654.8
45	303.1	54.5	35.7	77.2	470.5
31.5	255.9	35.7	106.5	60.1	458.2
22.4	166.4	37.2	26.7	32.3	262.5
16.0	93.6	85.2	78.1	19.0	275.8
11.2	79.0	71.4	12.2	13.7	176.3
8.0	45.1	24.2	11.3	15.5	96.0
5.6	38.2	11.5	4.5	7.1	61.3
4.0	28.9	7.8	8.4	4.5	49.5
2.8	30.8	10.0	0.5	5.6	46.9
2.0	15.1	8.3	3.3	4.6	31.2
1.4	14.1	5.7	5.5	5.6	30.8
1.0	27.6	7.0	6.3	4.7	45.6
Total mass	**1889.7**	**591.6**	**380.9**	**361.6**	**3223.8**

Table A4- 11 : Mass (kg) of metal scrap emptied out from each slice along the mill

	Slice 1	Slice 2	Slice 3	Slice 4	Total
Metal Scrap	25.2	26.2	41.0	59.3	**151.7**

Table A4- 12 : Raw steel balls mass (kg) emptied out from the mill

Size (mm)	Slice 1	Slice 2	Slice 3	Slice 4	total
125	0.0	0.0	0.0	0.0	0.0
90	66.9	75.2	96.5	216.2	454.9
63	3100.9	4244.6	3095.0	3761.5	14202.0
45	6112.4	5295.9	3699.1	4606.8	19714.2
31.5	2418.2	2163.9	1758.4	2373.3	8713.7
22.4	474.7	673.3	473.3	892.6	2513.8
16.0	183.5	1.4	63.2	366.1	614.2
11.2	24.3	1.2	34.1	100.8	160.4
8.0	3.2	2.0	4.4	11.1	20.7
5.6	0.7	0.4	0.8	3.1	5.1
4.0	0.0	0.1	0.2	0.4	0.7
2.8					
Total	*12384.8*	*12457.9*	*9225.0*	*12331.8*	*46399.5*
Tons	*12.4*	*12.5*	*9.2*	*12.3*	*46.4*

A4.6 CUMULATIVE PERCENT PASSING DATA

The cumulative percent passing data for the different streams and particle specifies emptied out from the mill are given in Table A4- 13 to Table A4- 19.

Table A4- 13 : Cumulative percent passing for streams around the milling circuit

Size (mm)	RoM feed	Total mill charge	Pebbles	Cyclone O/F	Cyclone U/F
180	100.0	100.0	100.0	100.0	100.0
125	94.3	99.4	100.0	100.0	100.0
90	85.4	96.4	100.0	100.0	100.0
63	74.3	92.2	100.0	100.0	100.0
45	63.4	89.2	100.0	100.0	100.0
31.5	53.0	86.3	80.3	100.0	100.0
22.4	44.3	84.6	49.7	100.0	100.0
16.0	37.2	82.9	20.9	100.0	100.0
11.2	31.9	81.7	0.6	100.0	100.0
8.0	28.6	81.1	0.0	100.0	100.0
5.6	25.3	80.7	0.0	100.0	100.0
4.0	23.3	80.4	0.0	100.0	100.0
2.8	21.2	80.1	0.0	100.0	100.0
2.0	19.0	79.9	0.0	100.0	100.0
1.4	17.6	79.6	0.0	100.0	100.0
1.0	15.8	79.3	0.0	100.0	100.0
0.710	14.5	78.9	0.0	99.9	99.6
0.500	11.7	78.0	0.0	99.8	98.6
0.355	8.4	75.7	0.0	99.4	95.4
0.250	5.8	70.3	0.0	97.8	86.8
0.180	3.9	59.3	0.0	92.3	67.6
0.125	3.0	47.4	0.0	83.3	47.8
0.090	2.2	35.3	0.0	69.7	27.9
0.063	1.6	25.6	0.0	54.9	16.1
0.045	1.4	20.4	0.0	44.3	12.1
0.032	1.1	16.8	0.0	37.2	8.7

Table A4- 14 : Cumulative percent passing of slurry drained from bolt holes along the mill shell

Size (mm)	drained slice 1	drained slice 2	drained slice 3	drained slice 4	average drained
1.0	100.0	100.0	100.0	100.0	100.0
0.710	99.6	99.5	99.7	99.8	99.7
0.500	99.1	98.9	99.1	99.4	99.1
0.355	97.9	97.5	97.8	98.3	97.9
0.250	95.4	94.1	94.6	95.2	94.8
0.180	90.0	86.6	87.8	88.0	88.3
0.125	83.2	77.5	79.4	79.0	80.1
0.090	74.2	66.0	69.1	67.3	69.8
0.063	65.2	55.5	59.4	56.2	59.9
0.045	58.4	47.1	52.6	47.5	52.5
0.032	53.0	43.0	47.1	42.3	47.3

Table A4- 15 : Cumulative percent passing of all fine particles (slurry) collected from the mill

Size (mm)	total slice 1	total slice 2	total slice 3	total slice 4	average total
1.0	100.0	100.0	100.0	100.0	100.0
0.710	99.4	99.4	99.7	99.7	99.5
0.500	98.1	98.1	98.7	98.8	98.4
0.355	94.7	94.9	96.2	96.6	95.5
0.250	86.7	87.6	89.8	90.9	88.6
0.180	71.9	73.2	76.8	78.2	74.8
0.125	56.4	57.9	62.7	63.1	59.8
0.090	42.0	42.9	47.6	46.1	44.5
0.063	31.0	31.1	35.1	32.3	32.3
0.045	25.3	24.4	28.3	24.8	25.7
0.032	21.3	19.4	23.3	20.6	21.2

Table A4- 16 : Cumulative percent passing for all rock solids emptied out from the mill

Size (mm)	Slice 1	Slice 2	Slice 3	Slice 4	total
180	100.00	100.00	100.00	100.00	100.00
125	98.56	99.35	100.00	100.00	99.31
90	92.81	96.22	98.90	98.89	96.00
63	85.55	91.60	97.07	96.36	91.37
45	80.03	89.63	95.79	93.85	88.04
31.5	75.36	88.35	91.98	91.89	84.80
22.4	72.32	87.01	91.03	90.84	82.94
16.0	70.62	83.94	88.24	90.22	80.99
11.2	69.17	81.37	87.80	89.77	79.74
8.0	68.35	80.50	87.40	89.27	79.06
5.6	67.66	80.09	87.24	89.03	78.62
4.0	67.13	79.81	86.94	88.89	78.27
2.8	66.57	79.45	86.92	88.71	77.94
2.0	66.29	79.15	86.80	88.56	77.72
1.4	66.03	78.95	86.61	88.37	77.50
1.0	65.53	78.70	86.38	88.22	77.18
0.710	65.14	78.23	86.08	87.90	76.81
0.500	64.16	77.11	85.17	87.10	75.85
0.355	61.74	74.43	82.79	85.07	73.47
0.250	56.04	68.22	76.79	79.88	67.73
0.180	45.50	56.11	64.42	68.16	56.26
0.125	34.65	43.40	51.31	54.36	43.95
0.090	24.71	31.17	37.44	38.99	31.60
0.063	17.32	21.70	26.18	26.52	21.94
0.045	13.69	16.65	20.33	20.05	16.97
0.032	11.16	12.59	16.08	16.38	13.55

Table A4- 17 : Cumulative percent passing of + 1 mm sized rocks

Size (mm)	Slice 1	Slice 2	Slice 3	Slice 4	Total rocks
180	100.0	100.0	100.0	100.0	100.0
125	95.8	96.9	100.0	100.0	97.0
90	79.1	82.2	91.9	90.5	82.5
63	58.1	60.6	78.5	69.1	62.2
45	42.1	51.3	69.1	47.8	47.6
31.5	28.5	45.3	41.1	31.1	33.4
22.4	19.7	39.0	34.1	22.2	25.2
16.0	14.8	24.6	13.6	17.0	16.7
11.2	10.6	12.6	10.4	13.2	11.2
8.0	8.2	8.5	7.5	8.9	8.2
5.6	6.2	6.5	6.3	6.9	6.3
4.0	4.6	5.2	4.1	5.7	4.8
2.8	3.0	3.5	3.9	4.1	3.3
2.0	2.2	2.1	3.1	2.9	2.4
1.4	1.5	1.2	1.6	1.3	1.4

Table A4- 18 : Cumulative percent passing of steel balls along the mill

Size (mm)	Slice 1	Slice 2	Slice 3	Slice 4	total
125	100.0	100.0	100.0	100.0	100.0
90	99.5	99.4	99.0	98.2	99.0
63	74.4	65.3	65.4	67.7	68.4
45	25.1	22.8	25.3	30.4	25.9
31.5	5.5	5.4	6.2	11.1	7.1
22.4	1.71	0.04	1.11	3.90	1.73
16.0	0.23	0.03	0.43	0.94	0.40
11.2	0.03	0.02	0.06	0.12	0.06
8.0	0.006	0.004	0.012	0.028	0.012
5.6	0.000	0.000	0.003	0.003	0.001
4.0	0.000	0.000	0.000	0.000	0.000

Table A4- 19 : Cumulative percent passing of defined + 1 mm rock sizes

	Slice 1	Slice 2	Slice 3	Slice 4
Big rocks (mm)				
125	100.0	100.0	100.0	100.0
90	92.8	94.4	100.0	100.0
63	64.0	67.9	73.8	81.9
45	27.7	28.8	30.3	40.8
S80	78.0	75.3	69.4	62.2
Critical size rocks (mm)				
45.0	100.0	100.0	100.0	100.0
31.5	63.0	62.7	85.5	59.1
22.4	31.7	48.5	42.4	27.2
16.0	11.4	33.8	31.6	10.1
S80	37.7	37.8	30.3	38.4
Small rocks (mm)				
16.0	100.0	100.0	100.0	100.0
11.2	75.1	65.1	42.9	76.4
8.0	54.1	35.8	34.0	59.4
5.6	42.1	25.9	25.7	40.1
4.0	32.0	21.2	22.4	31.3
2.8	24.3	16.3	15.4	25.6
2.0	16.1	11.6	14.6	18.7
1.4	12.0	7.7	11.8	13.0
1.0	8.1	4.8	7.4	6.1
S80	12.1	13.2	14.3	11.9

Table A4- 20: Drop weight test product size distribution at 0.25 kWh/t Ecs energy

57.8 mm						14.1 mm				
Size, mm	Mill feed	Slice 1	Slice 2	Slice 3	Slice 4	Mill feed	Slice 1	Slice 2	Slice 3	Slice 4
53.0	100.0	100.0	100.0	100.0	100.0	100.0	100.0	100.0	96.8	100.0
37.5	100.0	95.3	100.0	100.0	100.0	100.0	97.0	90.5	90.7	98.7
26.5	98.5	61.2	91.7	73.2	63.9	92.8	76.2	65.0	68.5	75.8
19.0	87.9	62.4	69.4	41.4	37.4	77.0	55.1	43.1	40.5	46.3
13.2	70.3	48.5	46.3	28.2	25.7	65.7	42.5	33.0	31.4	33.7
9.50	58.0	38.9	37.1	23.0	20.5	51.5	32.1	24.0	23.1	24.9
6.70	47.9	30.5	29.2	17.9	15.9	41.6	25.2	18.9	18.1	19.4
4.75	40.0	25.2	23.9	14.3	12.8	35.1	21.3	15.6	14.9	16.3
3.35	34.4	21.5	20.9	12.0	10.6	30.1	18.3	13.4	12.7	14.0
2.36	29.9	18.7	18.5	10.3	8.8	26.9	16.3	11.8	11.2	12.6
1.70	26.9	16.7	17.1	9.1	7.4	24.4	14.7	10.7	10.0	11.5
1.18	24.2	15.0	15.9	8.1	6.1	22.7	13.7	9.9	9.2	10.7
0.850	22.5	13.9	15.2	7.4	5.2	20.0	12.1	8.7	8.0	9.6
0.600	19.6	12.3	14.0	6.5	4.3	16.5	10.3	7.2	6.8	8.4
0.425	15.9	10.4	11.9	5.5	3.6	11.8	7.5	5.3	5.2	6.4
28.9 mm						**20.6 mm**				
Size, mm	Mill feed	Slice 1	Slice 2	Slice 3	Slice 4	Mill feed	Slice 1	Slice 2	Slice 3	Slice 4
53.0	100.0	100.0	100.0	100.0	100.0	100.0	100.0	91.7	100.0	100.0
37.5	94.8	94.8	97.1	90.8	93.8	92.0	88.9	77.2	91.2	81.1
26.5	79.1	75.5	77.9	69.4	65.4	82.7	75.5	58.9	72.2	59.0
19.0	68.9	60.3	58.4	44.0	47.1	64.4	61.1	39.1	49.5	45.8
13.2	52.4	43.7	42.6	32.0	34.3	47.7	47.6	27.5	34.6	34.2
9.50	41.4	33.9	31.8	24.7	26.4	37.7	39.2	21.5	27.5	27.7
6.70	33.9	27.9	25.4	20.3	21.8	30.9	32.3	18.1	22.7	22.9
4.75	28.4	23.6	21.8	17.2	18.4	27.0	28.4	15.8	19.9	20.1
3.35	25.2	20.9	19.4	15.0	16.3	24.2	25.7	14.0	17.7	17.8
2.36	22.6	18.7	17.7	13.3	14.6	22.1	23.8	12.8	16.2	16.2
1.70	20.9	17.3	16.6	12.1	13.4	19.2	21.3	11.2	14.3	14.2
1.18	18.4	15.3	15.1	10.6	11.9	15.6	17.6	9.2	12.0	11.7
0.850	15.1	12.8	13.1	8.8	10.2	10.8	12.1	6.6	8.8	8.4
0.600	10.5	9.1	9.9	6.6	7.7	7.2	7.8	4.6	6.2	5.6
0.425	7.1	6.2	7.0	4.7	5.5	4.6	4.7	3.1	4.1	3.6
14.5 mm										
Size, mm	Mill feed	Slice 1	Slice 2	Slice 3	Slice 4					
53.0	100.0	100.0	93.6	97.9	100.0					
37.5	91.6	96.0	84.5	88.3	87.6					
26.5	85.8	82.2	67.8	64.5	63.3					
19.0	71.8	64.5	48.6	46.3	42.0					
13.2	56.7	49.0	36.5	36.1	32.4					
9.50	44.0	39.0	26.0	28.6	25.8					
6.70	33.7	33.4	24.0	24.2	21.8					
4.75	28.6	29.7	21.1	21.0	19.1					
3.35	25.0	27.2	19.3	18.9	17.2					
2.36	22.7	23.6	17.1	16.2	14.9					
1.70	19.6	19.3	14.5	13.3	12.4					
1.18	16.0	13.1	10.7	9.6	9.1					
0.850	11.4	8.4	7.4	6.7	6.3					
0.600	7.7	5.0	4.7	4.4	4.2					
0.425	4.8	3.3	3.2	3.0	3.0					

Appendix 5

A5 DEM ENERGY SPECTRA DATA

Appendix A5 gives the raw energy spectra data obtained from the DEM simulations.

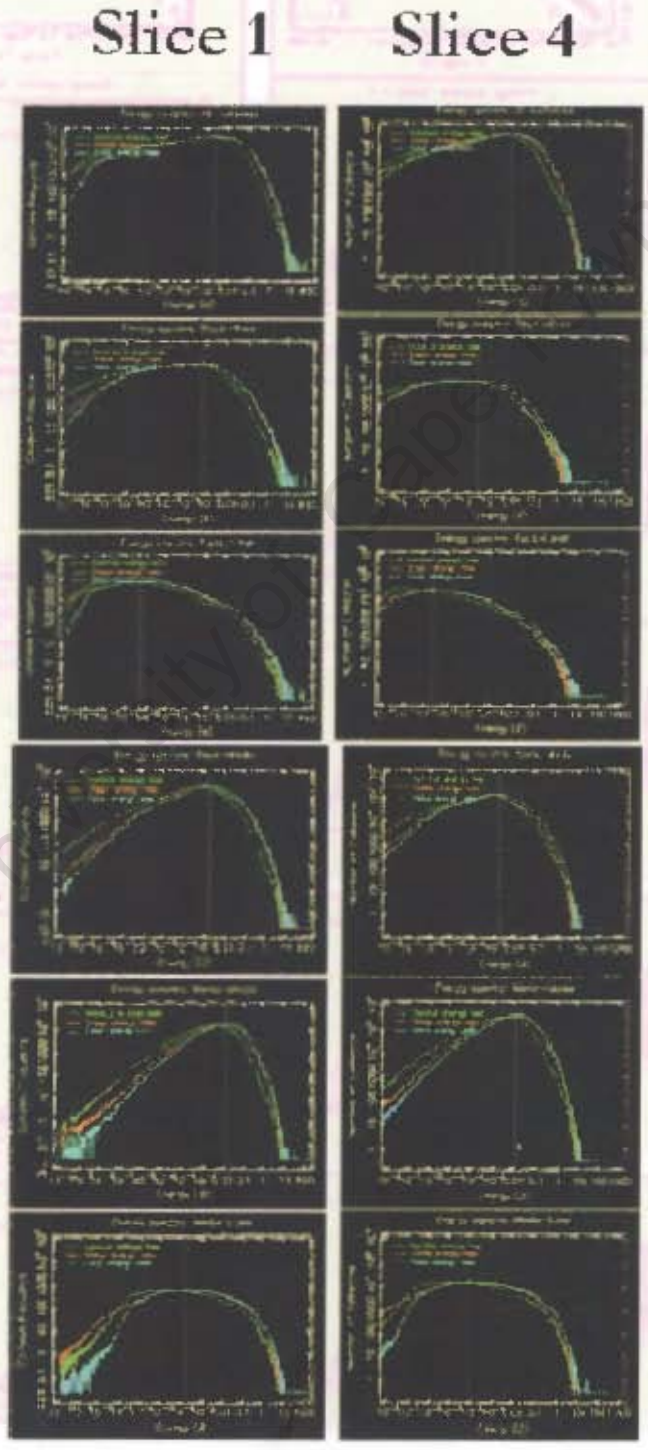

Figure A5- 1 : Energy spectra top to bottom; All collisions, Rock – Rock, Rock – L ner, Rock – Ball, Ball – Ball, and Ball – Liner

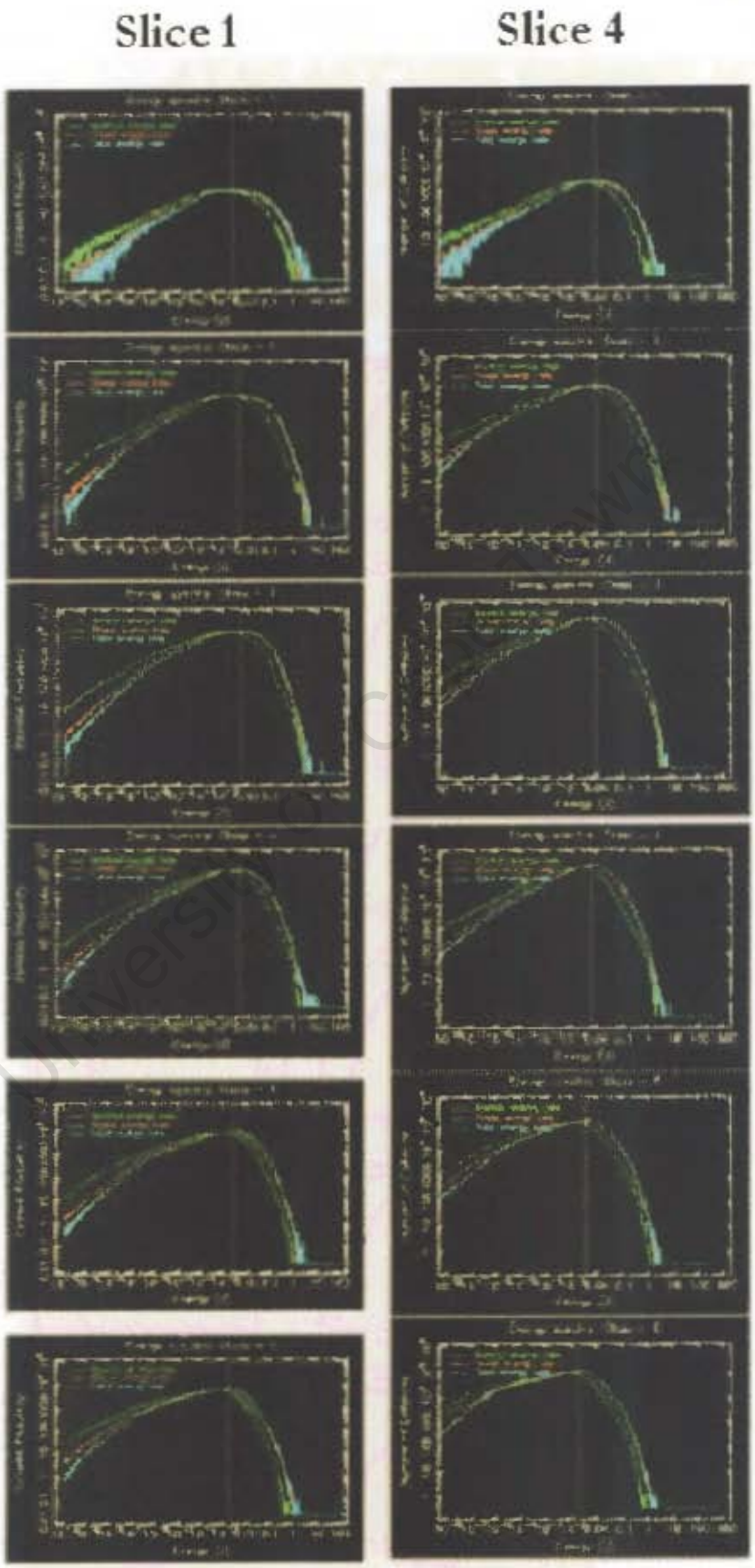

Figure A5- 2 : Balls size classes from top to bottom; 90, 63, 45, 22.4, 16 and 11.2 mm

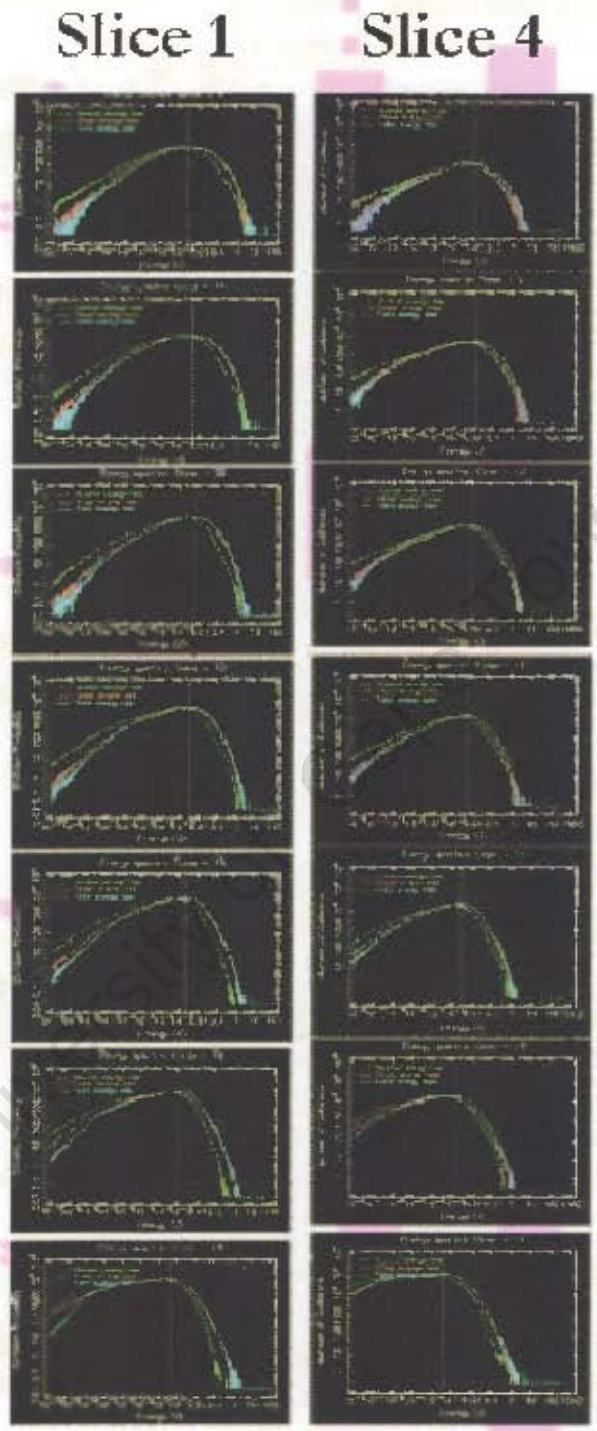

Figure A5- 3 : Rocks size classes from top to bottom; 125, 90, 63, 45, 22.4, 16 and 11.2 mm

Table A5- 1 : Energy conversion

DEM energy ranges, J	kWh/t
0.03	0.00001
0.09	0.000025
0.90	0.00025
2.25	0.001

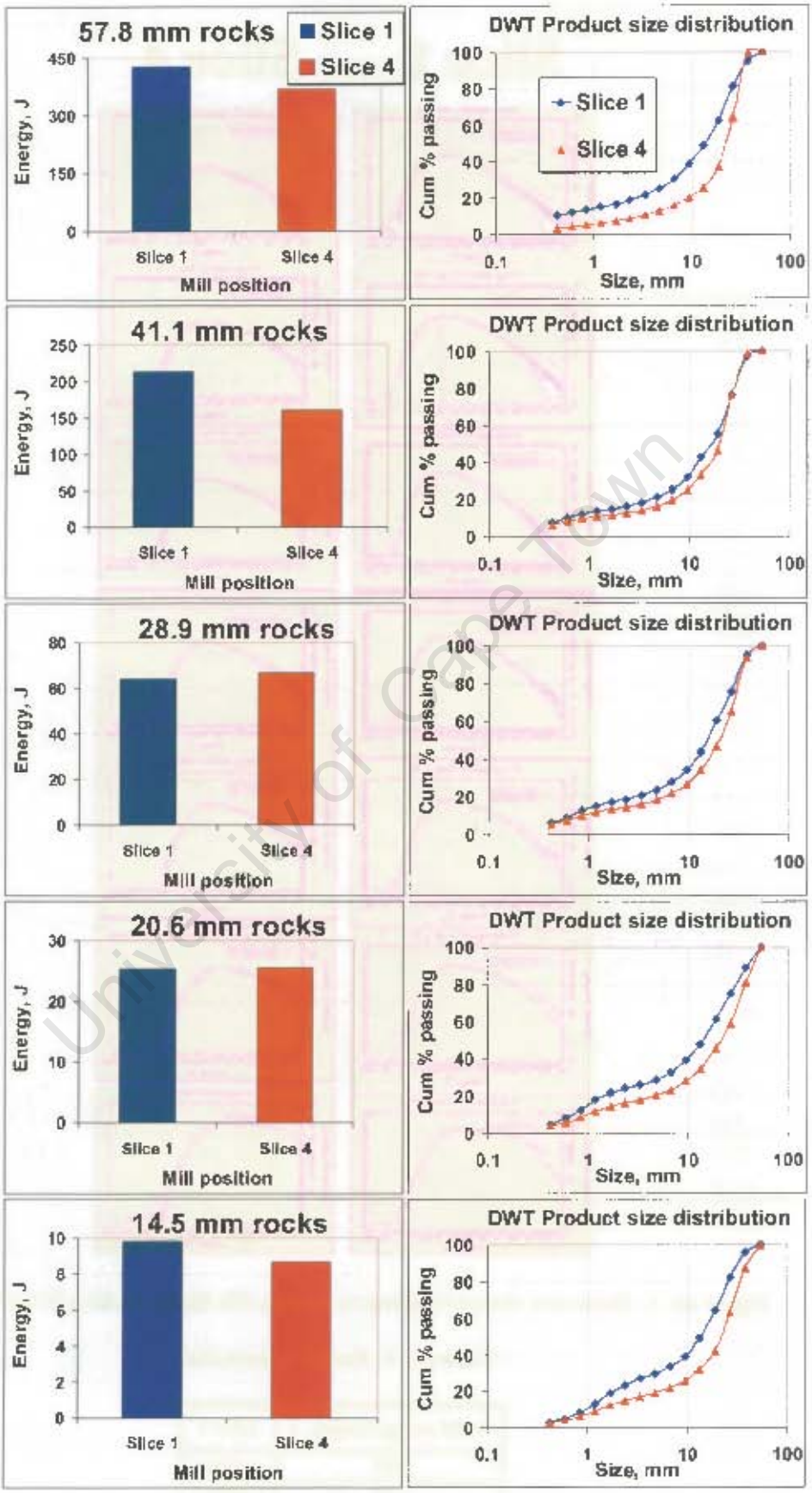

Figure A5- 4 : DWT input energy and the product size distribution at 0.25 kWh/t

Table A5- 2 : Predicted appearance function data at four energy ranges

Minimum breakage energy, E_{crit} = 0. 05 kWh/t							
	Breakage distribution -appearance function						
Size, mm	t_2	t_4	t_{10}	t_{25}	t_{50}	t_{75}	
57.8	26.0	9.7	5.3	3.5	2.1	1.55	Slice 1
41.1	27.0	10.2	5.5	3.7	2.2	1.63	
28.9	30.4	11.7	6.3	4.2	2.6	1.9	
20.6	36.1	14.2	7.7	5.2	3.2	2.4	
14.5	36.2	14.3	7.7	5.2	3.2	2.4	
57.8	19.3	5.6	3.1	2.0	1.3	1.0	Slice 4
41.1	29.0	8.9	4.9	3.2	2.2	1.6	
28.9	28.2	8.6	4.7	3.1	2.1	1.6	
20.6	30.4	9.3	5.1	3.4	2.3	1.7	
14.5	27.9	8.5	4.7	3.1	2.1	1.6	
0.1 and 0.9 J - energy range = cyclic energy to breakage, E_{crit} t_{10} used							
57.8	26.0	9.7	5.3	3.5	2.1	1.55	Slice 1
41.1	27.0	10.2	5.5	3.7	2.2	1.63	
28.9	30.4	11.7	6.3	4.2	2.6	1.9	
20.6	36.1	14.2	7.7	5.2	3.2	2.4	
14.5	36.2	14.3	7.7	5.2	3.2	2.4	
57.8	19.3	5.6	3.1	2.0	1.3	1.0	Slice 4
41.1	29.0	8.9	4.9	3.2	2.2	1.6	
28.9	28.2	8.6	4.7	3.1	2.1	1.6	
20.6	30.4	9.3	5.1	3.4	2.3	1.7	
14.5	27.9	8.5	4.7	3.1	2.1	1.6	
2.25 J - energy range = E_{crit} t map used for top four sizes							
57.8	26.0	9.7	5.3	3.5	2.1	1.55	Slice 1
41.1	27.0	10.2	5.5	3.7	2.2	1.63	
28.9	30.4	11.7	6.3	4.2	2.6	1.9	
20.6	36.1	14.2	7.7	5.2	3.2	2.4	
14.5	58.9	26.5	14.3	9.7	6.7	5.2	
57.8	19.3	5.6	3.1	2.0	1.3	1.0	Slice 4
41.1	29.0	8.9	4.9	3.2	2.2	1.6	
28.9	28.2	8.6	4.7	3.1	2.1	1.6	
20.6	30.4	9.3	5.1	3.4	2.3	1.7	
14.5	48.7	16.6	9.0	6.0	4.2	3.2	
	t_2	t_4	t_{10}	t_{25}	t_{50}	t_{75}	
14.5	Breakage achieved by single hit. Ecs is greater than E_{crit} used in DWT						

Table A5- 3 : Summary of collision rates obtained from the energy spectra at four energy ranges

Detectected rock collisions during 15 s simulation period				
	0.03 J energy range		0.1 J energy range	
Collision type	Slice 1	Slice 4	Slice 1	Slice 4
Rock - Rock	4000	5000	1500	1500
Rock - Liner	600	2000	200	1200
All - 106 mm rocks	800	1000	600	700
All - 53 mm rocks	3000	10000	1800	6000
All - 37.6 mm rocks	4000	19000	1500	5000
All - 26.6 mm rocks	4000	15000	1000	3000
All - 19 mm rocks	2000	6000	400	1500
All - 13.4 mm rocks	1500	20000	200	3000
Rock - Ball	20000	70000	8000	40000
	0.9 J energy range		2.25 J energy range	
Rock - Rock	80	60	20	18
Rock - Liner	25	100	10	40
All - 106 mm rocks	70	100	10	27
All - 53 mm rocks	40	300	4	70
All - 37.6 mm rocks	20	100	2	20
All - 26.6 mm rocks	10	10	0.4	1
All - 19 mm rocks	2	8	0.1	0.2
All - 13.4 mm rocks	2	10	0.06	2
Rock - Ball	100	3000	100	400
Total number of rocks	58952	16417	58952	16417
Total number of balls	27544	36188	27544	36188

Table A5- 4 : Degree of breakage and impact parameters for E_{crit} energy for five distinct sizes

Slice 1				
Size, mm	A	b	Energy, kWh/t	t_{10}
57.8	100.00	1.08	0.05	5.3
41.1	70.96	1.62	0.05	5.5
28.9	58.24	2.29	0.05	6.3
20.6	61.76	2.65	0.05	7.7
14.5	68.35	2.39	0.05	7.7
Slice 4				
57.8	100.00	0.63	0.05	3.1
41.1	49.48	2.08	0.05	4.9
28.9	58.72	1.67	0.05	4.7
20.6	60.43	1.77	0.05	5.1
14.5	63.85	1.51	0.05	4.7

Table A5- 5 : Predicted product size distribution for three selected energy ranges

DEM energy spectra and predicted fines production data

57.8 mm parent rock	$E_{cs} \geq 0.05$ kWh/t		0.1 J energy range		0.9 J energy range		2.25 J energy range	
Size, mm	Slice 1	Slice 4	Slice 1	Slice 4	Slice 1	Slice 4	Slice 1	Slice 4
0.8	1.55	1.02	0	0	1.6	1.0	1.6	1.0
1.2	2.12	1.35	0	0	2.1	1.3	2.1	1.3
2.3	3.53	2.04	0	0	3.5	2.0	3.5	2.0
5.8	5.27	3.12	0	0	5.3	3.1	5.3	3.1
14.4	9.75	5.63	0	0	9.7	5.6	9.7	5.6
28.9	25.95	19.32	0	0	26.0	19.3	26.0	19.3
41.1 mm parent rock								
Size, mm								
0.5	1.63	1.65	0	0	1.6	1.6	1.6	1.6
0.8	2.23	2.15	0	0	2.2	2.2	2.2	2.2
1.6	3.69	3.20	0	0	3.7	3.2	3.7	3.2
4.1	5.51	4.88	0	0	5.5	4.9	5.5	4.9
10.3	10.19	8.88	0	0	10.2	8.9	10.2	8.9
20.5	27.01	29.04	0	0	27.0	29.0	27.0	29.0
28.9 mm parent rock								
Size, mm								
0.4	1.9	1.6	0	0	1.9	1.6	1.9	1.6
0.6	2.6	2.1	0	0	2.6	2.1	2.6	2.1
1.2	4.2	3.1	0	0	4.2	3.1	4.2	3.1
2.9	6.3	4.7	0	0	6.3	4.7	6.3	4.7
7.2	11.7	8.6	0	0	11.7	8.6	11.7	8.6
14.4	30.4	28.2	0	0	30.4	28.2	30.4	28.2
20.6 mm parent rock								
Size, mm								
0.3	2.4	1.7	2.4	1.7	2.4	1.7	2.4	1.7
0.4	3.2	2.3	3.2	2.3	3.2	2.3	3.2	2.3
0.8	5.2	3.4	5.2	3.4	5.2	3.4	5.2	3.4
2.1	7.7	5.1	7.7	5.1	7.7	5.1	7.7	5.1
5.2	14.2	9.3	14.2	9.3	14.2	9.3	14.2	9.3
10.3	36.1	30.4	36.1	30.4	36.1	30.4	36.1	30.4
14.5 mm parent rock								
Size, mm								
0.2	2.4	1.6	2.4	1.6	2.4	1.6	5.2	3.2
0.3	3.2	2.1	3.2	2.1	3.2	2.1	6.7	4.2
0.6	5.2	3.1	5.2	3.1	5.2	3.1	9.7	6.0
1.5	7.7	4.7	7.7	4.7	7.7	4.7	14.3	9.0
3.6	14.3	8.5	14.3	8.5	14.3	8.5	26.5	16.6
7.3	36.2	27.9	36.2	27.9	36.2	27.9	58.9	48.7
	Cummulative % passing							

Table A5- 6: Predicted mass (g) produced per second from three DEM energy ranges

DEM energy spectra and predicted fines production data

57.8 mm rock	0.1 J energy range		0.9 J energy range		2.25 J energy range	
Size, mm	Slice 1	Slice 4	Slice 1	Slice 4	Slice 1	Slice 4
0.8	0	0	0.2	1.0	0.05	0.6
1.2	0	0	0.1	0.3	0.02	0.2
2.3	0	0	0.4	1.7	0.10	1.0
5.8	0	0	0.3	1.4	0.08	0.8
14.4	0	0	1.0	4.2	0.25	2.5
28.9	0	0	2.5	15.1	0.62	8.8
41.1 mm parent rock						
Size, mm						
0.5	0	0	0.1	0.5	0.03	0.3
0.8	0	0	0.04	0.2	0.01	0.1
1.6	0	0	0.2	0.9	0.05	0.4
4.1	0	0	0.2	0.7	0.04	0.4
10.3	0	0	0.5	2.2	0.13	1.1
20.5	0	0	1.3	7.4	0.32	3.7
28.9 mm parent rock						
Size, mm						
0.4	0	0	0.1	0.1	0.006	0.01
0.6	0	0	0.02	0.02	0.002	0.004
1.2	0	0	0.12	0.09	0.012	0.02
2.9	0	0	0.09	0.07	0.009	0.02
7.2	0	0	0.30	0.22	0.030	0.05
14.4	0	0	0.72	0.72	0.072	0.18
20.6 mm parent rock						
Size, mm						
0.3	0.3	0.9	0.02	0.05	0.002	0.003
0.4	0.1	0.3	0.01	0.01	0.001	0.001
0.8	0.6	1.4	0.03	0.08	0.004	0.005
2.1	0.4	1.1	0.02	0.06	0.003	0.004
5.2	1.5	3.5	0.1	0.2	0.01	0.01
10.3	3.4	11.7	0.2	0.6	0.02	0.04
14.5 mm parent rock						
Size, mm						
0.2	0.2	1.6	0.02	0.05	0.001	0.03
0.3	0.1	0.5	0.01	0.02	0.0004	0.01
0.6	0.3	2.6	0.03	0.09	0.002	0.04
1.5	0.2	2.1	0.02	0.07	0.002	0.03
3.6	0.7	6.4	0.1	0.2	0.005	0.1
7.3	1.7	21.5	0.2	0.7	0.01	0.3
Total mass, g	9.4	53.5	8.7	39.1	1.9	20.8